THE FORMATION OF SPRAY-ICE AND A SELECTION OF ITS CONSTITUTIVE PROPERTIES WITH COMPARISONS TO ICE AND SNOW

M. ABIGAIL STEEL

THE FORMATION OF SPRAY-ICE AND A SELECTION OF ITS CONSTITUTIVE PROPERTIES WITH COMPARISONS TO ICE AND SNOW

BY

M. ABIGAIL STEEL, B.SC.(ENG)

A thesis submitted to the School of Graduate Studies in partial fulfillment of the requirements for the degree of Masters of Engineering

Faculty of Engineering and Applied Science
Memorial University of Newfoundland

March, 1989

St. John's Newfoundland

ISBN 0-315-50470-6

ABSTRACT

This thesis examines the production of the material spray-ice, and several of its constitutive properties with comparisons drawn to existing spray-ice data as well as snow, ice and soil. Consideration was given as to how spray-ice was best represented as an engineering material and what factors effect its behavior. It was also important to add to the limited existing data base on spray-ice and to review the methods of production.

After a fairly extensive literature review on spray-ice, solid ice, granular ice and snow and a brief overview of the pressuremeter, the experimental results are presented. A total of thirty-seven pressuremeter tests were performed on first year ice and spray-ice. The production of spray-ice was evaluated through a large-scale test program and laboratory simulation. Finally a series of triaxial tests were performed on the laboratory made spray-ice.

From these experiments it was found that spray-ice behaved in a manner similar to granular ice or loose sand. However, its failure envelope has a shape that agrees with solid ice or snow. The cohesive properties of spray-ice plays an important role in determining its behaviour. It was found that spray-ice strength and failure type was highly dependent on the confining pressure and consolidation time as well as being affected by the test temperature, strain

rate and sample density. The strength trends found in this study do not entirely agree with the results of others on spray-ice, but the strength values and stress-strain curves are similar. The behaviour was comparable in some cases to that of solid, granular ice and snow. The pressuremeter tests performed on spray-ice did not compare well with values in the literature but, in general, agreed with the derived triaxial results. Generally, these tests were effective in evaluating spray-ice but additional work is required to understand this interesting and important material.

ACKNOWLEDGEMENTS

I would like to offer my sincere thanks to Dr. Pierre Morin and Dr. Jack Clark for their invaluable guidance, without which this work would not have reached fruition. I am also indebted to my supervisors, Memorial University and C-CORE for their generous funding provided for this project.

I would also like to thank Dr. Jeff Weaver and Esso Resources Ltd. of Calgary for their assistance and for the opportunity to take part in their spray-ice project.

I would like to thank my husband, Andrew, for his never ending support and encouragement thoughout this endeavour.

Finally, I dedicate this work to my father, John Steel, who passed away in October, 1988.

TABLE OF CONTENTS

LIST OF FIGURES

LIST OF TABLES

I INTRODUCTION

With the advancement of ice technology in North America in the past decade and the increasing costs of construction in the Arctic, many oil producers are looking at the use of spray-ice as a viable construction material. Spray-ice is a fine granular material formed through the high pressure spraying of water into a cold environment.

As spray-ice is a relatively new material only a limited amount of tests have been completed to determine its basic strength characteristics. In order to be able to increase its production while maintaining a competent material additional research work was thought necessary. The objectives of the following report are: (1) to help understand what affects spray-ice behaviour and to consider how it is best represented as an engineering material; (2) to add to the existing data base of strength information on spray-ice while assessing a means of performing insitu and laboratory tests on the ice and (3) to evaluate the production of spray-ice in the laboratory as well as through a full-scale experiment.

In preparing the test program it was important that the results could be correlated to previously attained field and laboratory data, while providing the greatest amount of information possible. It was therefore decided to look at spray-ice under field and laboratory conditions. The pressuremeter was selected to evaluate spray-ice insitu and

triaxial tests were employed to test laboratory made spray-ice.

To accomplish the above described objectives the work will proceed according to the following schedule: (1) A literature review is presented on spray-ice, other types of ice and the pressuremeter; (2) the spray-ice is assessed in detail with consideration given to the material, its formation and its uses; (3) the strength properties of solid ice, granular ice and snow are summarized and finally (4) the pressuremeter equipment is described in detail along with the test interpretation and its application to ice.

In the experimental section the field and laboratory tests are considered, the production of spray-ice is assessed and the ice crystallography is examined. A series of field pressuremeter tests on spray-ice and other first-year ice is presented. The production of spray-ice is evaluated through considering a large-scale experiment performed by ERCL (Esso Research Co. Ltd.) and by looking at the laboratory production of spray-ice. Triaxial tests have been performed on laboratory made spray-ice and the ice crystallography was determined for samples from the field as well as samples prepared in the laboratory and subjected to triaxial tests.

In the discussion of the results the success of the spray-ice production experiments is assessed along with the insitu and laboratory tests. Also, the findings from the

field and laboratory tests are compared with results from the literature on soil, solid ice, granular ice, snow and spray-ice where the data are available. These comparisons assist in providing information on the behavior of spray-ice.

II LITERATURE REVIEW

II.1 Spray-Ice

II.1.1 Introduction

From the construction already completed in the Arctic, it seems that spray-ice islands could cut exploration drilling costs by at least fifty percent in shallow to moderate water depths (Williams, 1985; Juvkam-Wold, 1986). Recently, spray-ice has also been used in the construction of barriers around offshore structures and floating ice islands. The spray-ice barrier protects a structure from the forces of the arctic ice sheet and creates an ice rubble mound that in itself defends the structure. Spray-ice has been employed to artificially thicken the ice sheet in the deep waters of the high Arctic and it has been used in the construction of a grounded island in the Beaufort Sea (Masterson et al, 1986(b); Goff et al, 1987). The general location of the Arctic exploration activities is shown in the map on Figure 2.1.1.

Spray-ice islands are not only economical in terms of the actual island construction, but there is also a saving due to the shorter construction period. A spray-ice island requires 30 to 45 days construction time while a gravel island needs 60 to 90 days (Williams, 1985). In addition, for gravel island construction there is a need for construction permits, dredging and transporting gravel, as well as having the drill rig ready well in advance because

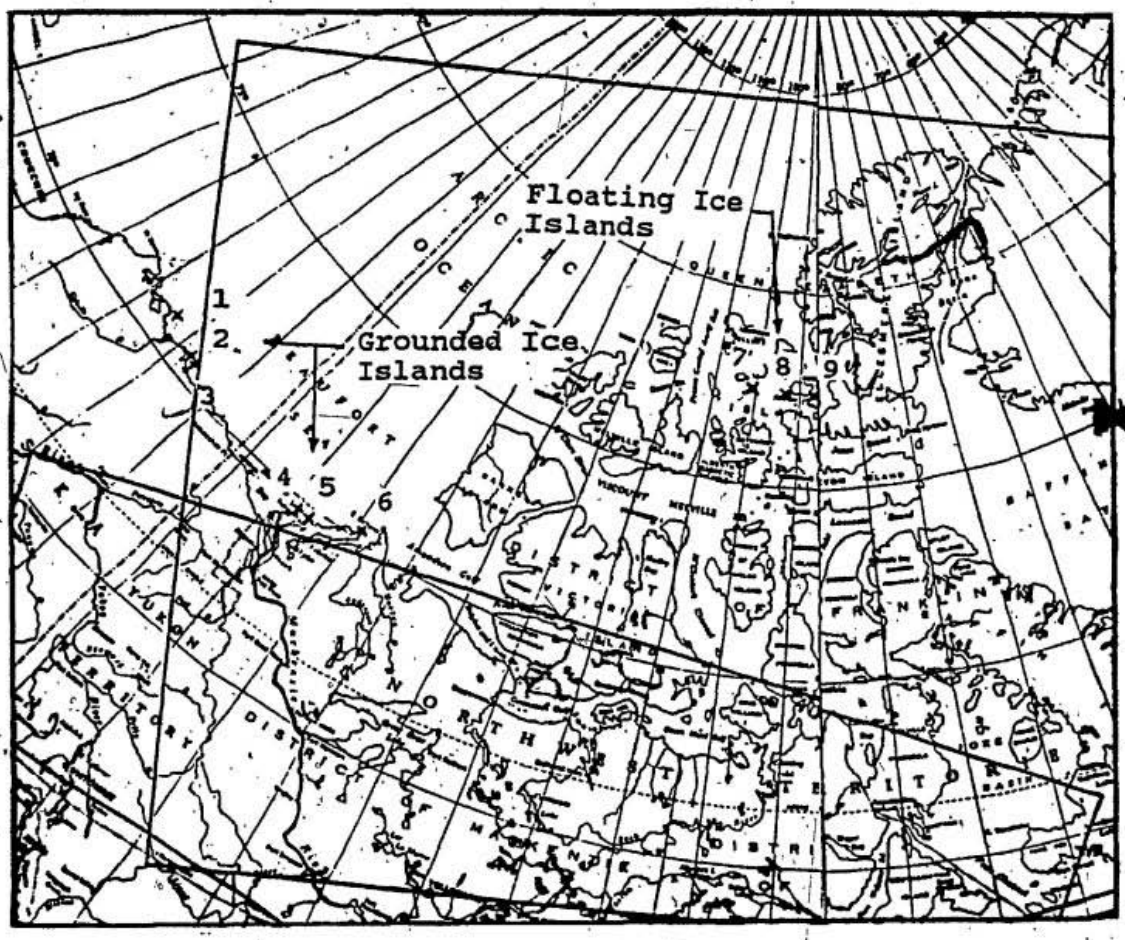

EXAMPLES OF SPRAY-ICE CONSTRUCTION

1 Mars, Amoco, 1986.
2 Ice Island Experiment, Joint Venture, 1978-79.
3 Experimental Island, Exxon, 1978-79.
4 Issungnak, Esso, 1980.
5 Alerk, Esso, 1982.
6 Angasak L-03, Esso & Exxon, 1986-87.
7 Cape Allison C-47, Panarctic, 1984-85.
8 Cornwall, 1985-86.
9 Buckingham O-68, 1985-86.

Figure 2.1.1

Location of Arctic Exploration Activities

of the necessarily brief drilling season. From an environmental point of view, the spray-ice island also has the advantage that, once the drilling is completed in the spring or summer, the island will melt. This means there will be few or no long term effects on the surrounding area.

The purpose of this section is to review the current literature on spray-ice. Spray-ice will first be described as a material and examples of how it has been used in construction will be illustrated. The physical and mechanical properties will be summarized from existing field and laboratory tests as found in the literature. Design aspects for spray-ice construction will be examined. The advantages and disadvantages of spray-ice will then be reviewed and consideration given to the future of spray-ice.

II.1.2 Spray-Ice Production

Ice has been used as a structural material for many years in the Arctic. The military developed its use in the 1950's for the construction of roads, bridges and runways (Duthweiller et al, 1985). More recently, floating ice islands have been constructed for exploratory drilling purposes by flooding sheet ice with water to build up a frozen mass (Masterson et al, 1986(a)). The major problems associated with flooding an ice sheet were the low build-up rate of the ice sheet (ie. approximately 7-10 cm/day at the

Panarctic ice platform), the limitations imposed by warm summer months, and the dependency of strength on the climatic conditions during construction.

The discovery of spray-ice, as it applies to the exploratory drilling operation, has renewed the use of ice as a structural material. Spray-ice has significantly higher build-up rates than flooded ice, with rates of up to 60 cm/day having been achieved in the experimental island constructed by Sohio and Partners in 1985 (Goff et al, 1986).

Spray-ice is formed by high pressure spraying of salt water through the cold Arctic air. Latent heat is rapidly transmitted to the air from the travelling water droplets, creating ice crystals before the droplets reach the ground. The material consistency depends on the air temperature, the initial flow rate and pressure, the distance of travel, and the salinity of the water. Once on the ground, it varies from a "snow" of ice crystals, to a "fluffy sleet", to a soft slush.

From observations on test and exploratory spray-ice islands, optimum conditions for making large quantities of spray-ice in a short time span have been ascertained. Generally, the lower the temperature, the higher the ice content of the spray-ice. Air temperatures should be at least -15 degrees C and preferably -20 to -40 degrees C. The spray nozzle is set at an angle of between 45 and 60

degrees to the horizontal with a spraying distance of between 60 and 90 metres and, ideally, no wind. During the spraying there may be losses of 65 to 75 percent of the estimated volume due to brine drainage and wind dispersion (Kemp, 1984).

In order to produce the very large volumes of spray-ice necessary for island construction, usually two to four pumps operate simultaneously to cover the area of the ice pad. The pumps are hooked up to a moveable skid or stationary swivel arrangement to which a fire nozzle is connected. The set up is similar to that shown in Figure 2.1.2. The pumps typically operate at a capacity of between 1500 and 18000 l/min. at 800 to 1500 kPa, depending on the type and number. During the construction of the CIDS (Concrete Island Drilling System owned by Global Marine) spray-ice barrier the pumps were stationed on board an ice breaker. This allowed for greater mobility and larger capacity pumps (Jahns et al, 1986).

II.1.3 Freezing and Sintering Processes of Spray-Ice

A better understanding of spray-ice can be attained by reviewing in more detail a few aspects of its formation including the formation of the ice granules and their sintering.

In the report by Zarling (1980) the heat and mass transfer from the water droplets is examined as described

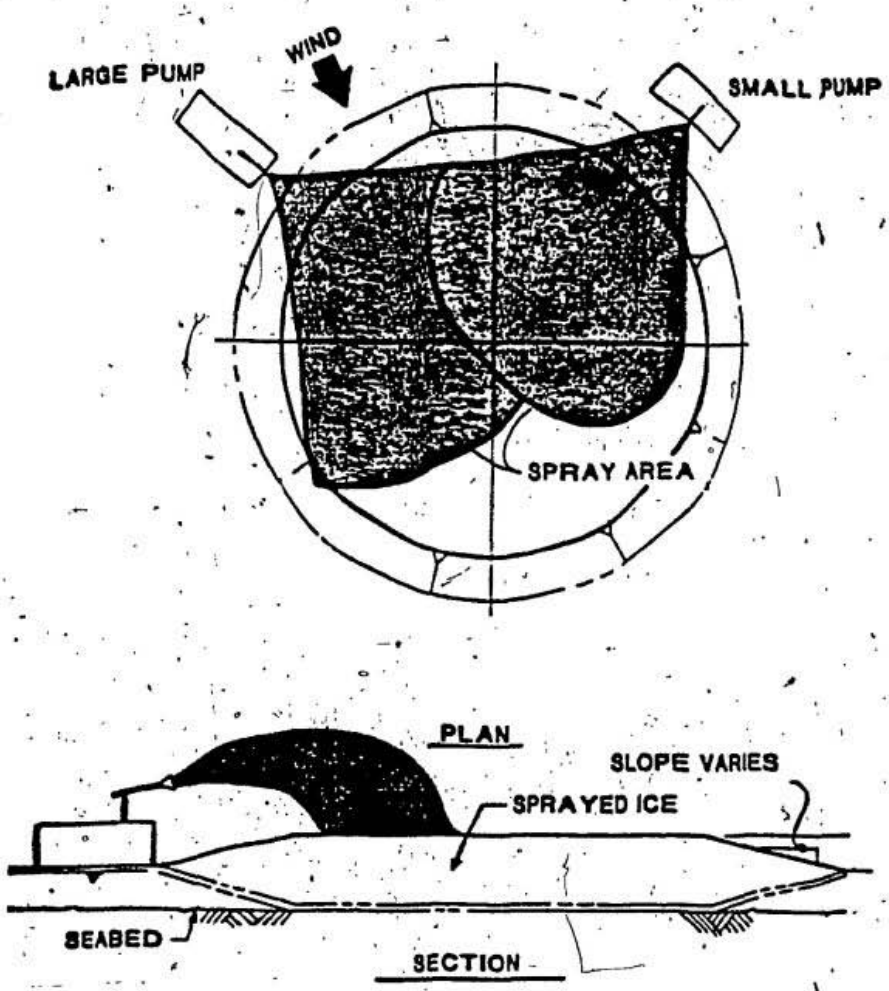

Figure 2.1.2

Spray-Ice Formation
(Jahns et al, 1986)

below. Sea water has not been considered in this explanation, it will be dealt with later.

As soon as the water leaves the nozzle the jet breaks up into drops. The pump pressure and the initial velocity of the jet are known and the initial water temperature is

assumed to be at zero degrees C.

When the jet breaks up due to inertial, aerodynamic and surface tension forces a large surface area versus volume ratio results. This causes high heat transfer rates and the supercooling of drops. Depending on the location of the water droplets in the stream, the air temperature and characteristics of the trajectory the water may nucleate before it hits the ground.

The analysis of the problem can be looked at in three ways; the velocity of the drops in the stream, the heat and mass transfer of a single drop in comparison to the evaporation rates and the heat and mass transfer of a system of drops.

The water jet behaves as a trajectory however as it breaks into drops the horizontal speed of the drop decreases with distance from the nozzle and the vertical speed of the drop decreases to zero as it reaches the top of the trajectory then increases again. It is important in this problem to know the drop diameter throughout the distance. This diameter is not necessarily the grain size of the material on the ground.

The heat and mass transfer of a single drop can be looked at in two ways. First it can be assumed that complete mixing occurs within the drop, and thermal and mass transfer occurs only at the drop surface, or no mixing can be assumed and the equation reduces to a transient heat flow

problem.

The heat and mass transfer of a system of drops can be analyzed by considering a steady flow condition from a volume of cold air and a falling water spray and the energy cross balance across the volume. Computer programs were used to step through the water trajectory in order to determine its properties.

These types of calculations have resulted in cooling curves for a system of water droplets falling from various heights. The curves are also used to determine the drop diameter for a given flow ratio and temperature.

From this type of calculation the following information has been ascertained:

- Drops falling from a greater distance cool more.
- As drop size decreases the thermal equilibrium condition between drops and air is approached. It is possible that drops falling from different distances have the same final temperature.
- If equilibrium is reached between drop and air, no further cooling of the drops takes place.
- As flow ratio increases, cooling of drops decreases due to the increase of water in the air column.

The flow ratio is directly a function of water drop temperature, water flow rate, air flow rate, change in air stream enthalpy, and humidity ratio.

Sackinger et al (1978) investigated the effect of the

salinity on the droplet formation. As the sea water droplets are forced from the spray nozzle into the cold air they experience accelerated cooling. Initially the heat is lost by convective heat transfer and evaporation. When the front side of the water droplet reaches -1.8 degrees C ice crystals begin to form.

Most water droplets contain a particle of sediment, which aids in crystal nucleation, and only a limited amount of super cooling is possible. Once the surface of the droplet is ice covered the transfer of heat by evaporation, is less and flow through the shell increases. As the droplet freezes the brine concentration of the remaining liquid rises and the freezing temperature decreases.

If the size of the water droplet is increased the quantity of material to freeze also increases. The larger the water droplet the faster it will move, this improves the local heat transfer in proportion to the square of the radius. Also an increase in the nozzle pressure does not necessarily increase the throw distance due to increased turbulence.

From actual observations of spray-ice, the mean diameter of the particles varies as follows: 99 percent are between 1 and 10 mm, 30 percent less than 4 mm and 0.1 percent less than 1 mm.

Experimentation shows that to ensure an ice content of 83 percent the droplet should be less than 1 mm in diameter

with the remaining brine at a salinity of 200 ppt. Spray-ice often contains entrapped air so that the density varies between 0.7 to 0.85 g/cm^3.

Once the material has reached the ground, various processes occur. The brine in the droplets starts to drain and the droplets sinter. Sintering bonds the individual grains together thus increasing the material strength. According to Ramseier et al (1967) sintering is the process by which ice and snow particles bond together at temperatures below the melting point. The growth of the bonds is a result surface diffusion, volume diffusion and evaporation condensation.

II.1.4 Spray-Ice Construction History

As previously mentioned, ice has been used as a construction material in the Arctic for many years. Since 1970 the oil industry has been using flooding, sprinkling and finally spray ice techniques for various construction applications (Goff et al, 1987).

The use of ice as an engineering material is limited by the extent of the "temperature window" throughout the year. In the Arctic, construction of an island or breakwater cannot commence until the summer breakup has been completed and temperatures are cool enough for ice formation and stabilization. This usually means December, in the Beaufort Sea, and both the construction and the exploratory drilling

must be completed by spring breakup and thaw in May (Goff et al, 1986). Therefore, the structures may only be used for one season unless special provisions are made to prptect the ice against warm temperatures.

The short construction period obviously limits the depth of water in which ice islands can be constructed and shortens the allowable exploration time for ice flooded and spray-ice islands in comparison to that of concrete caisson islands. Gravel and concrete islands, however, have very high construction costs for one time exploratory wells and only marginal success has been achieved in transporting concrete structures to new locations. Gravel islands, obviously, can not be relocated but they may, with additional maintenance costs, be used for a second season.

Panarctic Oils Ltd. has been constructing floating ice islands in the Canadian high Arctic since 1973. To date, 38 wells have been drilled on islands constructed in this manner in water depths of up to 500 metres. However, in the southern Arctic, the ice sheet is not solid (or stable) year round and it is not possible to drill from floating islands (Masterson et al, 1987).

In 1976/77, Union Oil and partners constructed a flooded, grounded ice island in about 2.7 metres of water in Harrison Bay, Alaska. The island was successfully used for the drilling of an exploration well (Cox et al,1986).

Exxon and partners, in the winter of 1979/80,

constructed an experimental, grounded ice island in Prudhoe Bay in 3.05 metres of water. The island was approximately 396 metres in diameter. Three techniques were used, free flooding, sprinkling from a central pivot, and spraying from a high volume nozzle. It was found that low density spray-ice could vastly improve the build-up rate and thus construction times for ice islands (Prodanovic, 1986).

The Tarsiut and Alerk caisson retained structures used thickened ice pads for their relief wells. Also, further protection against ice sheet forces was provided by using spray-ice to heighten the ice rubble mound around the island and to enlarge the pad diameter (Neth et al, 1983; Kemp, 1984).

In 1983/84 Standard Oil and Exxon constructed grounded spray-ice islands in relatively shallow water and confirmed the rapid build-up rates of spray-ice that had been anticipated. Exxon used a spray-ice barrier around the CIDS drilling unit in 15 metres of water located at Antares in the Beaufort Sea (Jahns et al, 1986). The same year, Standard Oil and partners constructed a 106 metre diameter spray-ice island off Prudhoe Bay in the Alaskan Sea. This experimental island was used to evaluate the engineering properties of spray-ice.

Amoco was the first to use a spray-ice island for exploration drilling. Mars was constructed in 1985/86 at Cape Halkett, west of Prudhoe Bay in moderate water depth

(Funegard et al, 1987).

Since 1980, Standard Oil Ltd. has been studying and making use of rubble ice. Rubble ice forms naturally on slopes of artificial islands and shoals. Standard Oil has designed and tested various rubble generating and collecting devices. An example of a full-scale field test is the proposed use of a barge mounted structure as the ice rubble generator and then using spray-ice techniques to add to the island's mass (Potter et al, 1984).

Another use of spray-ice was tested in 1984/85 by Panarctic Oils Ltd., on Cape Allison C-47. Cape Allison C-47 was a floating ice drilling platform constructed of first year sea ice which was thickened with spray-ice. The original ice thickness was approximately 0.8 metres, and the final total thickness was 6.97 metres. Cape Allison was located in the Canadian Arctic, offshore of Ellef Ringnes Island, in 260 metres of water, and it covered an area of 180 by 40 metres. The island was designed to support the Panarctic Rig A which weighs 1.6 thousand tonnes (Masterson et al, 1987). A year earlier, Panarctic Oils Ltd. gained experience with spray-ice during the construction of the Buckingham O-68 platform and relief platform, offshore of Graham Island. Originally, spray-ice was to be used solely for the relief platform, but due to its successful operation and high build-up rates, spray-ice was used in the later stages of construction of the main platform.

More recently, in 1986/87, Esso and partners constructed a grounded spray-ice platform, Angasak LO3 near Cape Dalhousie in the Beaufort Sea, for exploratory drilling and experimental purposes (Weaver et al, 1988).

II.1.5 Physical and Mechanical Properties of Spray-ice

Since its first use as a construction material, spray-ice has been tested to determine its physical and mechanical properties both in-situ and in the laboratory. The improved knowledge of the properties of spray-ice will enhance the design of various structures.

The properties of spray-ice vary with temperature, location of the water table, salinity, age, and production conditions. Depending on its use, the strength, volume, density or dryness of the spray-ice may be important. The borehole logs shown in Figure 2.1.3 show the ice stratigraphy on two spray-ice construction sites.

Spray-ice appears in various forms, and it is worth noting the layering and variability of the material. From the profiles in Figures 2.1.3 and 2.1.4, the increase in slush and the water content with depth is evident. Spray-ice above the waterline (a.w.l.) is drained, cold and quite strong, while spray-ice below the waterline (b.w.l.) is saturated, at sea water temperature (-1.8 degrees C) and contains soft layers. Generally, spray-ice is a fairly competent material. It is composed of fine, subrounded

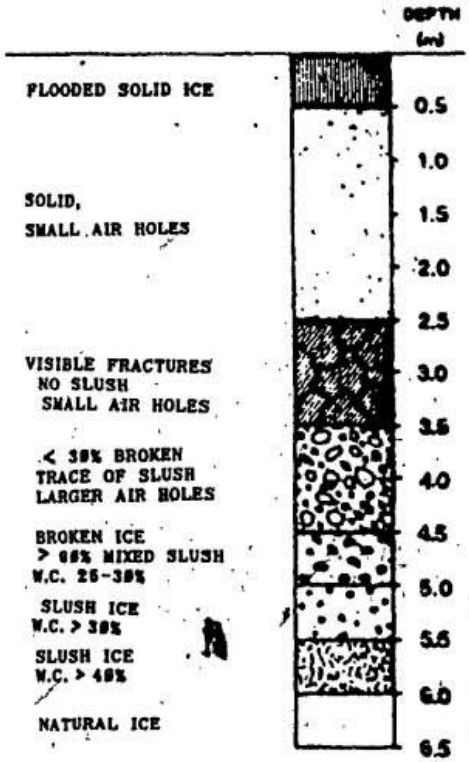

Figure 2.1.3

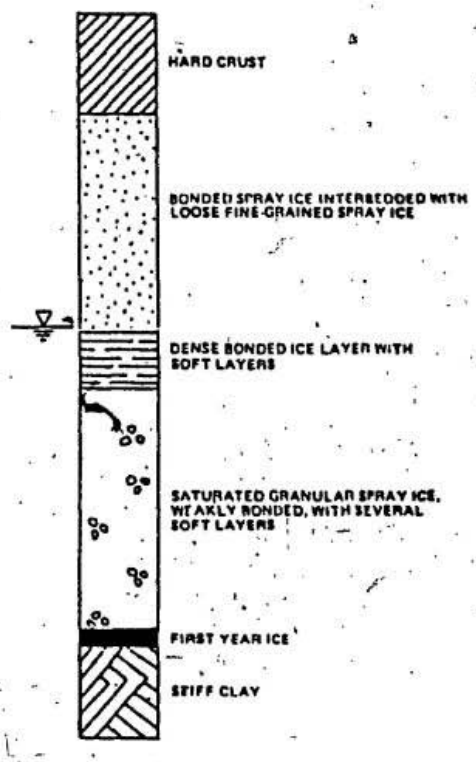

Figure 2.1.4

Typical Spray-Ice Core Profiles
(Masterson et al, 1987 (left);
Jahns et al, 1986 (right))

granules of ice which may be bonded or partially bonded. It tends to consolidate and become more dense with increasing overburden pressure. Above the water table, spray-ice is deposited in layers, as a solid granular material including unfrozen brine. Over time the brine drains from the

partially bonded material. Below the water table, the spray-ice maintains a thermodynamic equilibrium with the saline pore fluid (Goff et al, 1987).

The properties of spray-ice are highly dependent on ice type and, therefore, distance to the water level. The salinity of spray-ice also changes with depth and time. The a.w.l. salinity averages lower than the b.w.l. salinity. Over time, the a.w.l. salinity decreases due to brine drainage and brine migration. Brine drainage and migration are initiated due to the force of gravity and temperature gradient acting on the denser brine over the surrounding spray-ice. These effects cause a corresponding increase in the b.w.l. salinity of the ice. On average, the salinity is around 7.4 ppt. a.w.l. and 16 ppt. b.w.l. spray-ice (Prodanovic, 1981(a)). The salinity of sea water is approximately 35 ppt..

The grain size of spray-ice depends mainly on the type of spray nozzle used and the climatic conditions during construction. Grain sizes for spray-ice vary from 0.5 to 5.0 mm.

The spray-ice is initially formed at a temperature of about -1.8 degrees C. The ice then quickly cools in the cold arctic air. In the early life of the island the ice temperature is quite variable, but as time progresses the ice surface comes close to air temperature and the ice temperature gradually increases with depth until the water

level is reached. Below the water line the ice assumes the water temperature of about -1.8 degrees C (Jahns et al, 1986).

The density of spray-ice not only depends on its salinity, temperature and distance to the water surface, but is also a function of the meteorological conditions during construction and of the production equipment. This porous material has a bulk density on average of 0.74 g/cm^3 which is lower than solid ice. Bulk densities vary between 0.52-0.86 g/cm^3 for a.w.l. and 0.85-0.92 g/cm^3 for b.w.l. spray-ice. By coring through islands the existence of layering of the spray-ice has been established, some of these layers are solid ice. During ice production spraying is stopped intermittently to allow the material to solidify. At times, when the air temperature is relatively high ice lenses form. A density and brine volume profile from the Esso Resources Ltd. Alerk grounded spray-ice pad is shown in Figure 2.1.5..

Several types of field and laboratory tests have been conducted in order to determine the strength and deformation properties of spray-ice. The strength of spray-ice has been estimated from in-situ penetrometer tests, flatjack tests and pressuremeter tests. Vertical and horizontal settlement of the spray-ice structures was examined through the use of Sondex tubes, vertical and horizontal slope indicators and surveying equipment.

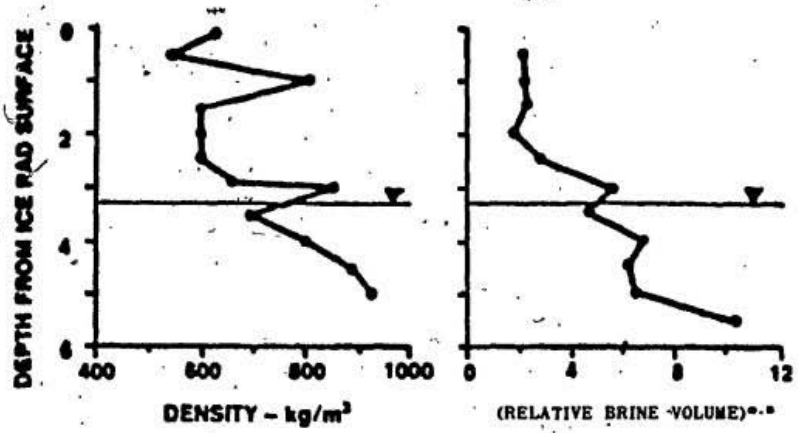

Figure 2.1.5

Ice Island Density & Salinity Profile
(Kemp, 1984)

It appears that mechanical properties of spray-ice are functions of the particle bonding, loading rate, stress level, temperature, salinity, density, and air and void volumes. The shear strength is generally considered to be about half of the uniaxial compressive strength. The strength of spray-ice has been measured from triaxial tests pefformed on ice cores in a field testing facility as well as from insitu tests. Pressuremeter and flatjack tests, provide an estimate of Young's Modulus for spray-ice, that is useful in predicting the settlement.

Field tests have the advantage of testing in place material. However, these tests are expensive and subject to the time constraints imposed by island or barrier construction and drilling times. Because of this, there has

been increasing interest in producing spray-ice in the laboratory or in transporting block samples and conducting ontrolled laboratory experiments.

Spray-ice can be produced in the laboratory in a manner similar to the method used in the field. A nozzle is used to spray water droplets in the air, where it freezes into ice granules. The nozzle is fed with compressed air and saline water. Equipment used to make artificial snow can be adapted for use in producing spray-ice.

In the laboratory, triaxial tests are used to determine ice properties. To simulate site conditions, drained and undrained tests have been carried out at different confining pressures, temperatures and strain rates. These tests are conducted on spray-ice core samples transported to the laboratory, and on samples made from reconstituted field spray-ice.

The stress-strain strength characteristics of the spray-ice as determined in controlled triaxial tests can be used to estimate the deformation modulus and anticipated settlement. However, it has been found that it is difficult to extrapolate laboratory data to long term settlement determination (Man, 1988). More recently, the creep behaviour for spray-ice has been determined through constitutive law and numerical modelling (Man, 1988). These analyses make use of the limited field observations. An example of a simplified stress-strain curve from Angasak

spray-ice island is shown in Figure 2.1.6. The strain hardening behaviour of the material is quite evident.

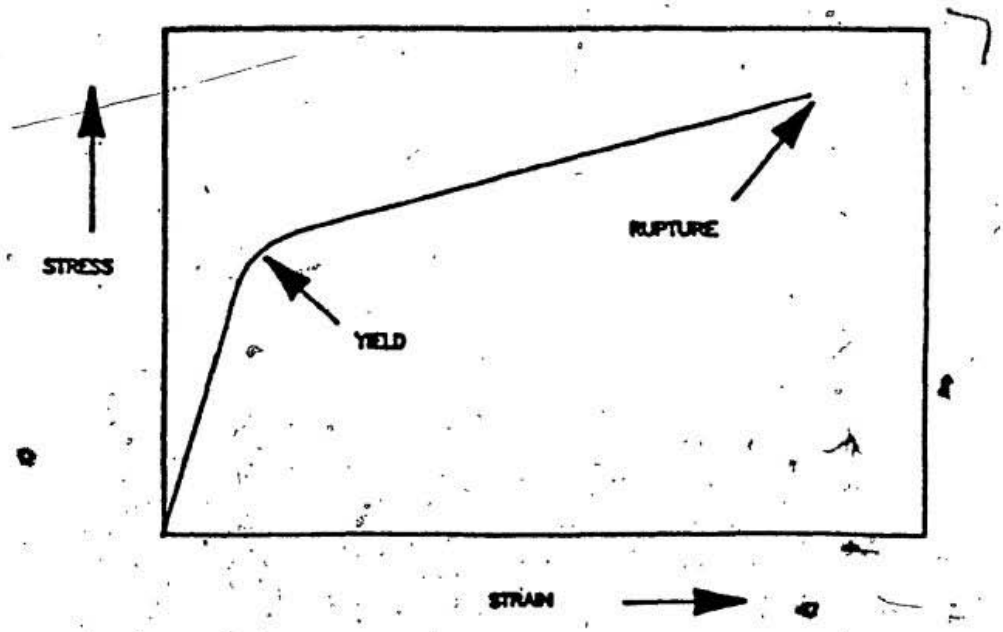

Figure 2.1.6

Simplified Stress-Strain Curve
(Weaver et al, 1988)

Table 2.1.1 and 2.1.2 show some typical values for the elastic modulus and compression strength of spray-ice from laboratory and field data.

From the test data collected on spray-ice, it appears that laboratory experiments on field or laboratory spray-ice samples give reasonable estimates of the field compressive strength and elastic modulus values. The laboratory tests tend to underestimate both the elastic modulus and the strength values, although they are within the range of various field tests conducted. It is difficult

ICE QUALITY TEST RESULTS

COMPRESSIVE STRENGTH

TEST	STRAIN RATE (s^{-1})	MEAN (MPa)	STD. DEV. (Mpa)
Lab uniaxial	10^{-3}	2.3	1.02
Lab triaxial (confining pressure 10.3 MPa)	10^{-3}	13.3	1.23
Flatjack	10^{-6}	1.87	0.22
Borehole jack	10^{-3}	15.2	4.5

ELASTIC MODULUS

TEST	STRAIN RATE (s^{-1})	MEAN (MPa)	STD. DEV. (Mpa)
Lab uniaxial	10^{-3}	1285	382
Lab triaxial (confining pressure 10.3 MPa)	10^{-3}	1672	021
Flatjack	10^{-6}	1060	285
Borehole jack	10^{-3}	2396	2371

Table 2.1.1

Spray-Ice Properties I
(Masterson et al, 1986)

ICE PROPERTIES				
	DENSITY kg/m³	SALINITY 0.00	CONFINED COMPRESSIVE STRENGTH MPa	UNCONFINED COMPRESSIVE STRENGTH MPa
SPRAYED ICE	540 to 870	0.5 to 8.0	MEAN 7.3	0.2 at −2°C to 3.4 at −22°C
CONSOLIDATED ICE RUBBLE	810 to 940	4.0 to 15.0	MEAN 13.4	0.81 at −13°C to 5.27 at −22°C

Table 2.1.2

Spray-Ice Properties II
(Kemp, 1984)

to compare the results without knowing all the test conditions and individual spray-ice properties.

In a paper by D.M. Masterson et al (1987) on the Cape Allison C-47 island, quality tests were performed to compare flooded and spray-ice properties. As shown in Figure 2.1.7, the materials are not significantly different for the testing techniques employed, but the range of values can be large.

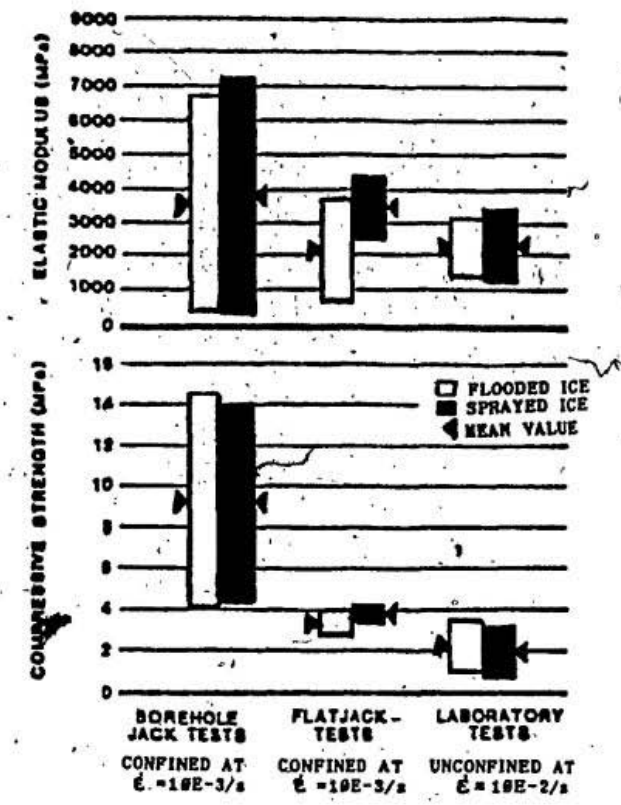

Figure 2.1.7

Ice Quality Tests on Spray and Flooded Ice
(Masterson et al, 1987)

II.1.6 Design Considerations using Spray-Ice

As mentioned previously, spray-ice can be used for many construction purposes including barriers, floating islands and grounded islands. In order to attain a perspective on the design concerns of structures using spray-ice, the issues pertinent to a grounded spray-ice island will be briefly outlined.

Several grounded ice islands have been constructed, but few have been actually used for exploratory drilling. Reasons for this are: the newness of the spray-ice technology, its somewhat limited applications and the decline in oil prices. During the feasibility studies, two cases are addressed: the practicality of constructing an island within the given time constraints and the stability of an ice island under lateral loading. Other important issues are the thermal stability (especially during spring breakup), the settlement of the pad, the rig stability and the cost of constructing and operating the island.

Construction can not commence until the ice sheet is stable so that supplies and equipment can be brought in on ice roads. It is also required to construct the island in a restricted time period in order to complete the exploratory drilling before the spring breakup. A typical construction schedule is shown on Figure 2.1.8.

The major forces acting on the ice island are lateral loads imposed by the ice sheet and the weight of the

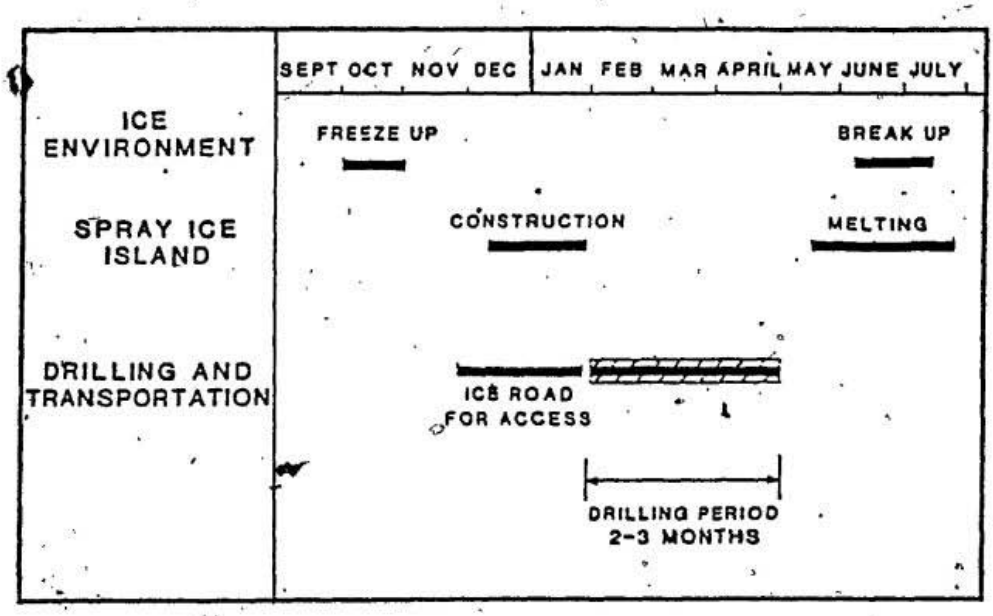

SPRAY ICE ISLANDS ALLOW CONSTRUCTION AND USE FOR EXPLORATION DRILLING IN ONE WINTER SEASON.

Figure 2.1.8

Construction Schedule
(Goff et al, 1986)

equipment on the island. The ice forces acting on the island in a landfast ice zone are usually described by discrete events, characterized by large, sudden, ice-field motions.

Failure can occur in several ways, due to the interaction of the spray-ice island and the ice sheet. There may be initial crushing of the ice sheet, local failure of the spray-ice at the edge of the island, or

global movement of the island due to shear failure between the island and the seabed or other critical sliding planes through the island. In the design of the island, it is important to ensure that the latter, global movement of the island, does not occur. Therefore, the island is designed with an outer sacrificial edge zone, or interaction fringe, which may be penetrated without affecting the actual island. It is anticipated that the outer fringe will fail in a passive wedge failure which will induce a bending moment in the natural ice sheet. This will cause the ice sheet to break into rubble and thus lower the lateral load on the island as the flexural strength of the ice sheet is much less than its crushing strength. The different modes of failure of the ice pad are shown in Figure 2.1.9.

II.1.7 Problems and Improvements in Spray-Ice Structure Design

Problems that can arise during spray-ice construction include the variability of the material, the loss of spray-ice due to adverse wind conditions, the creation of brine pools throughout construction, the fairly large settlements during the life time of the pad, the short construction period, the partial melting of the islands, the water depth limitations and the development of cracks in the island.

The problems associated with the formation of spray-ice

are difficult to correct. However various additives have

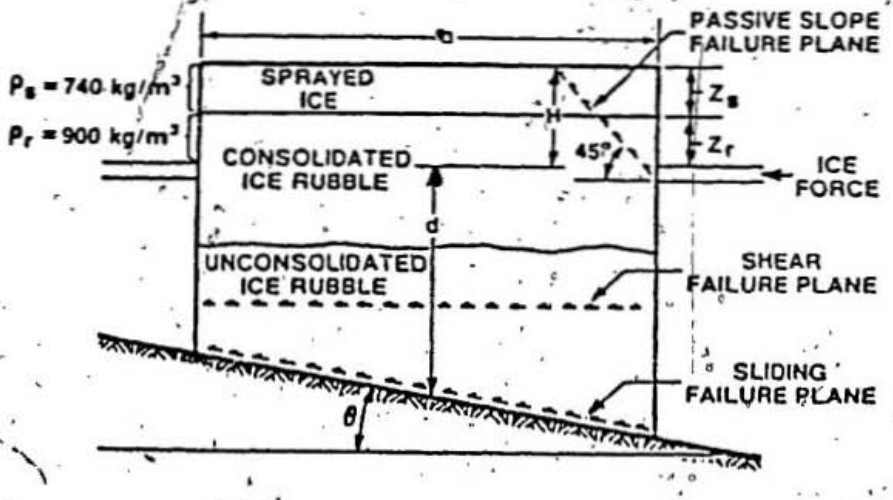

Figure 2.1.9

Failure Modes of Grounded Ice Islands (Kemp, 1984)

been tried to improve the characteristics of spray-ice during warm temperature construction (Pare et al, 1987). As much as 60 percent of the produced spray-ice is lost due to wind conditions (Kemp, 1984). This can be improved by locating several pumps and nozzles around the circumference of the proposed island. In this way only those nozzles in the correct orientation with respect to the wind are used, enhancing the production. Brine pools are usually formed when the temperature is not sufficiently low. Careful drainage procedures or additives might alleviate this

problem.

Settlement of spray-ice islands is significant. Settlement is caused by partial melting and consolidation. To reduce the settlement near the well, the area can be insulated or cooling units can be installed. An alternative to these measures is to shim up the drill area or to support the drill rig on piles set into the seabed. In most areas of the island the low regions can be simply built up by making more spray-ice.

Besides settlement through consolidation and creep, the island may settle due to partial melting. The island will melt from the top, sides or bottom. Melting from the top can be controlled by covering the island with a gravel pad or mats. Melting from the bottom is not a major concern because the sea water is usually near the freezing point and, in fact, the ice may actually grow. Melting on the sides of the island at the water line can, however, be a serious problem if the island is to be kept late into the spring. This melting may be reduced by: pumping colder bottom water up to the island perimeter, covering the side slopes of the island with a plastic or rubber sheet, or installing cooling tubes along the island perimeter.

It has been found that when the ice island grounds onto the seabed, cracks in the island often develop. To date, these cracks have been simply mended by using more spray-ice (Weaver et al, 1988).

The spray-ice island has so far been limited to shallow waters and to one season construction and utilization. However, as spray-ice technology advances it may be possible to overcome these limitations. Recently, spray-ice/rubble islands have been considered for water depths of up to 15 metres. As the water depth increases, however, the volume of ice required increases very quickly due to the larger island diameter required to keep the island pad above the water surface. It may be impractical to consider islands in deeper water because of the short construction season. Experiments are also being conducted in maintaining the ice islands over the summer season, although this would involve large expenditures.

II.1.8 Advantages and Future of Spray-Ice Technology

As previously indicated, spray-ice islands have low capital and operating costs, (approximately 50 percent of the cost for a similar concrete or gravel island). Due to the low bulk density of the material and the large diameter of the islands, the contact pressures are reduced and the islands can be built even on very weak soils with little preparation. The large diameters also provide ample space for equipment and supplies. The construction periods are relatively short. These structures are easily repaired and have low restoration costs, with minimal environmental damage. Spray-ice islands use local construction materials

and can be constructed without open water in a fairly wide range of water depths.

As exploration costs increase for the oil companies, it is likely that greater use will be made of proven spray-ice technology. We can anticipate spray-ice islands in deeper water. However, even though spray-ice has demonstrated acceptable strength characteristics, more work is needed to improve the quality and efficiency of spray-ice production and enhance the design quality.

II.2 Insitu and Laboratory Testing of Solid, Granular Ice and Snow

II.2.1 Introduction

A cursory look at what types of tests have been performed on snow and ice is presented in the following sections. Spray-ice cannot be described as either of these substances and since it is highly variable in itself, an overview of experimental results of similar material will aid in the understanding of the constitutive properties of spray-ice.

II.2.2 Field and Laboratory Tests on Solid and Snow Ice

A wide range of field and laboratory tests have been performed on solid and snow ice. Ice is a visco-elastic material with strain rate dependent strength and deformation properties. Tests have generally been carried out to examine the brittle behaviour of ice (fracture mechanics) or the ductile behavior (creep). The frictional characteristics, density, salinity and porosity to name a few are also critical to design criteria.

The field experiments which have been successfully employed in ice are: flatjack, borehole jack and pressuremeter test, cone penetrometer, plate bearing test, indentor and impact test and cantilever beam test. The length of time required to perform creep tests in the field

can cause many logistical problems. The pressuremeter has been used successfully for this purpose (Ladanyi et al, 1978(a)).

The plate bearing, flatjack, borehole jack and pressuremeter tests will give information on the bearing capacity and deformation of the ice. The cantilever beam test is generally performed on ice sheets and will provide information on the flexural strength of the ice. The indentor and impact tests are high to very high speed compressive strength tests.

Examples of insitu test results are illustrated below. Since flatjack, borehole jack and pressuremeter all operate on the same principle only pressuremeter tests will be examined. The pressuremeter is described in greater detail later, however two main types of tests have been performed in ice i.e. high speed crushing tests and stress-relaxation tests. During crushing tests it is possible to relate the shear resistance (Ty) derived from the pressuremeter curve to the uniaxial compressive strength of ice through an indentation coefficient (Michel, 1986). Also the shear resistance (Ty) and pressure limit (Py) were found to vary with ice type and with temperature. When tests are performed at varying strain rates encompassing the brittle to the ductile range for ice, stress-strain curves similar to those for uniaxial compression tests can be derived.

The pressuremeter is also useful in determining creep parameters for materials whose deformation follows a generalized power law such as ice (Ladanyi et al, 1978(b)). In a paper by Ladanyi et al, 1987 the flow creep theory was used to interpret data from tests. The stress relaxation test consists of inflating the pressuremeter probe in equally increasing volume steps and recording the pressure in the probe over a period of time for each volume level. The results are in the form of a set of relaxation curves. By applying the flow creep theory to these curves the strain in the ice can be summarized by:

$$\varepsilon_e = A \sigma_e^B t^C$$

where: A,B,C = derived constants
t = time
ε_e, σ_e = equivalent Von Mises strain and stress

Large scale cantilever beam tests have been used both in the laboratory and in the field to determine the flexural strength of ice. The test is conducted by cutting three edges of a cantilever beam out of the ice sheet; the beam is supported by its buoyancy in the water. A load is applied to the end of the beam while deflection is measured. The flexural strength is calculated by considering the beam on an elastic foundation. The ice can be assessed as either a homogeneous or nonhomogeneous material, depending on the influence of the temperature gradient over the thickness of the ice. Frederking et al (1978) evaluated an average strain modulus of 2.0 GPa and

flexural strength of 0.32 MPa for sea ice.

Impact tests can be illustrated by the impact hardness test devised by Pounder et al (1959). In this test a calibrated sphere is dropped from a standard height onto the ice. By measuring the depth of penetration, the impact compressive strength of the ice is determined according to:

$$\sigma = \frac{Wh}{\pi (A_o[x^2] - [x^3]/3)}$$

Where: σ = compressive strength
W = weight of sphere
h = height of drop
x = depth of penetration
A_o = radius of sphere

Lane (1979) reports measurements of 4550 kPa to 6200 kPa for this type of confined test.

A commonly used indentor test is the fracture toughness test on sea ice. The experimental set up is shown in Figure 2.2.1.

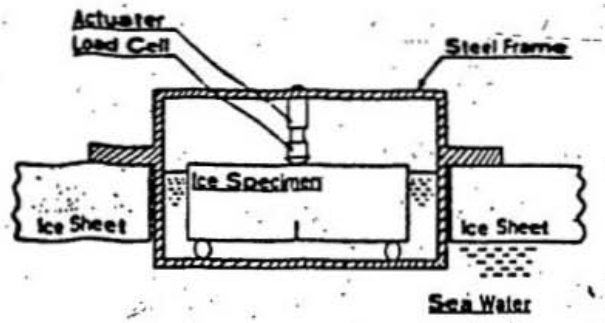

Figure 2.2.1

Experimental Setup for Fracture Toughness Test (Wrabe et al, 1980)

A notch is cut in the middle of the bottom of the ice specimen which is loaded to failure. The load is recorded with displacement and time. The fracture toughness (Klc) is a function of the geometry of the beam and the applied moment. Klc is shown to remain fairly constant at approximately 8 kg. $cm^{-1.5}$ until a rate of 10E-3 s^{-1} is attained when it decreases rapidly. Urabe et al (1979) also found that the scatter in fracture toughness values is very small when compared to other means of measuring fracture strength such as compressive tests.

A variety of laboratory tests have been employed to test solid ice. The most popular are probably the triaxial and uniaxial tests. These tests may be performed as a creep or fracture type tests. In the triaxial test, various confining pressures can be applied to the specimen. The uniaxial tensile strength of ice can also be determined using similar equipment.

Indentation and impact tests have also been performed in the laboratory. The indentor may be flat, spherical or the pyramid-shaped Vickers indentor. Impact tests have been performed using a steel ball or cylinder of various sizes. These tests are conducted on large blocks of ice. These types of tests were mentioned earlier in their application to insitu testing.

Flexural beam tests, shear tests and a variety of tension tests have also been performed on polycrystalline ice.

Laboratory tests have been conducted on what is known as snow ice (El Tahan et al, 1984). Snow ice is formed by collecting natural snow or artificial snow, sieving it to the desired grain size, placing and compacting it in a mold and flooding the mold with fresh water. The resulting frozen sample is called snow ice and is classified as T1 ice. It can be formed naturally when snow falls on top of river ice which subsequentially floods.

The uniaxial test was the first broadly accepted laboratory test to be performed on solid ice and much of the information on the mechanical properties of ice have been derived from this test. There are basically two types of tests; the creep test (constant stress), and the strength test (constant strain). Typical curves from these tests are shown in Figures 2.2.2 and 2.2.3.

The strain versus time curve is divided into four parts; the instantaneous elastic strain, the decelerating primary creep, the transitional secondary creep and the accelerating tertiary creep. During the secondary creep the deceleration in strain rate reaches zero and then reverses sign, it is sometimes termed "steady state creep". During each of these stages different internal mechanisms are acting on the ice as a result of the deformation such as strain hardening or softening and recrystallization.

The stress versus strain curve can be broken down into three stages the initial linear increase in stress with

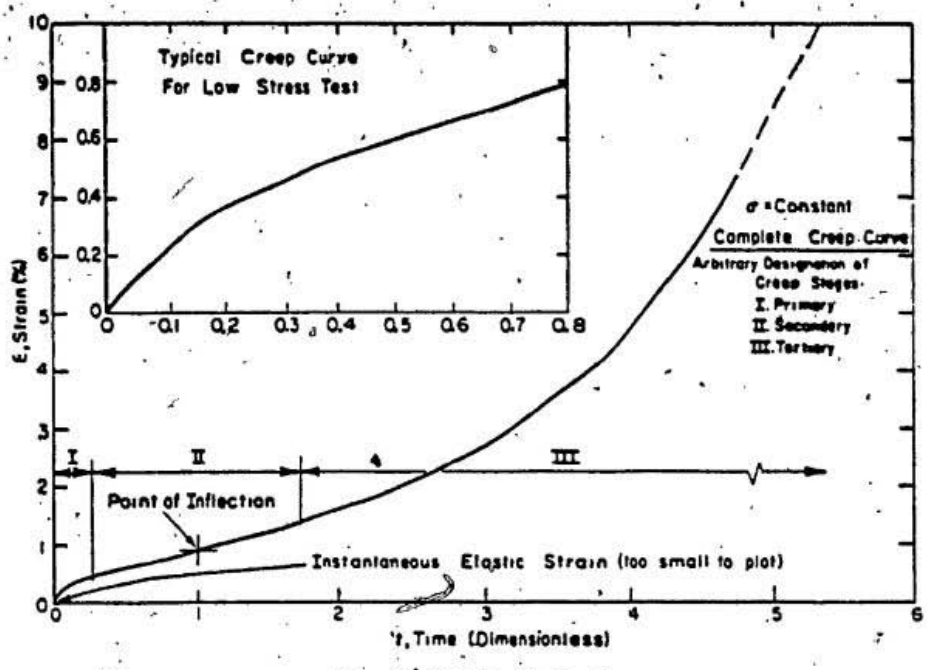

Figure 2.2.2
Creep Curve for a Constant Stress Test on Ice
(Mellor, 1979)

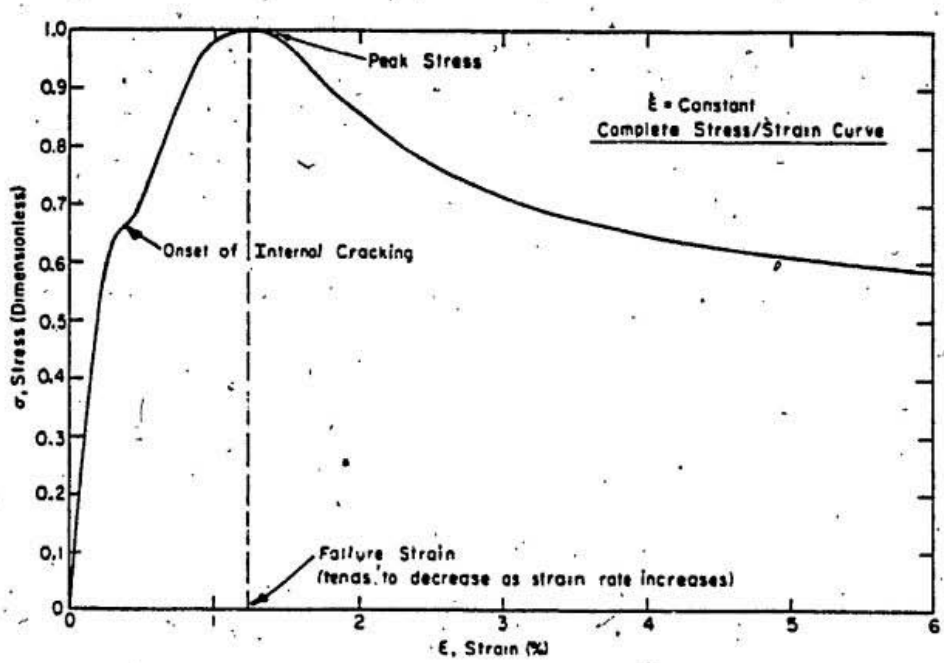

Figure 2.2.3
Stress-Strain Curve for Constant Strain Test (Moderate Rate)
(Mellor, 1979)

strain, from which Young's Modulus can be derived, a peak or maximum stress and the "failure strain", and a non-linear decrease in stress with strain during which the stress approaches a constant value.

To describe the creep curves, two theories are often combined: the 'flow law for ice' and the Arrhenius equation. The flow law describes the creep curve by the equation:

$$\dot{\varepsilon}_{min} = A\sigma^n$$

where: $\dot{\varepsilon}_{min}$ is determined from the inflection point on the creep curve.
A = temperature dependent constant
σ = level of stress during the test
n = stress dependent constant

Arrhenius' equation describes the effect of temperature on the creep of ice with the equation:

$$\dot{\varepsilon} = A\, e^{(-Q/RT)}$$

where: Q = activation energy
R = gas constant
T = absolute temperature

Uniaxial strength tests have also been performed on T1 or snow ice. Examples are shown in Figure 2.2.4. The strain rate has, undoubtedly, a strong effect on ice strength.

Figure 2.2.5 shows the peak strength of the snow ice as a function of the logarithm of the strain rate. This plot is similar in shape to that of polycrystalline ice.

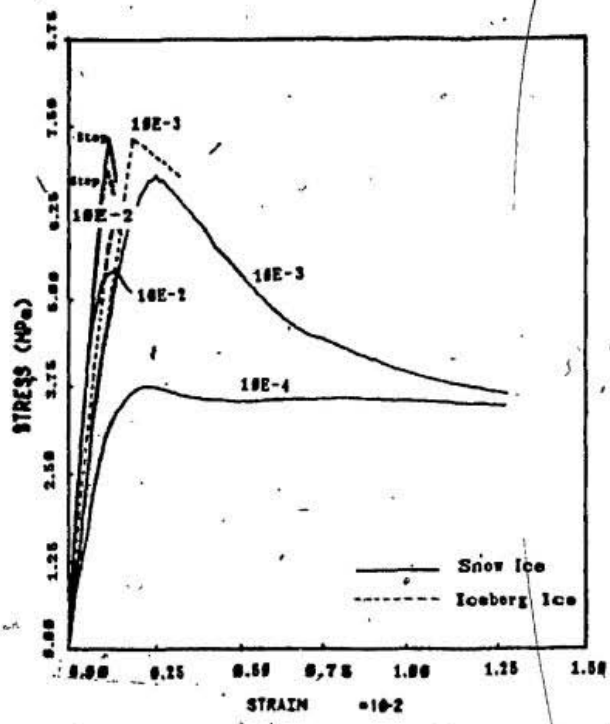

Figure 2.2.4

Stress-Strain Curves for Snow Ice and Iceberg Ice at Different Strain Rates
(El-Tahan et al, 1984)

More recently, the triaxial test has become the most widespread laboratory strength test for ice, with the uniaxial test being performed in field laboratory situations or where triaxial equipment is not available. Triaxial creep or strength tests have the same general shape as the uniaxial curves described earlier, but incorporate confining pressure. Also, the triaxial equipment tends to have greater stiffness and be more accurate.

An example of how confining pressure affects the stress-strain curve is depicted in Figure 2.2.6. It can be

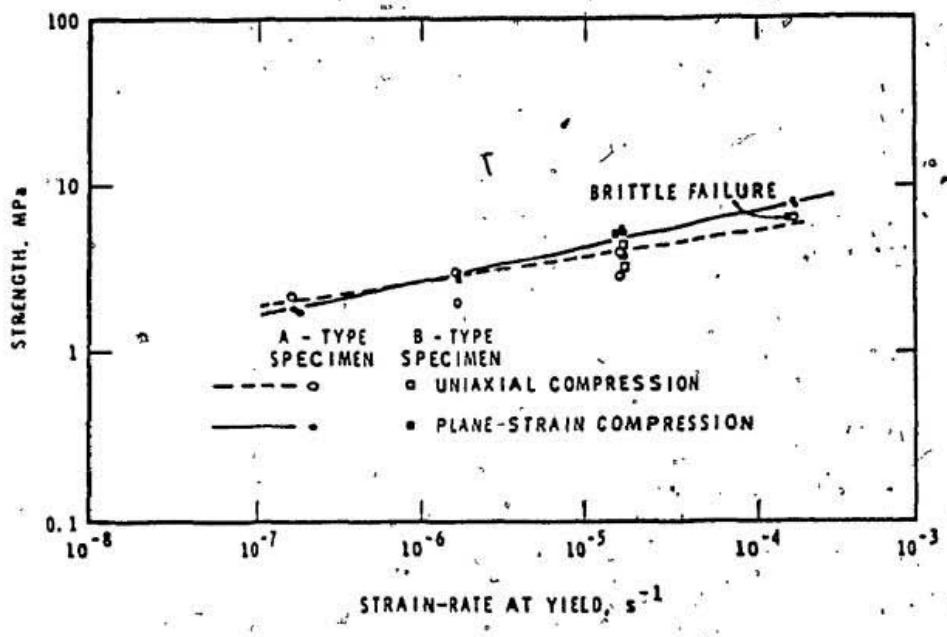

Figure 2.2.5

Strain Rate Dependence of Strength for T1, Granular Snow Ice (Frederking, 1977)

seen that applying a confining pressure suppresses brittle failure and causes an increase in the maximum stress or the yield stress, while at very high confining pressures the yield stress decreases. In Figure 2.2.7 the dependence of yield stress on confining pressure and strain rate is illustrated. It appears that as the strain rate for the test is increased, the effect of the confining pressure becomes more pronounced.

Hausler (1981) performed work recently on the multiaxial compressive strength of ice. During these trials a cubical specimen was placed in a loading frame

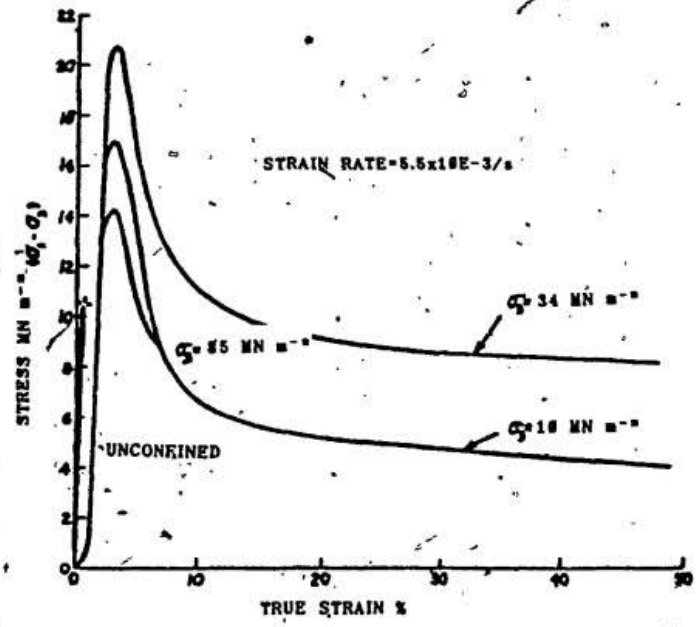

Figure 2.2.6
Stress-Strain Curves for Polycrystalline Ice for Various Confining Pressures
(Jones, 1982)

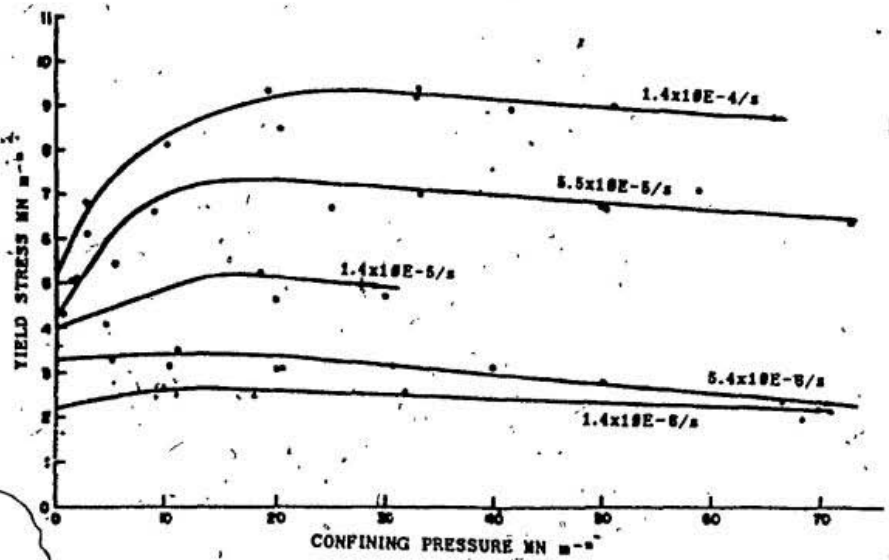

Figure 2.2.7
Maximum Stress vs. Confining Pressure at Different Strain Rates (Jones, 1982)

which allowed the ratio of the three stresses applied to the sample to remain constant throughout the test. From this series of tests it was found that the biaxial strength of saline ice is several times the uniaxial strength, depending on the direction of ice crystal growth with respect to the major principal stress. For isotropic snow ice the strength increase was only 25 percent. From these tests it was also possible to project the failure surface for saline ice in three dimensions.

Lane (1979) described a number of laboratory strength experiments on ice. He reported on beam tests, tensile tests and shear tests among others. The beam test in the laboratory is very similar to the in situ test described earlier.

Three types of tensile tests have been performed in the laboratory on solid ice; the ring test, the Brazil test and the tension test. The ring test is conducted on a solid cylinder of ice from which a hole is drilled through the long axis. The sample is loaded compressively across its diameter until failure. The tensile strength is derived from the following formula:

$$\sigma_T = \frac{PC}{\pi L_o R_o}$$

where: σ_T = ultimate tensile strength
P = applied load
C = concentration factor, $f(R_i/R_o)$
L_o = length of cylinder
R_o = outer ring radius
R_i = inner ring radius

This test should be performed at a strain rate which will ensure brittle failure, as the test interpretation assumes an elastic material. The tensile strength for solid ice is in the range of 300 to 3000 kPa.

The Brazil test is similar to the ring test except no hole is drilled in the center of the sample. The strength formula also resembles that outlined above and leads to comparable strength values.

The tension test is conducted in a standard tensile test frame on a dumbbell-shaped sample, or a cylindrical-shaped sample which have ends that are in some manner fixed to end caps on the test frame. The tensile strength is computed from the formula:

$$\sigma_u = P / A$$

where: σ_u = ultimate tensile strength
P = applied load
A = cross-sectional area

Peyton (1962) found sea ice to have tensile strengths in the range of 100 to 2500 kPa.

Single and double shear tests have been performed on solid ice. The single shear apparatus is made up of two aligned plates which are placed on either side of the sample. When a compressive load is applied to the plates the sample is sheared. For the double shear test a cylindrical sample is fixed at either end by holders while a center section is pressed out along two parallel planes. The value of the shear resistance of sea ice ranges from 300

to 1300 kPa (Pounder et al, 1959) and 950 to 3300 kPa (Butkovitch, 1962) respectively.

II.2.3 Crushed and Granular Ice, Laboratory Tests

Various laboratory tests have been completed on crushed, granular or broken ice, including shearbox, triaxial and consolidation tests, as well as kinematic and piling tests. For all of these tests the physical properties of the ice (eg. grain size distribution, porosity, amount of slush, salinity, etc.) have a major effect on results and must be thoroughly stated. The name given to the ice types is as stated by the investigator.

In a paper entitled "Shear Box Tests on Broken Ice", Wong et al (1987), concluded that the shear stress - displacement relationship is nonlinear and the normalized shear-displacement curve was hyperbolic. No peak or ultimate shear resistance was observed so that the use of a Mohr-Coulomb failure criterion was not satisfactory. These authors also suggest that the mechanical behaviors of the broken ice is not significantly affected by particle size or displacement rate. The material tested was fairly uniform, unconsolidated, made from ice cubes of two sizes; either less than 9.5 or less than 4.75 mm in diameter. In addition, the presence of brine reduces the shearing resistance and higher normal loads cause an increase in shear strength.

Gale et al (1986) also performed large scale shear box

tests on broken ice. The model ice particles were less than 25mm in diameter. In this case the results were presented using a linear Mohr-Coulomb envelope as shown in Figure 2.2.8. The ice was found to have an angle of internal friction of 36 to 45 degrees and no cohesion. Again, no maximum shear stress was realized during the tests and the shear stress increased with increasing normal stress.

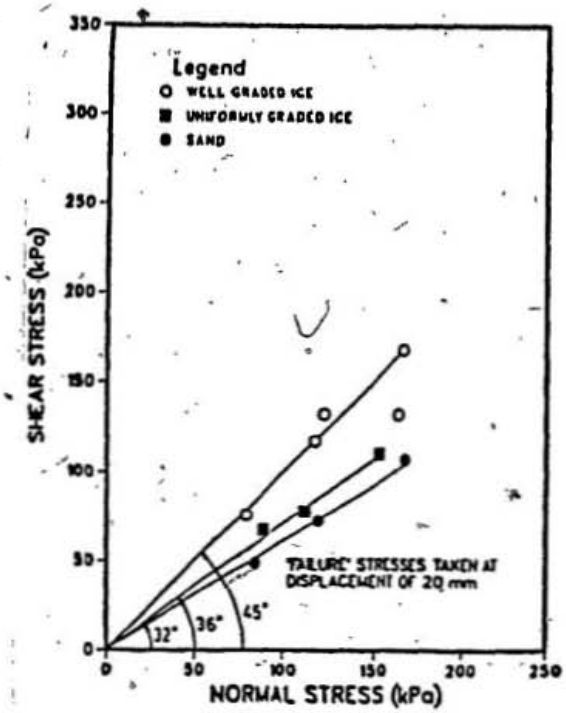

Figure 2.2.8

Mohr Coulomb Envelope on Broken Ice
(Gale et al, 1986)

A series of oedometer tests also completed by Gale on samples of varying gradation, reveals the high

compressibility of the material and the increasing volumetric strain with decreasing grain size as shown in Figure 2.2.9.

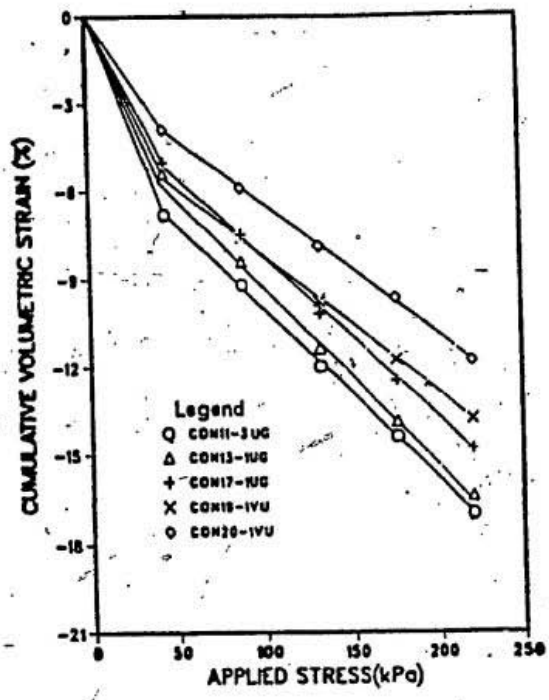

Figure 2.2.9

Oedometer Test on Broken Ice
(Gale et al, 1986)

A second paper by Gale et al (1987) describes the results of triaxial compression tests conducted on cohesionless broken ice in comparison to loose sand. The ice was less than 9mm in diameter and was tested at -2.5 degrees C and at a rate of 0.05 cm/min. The stress-strain curves (Figure 2.2.10) show a distinctive bilinear slope.

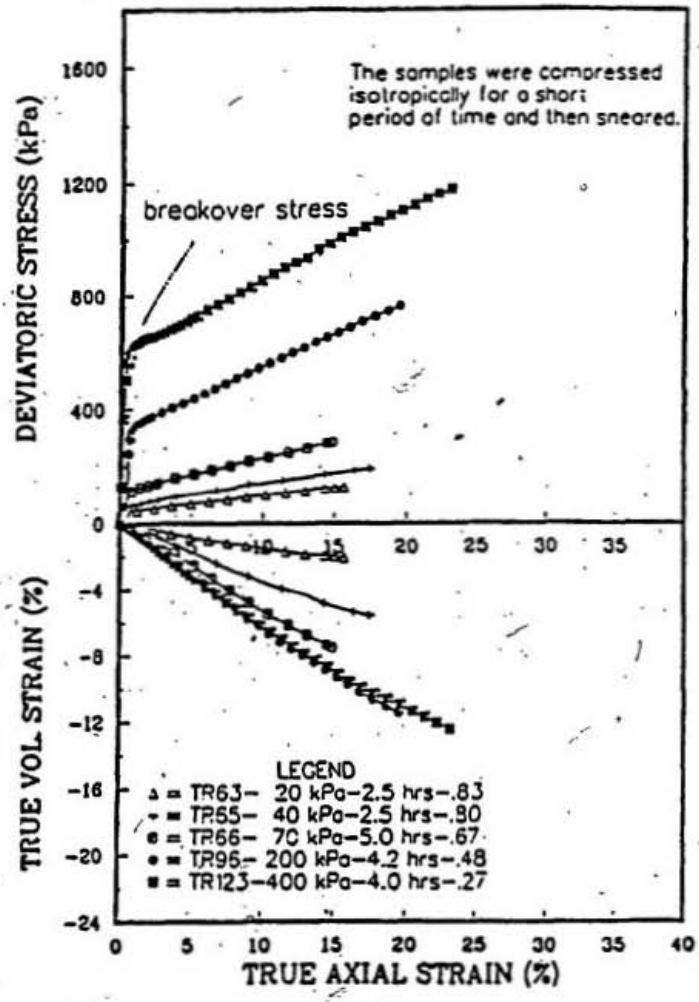

Figure 2.2.10

Triaxial Compression Test on Broken Ice
(Gale et al, 1986)

Again the ice is very compressible and exhibits no limiting average shear stress. The breakover stress was at approximately 1 percent strain. It was found that an increase in the loading prior to shear or an increase in the

confining pressure changed the stress-strain curve by augmenting the breakover stress, and in the case of prior loading flattening the second portion of the curve.

In the work performed by Keinonen et al (1978) the structure of an ice ridge was modelled. This was simulated by analyzing the behavior of an ice-block mass during shear, compression, kinematic and piling tests. The model ice was roughly cubic (mean block thickness of 23 mm), was well-graded, saturated and contained slush ice.

All of the tests were conducted in a test box measuring 1.0 metre, by 0.3 metre, by 0.3 metres. The kinematic tests were used to model a ship's keel moving through an ice-block mass. This was performed by pushing a plate, inclined at varying angles, through the ice. The piling tests determined the maximum angle that can be built up above and below the water surface; they were 38.5 and 32.9 degrees respectively. The compression and shear tests were similar to those previously described but were performed under full saturation. Two possible sources of error in this work were the small test box and the deterioration of the ice during the course of the experiment.

II.2.3 Field and Laboratory Tests on Snow

According to Mellor (1966), "Snow is considered to be a non-linear viscoelastic material. Its rheological behavior is similar to that of polycrystalline ice except for its

high compressibility". When looking at long term conditions the viscosity and creep processes of snow become important.

The field tests that have been conducted on snow were originally performed to understand the risk of avalanches or snow slides. The major test used was the Rammsonde cone penetrometer. The military became interested in snow as a material as they ventured into the arctic (Haas et al, 1985), then oil industry conducted several studies on snow. Other field tests which have been completed are the CBR penetrometer and the plate bearing test.

The Rammsonde cone penetrometer provides what is known as ram hardness measurements. The instrument consists of a penetrometer with a cone tip; rods are attached to the penetrometer and it is hammered into the snow. The hammer is dropped from a given height much like the standard penetration test for soil and the number of 'blows' are counted. An example of a ram hardness curve for aging snow is shown in Figure 2.2.11..

In a paper by Haas et al (1985), the CBR (California Bearing Ratio) test has been described along with results on processed and compacted snow. This test which may be performed both in the field and laboratory was adapted initially from highway design and then from the design of U.S. military airfields around the time of World War II. Since that time it has been employed periodically during the

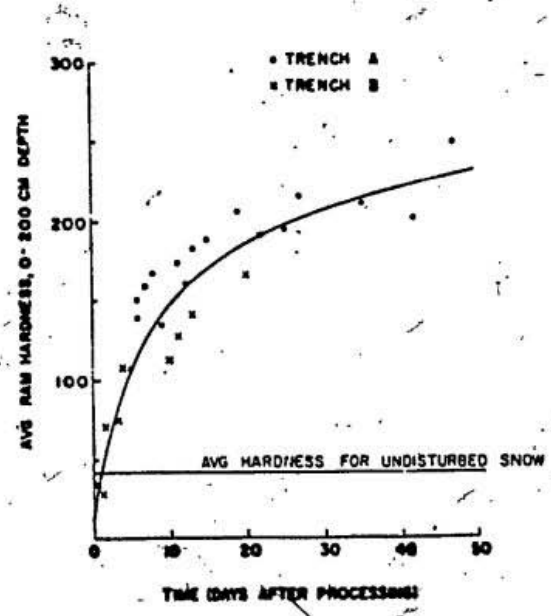

Figure 2.2.11

Ram Hardness vs Age for Processed Snow
(Butkovich, 1962)

construction of snow roads and runways and for evaluating the bearing capacity of processed snow.

The test makes use of a cylindrical penetrometer with a flat end, which is forced into the soil or snow at a constant rate of 1.27 mm/min to a depth of 12.7 mm. The required load in psi for 2.54 mm penetration is divided by 1000 psi to attain the CBR ratio. A CBR ratio equal to 100 relates to a high quality crushed rock. In order to perform the test in the laboratory the test material is initially placed in a mold.

This test has been used to examine the sintering and

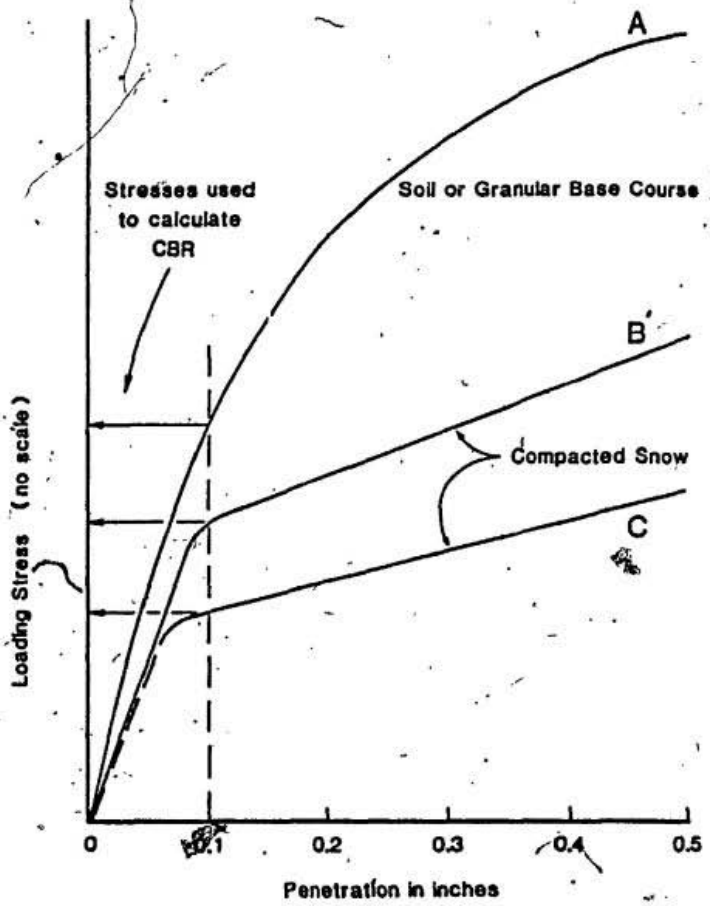

Figure 2.2.12

Sample CBR Loading Curves
(Haas et al, 1985)

age hardening processes of processed snow. As expected the higher the density of the snow the greater the CBR ratio. In addition if the snow was worked and disaggregated, the CBR ratio increased. The stress-strain curve for the tests on compacted snow and soil are shown in Figure 2.2.12. The distinctive bilinear relationship of snow is very different from soil and indicates a more brittle type failure. The

inflection point for all tests occurred at somewhat less than 0.1 inches.

The plate bearing test has also been performed on snow in various forms. In Figure 2.2.13 the non-dimensional stress distribution within the snow from field tests is compared to Boussinesq analysis for soils. The majority of the stress profiles fall within the Boussinesq envelope for soils with the notable exception of Stehle's data which may not be applicable due to the low applied load.

An extensive amount of data has been collected on snow through laboratory testing. These include unconfined compressive tests, creep tests, tensile tests, shear tests and torsional shear tests. Important factors to consider during these tests are snow density and grain size, snow age and test temperature.

The stress-strain relationship of snow under uniaxial compression has been described by Landauer (1955). His work shows that initially the stresses increase quickly at a continuously decreasing rate, then there is a region where the stress rate decreases abruptly and eventually an equilibrium stress is attained. It is assumed that the stresses increase due to sample compression and are reduced by relaxation, with strain hardening also being an important factor.

Other compression tests have been performed to

delineate the effect snow age and density have on unconfined compressive strength (Butkovich, 1962; Jellinek, 1957; SIPRE Report 18, 1956). Generally, the compressive

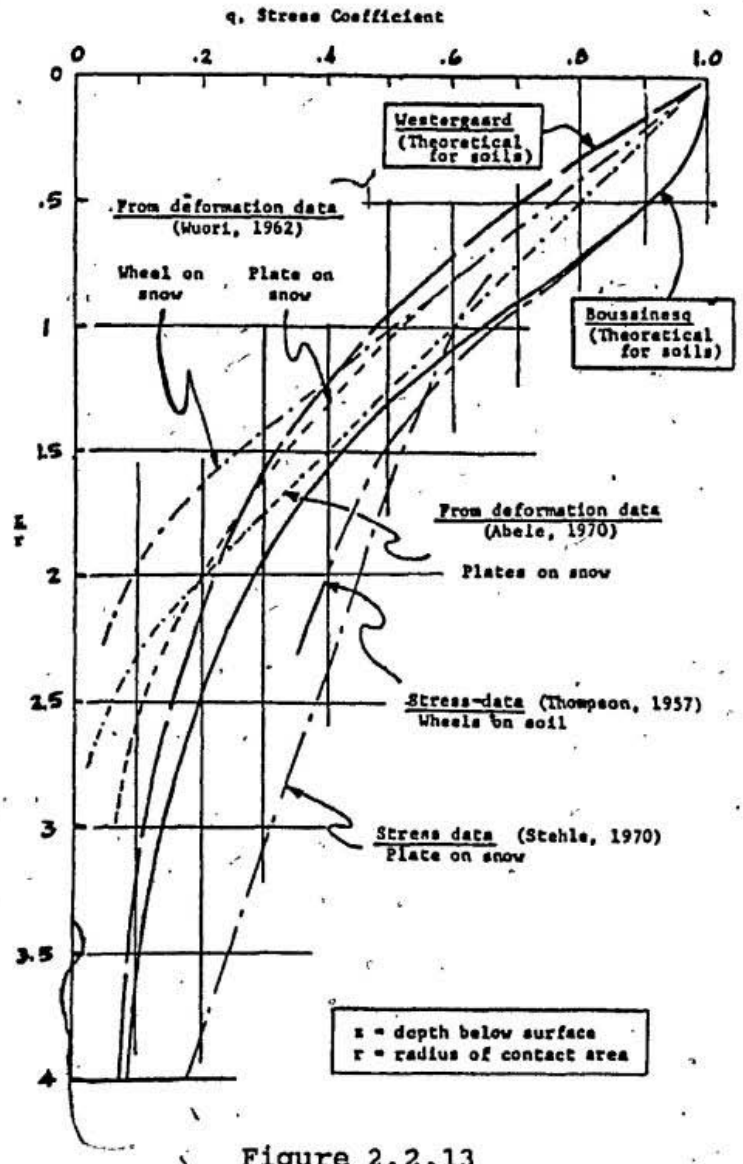

Figure 2.2.13

Stress Distribution in Snow
(Wuori, 1973)

strength of processed snow increases with age and approaches a limit close to the strength of naturally compacted snow. Tests performed on the crushing strength of high density snow predict a linear relationship between density and strength.

In the creep curves studied by Landauer (1955) and Butkovich (1962), it was found that the slope of the curve decreased with time but this did not imply a strong linear term. The deformation that did occur was linearly dependent on stress and void ratio.

In the SIPRE Report #18 (1956), several other strength tests have been described and carried out. The tensile strength of snow has been calculated from the centrifugal and ring test. The centrifugal test is consists of a cylindrical container in which the specimen is placed and secured at the base. The cylinder is rotated at a speed which will fail the sample. The second type of test, the ring test, was previously described in this report. The tensile strength is derived by assuming that the snow is an elastic, brittle material. This assumption is accepted if the test is conducted very rapidly on a high density snow. Of the tests conducted a mean tensile value of 1117 kPa was attained at an average density of 0.673 g/cm3. A plot of tensile strength versus density shows a sharp, almost linear increase in strength with density (Figure 2.2.14).

Cylindrical samples have been tested in double shear

and torsional shear. The double shear apparatus at times caused the sample to fail in the center in a tensile type failure. Generally the shear strength increased with density and applied confining pressure (Figure 2.2.15). The torsional shear test could be employed only on samples with higher densities. The torsional shear values were lower than that of normal shear with the samples failing in a 45 degree helical break, typical of a brittle material.

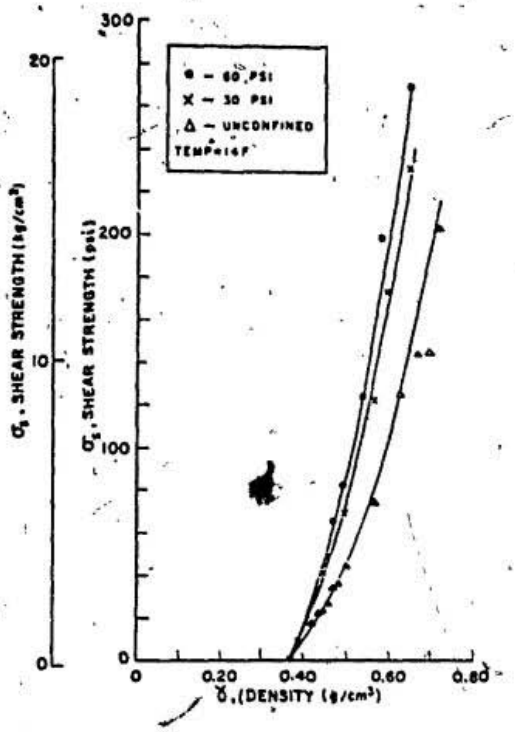

Figure 2.2.14

Shear Strength vs. Density

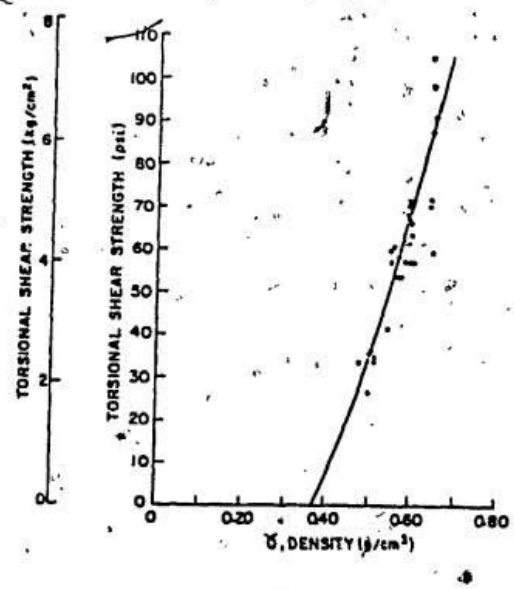

Figure 2.2.15

Torsional Shear vs. Density

(SIPRE Report #18, 1956)

II.3 Pressuremeter Testing

II.3.1 Introduction and History

The pressuremeter has gained wide-spread use in Europe and more recently in North America due not only to its versatility in all types of soil, permafrost, rock and ice but also because the results can be used directly for estimating bearing capacity and settlement (Shields et al, 1987).

In "The Pressuremeter and Foundation Engineering", Baguelin et al, 1978, fundamental information and history on the pressuremeter can be found. The pressuremeter test is an in-situ load test, in which the radial expansion of a probe in a borehole provides the relationship between pressure and deformation of the soil. Analysis of the pressuremeter curve allows for the estimation of mechanical soil properties, bearing capacity and settlement.

The pressuremeter test has many advantages over other types of in-situ or laboratory testing. Some of the advantages are outlined below.

-the pressuremeter is a simple device, which is easy to operate and calibrate.

-the pressuremeter test applies an axisymetric stress field in the ground similar to that of a foundation.

-the test measures both limit resistance and deformation properties of the soil.

-the test involves a large volume of soil.

-the test results are used directly to predict foundation performance.

-the test method has been standardized, and a considerable amount of published results are available.

The pressuremeter has evolved considerably from the three-cell probe Louis Menard constructed in 1954. Menard's probe had a central measuring cell which was water-filled and two gas-filled guard cells which were intended to reduce the end effects of the central unit. After this probe had been in use for several years it became apparent that disturbance of the borehole walls had considerable effect on the pressuremeter results. During the 1960's the self-boring pressuremeter (SBP) was developed. This instrument greatly reduced the unloading and reloading effects of Menard's probe. The SBP is used mostly in fine-grained materials. Also around this period, a one-celled water-filled pressuremeter was constructed, this somewhat simpler device has been used extensively in rock mechanics.

Not only has the pressuremeter evolved as a piece of equipment but also the analysis of the pressuremeter curve and the types of tests have under gone changes over the years. Menard made use of Lame's elastic theory and Bishop, Hill and Mott's (1945) elastic-plastic theory for metals to model the soils reaction. In his analysis of the

pressuremeter curve, the pressure limit was related to the yield strength of the material. He also tried to apply Tresca's and Mohr-Coulomb's failure criterion. From a number of field load tests Menard was able to construct a series of design equations and charts for the pressuremeter.

Over the years attempts have been made to determine the cohesion (c) and the angle of internal friction (ϕ) of the soil from the pressuremeter results and thus determine the shear strength of the soil. Progress was made when Ladanyi (1963), considered the volume change of the soil due to compression and dilantancy. In 1972, Baguelin, Jezequel and Lame determined the shearing resistance (C_u) of the soil. It was found that the volume change of the soil and the pore-water pressures were both important.

More recently, many creep and relaxation tests have been performed on soils to evaluate long-term effects of loading. The use of computers has also made possible the refinement of tests result interpretation. In the past decade a considerable amount of work has been concentrated on the pressuremeter testing of permafrost and ice.

II.3.2 Description of Apparatus

There are several types of pressuremeters available on the market today. They basically all consist of three parts: the probe, the control unit and the tubing. When inflated under pressure the probe expands in the borehole.

It can be single or three celled.

The tubing allows the fluid, either compressed air or a liquid, to connect the probe to the control unit. From the control unit the amount of fluid and the pressure of the fluid in the probe and guard cell if present are monitored. The liquid may be injected into the probe by a hydraulic actuator which also digitalize the volume.

Further advances have been made in the equipment including different versions of a self-boring pressuremeter that have the advantage of reduced soil disturbance. Another type of equipment is based on the measurement of the diameter of the borehole using LVDT's (linear variable differential transducers). The equipment used in this work, called the Texam pressuremeter, is a single-celled unit and makes use of a mechanical actuator in lieu of the compressed air to apply the fluid pressure.

II.3.3 Operation and Calibration of Pressuremeter

Prior to using the pressuremeter in the field it has to be saturated and calibrated. The operation, calibration and test performance of the Texam pressuremeter is derived from concepts common to several types of pressuremeters. The pressuremeter is initially assembled as shown in Figure 2.3.1. To ensure meaningful results all air must be removed from the probe, lines and gauges.

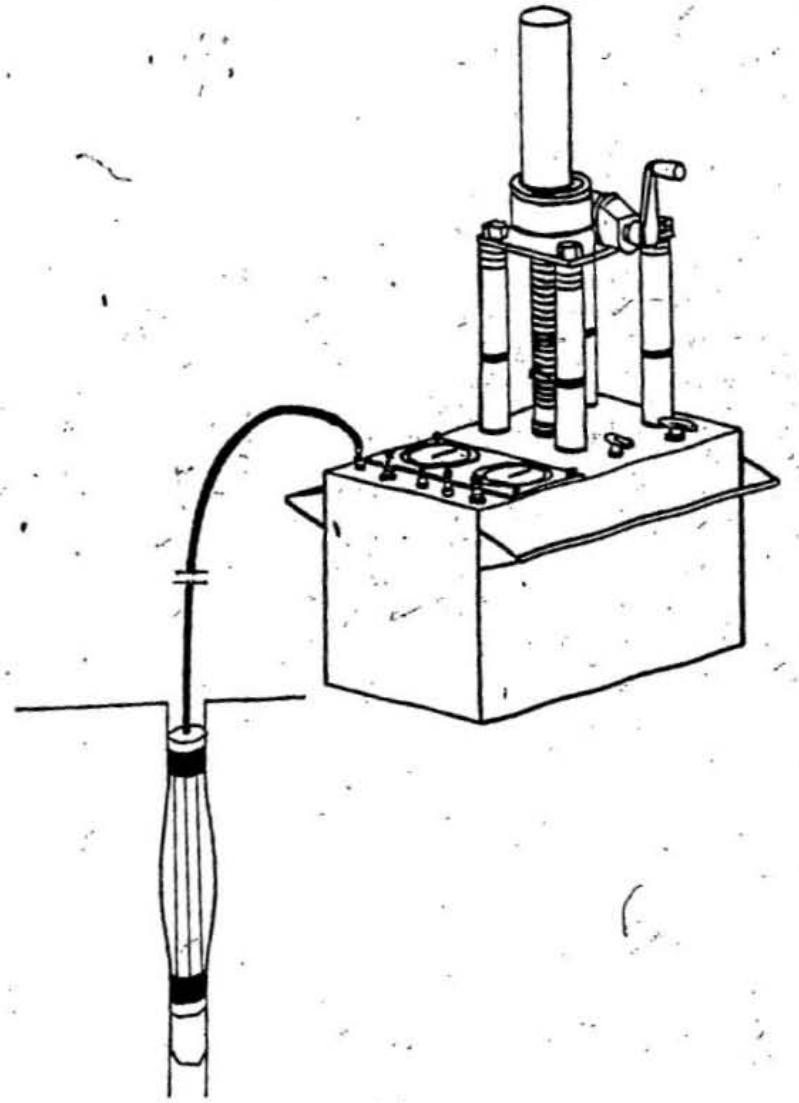

Figure 2.3.1

The Roctest Pressuremeter
(Sols Soils, 1975)

The fluid is first drawn into the actuator, then into all the lines. The fluid is 60 percent ethylene glycol and 40 percent water; which should be stable to -64 degrees C. The lines are checked to ensure they are bubble free. Once the probe and tubing is attached to the control box, they are filled and the entire system is saturated.

The pressuremeter must be calibrated at the temperature of operation to take into account two corrections. (1) The pressure that is applied to the soil or ice is less than that measured in the probe due to the resistance of the rubber membrane. (2) The volume of fluid in the probe is less than that measured from the reservoir because of the expansion of the plastic tubing and compression of the membrane and the fluid.

To perform a correction for membrane resistance the probe is placed at the level of the pressure gauges and inflated in steps of constant volume, while recording pressure. After the maximum volume is reached the probe is deflated. The pressure readings from this curve must be subtracted from the measured test pressures at the corresponding volumes.

To perform a volume correction the pressuremeter and probe are first saturated. The probe is then placed in a rigid steel tube. The pressure is increased in steps and the volume is recorded after stabilization. When the pressure reaches 10,000 kPa the test is stopped and the

fluid is removed from the probe. A curve of pressure versus volume shows that once the membrane touches the sides of the casing the pressure very quickly increases with the volume.

II.3.4 Performing a Test

The first step in conducting a test is to drill a borehole in the soil, permafrost or ice. The borehole diameter should be as close to the probe diameter as possible. The borehole walls should ideally be smooth and without ridges, the surrounding material being undisturbed and the hole vertical. Various drilling methods can be used as long as they meet the above constraints. The self-boring pressuremeter has the advantage that the hole size is correct for the probe and there is little material disturbance.

Once the hole is made the probe should be quickly lowered into place thus limiting the expansion of the soil. Time is then allowed for thermal stabilization of the probe in ice type materials.

There are basically two types of pressuremeter tests; the stress-controlled test and the strain-controlled test. In the stress-controlled test the pressure is quickly increased to a predetermined level and maintained at that pressure for a period of two minutes for a short-term test, after which as volume measurement is taken. The pressure

is then increased to the next level. Ten such steps are completed or to the maximum volume of the probe. If an estimate of the pressure limit can be obtained before the test, it is convenient to divide this pressure into ten increments. Plots of the pressures and final volumes delineates the uncorrected pressuremeter curve.

The second type of test is strain-controlled. In this test the volume of the probe is increased in 20 equal increments to the probe's capacity (1200 cc for the Texam pressuremeter). Two minutes after each volume increase the pressure of the fluid is noted. Once again pressure versus volume curves are plotted. In order to test the material over its elastic range a cycled test may be used. After a test is completed the fluid is pumped back into the reservoir so that the probe can be removed from the borehole.

The stress-controlled test can also be adopted to perform creep tests on a material. In this test the pressure is held for much longer periods of time while volume measurements are taken, this test can be single or multi-staged. Relaxation tests can also be used to determine creep characteristics of the material. During these tests the surrounding material is loaded and unloaded by removing fluid from the probe.

The correction of the raw pressuremeter curves is completed as follows. First, the volume readings are

reduced by the volume correction (from the volume calibration curve). Then the corrected volume is entered into the pressure calibration curve. The membrane resistance derived from this plot is subtracted from the test pressure. The procedure is simplified by deriving equations for the calibration curves and using a simple calculator program.

II.3.5 Interpretation of Test Results

The corrected pressuremeter curve is ordinarily divided in three distinct sections as shown in Figure 2.3.2. The initial portion of the curve corresponds to the expansion of the probe required to restore the pressure to that prevailing in the ground before drilling. From this information the initial volume of the cavity can be established. The curve then approaches a straight line portion. The pressuremeter modulus is determined from this pseudo-elastic phase. The end of the straight line segment is designated by the accelerated pressure increase. As the material being tested begins to creep the curve bends until it approaches an asymptote with the pressure. The pressure limit is defined as either the pressure at which the initial volume of the cavity is doubled or the asymptote pressure.

The net pressure limit (pl) is the pressure limit (pL) minus the horizontal pressure at rest of the material (po) (ie. pl = pL-po).

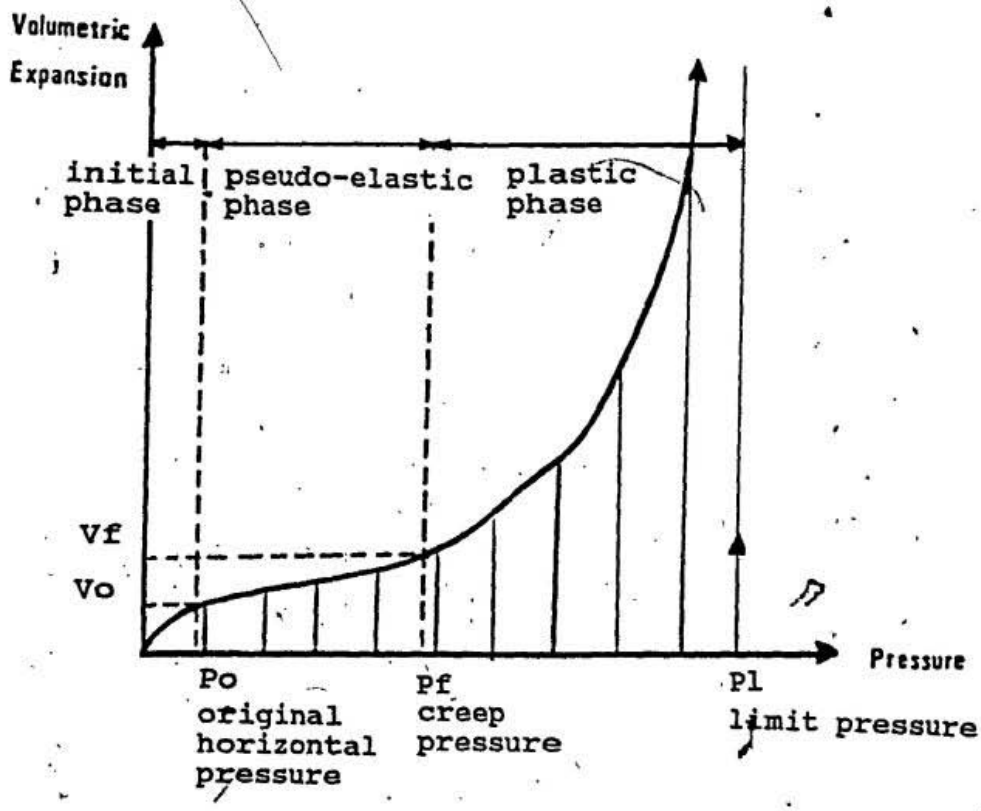

Figure 2.3.2

Corrected Pressuremeter Curve
(Sols Soils, 1975)

The pressuremeter modulus Em is derived from the radial expansion of a cylindrical cavity in an infinite elastic medium. After Lame $Gm = Vm\ \Delta P/\Delta V$

Gm: shear modulus
ΔP: pf - po
ΔV: vf - vo
Vc: volume of cavity

$$Vm = (vf + vo)/2 + Vc$$

or $Gm = Em / [2(1 + \nu)]$

where ν = Poisson's ratio (0.33 to 0.5)
Em: pressuremeter modulus

assuming $\nu = 0.33$

$$Em = 2.66 \left[Vc + \frac{(vf + vo)}{2 (vf - vo)}\right] [(pf - po)]$$

The preceding interpretation is an acceptable work frame for short-term tests; creep and relaxation tests will be discussed in more detail in the following section.

The shear strength formulation was derived for the case of total stresses for the elastic and plastic zones by Stordal et al (1985) and are as follows.

$$\Delta P / Su = \ln (e_v G/Su) + 1$$

$$R / ri = (ev\ G/Su)^{-0.5}$$

where ev: volumetric expansion
ri: initial cavity radius
Su: undrained shear strength
R: radius of plastic zone limit

The stress-strain curve as plotted from pressuremeter results requires values of $\sigma_1 - \sigma_3$ (principal stress difference) and γ_i (shear strain). Ladanyi et al (1978(b)) provides these values as follows:

$$\sigma_1 - \sigma_3 = 2(Pc,i - Pc,i+1) / [\ln(\Delta V/V)i - \ln(\Delta V/V)i+1]$$

where Pc: corrected pressure

$V = Vo + \Delta V$

i, i+1: two neighboring points on the true pressuremeter curve.

$$\gamma_{i,i+1} = 0.5 [(\Delta V/V)i + (\Delta V/V)i+1]$$

The average plane-strain compressive strength (Qps) can be calculated from the formula (Ladanyi, 1978 (b)).

$$Qps = 2\ Pias\ /\ [1 - \ln(2e_f)]$$

where Pias: ultimate asymptotic pressure, from extending $\Delta V/V = 1$ in a semi-log plot of the pressuremeter curve.

e_f: average failure strain in compression

II.3.6 Pressuremeter Theory

It is of interest when analyzing pressuremeter results to understand the basics of the theory behind the pressuremeter. Two frequently used methods of interpretation are based on theories by Gibson et al (1961) and Menard (1957) which consider an ideally elastic perfectly plastic material. The following work was derived by Ladanyi (1972) and combines the original Gibson theory with a strain-displacement relationship (Ladanyi, 1961, 1963). This simple presssuremeter curve evaluation method makes use of an arbitrary nonlinear soil behaviour.

In the following description the case for a saturated clay will be detailed. Although spray-ice does not react exactly like this material, it will provide a basis for understanding the pressuremeter theory.

The pressuremeter can be considered a cylindrical cavity in an infinite medium expanding from a radius of zero. The state of stress and strain around the cavity is obtained by

integrating the equilibrium differential equation, and assuming cylindrical symmetry with no body forces.

$$d\sigma_r/dr + (\sigma_r - \sigma_\theta)/r = 0 \qquad (1)$$

where: σ_r and σ_θ are principal stresses in the radial and circumferential directions.

r is the radius from the centerline of the cavity.

In the field of metal plasticity the solution of the problem of an expanding thick-walled cylinder can be solved approximately for any given stress-strain law for the material. This is done by assuming the cylinder consists of many thin concentric cylinders, each complying to a common stress-strain law. Assuming a constant volume, the average strain in each cylinder can be directly related to the expansion of the borehole. The complete pressure versus volume curve can be derived by numerical integration of this method. Considering the medium is composed of cylinders, the mobilized undrained, plane-strain compressive strength can be expressed by:

$$q_{i,i+1} = (\sigma_1 - \sigma_3)_{i,i+1} \qquad (2)$$

and the average shear strain by:

$$\gamma_{i,i+1} = (\varepsilon_1 - \varepsilon_3)_{i,i+1} \qquad (3)$$

Integrating equation (1) and substituting in equation (2) derives:

$$\sigma_{r,i} - \sigma_{r,i+1} = q_{i,i+1} \ln(r_{i+1}/r_i) \qquad (4)$$

Given the boundary conditions, the state of stress and

strain around the cavity can be derived, then this equation can use the pressuremeter curve to solve for the strength.

$$q_{i,i+1} = (\sigma_{r,i} - \sigma_{r,i+1})/(\ln r_{i,i+1} - \ln r_i) \qquad (5)$$

The denominator in equation (5) can be written in terms of displacement.

Where a = current borehole radius and varies from a_o to a.

u_r = the radial displacement.

If $r = r^* + u_r$

Where r^* = the radial distance to a point before expansion.

r = the radial distance to a point after expansion.

Then $(r/a)^2 = (1 + u_r/r^*)^2 / [(1 + u_r/r^*)^2 - 1]$

Using the similarity principle the relative displacement caused by stresses ($\sigma_{r,i}$, $\sigma_{r,i+1}$) can be considered as relative expansion produced by borehole pressures (p_i, p_{i+1}).

Thus $(1 + u/r_*)_2 = (1 + \Delta a/a_o)_2 = 1 / (1 - \Delta V$

where $V_o = a_o^2 \pi L$ (initial) and $V = a^2 \pi L$ (current)

So $\ln(r_{i+1}/r)$ [redacted] $5\,[\ln(\Delta V/V)_i - \ln(\Delta V/V)_{i+1}]$

Equation (5) becomes:

$$q_{i,i+1} = (p_i - p_{i+1}) / 0.5[\ln(\Delta V/V)_i - \ln(\Delta V/V)_{i+1}] \qquad (6)$$

Equation (6) allows the average strength to be determined for any two points on the pressuremeter curve. The average shear strain (γ_i, γ_{i+1}) corresponding to the applied pressure (p_{i+1}, p_i) can be computed in a similar

fashion as that for displacements.

Assuming $\gamma = (a/r)^2$, it follows that $\gamma = \Delta V/V$

$$\gamma_{i,i+1} = 0.5[(\Delta V/V)_i + (\Delta V/V)_{i+1}] \qquad (7)$$

For the practical computation, the results of the pressuremeter test are plotted as a corrected pressuremeter curve with $V_m = f(p_o)$, where V_m is the total volume. The strength evaluation method uses the true pressuremeter curve of $\Delta V = f(p)$.

where $p = p_c - p_o$ (p_o is the original ground pressure)

$$\Delta V = V_m - V_{mo}$$

V_{mo} is the volume injected in the probe to attain $p_c = p_o$

$$V = V_{empty} + V_m$$

A plot of $\log(\Delta V/V)$ versus p provides a s-shaped curve. The pseudo-elastic portion of this curve can be used for strength determination for normally-consolidated clay, which exhibits plastic strain-hardening behaviour. For over-consolidated clays the slope of the pseudo-elastic portion of the normal pressuremeter curve provides the best estimate of pressuremeter modulus, by the equation $E = 3\Delta p/\Delta(\Delta V/V)$. The upper, pseudo-plastic, part of the semi-log curve shows the strain-softening of the material. The pressure limit can be derived by extending the curve on this semi-log plot. From equations (6) and (7) the stress-strain information on the test can also be calculated.

II.3.7 The Pressuremeter in Ice

The pressuremeter has been successfully used in the testing of ice since the late seventies and in the testing of permafrost and ice-rich soil for several years previous to that time (Ladanyi et al, 1982). There are basically two types of tests that have been performed in ice with the pressuremeter or borehole dilatometer; the short-term strength test and the long-term creep test.

The short-term test consists of increasing the pressure in the probe until the volume limit of the cell is reached in a series of 10 to 20 steps. The short-term tests can either be stress-controlled or strain-controlled as described earlier. After each increment the pressure is held while volume readings are recorded for two minutes. From this type of test the following information can be obtained; Young's modulus and the stress-strain curve in compression, the minimum tensile strength and minimum compressive stress normal to the borehole axis.

Michel (1986), have reported on a series of high rate pressuremeter tests conducted to verify the crushing strength of ice. He made use of a high pressure rock testing instrument to perform these tests which was well suited to the cold environment and demanding operating conditions. He considered that under quick loading conditions the ice can be treated as an elastic material

until failure is initiated at which time it behaves as a perfectly plastic material.

Several hundred tests were performed on lake ice near Quebec City during a three year period, the ice included snow ice, columnar ice and superimposed layered ice, Table 2.3.1 below, illustrates a summary of the test results. From the results it was found that:

(1) Ti (shear strength) and Py (yield pressure) are lower in

Number of Tests	Type of Ice	T° °C	$\dot{\epsilon} \times 10^{-3}$ s^{-1}	T_i MPA and PSI Average ± st. deviation	P_y MPA and PSI Average ± st. deviation
90	S2	0	1	6.0 ± 0.5 860 ± 72	8.0 ± 0.0 1150 ± 15
6	S2	0	2	4.8 ± 0.3 690 ± 42	7.9 ± 0.3 1135 ± 42
36	S2	0	3	4.7 ± 0.5 675 ± 72	8.2 ± 0.1 1180 ± 15
6	S2	0	5	5.2 ± 0.2 745 ± 28	8.2 ± 0.1 1180 ± 15
18	S2	0	0.5	5.1 ± 0.6 730 ± 85	7.7 ± 0.2 1120 ± 28
18	S2	0	0.25	4.4 ± 0.7 635 ± 100	7.3 ± 0.5 1050 ± 72
18	S2	0	0.1	3.2 ± 0.5 460 ± 72	6.3 ± 0.8 900 ± 115
36	S1	0	1	7.1 ± 0.5 1010 ± 72	8.0 ± 0.0 1150 ± 0
29	T1	0	1	2.8 ± 0.4 400 ± 60	5.3 ± 3.8 760 ± 85
7	T3	0	1	4.7 ± 0.3 675 ± 42	7.4 ± 0.6 1065 ± 85
18	T3	-5	1	6.4 ± 0.8 920 ± 115	8.0 ± 0.1 1120 ± 15

Table 2.3.1

Summary of High-Speed Pressuremeter Test Results (Michel et al, 1986)

the T1 than in S1 ice.

(2) The uniaxial strength of the ice can be related to the shear strength by the formulation:

$\sigma o = 2Ti / Ci$ where Ci is a coefficient that varies between 2.5 to 4 depending on ice type.

(3) The position of the probe in the hole whether it was close to the surface or not did not influence the results.

(4) Tests indicated that the strength was strongly influenced by strain rate and the brittle range started at a strain rate of about 2x10E-3 s^{-1}.

Ladanyi has reported on a series of short term pressuremeter tests that were completed near the community of Igloolik, NWT in 1977. These tests were performed with type G Menard pressuremeter on columnar-grained sea ice which was approximately 1.5 m thick and at about -4 degrees C. Table 2.3.2 shows the results.

The values of Michel's Py, (5.3 to 8.2 MPa) yield pressure compares well with Ladanyi's Pi,as, asymptotic pressure (4.2 to 6.7 MPa). The discrepancy may be due to different types of tests, ice types or ice temperature.

The second type of pressuremeter test being performed in ice is the long-term creep test. This test will provide information on the long-term bearing capacity of ice covers or on the effect of permanent ice loading on vertical structures. There are two types of stress-controlled tests that are usually performed ,these are the one-stage and

Short-term parameters

Test No.	Time per stage	Average loading rate	$P_{i,max}$	$P_{i,as}$	E_p	c_{ps} max	ϵ_f	T_s	c_{ps}	c_{ps} Eq. 9
	min	kPa/min	MPa	MPa	MPa	MPa	%	MPa	MPa	MPa
2	2	250	4.427	5.95	212	3.10	4.03	-0.40	1.56	1.40
3	2	250	3.443	5.93	212	2.39	1.55	-1.08	1.18	1.40
5	2	250	3.475	-	139	1.83	2.38	-3.52	1.25	-
7	2	100	1.494	-	127	3.11	1.10	-1.86	1.55	-
8	2	100	1.951	-	124	2.14	2.47	-1.07	1.05	-
9	2	100	3.559	5.00	149	3.21	1.16	-2.13	1.12	1.18
10	2	100	4.105	5.70	165	2.58	1.54	-1.14	1.30	1.34
11	1	400	4.652	6.70	165	3.71	4.18	-0.81	1.56	1.58
15	2	100	3.158	4.50	96	2.15	2.24	-1.23	1.04	1.06
16	1	200	4.125	5.60	175	3.19	1.16	-1.93	1.15	1.32
18	2	100	1.993	-	165	1.35	1.61	0	0.68	-
19	2	100	3.329	4.75	186	2.82	0.70	-1.76	1.00	1.12
20	2	100	1.595	-	124	1.91	1.09	-0.76	0.95	-
21	2	100	2.962	4.30	169	1.48	2.08	0	0.75	1.01
22	2	100	2.479	4.20	149	1.73	2.04	-0.21	0.80	0.99

Table 2.3.2

Short-Term Pressuremeter Test Results in Ice (Ladanyi et al, 1978(b)).

multi-stage creep test. In the single-stage test the pressure is rapidly brought to a predetermined level in the probe and maintained as long as the volume capacity of the probe allows. In the multi-stage test the pressure is increased in several steps. During each step the pressure is held for 15 minutes or more.

Strain-controlled tests may also be performed but their interpretation is more complex. These relaxation tests allow for the determination of creep parameters while providing adequate test time and probe capacity.

The creep tests are interpreted by adopting a creep law and determining its constants. The problem is defined as the creep from the internal pressure of a cylindrical cavity of infinite length in an infinite medium. The formulation most often employed for frozen soil and ice is the generalized Andrade creep law which has the form:

$$\varepsilon_e^c = (\dot{\varepsilon}_c/b)^b \, (\sigma_e/\sigma_c)^n \, t^b$$

where: ε_e^c: Von Mises equivalent creep strain
σ_e: Von Mises equivalent creep stress
σ_c: reference stress
$\dot{\varepsilon}_c$: arbitrary strain rate
t: time
n, b: creep exponents

(Ladanyi, 1984(a))

The parameters n, b and σ_c can be determined from graphical procedures performed on the creep test data. If the failure strain is also determined this provides information on the variability of the ice strength with strain rate.

Ladanyi performed a number of stage-loaded and long-term creep tests during the experiments in Igloolik in 1977. The results of these tests are shown in Table 2.3.3. It appears from the results that the exponent 'b' increases with increasing stress level, and decreases with time in each stage. The exponent 'n' was close to 2.1 which compares to findings by Gold (1965) for columnar ice of 1.5 to 2.0 in primary creep and 3.0 in steady state creep.

In 1979, Ladanyi et al reported on a number of relaxation tests that were performed with a CSM pressuremeter on fresh water ice. The CSM cell was

Long-term parameters

Test No.	Time per stage	Average loading rate	$p_{i,max}$	Creep pressure range	b (range)	b (aver. at 15 min)	n	σ_c for $\dot{\varepsilon}_c = 10^{-5}$ min^{-1}
	min	kPa/min	MPa	MPa				MPa
3	15	-	3.443	3.443	0.941-0.787	0.941	-	-
4	15	33.3	2.989	0.996-2.989	0.222-0.933	0.933	1.540	0.104
5	15	-	3.475	3.475	1.000-0.917	1.000	-	-
6	15	33.3	2.987	0.995-2.987	0.615-0.840	0.713	4.010	0.494
7	720	-	1.494	1.494	0.620-0.420	0.620	-	-
8	75	-	1.951	1.951	0.769-0.526	0.769	-	-
12	15	13.3	2.388	1.193-2.388	0.580-0.905	0.745	2.175	0.436
13	30	6.7	2.188	0.993-2.188	0.698-0.929	0.706	2.048	0.634
14	15	13.3	2.388	0.993-2.388	0.669-1.000	0.805	2.054	0.321
17	15	13.3	2.189	0.994-2.189	0.733-0.882	0.882	2.145	0.184
18	120	-	1.993	1.993	0.828-0.627	0.828	-	-
20	300	-	1.595	1.595	0.740-0.669	0.740	-	-
22	20	-	2.479	2.479	1.000-0.813	1.000	-	-

Table 2.3.3

Long-term Creep Parameters from pressuremeter Tests on Ice (Ladanyi et al, 1978(b))

developed for testing rock. It can be used for stress or strain-controlled tests and has a higher pressure capacity than the Menard system. The tests were performed in a 54 cm diameter cylinder of ice with a length of 40 cm. The relaxation tests performed consisted of a 12 step volume increase with each step being followed by a relaxation stage of 16 minutes, during which pressure readings were recorded. These tests resulted in a set of isochronous pressure-volume curves as shown in Figure 2.3.3.

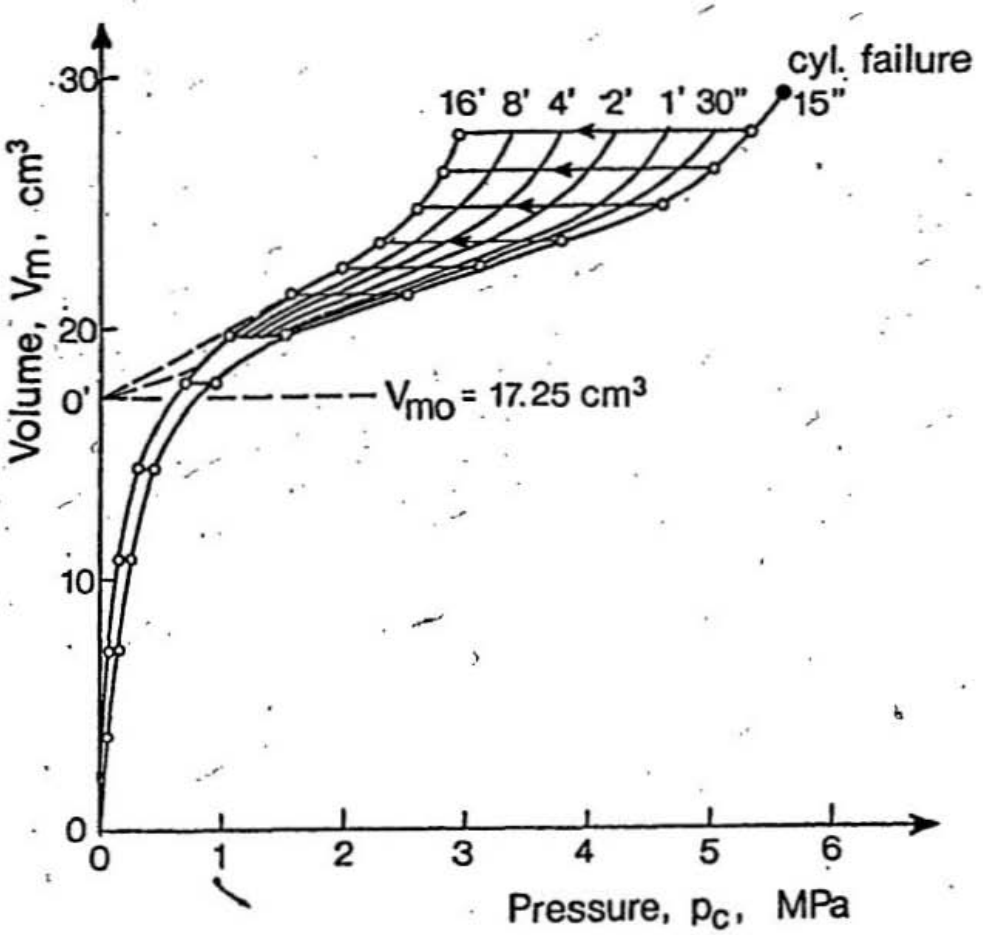

Figure 2.3.3

Relaxation Test on a Fresh Water Ice Cylinder (Ladanyi et al, 1978(a))

These curves can be interpreted in a manner similar to the creep curves to determine the deformation modulus and the compressive strength versus time and the stress-strain curves for various time steps. It is more difficult to calculate the creep parameters from this type of test as the initial elastic state is not known. An approximate solution similar to that derived by Vyalov et al (1966) for

the compression testing of ice has been employed. More recently, an exact solution has been adapted by Ladanyi (1979) from the power law creep equation developed by Spence et al (1973) for kinematically determinate structures including a hollow sphere.

Using the approximate solution Ladanyi found the following sets of creep parameters from the relaxation curves for a strain rate of 10E-5 min^{-1}.

(1) In the low strain region b = 0.1388, n = 1.095 and σc = 63.39 MPa.

(2) In the middle strain region b = 0.28, n = 1.75 and σc = 7.49 MPa.

(3) In the high strain region b = 0.4247, n = 2.4 and σc = 0.4247 MPa.

Ladanyi (1978(b)) makes a comparison between the approximate and exact solutions for the relaxation curves. The comparison shows that the agreement increases with decreasing creep coefficient 'n'. The exact solution has the advantage that it is more general and takes into account the rate of loading and the eventual non-linear short-term response of the material thus providing more exact creep parameters. However it does not account for the effect of previous strain history in staged tests nor provide information on the unloading Young's modulus.

Some work has been done on comparing the relaxation parameters to the creep parameters by Ladanyi (1982) in

ice-rich permafrost. It was found that the relaxation tests give slightly lower values of 'b' and 'σ_c' and higher 'n' values than the creep tests although within acceptable agreement. The difference may be due to the different types of tests, the different equipment, theoretical considerations or the limited number of tests conducted.

It was generally found that both the short-term and long-term tests provide valuable insitu information on the mechanical properties of ice. However tests must be conducted with proper technique and care taken in their interpretation and in predicting long-term behavior.

III THESIS OBJECTIVES AND RESEARCH PLAN

The specific objectives of this present work were outlined in the introduction of this report. They were: (1) to provide information on the behaviour of spray-ice and consider how it is best represented as an engineering material; (2) to add to the existing data base on the material and to evaluate a means of performing insitu and laboratory tests on spray-ice; (3) to assess the production of spray-ice in the laboratory and the field.

The need for adequately controlled information on spray-ice properties and the high costs of field tests lead to an experimental program at M.U.N. in which a series of tests have been conducted on laboratory made spray-ice. In preparing the testing program it was important that the laboratory results could be correlated to previously attained information. Also the type of tests chosen should provide the greatest information on spray-ice strength characteristics. It was therefore decided to conduct a series of triaxial tests on laboratory made spray-ice.

The Texam pressuremeter was selected for conducting field tests on spray-ice due to its operating advantages previously mentioned and because a fair amount of work on pressuremeter tests in ice has been published. The same type of pressuremeter tests were also performed on two types of sea ice and the results were compared with those of the

spray-ice. The production of spray-ice was evaluated on a small-scale in the laboratory and full-scale through a project conducted by ERCL in Calgary, Alberta. Additional information on the ice tested was provided by a crystallographic study of selected samples.

Through the above described testing program a large amount of information could be attained on spray-ice and the objectives for the present work could be met.

IV EXPERIMENTAL RESULTS

IV.1 Field Experience with the Pressuremeter

IV.1.1 Introduction

During the course of this research three field trips were undertaken with the pressuremeter. The TEXAM pressuremeter manufactured by Roctest Ltd. was used to evaluate ice in each case. A total of thirty-seven tests were conducted; 13 stress and 24 strain-controlled tests. Presented below is a description of the experiments and a summary of the results. In Appendix A the results corrected and uncorrected for pressure and volume effects are detailed along with the spray-ice corrected curves for spray-ice, the calibration curves and an account of the ice core samples retrieved from each field trip.

A table of the results is provided for each of the field experiments conducted. The tables show test conditions as well as values for the pressuremeter modulus and pressure limit. The modulus was derived from the corrected pressuremeter curve by the formula outlined in the literature review. The pressure limit was taken as the asymptote of the corrected curve. Additional strength properties were calculated from the spray-ice data, to enable comparison with pressuremeter test results from the literature.

The pressuremeter indentation fracture strength (T1) and the pressuremeter crushing strength (σop) were derived from

the formula provided by Michel (1986).

$T1 = \Delta p / (\Delta \ln (\Delta V / Vo))$

$\sigma_{op} = 2T1$

where: Δp and ΔV from the slope of the corrected curve.

Vo is the initial volume of the probe.

IV.1.2 LIMEX Experiment

LIMEX or the Labrador Ice Margin Experiment was a joint government, industry and university venture in which an extensive set of data was collected on the physical processes and the nature of the ice pack in the marginal ice zone. In order to conduct drilling operations more safely and efficiently offshore Newfoundland, a greater knowledge of the ice loads and the behaviour and properties of the ice was necessary. It was anticipated that direct measurements of ice strength with the pressuremeter would increase the limited available information. The experiment was conducted from the coast guard ship the CSS Baffin, in March, 1987, along the South-East coast of Newfoundland as depicted on the map in Figure 4.1.1.

In preparation for departure the equipment was assembled, calibrated and tested in the laboratory cold room of IMD (Institute of Marine Dynamics). The pressuremeter and probes were calibrated at various temperatures in the laboratory before and after the cruise, as well as on board the Baffin. To check the operation of

the pressuremeter and auger, several actual tests were performed in an ice-filled barrel prior to LIMEX.

To perform a test equipment and personnel were lowered over the side of the ship onto a selected ice floe.

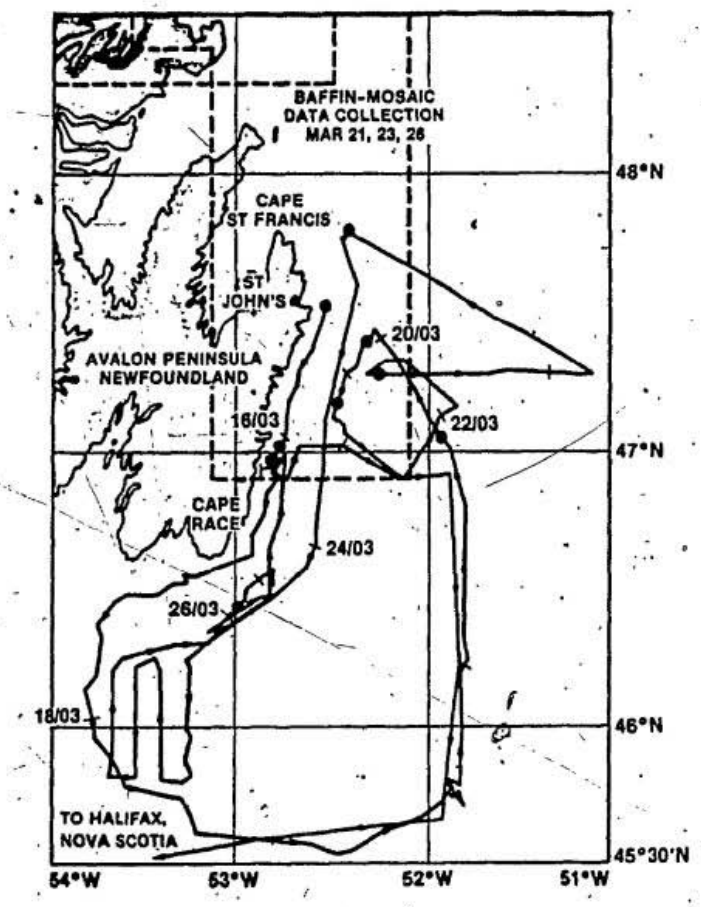

Figure 4.1.1

Path of CSS Baffin during LIMEX

Initially thickness measurements were taken across the floe to ensure adequate depth for testing. A 75 mm (3 inch) hole was then augered into the ice and the probe was inserted

to a depth of approximately 150 mm from the surface. Eleven strain-controlled tests were performed during the cruise; nine vertical and two inclined. The tests were taken to the maximum volume of the probe, 1200 cc, in twenty steps at a strain rate of 2x10E-3 s^{-1}. For each step pressure readings were recorded at mostly 2 minute intervals with 3 or minute measurements taken when possible.

A summary of the pressuremeter results is shown in Table 4.1.1 with a typical plot of the corrected pressuremeter curve in the Figure 4.1.2. It is interesting to note that the inclined orientation tests (test #3 and test #8) produced the highest pressure limits and generally greater pressuremeter moduli. The values for the pressuremeter modulus varied from 31.25 MPa to 8.18 MPa with an average of 17 MPa. The pressure limit showed less variation than the modulus with a range of 790 to 470 kPa and an average of 654 kPa. The range in the results may be partially due to the different types of ice encountered in the field. The results of the tests #5 and #6 are not included as the probe most likely penetrated the thickness of the ice floe.

After a test was completed a 100 mm (4 inch) diameter core was taken close to the test site with a fiberglass CRREL ice corer, which was driven by a gas power head. The core was examined for ice type, condition and temperature on site then packaged in polyethylene sleeves and stored in

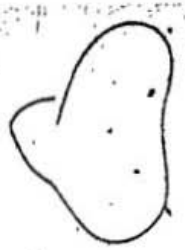

Summary of LIMEX Pressuremeter Test Results

Test	Date Time (NST)	Lat. deg °	Long. deg °	Test Orientation	Air Temperature	Ice Thickness Metres	Pressuremeter Modulus, E_p MPa	Pressure Limit, p_l kPa	Remarks
1	87/03/16 0920h	47.0100	52.8101	vertical	+2°C	1.00	probe penetrated ice thickness		1.0m-1.7m brash ice
2	87/03/20 0824h	47.4379	52.2693	vertical	+2	1.45	31.25	785	ice core taken
3	87/03/20 -	-	-	55° to horiz	+2	1.45	18.95	790	ice cracked; ice core taken
4	87/03/20 1317h	47.4325	52.2852	vertical		1.40	13.25	720	
5	87/03/20 1540h	47.4218	52.2964	vertical		0.70	-	270*	probe penetrated ice thickness
6	87/03/21 0937h			vertical		1.09	results questionable		greyish white ice
7	87/03/21 -	47.004	52.2947	vertical		≈1.09	8.18	470	ice crushed around hole; blue ice
8	87/03/21 1400h			60° to horiz	0	≈1.09	24.00	790	
9	87/03/23 1005h	-	-	vertical		2.5	8.57	520	salinity profile
10	87/03/23 1235h			vertical	+1	≈2.5	21.43	550	
11	87/03/26 1420h	46.973	52.793	vertical	+2	1.6	9.52	610	whitish blue ice
							E_p(avg) = 17MPa	p_l(avg) = 654kPa	

Notes: - salinity profile on core #9 ranged from 0.0226‰ - 0.3915‰
- all test holes were water filled after augering
* test result not included in average
- strain rate constant for all tests at $2.0 \times 10^{-3} s^{-1}$

Table 4.1.1
Summary of LIMEX Pressuremeter Test Results

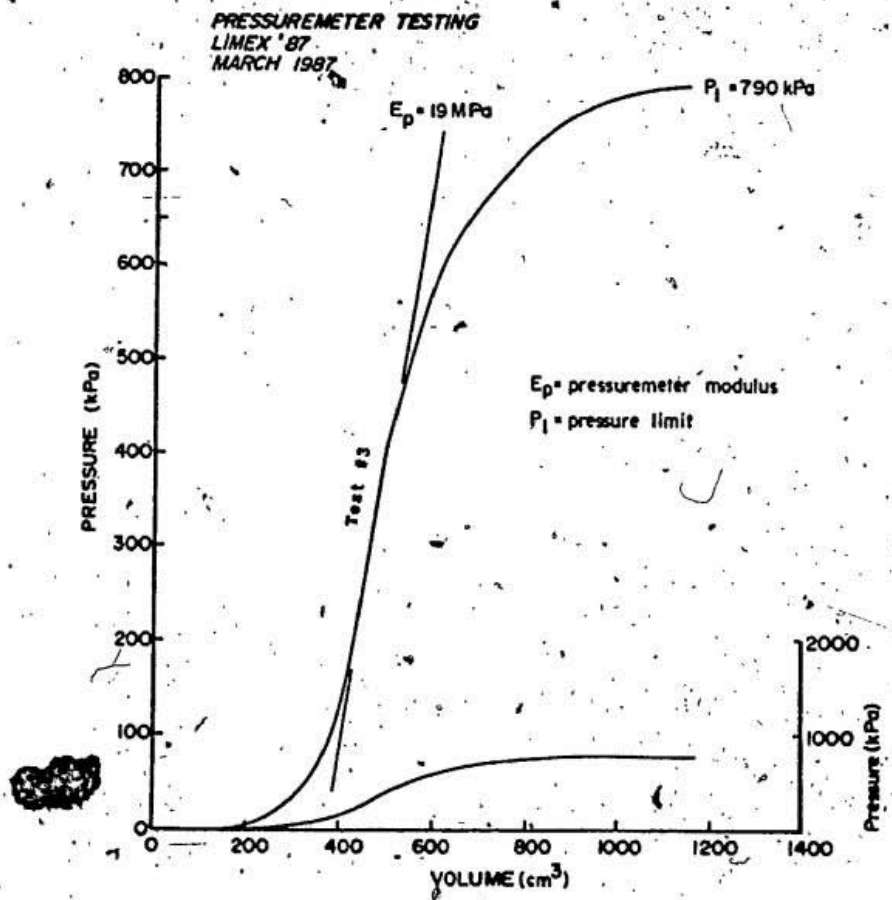

Figure 4.1.2
Example of LIMEX Corrected Pressuremeter Curve

Sample No.	Section Depth (mm)	Salinity ‰
025401	50	0.226
025402	110	0.287
025403	170	0.806
025404	230	2.154
025405	340	2.520
025406	450	2.044
025407	560	3.213
025408	670	3.617
025409	780	3.915

Table 4.1.2
Salinity Profile (Core #9)

insulated boxes in the ship's cold room until being transported to St.John's. A salinity profile was taken on a selected core and is illustrated in Table 4.1.2. In some cases more than one test was completed on a floe or if possible tests were performed on adjacent floes by simply moving the equipment to the next floe while the control box remained stationary. As many tests were performed as possible during a given period on the ice. When completed the equipment and personnel were retrieved by a cage over the side of the ship.

The ice tested during the experiment varied from consolidated brash ice to columnar first-year ice. The floe size depended on location but was generally less than 15 m in diameter in the vicinity of the ship. The floe thickness was in the order of one meter. In some cases it was anticipated that floes were rafted, no multi-year floes or growlers were evident. Generally the weather during the experiment was warm, hovering around 0 degrees C, with fog, sun or rain. The ice temperature was close to melting at about -2 degrees C.

A number of difficulties were encountered during the experiment. Due to the wide range in tests being conducted it was not possible to have as much time testing on the ice as anticipated. The cold storage available on the ship was far from ideal for properly storing samples. For future work a small portable laboratory would be very useful, so

that salinity tests and compression tests on ice cores could be performed immediately after retrieval. The majority of the tests were conducted on the extreme ice edge where the ice was disintegrating and melting, it would be useful to perform tests on the ice further into the pack.

IV.1.3 Resolute Experiment

During April of 1987 and again in 1988, IMD and C-Core collaborated on a field project in Resolute NMT which was funded by NSERC. The researchers were based at the Polar Continental Shelf Project (PCSP) in Resolute throughout the experiment. The purpose of this investigation was to test the mechanical properties of the first-year ice in the area through a variety of test setups. The pressuremeter was one method used to predict ice strength. The general location of this field experiment is shown in Figure 4.1.3.

The experiments were conducted from a camp set up on the ice a few hundred meters offshore in a bay about 4 kilometers from PCSP. The pressuremeter tests were conducted at random locations around one of the camp tents. In this way the control box and researcher could be somewhat protected from the environment inside a tent during the course of the test.

A total of eight strain- and eight stress-controlled tests were completed during the trip. One of each type of

Figure 4.1.3
Location of Resolute Experiment

test was performed horizontally into the ice from the side of a trench. During the strain-controlled tests the volume was increased to 1200 cc, the capacity of the probe, in 20 steps and readings were taken at 30 s, 1, 2 and 4 min

intervals. Occasionally other intervals were used. The strain rate during these tests was 2x10E-3 s^{-1}. If failure occurred in the ice the test was stopped. The stress-controlled tests were taken to a maximum pressure of 8000 or 10000 kPa usually in ten steps or less if the volume of the probe was exceeded first. A summary of the results are shown in Table 4.1.3, with examples of the corrected pressuremeter curves depicted in Figure 4.1.4.

The results show, in general, the stress-controlled tests gave higher values of both pressure limit (65% higher) and pressuremeter modulus (10% higher) than the strain-controlled tests. In these tests orientation of the probe seemed to have little effect on the calculated ice properties. The values for the modulus ranged from 110.7 to 61.3 MPa with an average of 90 MPa. The pressure limit was found to be between 3.1 and 9.15 MPa with an average of 6.5 MPa. No pressure limit or modulus values were attained for tests #1 and #2 because of equipment problems. The crushing pressure ranged from less than 900 kPa to over 4500 kPa.

The ice around the camp was approximately two meters thick and was columnar-grained, first-year ice; some rubble and multi-year ice existed in the area but this was not tested. The temperature at the camp varied from -13 to -32 degrees C during the four week period, however the ice temperature was more consistent, from -10 to -15 degrees C.

During the field trip calibrations were performed on

Table 4.1.3 Summary of Resolute Pressuremeter Results

Summary of Resolute (NWT) Pressuremeter Test Results

Test	Date	Probe	Test Type	Temperature Air	Temperature Ice	Cracking Pressure	Pressuremeter Modulus, E_p	Limit Pressure, p_1	Remarks
1	87/04/11	1	strain	-32°C		884 kPa	-	-	High-pressure gage inoperative
2	87/04/11	1	strain	-28		1095	-	-	Probe not inserted deep enough in ice
3	87/04/12	1	strain	-28		2315	75.5 MPa	5.22 MPa	
4	87/04/13	1	strain	-22			61.3	4.73	Probe 5° off vertical
5	87/04/13	1	stress	-22			110.3	7.78	Hole drilled between 2 long cracks -- created 3rd crack thru hole
6	87/04/13	1	stress	-26		3781	101.5	8.60	
7	87/04/21	2	stress	-13	-10°C		62.9	6.85	Hard top layer 10cm
8	87/04/22	2	strain	-19	-15	4288	98.8	4.80	
9	87/04/22	2	stress	-17	-15		91.9	7.30	
10	87/04/23	2	strain	-18	-14	3840	103.7	4.35	
11	87/04/23	2	stress	-17	-11	3757	110.7	9.15	
12	87/04/24	2	stress	-17	-13	4499	83.3	7.75	
13	87/04/26	2	strain	-17	-11	2692	91.0	3.1	Horizontal (68 cm below surface) - test stopped prematurely due to major crack in pit wall...
14	87/04/27	2	stress	-19	-10	4534	101.7	7.00	Horizontal (1.24 m below surface)
15	87/04/27	2	strain	-16	-12	2931	87.7	4.7	Snow cover = 26 cm
16	87/04/28	2	stress	-17	-13	6928	152.2	8.0	6400kPa step missed

E_p(avg) = 90MPa P_1(avg) = 6.5MPa Only vertical standard tests considered

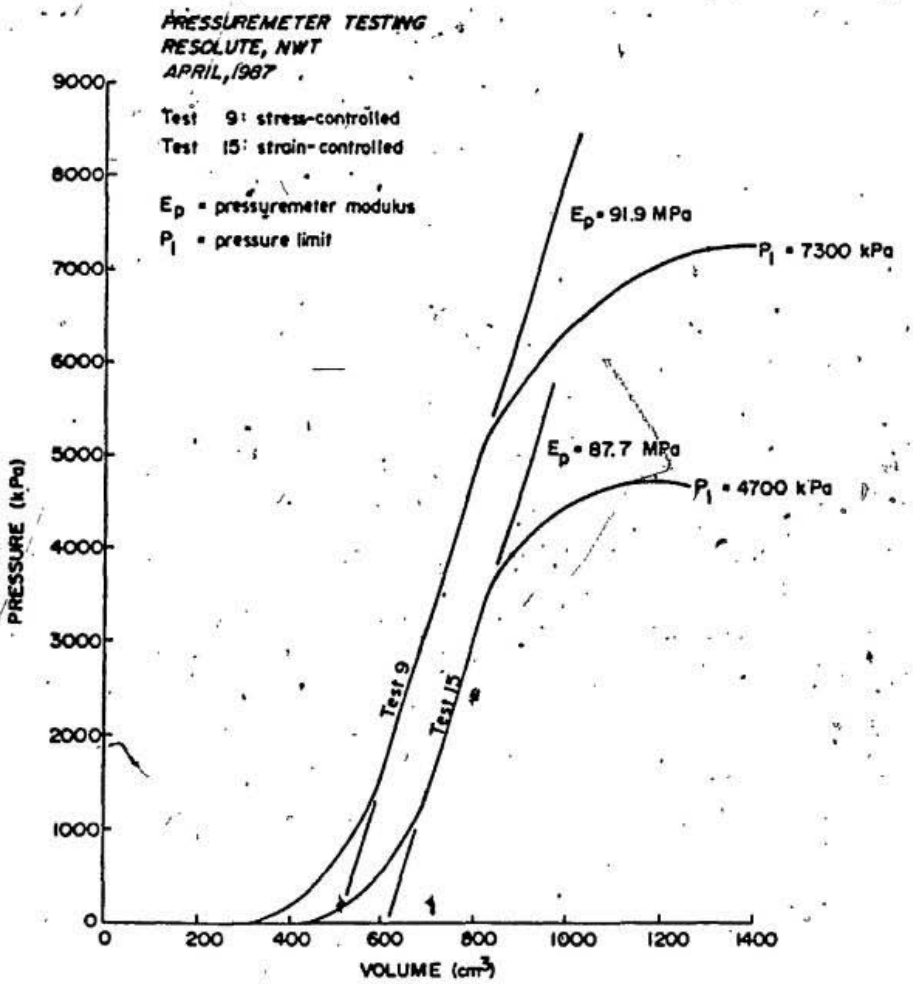

Figure 4.1.4
Examples of Resolute Corrected Pressuremeter Curves

the probes when the temperature changed dramatically. A limited number of core samples and several small block samples were taken close to the test locations, these were stored in insulated boxes outside then shipped to St. John's. Salinity tests were not performed during the

experiment. However, previous work undertaken in Igloolik (Ladanyi et al, 1978) on similar ice averaged a salinity of approximately 0.4 percent.

Several problems were encountered during this project. The cold temperatures caused a few concerns. The auger holes made for the tests were ridged on the sides partly due to the auger movement but enhanced because of the ice temperature. This caused the metal strips on the outside of the probe membrane to deform so that the probe had to be changed. As the temperature was low the fluid in the probe became very viscous and it took an unusually long time to deflate the probe. Finally the number of tests was limited by the amount of time it was possible to spend performing pressuremeter tests when other experiments also had to be completed.

IV.1.4 Calgary Spray-Ice Experiment

During the period from October 1987 to February 1988 Esso Resources Ltd. undertook a full-scale study on several factors affecting the material properties of spray-ice. This investigation will be described in greater detail in the next section while the pressuremeter tests this researcher performed on the spray-ice will be considered in the following paragraphs.

The pressuremeter tests were performed at an Esso Gas Plant located southwest of Calgary. The spray-ice was

formed over a frozen freshwater supply pond at the refinery. This granular ice varied from approximately 1.3 to 0.7 metres in depth and was a coarse to fine saturated, freshwater material. The air temperature during the testing period was +2 to -10 degrees C and the ice temperature hovered around its melting point.

To conduct a test the thickness of the ice was initially checked, if sufficient, a test was conducted at the same location. A stainless steel 75 mm (3 inch) diameter core barrel was used to make the hole. The core barrel was driven by an electric drill and had the advantage of taking an 42 mm (1.5 inch) diameter core at the exact same location of the pressuremeter test. This allowed the spray-ice to be examined prior to testing. In total five strain and five stress-controlled tests were performed on this site. The stress and strain-controlled tests were kept in close proximity to each other about 0.5 to 1.5 meters apart. The strain-controlled tests were completed in a similar fashion, at the same strain rate (2×10^{-3} s^{-1}) as in the previous experiments with readings taken solely at 0 s, 30 s, 1 min and 2 min intervals. The stress-controlled tests had maximum pressures of 750 to 1500 kPa with the same reading intervals as the previous tests.

For these tests the pressuremeter modulus averaged 3.82 MPa with a range of 1.93 to 6.84 MPa. On average the stress-

controlled tests gave moduli values 100 percent higher than the strain-controlled tests. The pressure limit values for stress-controlled tests #6 through #8 could not be computed due to the shape of the corrected stress-strain curve. For tests #9 and #10 the pressure limit averaged 800 kPa, more than 100 percent higher than that for the strain-controlled tests. The low accuracy of this value is caused by the poor shape of the corrected pressuremeter curve. The limit pressure for the strain-controlled tests averaged 291 kPa and ranged from 224 to 345 kPa. The values derived for the indentation fracture strength and pressuremeter crushing strength were approximately 289 and 578 kPa respectively. The ratio of Ep/Pl is sometimes used in describing a material, for these tests it varied from 9.0 to 18.3.

After the tests were completed 100 mm (4 inch) diameter cores were taken at each of the five main test locations with a fiberglass CRREL core barrel driven by a gas engine. Large block samples were also taken from the site. Calibrations of the pressuremeter were performed prior and during the testing period. A summary of the results is shown in Table 4.1.4 , and an example of a corrected pressuremeter curve is depicted in the following Figure 4.1.5.

Some of the problems encountered in this experiment are outlined below. As this testing was left until the end of the experiment there was a limited time in which to perform

SUMMARY OF CALGARY PRESSUREMETER TEST RESULTS

Test	Date	Test Type	Temperature (deg.C) Air	Ice	Water Depth in hole (m)	Pressuremeter Modulus, Ep (MPa)	Limit Pressure Pl (KPa)	Ep/Pl	Ti (KPa)	Qcp (KPa)	Remarks
1	Feb.6/88	strain	-2	-0.5	0.27	3.14	320	9.8	286	572	-
2	Feb.6/88	strain	-4	-1	0.23	1.93	271	7.1	195	390	-
3	Feb.6/88	strain	-6	-1	0.26	2.81	345	8.1	234	468	-probe bulged at top 75 mm
4	Feb.6/88	strain	-6	0	0.21	2.74	294	9.3	216	432	-probe didn't completely deflate
5	Feb.7/88	strain	-8	0	0.28	2.51	224	11.2	204	408	-
6	Feb.7/88	stress	-9	-0.5	0.26	5.31	-	-	185	370	-probe slightly bulged at top
7	Feb.7/88	stress	-7	0	0.25	4.65	-	-	195	390	-probe slightly bulged at top
8	Feb.7/88	stress	0	0	0.26	4.46	-	-	230	460	-
9	Feb.7/88	stress	2	0	0.29	10.24	866*	11.8*	601	1202	-
10	Feb.7/88	stress	2	0	0.25	6.84	734*	9.3*	542	1084	-
						Ep(avg)=3.82 MPa		Pl(avg)=291 MPa			

Notes: Probe centerline at 0.58 m below surface; test #10 at 0.64m.
Ice was saturated and layered, with 1-2 mm sub-rounded particles.
Core recovery: 1-100%, 2-90%, 3-100%, 4-75%, 5-85%
Depth of spray ice varied between 1.0 m and 1.13 m.
Ti-Indentation fracture strength; Qcp-pressuremeter crushing strength.
---* not included in average.

Table 4.1.4
Summary of Calgary Spray-Ice Pressuremeter Test Results

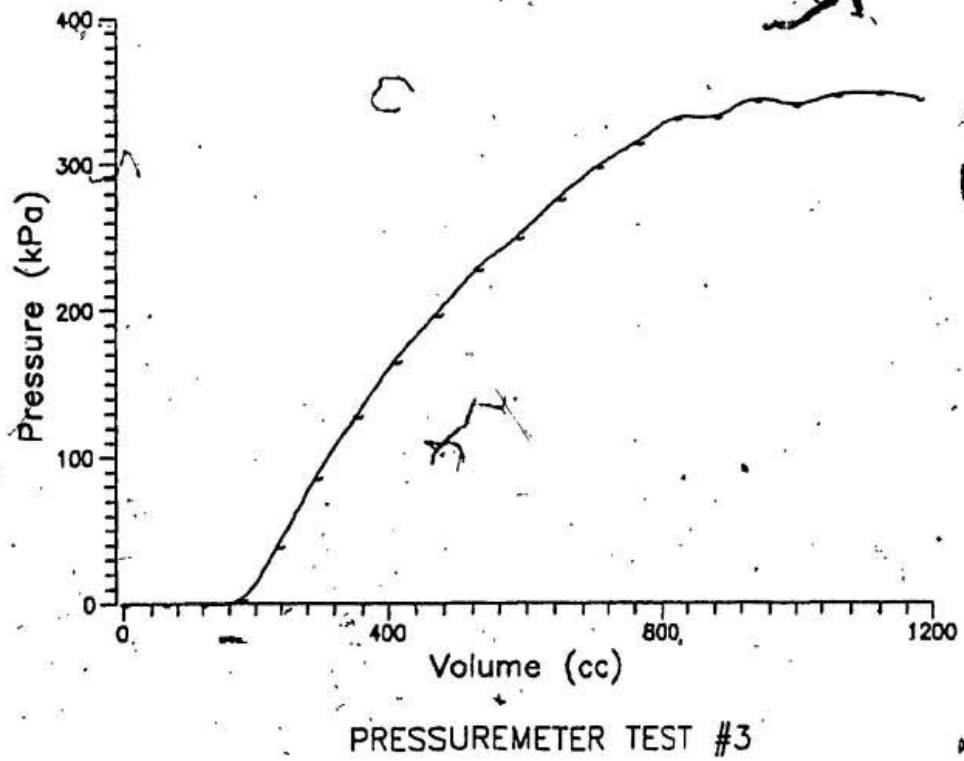

Figure 4.1.5
Example of Calgary Spray-Ice Corrected Pressuremeter Curve

the necessary tests. Also the space available for the trials was confined to a small area where there was adequate depth for the tests. Finally some problems with equipment were endured due to the design of the particular pressuremeter.

IV.1.5 Comparison of Results

The results will be looked at in greater detail in the section 'Discussion of Results'. As a brief comparison, the average pressure limit for the Resolute tests was ten times that of the LIMEX tests and twenty times that of the Calgary tests. The pressuremeter modulus was approximately five times higher in Resolute than LIMEX and again twenty times higher than Calgary. The differences between the LIMEX and Resolute results may be the temperature range in which the ice was tested. Also the ice was a slightly different type as will be described later. The Calgary tests were performed on spray-ice which has a very different structure and properties than first-year ice.

IV.2 Field Production of Spray-Ice

IV.2.1 Introduction

Esso Resources Canada Ltd. (ERCL) of Calgary and Exxon Production Research (EPR) of Houston, Texas have undertaken a full-scale spray-ice construction test experiment. Information on this project was derived from written documents by and verbal discussions with Dr. Jeff Weaver P.Eng. of ERCL and through personal observations. The purpose of this proposed three-phase experiment was to improve spray-ice construction techniques. The details of the project are not presented in this report as they are considered confidential.

IV.2.2 Project Outline and Equipment

This experiment was divided into three phase objectives by ERCL. The first phase was performed at the ERCL research facility in Calgary during non-freezing weather conditions. The purpose was to study the relationship between methods of reducing water drop size, water volume and throw distance. The second phase was conducted both in Calgary and at the final test site during cold weather. The intent was to examine the effectiveness of "Snowmax" in making spray-ice from fresh water for a range in drop sizes and temperatures. The final phase objective was to perform the same trials on salt water spray-ice. After the test completion a monitoring program was designed to examine the

engineering behaviour and properties of spray-ice.

The spray was produced by the high pressure pumping of water into the air through a nozzle. A skid-mounted, centrifugal pump was used. The flow through the pump was measured with a flow meter. The compressed air was to be injected downstream of the pump. The surfactant and "Snowmax" were to be injected in the water intake line, upstream of the pump inside a heated trailer.

IV.2.3 Results and Observations

During the phase 1 program, conducted at the end of December, a series of tests were completed in which the nozzle type and quantity of compressed air were varied. The trials were conducted over a five minute period in which the following parameters were recorded: the water flow rate and pressure, the compressed air injection rate and pressure, meteorological conditions, spray area outline, water drop size just before impact (by high speed photography) and nozzle configuration.

The phase two tests were conducted in January and early February, 1988 during colder weather. This researcher was involved in working for ERCL during this portion of the experiment. Three types of nozzles configurations were employed and the tests were performed over a range in temperatures from -25 to -10 degrees C.

During the early part of these experiments the

operation was moved from the ERCL research facility to the site of an ERCL gas refinery about 75 km southwest of Calgary, near Turner Valley. The tests were conducted over the refineries' cooling pond. This site provided more room for the tests and eliminated the necessity of constructing barriers around the test area. However it was not possible to put additives in the cooling pond, so the surfactant, "Snowmax" and saltwater were not incorporated in this experiment.

Throughout these tests similar measurements were made as in the previous phase with the addition of the following observations: the spray-ice build up, a qualitative description of the spray-ice, the temperature of the spray-ice just after impact, and the ice content of the spray-ice. Tests lasted for three to five minutes.

The pump and other equipment were set up on the bank facing the short axis of the oval-shaped pond, aligned with the predominant wind direction. Stakes were secured in the ice in a grid pattern over the spray area. They were used to measure the build up of spray-ice as well as the spray area. A photograph of the test site is portrayed in Figure 4.2.1, while Figure 4.2.2 depicts the spray-ice being formed. The ice content of the spray-ice was determined from calorimetry tests performed on the ice collected after each trial.

A few of the observations made during the tests are outlined below. The nature of the spray-ice depended on the

Figure 4.2.1
Spray-Ice Test Site, Turner Valley, ALT

temperature, the type of nozzle and the amount of air introduced. The temperature of the spray-ice on impact was measured by thermocouples placed on the ice. The thermocouples indicated the spray-ice temperature was 0 degrees C or just below. The ice content measurements were a very good indication of spray-ice quality. The quality of the spray varied over the area covered thus it was important to average results, especially at warmer temperatures and low ice contents.

The third phase of the experiment, the use of salt water could not be completed due to the location of the

site. The monitoring program was also not completed as the

Figure 4.2.2
Spray-Ice Formation, Turner Valley, ALT

budget did not allow for the additional expenditure. However pressuremeter tests were performed by the writer and core and block samples were retrieved so that further work could be done at a later date by interested parties. Thin sections were also completed on the block samples, these are

reported on in a later section.

The experiment showed that spray-ice could be successfully made on a large scale outside of the arctic and its quality and volume could be measured to a reasonable degree of accuracy. Thus it was possible to vary the additives or nozzles and determine their effect in the temperature range of -25 to -10 degrees C.

IV.3 Method of Making Laboratory Spray-Ice

IV.3.1 Introduction and Equipment

The intention of the initial phase of this experiment was to determine a method by which spray-ice could be made in the laboratory. The requirements of the operation were: that a reasonable quantity of spray-ice could be made with each spraying, that the spray-ice made should have similar properties as the material formed in the arctic and that the results should be repeatable.

The spray-ice for the experiments was made by spraying saline water through a nozzle with compressed air into a cold room which was initially at -20 to -25 degrees C. The nozzle was placed in a port on the back wall of the cold room. Compressed air and water were fed to the nozzle from outside the room. The cold room measured approximately 1.2 by 2.5 m in plan and 2 m in height.

Four nozzle configurations were tried before a standard was selected for the experiments. Three of the nozzles had single orifices while one had six. The larger nozzle was manufactured in an attempt to produce greater quantities of spray-ice during one session. This nozzle was not satisfactory for these experiments as high enough air pressure could not be maintained for all of the jets to work properly. The other three nozzles had similar designs except for variations in the intake diameter for the air and water apertures. After testing the three nozzles, one

was chosen for the project. No significant variation in the spray results was noticed amongst the three nozzles. Table 4.3.1 delineates the dimensions of the nozzles and a diagram of the selected nozzle is illustrated in Figure 4.3.1.

SPRAY-ICE NOZZLE DIMENSIONS

Nozzle No.	Compressed Air Orifice (mm)	Water Intake Orifice (mm)	Air Orifice (mm)
#1	4.00	1.422	3.619
#2	2.3-2.4	1.486	3.619
#3	4.05	2.197	3.607

Note: All dimensions are inside diameters.

Table 4.3.1
Spray-Ice Nozzle Dimensions

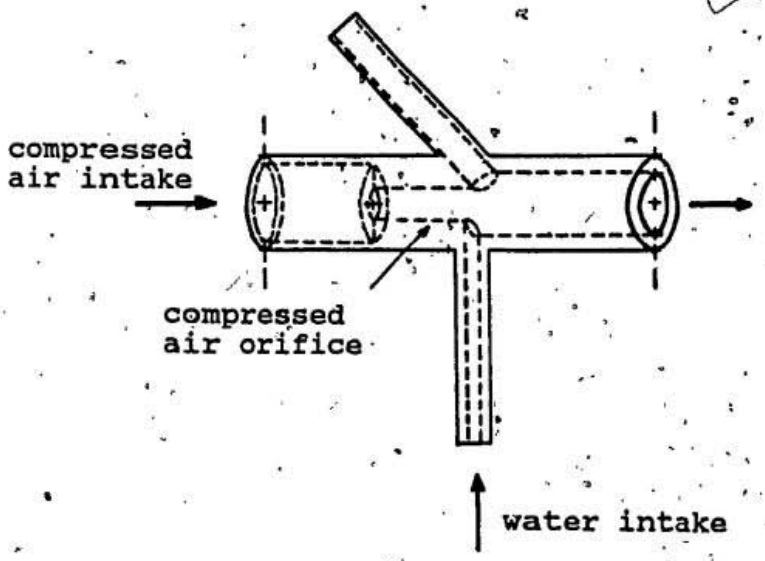

Figure 4.3.1
Spray-Ice Nozzle Configuration (scale 1:0.889)

IV.3.2 Spray-Ice Production and Results

The spray-ice produced in the cold room was created in the following manner. Compressed air was forced into the rear, larger aperture of the nozzle at a constant pressure of 550 kPa (80 psi), and through suction water was drawn up through the line running perpendicular to the air flow. The water used in the experiment was a mixture of two parts sea water to three parts fresh water combined to give a spray-ice salinity of between 7 and 16 ppt, which was in the range of salinities found on spray-ice islands as reported earlier in Section II.1 of the literature review. The line running at an angle to the flow was left open to the atmosphere to aid in the dispersion and cooling of the stream.

Initially the temperature of the cold room was fixed at its lowest setting about -25 degrees C. The spraying process continued, for 25 to 35 minutes, until the room temperature reached -15 degrees C, at which time the air pressure was turned off and the spray-ice was left to cool for approximately 30 minutes. The spray entered the cold room just below the air conditioning unit so that the water droplets were quickly caught in the flow of cold air. The additional cooling from the air stream greatly aided in the production of relatively dry spray-ice. The spray-ice formed covered three of the walls and the ceiling of the room. After a period of spraying the ice was 'harvested' from

the plastic covered walls with a broom and shovel and stored in sealed containers to help prevent sublimation.

The experimental arrangement for making spray-ice worked very well for this study. The spray-ice made could best be described as a damp to wet granular material, it was not slushy or very dry. Initial test runs were conducted with fresh water, once pleased with these results saline water was used for the experiment. Grain size analyses were performed on the spray-ice. Figure 4.3.2 illustrates the results of one such test. It is evident that the material is less than 2mm in diameter and fairly well-sorted. A number of thin sections on the samples were performed after the triaxial tests were completed. They are described in another section.

The spray-ice made in the cold room did not vary greatly from one batch to the next. However the spray-ice properties in-situ change immensely with climatic conditions, placement procedure and location with respect to the water line. This study dealt exclusively with fairly dry, above-water-line spray-ice.

During the test period the spray-ice changed while stored in the cold room. The spray-ice sintered, the grains grew and some brine drainage was noticeable. Therefore, in order to have relatively consistent samples, before constructing samples the salinity of the ice was checked, the material was broken up by hand and it was sieved.

The quantity of spray-ice made depended greatly on the ability of the cold room to maintain the cold temperatures

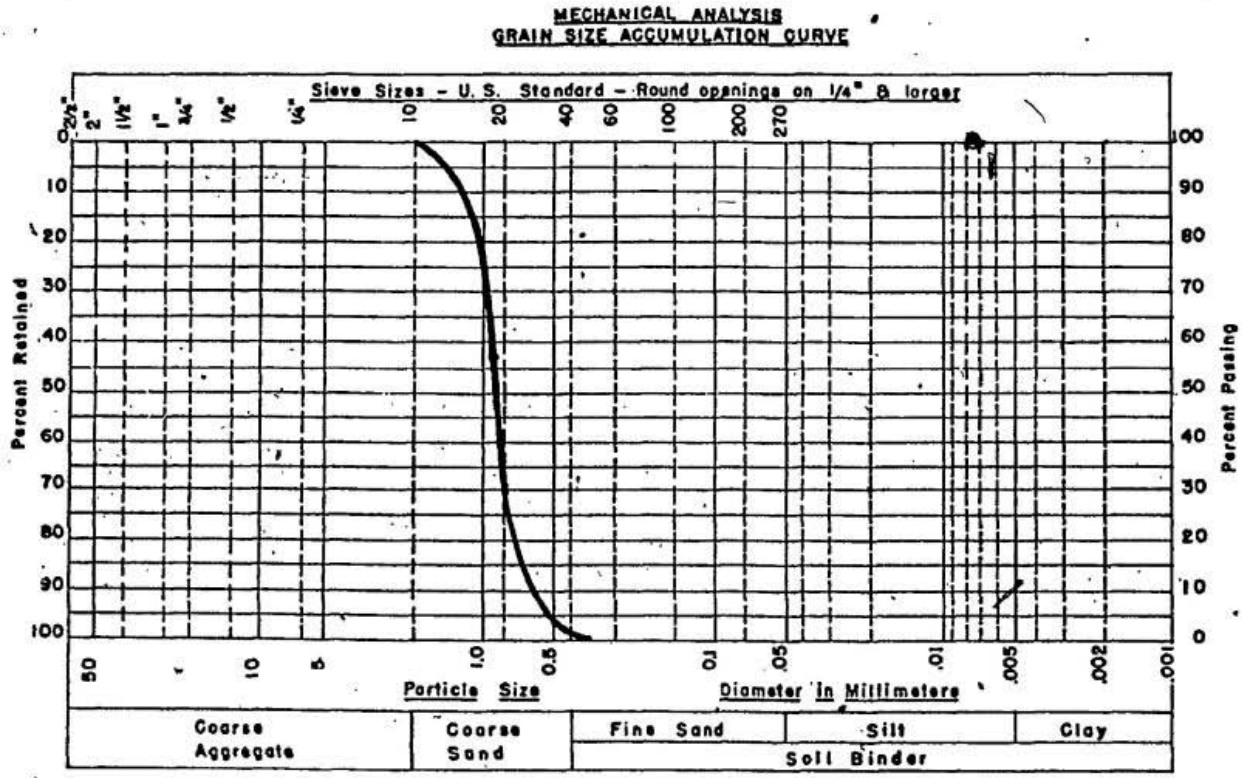

Figure 4.3.2
Grain Size Analysis on Spray-Ice

required. The size of the cold room and the amount of icing on the ventilation fan also affected the production time available. It was found that heats sinks helped to keep the room temperature low; containers of solid ice were used for this purpose. After spraying for 25 to 35 minutes anywhere from 15 to 30 litres of spray-ice was formed.

A few difficulties experienced during this portion of the experiment were, keeping the air orifice of the nozzle from icing over and ensuring that the water line and nozzle were ice free. As the cold room was not very efficient it was necessary to allow plenty of time for the room to cool before testing, and time for the ventilation system to defrost after spraying. Due to these restraints it was only possible to spray once a day. Given a more reliable cold room the production of spray-ice would have increased considerably.

IV.4 Triaxial Tests on Spray-Ice

IV.4.1 Introduction and Purpose

After successfully making the spray-ice, triaxial tests were performed to determine the material strength under various conditions. To determine how the material changed over time, these tests were performed after the sample had consolidated over a selected time period. Tests were also conducted at varying cell pressures to simulate conditions at depth below the surface. Finally, a series of tests were completed at a higher temperature and at a higher strain rate to assess the changes in spray-ice strength when the temperature or strain rate were changed.

IV.4.2 Preparation of Test Specimens

The triaxial samples were made from spray-ice that was first segregated and then sieved through a #12 (1.68 mm) sieve. After sieving the spray-ice a sample was taken for salinity testing. The results of salinity tests are shown in Appendix B. The samples were formed in a regular triaxial mold in much the same manner as a sand sample would be formed. A rubber membrane was placed inside the mold which was in turn put on the cell base. A partial vacuum in the mold kept the membrane tight against the mold walls during forming of the sample. The spray-ice was placed in the mold in five lifts and compacted with a

cylinder of wood which had a diameter slightly less than that of the mold. An initial height to diameter ratio of 2:1 was chosen, with an initial bulk density of 0.650 g/cm3. After the sample was formed the top cap was placed on the sample and the membrane secured with o-rings at both ends. The following photographs in Figure 4.4.1 depict the equipment used to form the sample.

IV.4.3 Test Procedure and Equipment

The triaxial tests were performed with standard triaxial equipment which incorporated cooling coils inside the cell to maintain the required test temperature. The coils were connected to a Haak controller and bath; the controller circulated an antifreeze liquid and held the bath at a constant temperature within 0.1 degrees C. During the test the cold room was kept close to the test temperature, within 2 degrees C. The cell was brought to the precise test temperature of -10 or -5 degrees C during the construction of the sample. In the most cases the sample began the consolidation phase of the testing immediately after it was formed.

Triaxial tests were performed at two nominal, constant strain rates of 1.45x10E-4 s^{-1} and 1.78x10E-5 s^{-1}. The actual strain rates of the samples varied slightly due to the accuracy of the press and stiffness of the equipment. As the platens for the samples were steel and the load

presses were of high capacity in comparison to the ice strength the equipment stiffness was not deemed to be a

Figure 4.4.1
Triaxial Sample Preparation

concern. Two presses were used in the present study; the faster tests were performed on a 55 kN capacity ELE, Hoskin Scientific press, with the slower on a 1000 kg Wykeham Farrance press. An LVDT mounted on the triaxial rod monitored the sample deformation during tests. The cell pressures used for the tests were 45, 83 and 172 kPa (6, 12, and 25 psi). The cell pressure was measured before and at the end of each test with an accurate pressure gage, and continuously monitored through a coarser gage located outside the test trailer. The consolidation time for the sample ranged from four hours to approximately nineteen hours. During the consolidation phase LVDT readings were recorded on a variable speed chart voltage recorder, and noted directly from a voltmeter. A thermistor located inside the cell was used to monitor the cell temperature. The experimental set-up is illustrated in the photographs in Figure 4.4.2.

To perform a test, the sample, while on the base, was weighed and diameter and height measurements were taken. The sample was then placed in the cell. The cell was filled with air to the required pressure and the sample was allowed to consolidate for the required time period. The pressure was maintained during consolidation and LVDT measurements were recorded. After consolidation the press was started and rod friction recorded. During each test a chart recorder monitored the vertical load through a load cell, and the

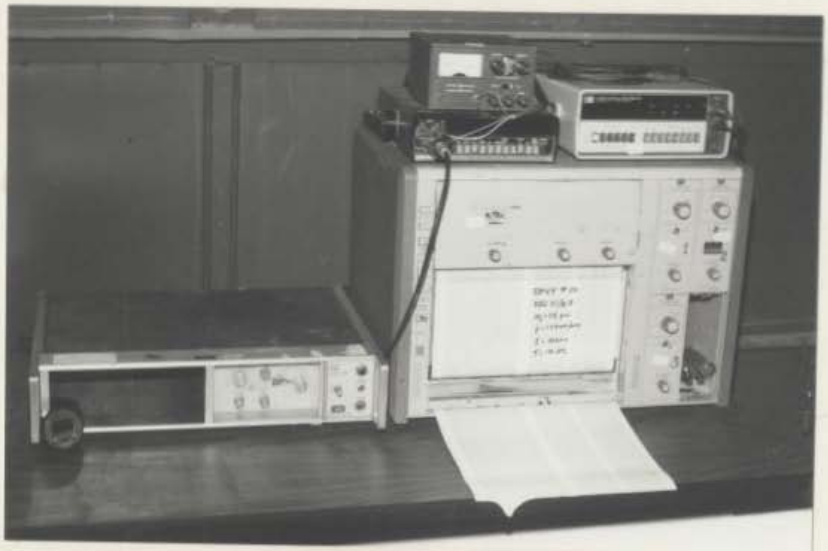

Figure 4.4.2
Triaxial Test Arrangement

LVDT deflection. The load cell was threaded into a ball joint at the top of the test frame. A ball bearing threaded under the load cell transferred the vertical load to the top cap and the sample. The data from each test was also recorded manually at time periods of 15 to 60 seconds.

At the end of a test, defined as being either visible failure or twenty percent strain of the sample, the press was stopped and the sample was removed. The sample was again weighed, carefully measured and photographed. Any pertinent observations on its condition were also recorded. Four height and five diameter measurements were taken on each sample and the results averaged. It was finally wrapped in plastic, labelled and stored at -20 degrees C in a freezer. The measured final sample height was compared to that calculated from the LVDT measurements. This provided a check on the results.

During the set up of the equipment several calibrations were performed. The load cell was calibrated in the cold room before and after performing the series of tests. The LVDT used in the experiment was changed a few times initially due to malfunctions; so each one was carefully calibrated. Finally the thermistor was calibrated over a range of temperatures. All these calibrations are shown in Appendix B.

The triaxial testing program is shown in Table 4.4.1. The table separates the tests into groups which have

similar conditions. Tests number 1 through 4 were preliminary trials and do not appear on the table. The consolidation time varied to some extent solely with the longer period which was felt would not greatly change the test results. The strain rate as calculated from the LVDT

TABLE OF TRIAXIAL TESTING PROGRAM

Test No.	Start Date	Cell Pressure KPa (psi)	Strain Rate (1/s)	Consolidation Time (hrs)	Temperature (deg.C)
5	Oct.21/87	86.2 (12.5)	1.49*10-4	4.17	-10
6	Oct.22/87	86.2 (12.5)	1.51*10-4	4.10	-10
8	Oct.27/87	93.1 (13.5)	1.45*10-4	4.00	-10
25	Dec.7/87	86.2 (12.5)	1.47*10-4	3.93	-10
9	Oct.28/87	44.8 (6.5)	1.23*10-4	4.00	-10
10	Oct.29/87	44.8 (6.5)	1.48*10-4	4.00	-10
11	Oct.30/87	44.8 (6.5)	1.50*10-4	4.03	-10
13	Nov.3/87	172.4 (25)	1.40*10-4	4.00	-10
14	Nov.4/87	172.4 (25)	1.44*10-4	4.05	-10
15	Nov.5/87	172.4 (25)	1.48*10-4	3.97	-10
7	Oct.26/87	86.2 (12.5)	1.21*10-4	19.00	-10
12	Nov.2/87	79.3 (11.5)	1.53*10-4	19.03	-10
16	Nov.7/87	79.3 (11.5)	1.42*10-4	20.28	-10
24	Dec.4/87	86.2 (12.5)	1.40*10-4	18.20	-10
17	Nov.24/87	86.2 (12.5)	1.78*10-5	4.00	-10
18	Nov.25/87	86.2 (12.5)	1.72*10-5	4.25	-10
19	Nov.26/87	86.2 (12.5)	1.79*10-5	4.00	-10
26	Dec.8/87	82.7 (12)	1.82*10-5	4.12	-10
20	Nov.30/87	44.8 (6.5)	1.42*10-4	17.66	-10
21	Dec.1/87	44.8 (6.5)	1.40*10-4	18.05	-10
22	Dec.2/87	172.4 (25)	1.46*10-4	17.92	-10
23	Dec.3/87	172.4 (25)	1.47*10-4	19.83	-10
29	Dec.10/87	172.4 (25	1.72*10-4	18.5	-10
27	Dec.9/87	82.7 (12)	1.47*10-4	4.00	-5
28	Dec.10/87	82.7 (12)	1.46*10-4	4.00	-5

Table 4.4.1
Table of Triaxial Testing Program

measurements differed from the average of either 1.45x10E-4 s^{-1} or 1.78x10E-5 s^{-1} by at most 17 percent. The cell pressure measurements remained close to constant during the test through careful monitoring. The deviation from the average was less than eight percent.

IV.4.4 Triaxial Test Results and Interpretation

The results of the twenty-five triaxial tests conducted on spray-ice are shown in various forms on the following pages and in Appendix B. The appendix contains information sheets on each of the tests. The tables summarize initial and final conditions and provide calibration data for each test. Also in the appendix are graphs of deviatoric stress (total vertical stress ($\sigma 1$)-cell pressure ($\sigma 3$)) versus percent strain, that is stress-strain curves, for each group of tests. From these plots a representative test has been selected from each group for the graphs shown hereafter. Finally, photographs of the samples after test completion are provided in the appendix.

The initial results of the triaxial tests are provided in the Table 4.4.2. This table gives information on sample initial and final density, consolidation and total test strain, data on the test cell pressure, sample strength, and the stress path strength parameters p' and q', as well as comments on the final condition of the sample. The

TABLE OF TRIAXIAL TEST INITIAL RESULTS

Test No.	Cell Pressure σ_3 (KPa)	Sample Consol. Delta H (cm)	Density (g/cm^3) initial	Test Strain(%)	Density (g/cm^3) final	Dev. Stress $\sigma_1-\sigma_3$ (kPa)	$p=(\sigma_1+\sigma_3)/2$ (kPa)	$q=(\sigma_1-\sigma_3)/2$ (kPa)	Comments
5	86.2	0.463	0.574	20.2	0.656	256	214.2	128.0	small hole at p.w. valve
6	86.2	0.257	0.597	18.3	0.675	216	194.2	108.0	small hole at p.w. valve
8	93.1	0.458	0.592	23.0	0.634	234	210.1	117.0	-
25	86.2	0.124	0.639	21.2	0.689	319	245.7	159.5	sample tilted & bulged
9	44.8	0.258	0.55	17.9	0.618	214	151.8	107.0	poor voltage readings
10	44.8	0.069	0.637	22.7	0.647	267	178.3	133.5	poor voltage readings
11	44.8	0.131	0.627	19.9	0.658	263	176.3	131.5	sample thin top & middle
13	172.4	0.359	0.678	20.5	0.747	462	403.4	231.0	-
14	172.4	0.301	0.638	17.7	0.718	405	374.9	202.5	test restarted
15	172.4	0.361	0.654	19.1	0.728	462	403.4	231.0	sample distorted
7	86.2	1.224	0.593	19.1	0.622	387	279.7	193.5	sample top tilted
12	79.3	0.177	0.652	22.6	0.709	535	346.8	267.5	-
16	79.9	0.063	0.656	19.0	0.655	540	349.3	270.0	top vertical cracks, bulged
24	86.2	0.151	0.656	21.0	0.701	467	319.7	233.5	-
17	86.2	0.267	0.731	19.0	0.752	319	245.7	159.5	bulged base, large crystals
18	86.2	0.153	0.687	18.6	0.769	169	170.7	84.5	-
19	86.2	0.178	0.697	19.3	0.771	174	173.2	87.0	-
26	82.7	0.161	0.61	19.8	0.701	196	150.7	68.0	-
20	44.8	0.192	0.622	22.0	0.659	362	225.8	181.0	bulged middle
21	44.8	0.145	0.659	21.2	0.66	377	233.3	188.9	bulged middle
22	172.4	0.459	0.684	21.8	0.798	673	508.9	336.5	slightly bulged middle
23	172.4	0.466	0.638	22.0	0.749	534	439.4	267.0	slightly bulged middle
29	172.4	0.525	0.643	19.9	0.66	682	513.4	341.0	straighten load cell
27	82.7	0.214	0.638	20.7	0.73	273	219.2	136.5	-
28	82.7	0.277	0.633	21.2	0.709	275	220.2	137.5	tilted, slightly bulged

Notes: Unless otherwise stated the sample deformed uniformly.
"p.w." = pore water

Table 4.4.2
Table of Triaxial Test Initial Results

average initial density of the samples was 0.640 g/cm^3 and the average weight was 387 g. When forming the samples it was relatively easy to make the sample close to the correct height for a 2:1, height to diameter ratio. However, although the same procedure was used to form each sample it was difficult to maintain the selected initial sample density. Also, the weight of the sample could not be accurately measured until after the test was completed. In cases where the sample densities were not in the correct range additional tests were performed to verify results. All but two of the tests were within ten percent of the average density. It appears from the table that strength increases with density.

The samples were isotropically consolidated for periods of four or nineteen hour. Examples of the consolidation phase are shown in Figures 4.4.3 and 4.4.4. The total specimen deformation during consolidation varied considerably depending on the conditions as well as the sample initial density. For the four hour period the average change in height was between 0.088 cm to 0.290 cm, for the nineteen hour period it was from 0.169 cm to 0.483 cm.

The final strain varied from 17.7 to 23.0 percent depending on several factors; the condition of the sample (tilted or not), the linear range of the LVDT and the final diameter of the sample (for removal from cell). As the portion of the test that was of interest was usually

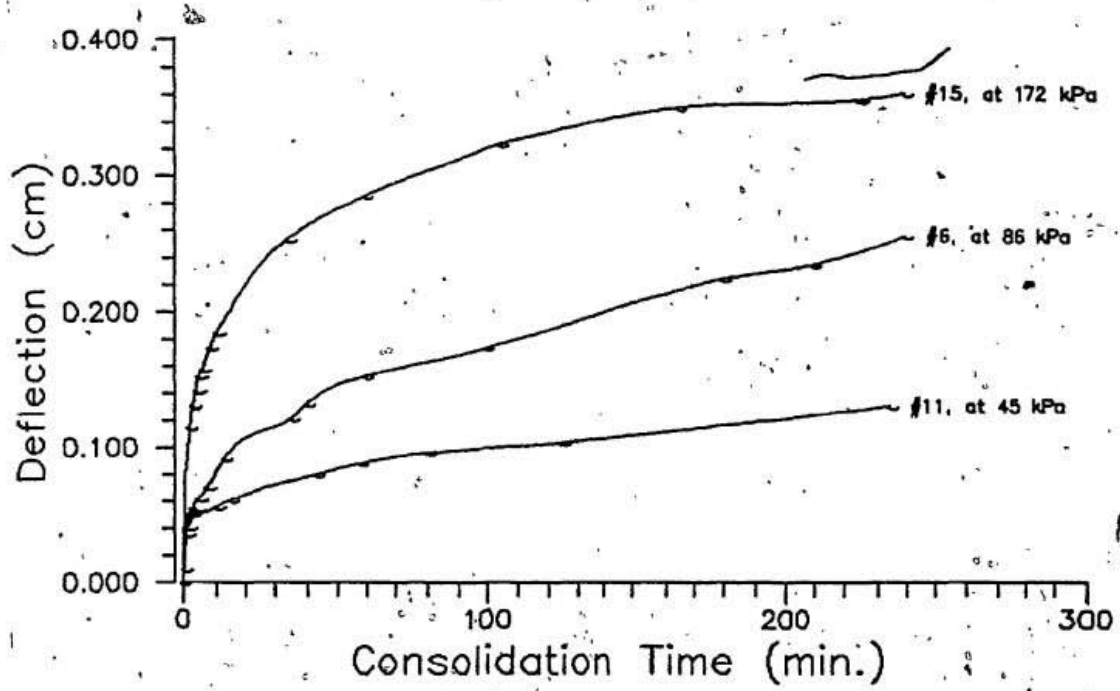

Figure 4.4.3
4 Hour Consolidation Phase, at Various Cell Pressures

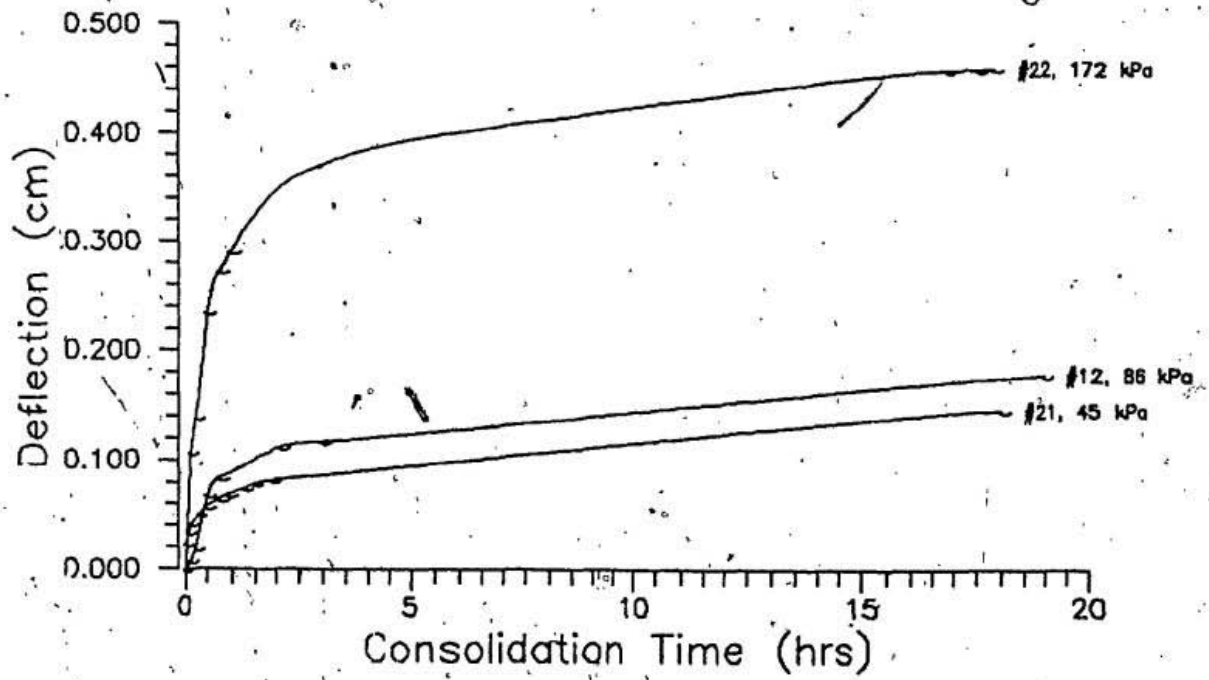

Figure 4.4.4
19 Hour Consolidation Phase, at Various Cell Pressures

completed by about 12 percent strain, all tests were performed to a sufficient extent.

The final condition of the sample is noted in the comment section of the Table 4.4.2. Further information can be also acquired from the photographs in the appendix. As expected the samples most distorted or bulged were those tested at low cell pressures and for short consolidation times. The final density measurements of the specimens were inaccurate because of the distorted shape of the sample. In all but one case the sample density increased after the test. The exception was test #16 where the sample cracked.

Figures 4.4.5 to 4.4.11 portray the results of the entire test history while only the peak, breakover stress or strength will be used later on in the discussion. The strength is defined as the deviatoric stress and is determined by the intersection of the initial slope of the stress-strain curve and the final linear segment of the curve. The breakover or peak stress is given for each test in Table 4.4.2. Seven stress-strain graphs are provided. They illustrate variations in one of the following parameters; cell pressure (4 hrs consolidation), cell pressure (19 hrs consolidation), strain rate, test temperature and consolidation time at 45, 86 or 172 kPa.

Several types of failure were observed. The majority of the samples deformed by strain hardening (see for example test #15). In this test a bi-linear relationship is

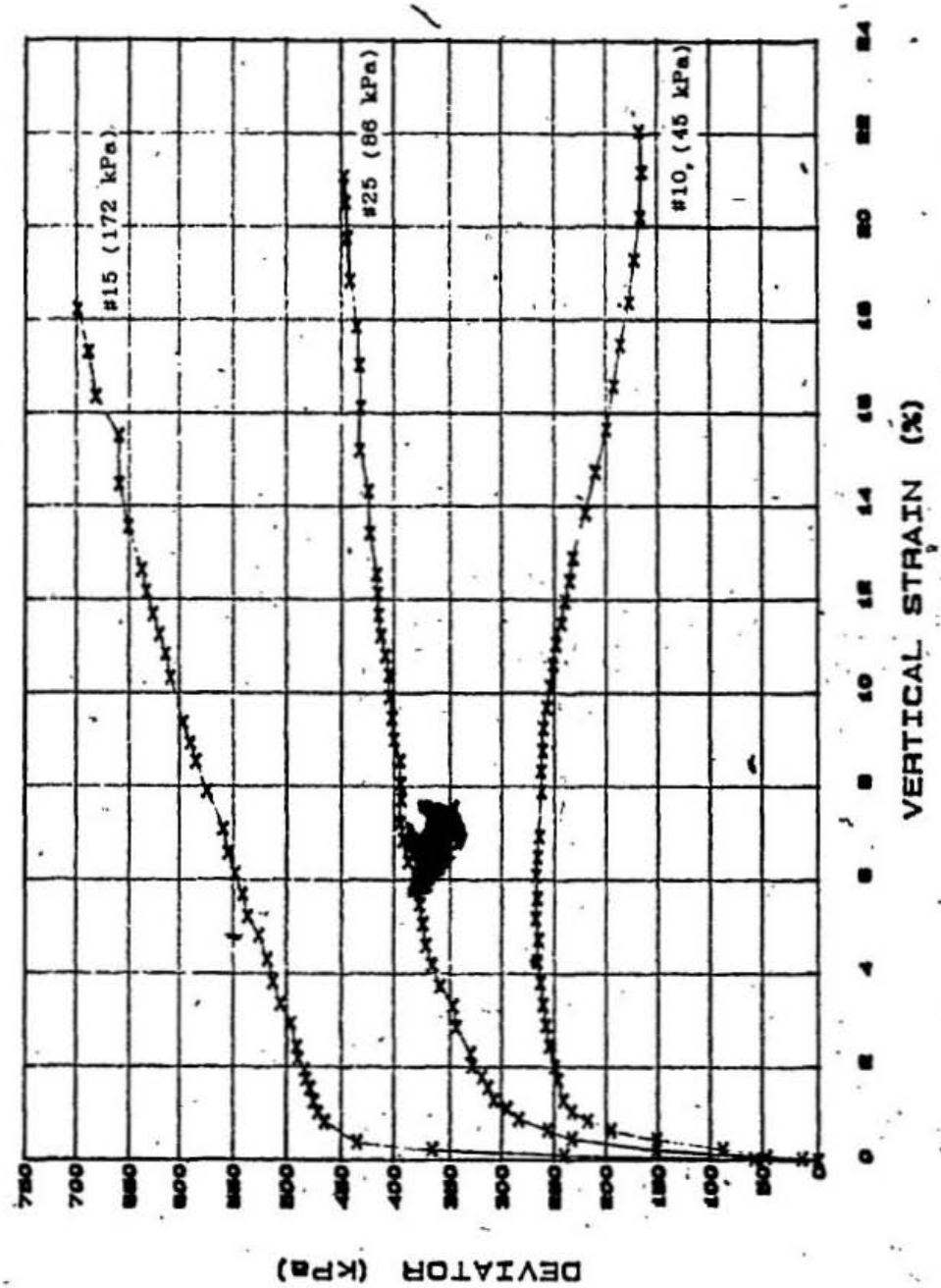

Figure 4.4.5
Stress-Strain Curves, at Three Cell Pressures
(4 Hour Consolidation)

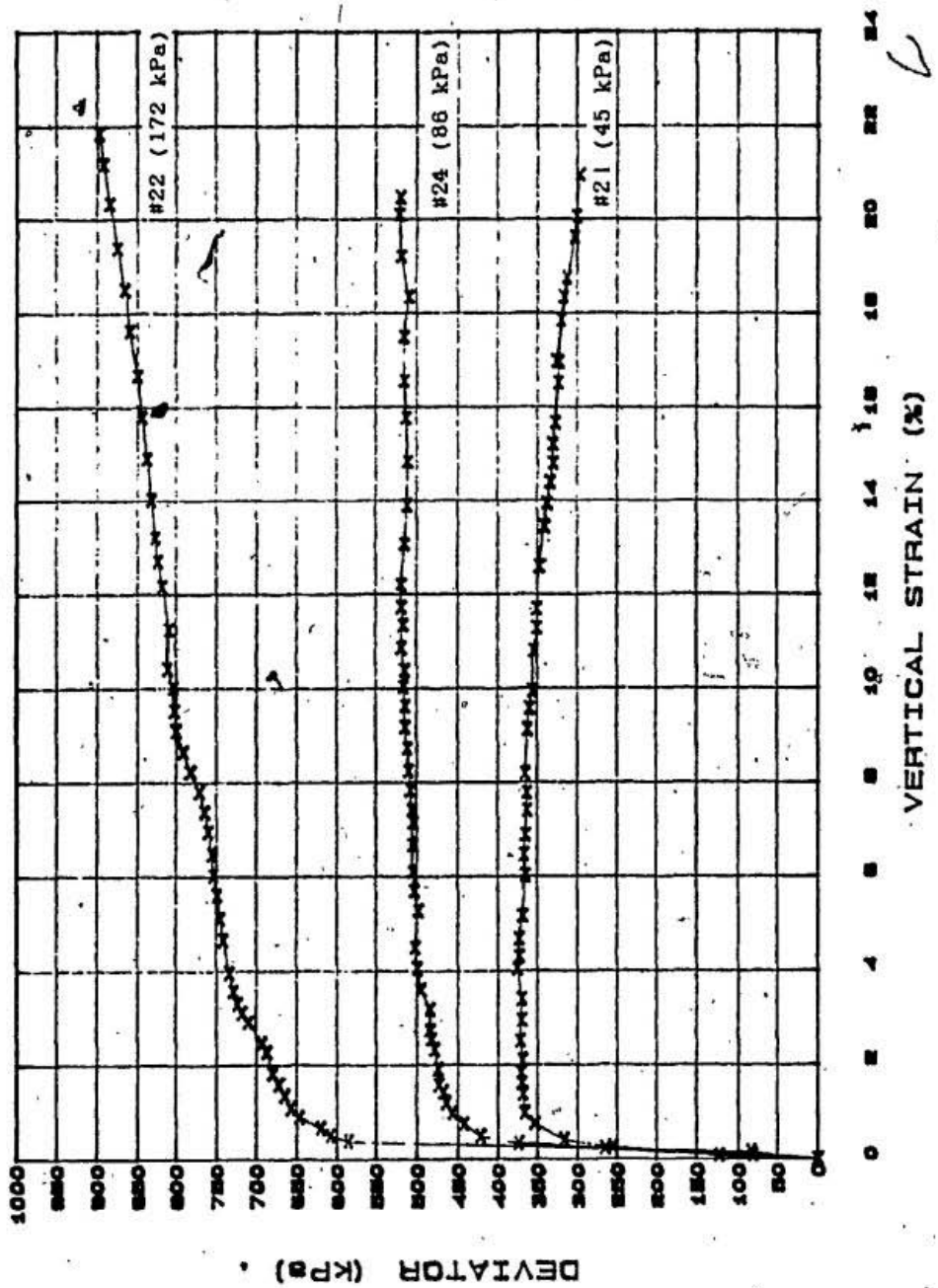

Figure 4.4.6
Stress-Strain Curves, at Three Cell Pressures
(19 Hour Consolidation)

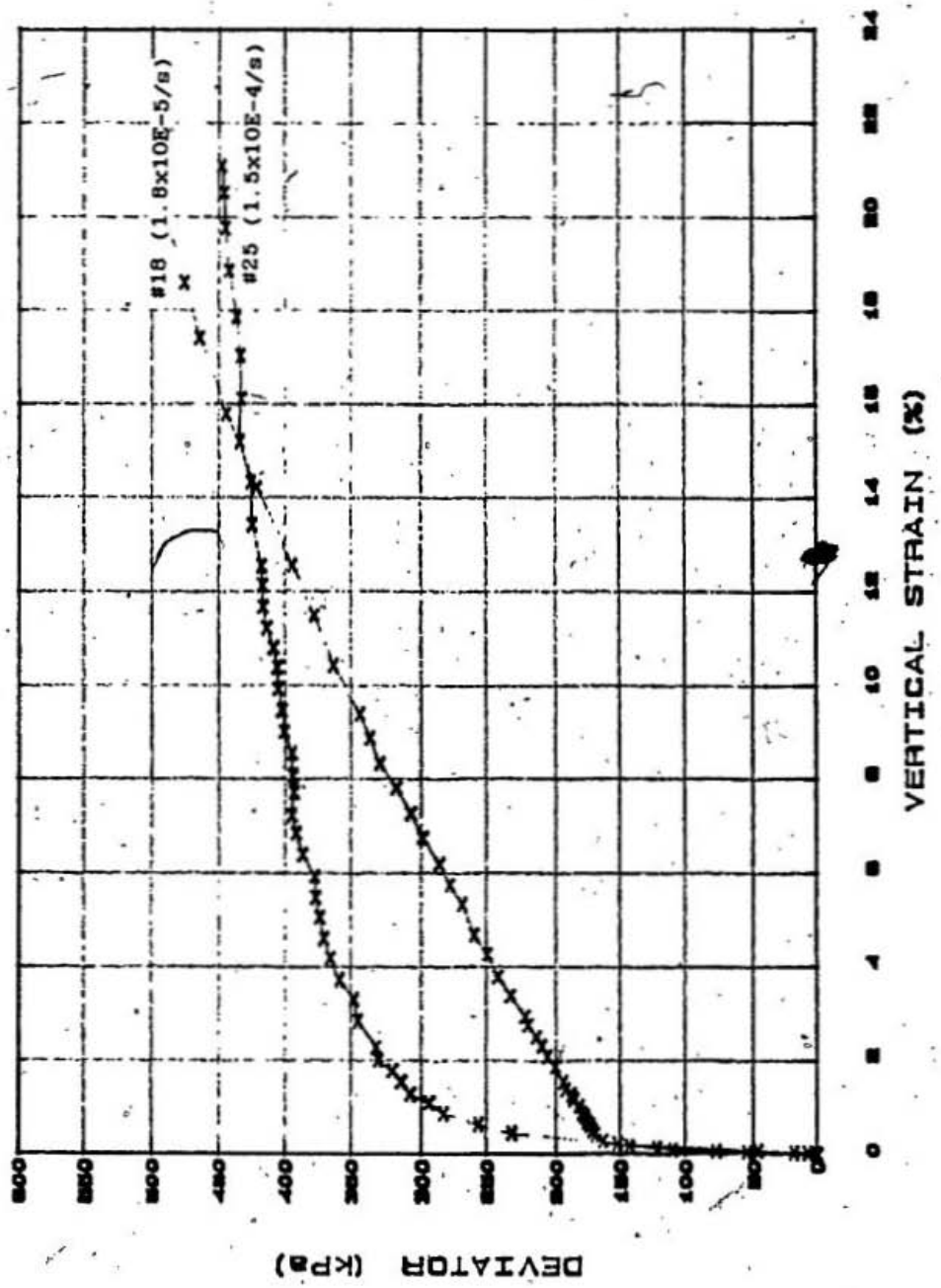

Figure 4.4.7
Stress-Strain Curves, at Two Strain Rates
(Cell Pressure 86 kPa)

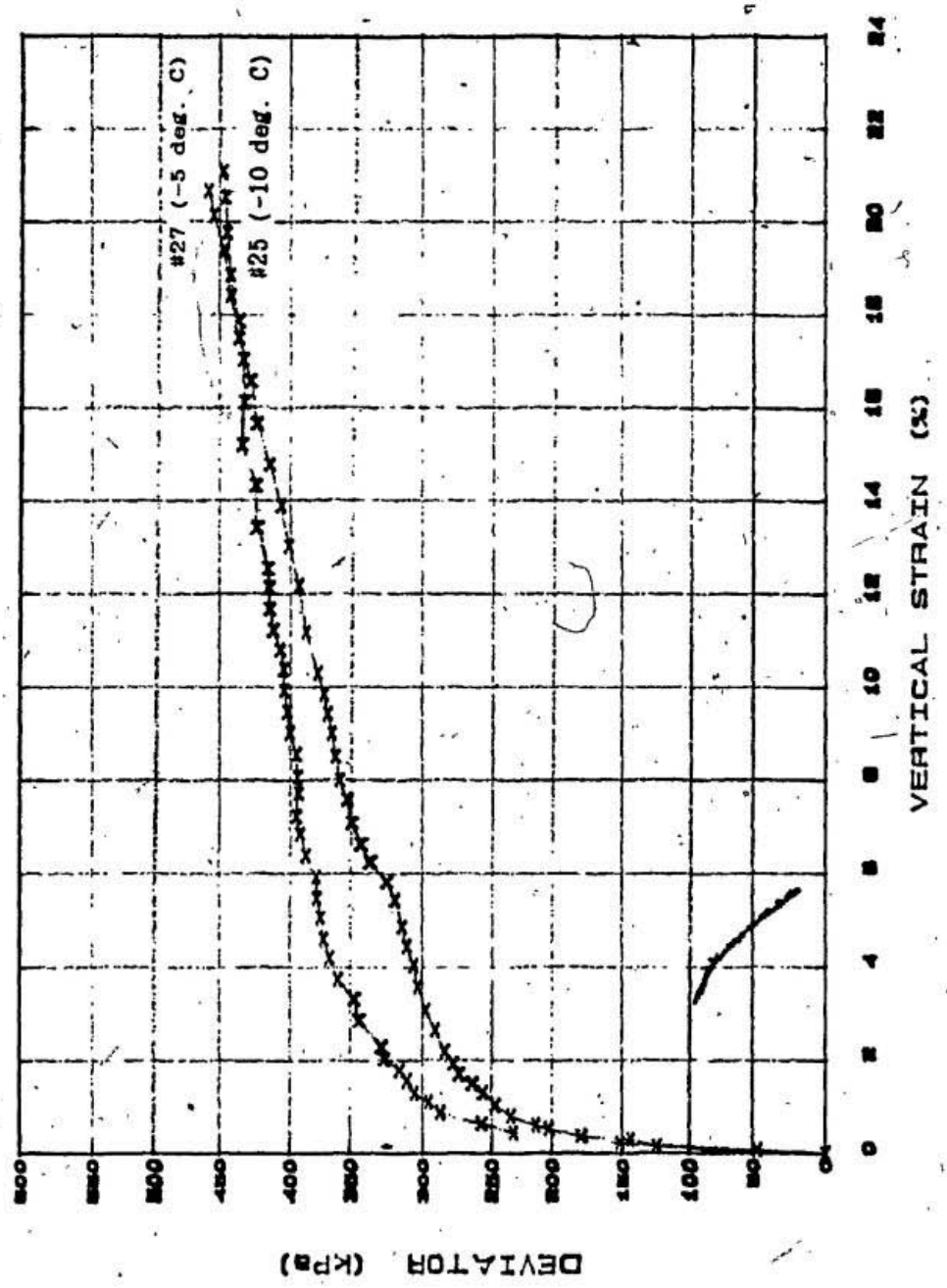

Figure 4.4.8
Stress-Strain Curves, at Two Test Temperatures
(Cell Pressure 86 kPa)

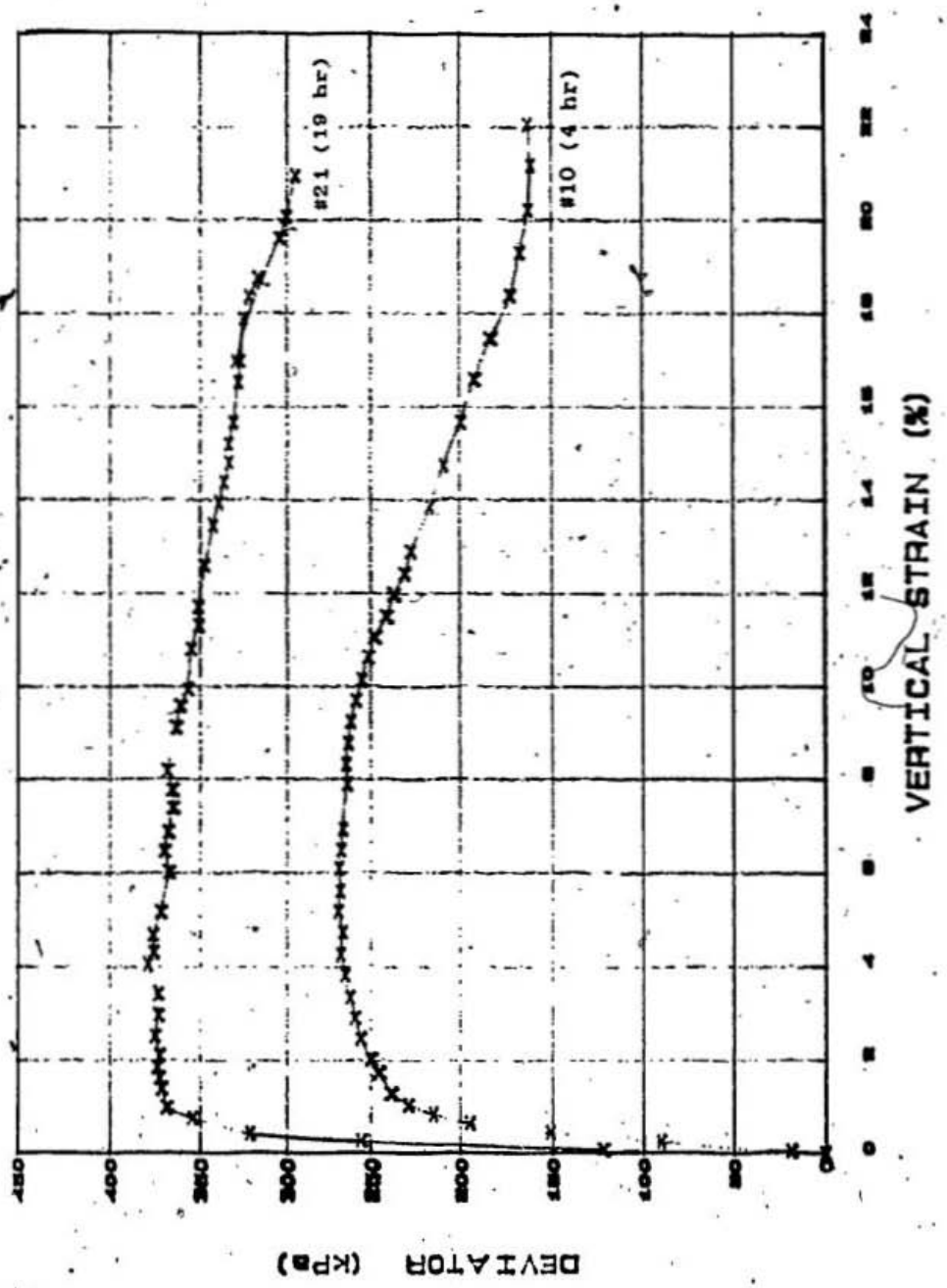

Figure 4.4.9
Stress-Strain Curves, at Two Consolidation Times
(Cell Pressure 45 kPa)

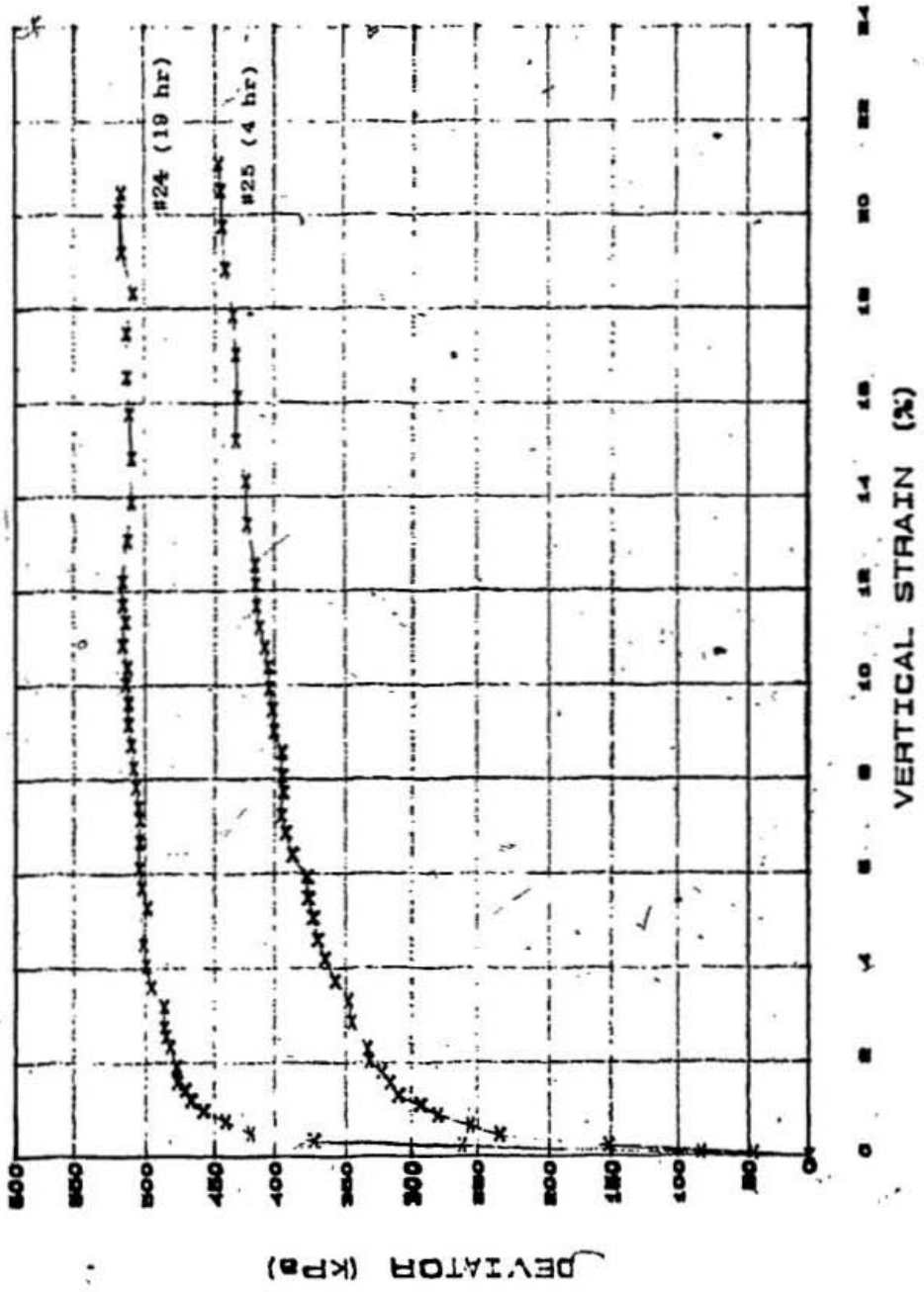

Figure 4.4.10
Stress-Strain Curves, at Two Consolidation Times
(Cell Pressure 86 kPa)

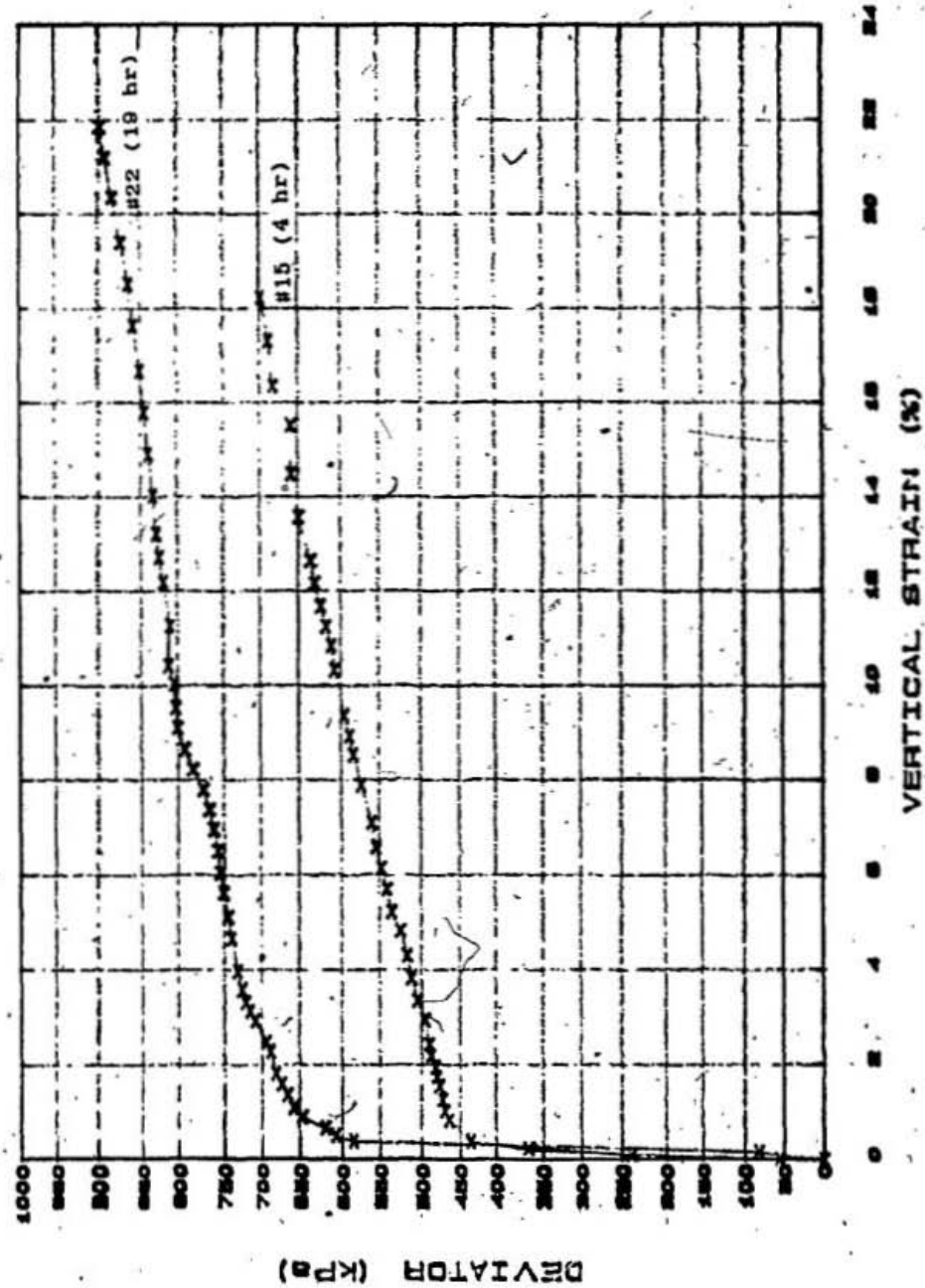

Figure 4.4.11
Stress-Strain Curves, at Two Consolidation Times
(Cell pressure 172 kPa)

evident, the stress increases rapidly with strain then reaches a breakover point, at about 0.75 percent strain, after which the stress continues to rise more gradually. This type of failure is characteristic of tests performed under moderate or high cell pressures and short consolidation times. The second type of failure is illustrated by test #24, in which the stress increases rapidly with strain then reaches a peak and levels off to a near constant residual value. This behaviour was noticed in tests with a longer consolidation time especially at the moderate cell pressure. The final main type of stress-strain curve expressed in the results was due to strain softening of the material, an example of which is test #10. In this test the stress initially increased quite rapidly with strain then the stress increase was reduced dramatically and it eventually decreased slightly. For this case the peak value may be at the breakover stress, at less than two percent strain, or later between six and eight percent strain. Generally this result was found in tests with low cell pressures.

One anomaly among the results was test #16, which failed in a more brittle fashion. The stress rapidly increased reached a peak value then rapidly decreased. Visual inspection of the sample after the test revealed cracks around the upper half of the specimen. This event could have been caused by the sample being formed the day before

consolidation commenced and the cold room undergoing a defrost cycle during that period.

A summary of the above full test results can be delineated by graphs of the strength of the spray-ice versus temperature, strain rate, consolidation time as well as confining stress, provided in Figures 4.4.12 through 4.4.18. Despite the limited data general tendencies are indicated in these figures. From the strength graphs the following is apparent; strength increases with increasing cell pressure, consolidation time and strain rate. It is felt that test #25 is the most representative test of the group of tests, with a cell pressure of 86 kPa and strain rate of 1.5x10E-4 s^{-1} as its sample initial density is in the correct range. That being the case the temperature graph shows an increase in strength with decreasing temperature.

The stress-strain curves depict further information on the behavior of the samples. Figures 4.4.5 and 4.4.6 show that as cell pressure increases the slope of the final portion of the curve also increases for the case of both the four and nineteen hour consolidation time. This increase in strain hardening with cell pressure can be expected as the samples will become more dense at a greater rate at higher confining pressures.

From the limited data available it is suggested that the reduction in strain rate causes a lowering of ice strength but an increase in the ability of the material to

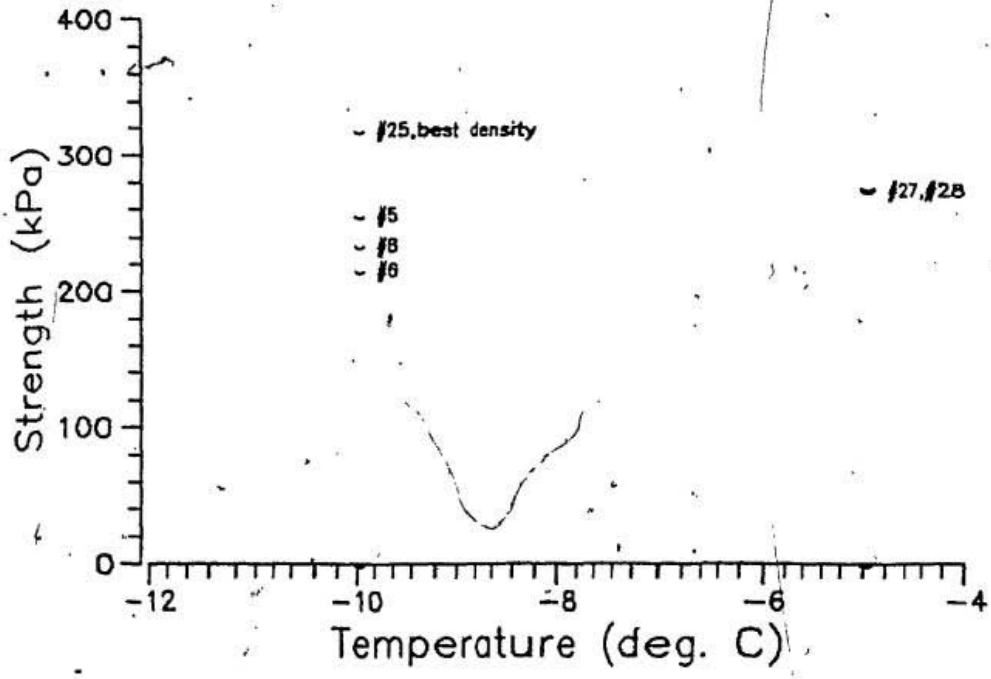

Figure 4.4.12
Strength versus Temperature

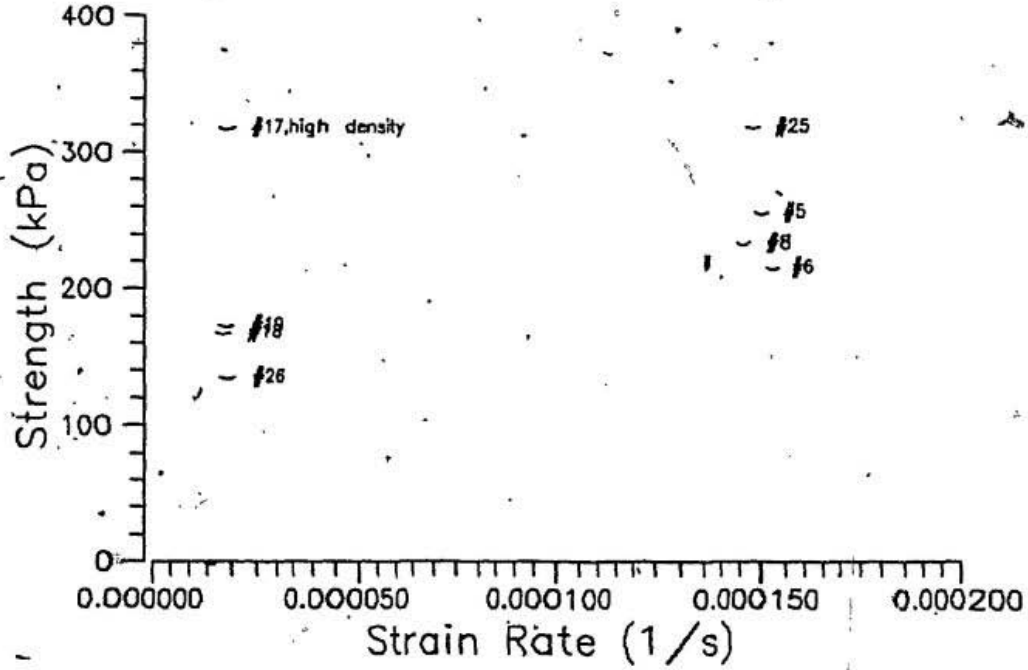

Figure 4.4.13
Strength versus Strain Rate

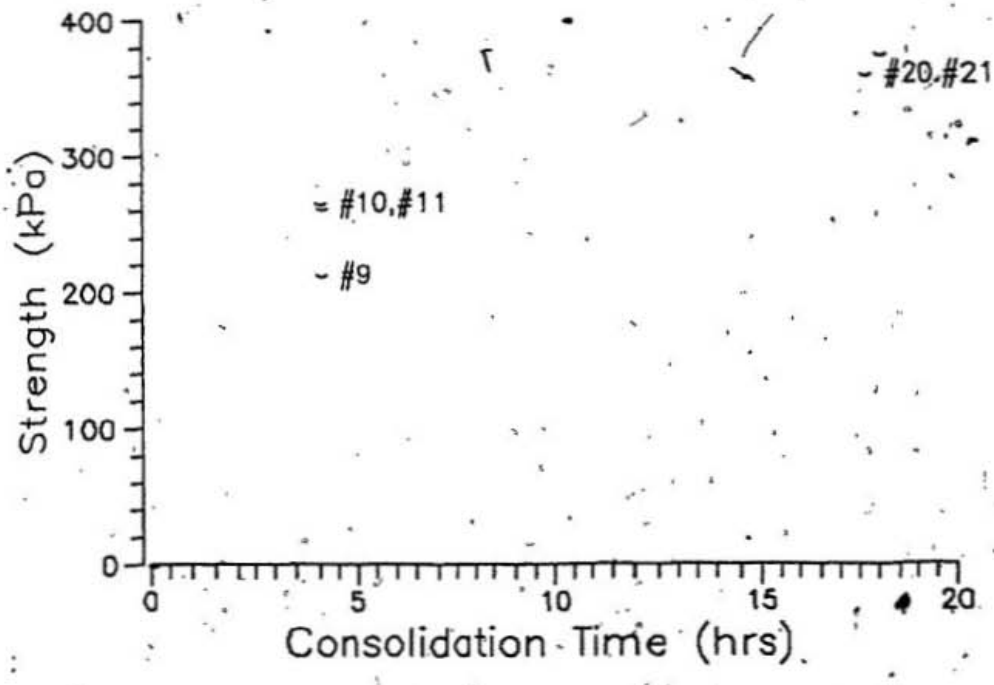

Figure 4.4.14
Strength versus Consolidation Time (45 kPa)

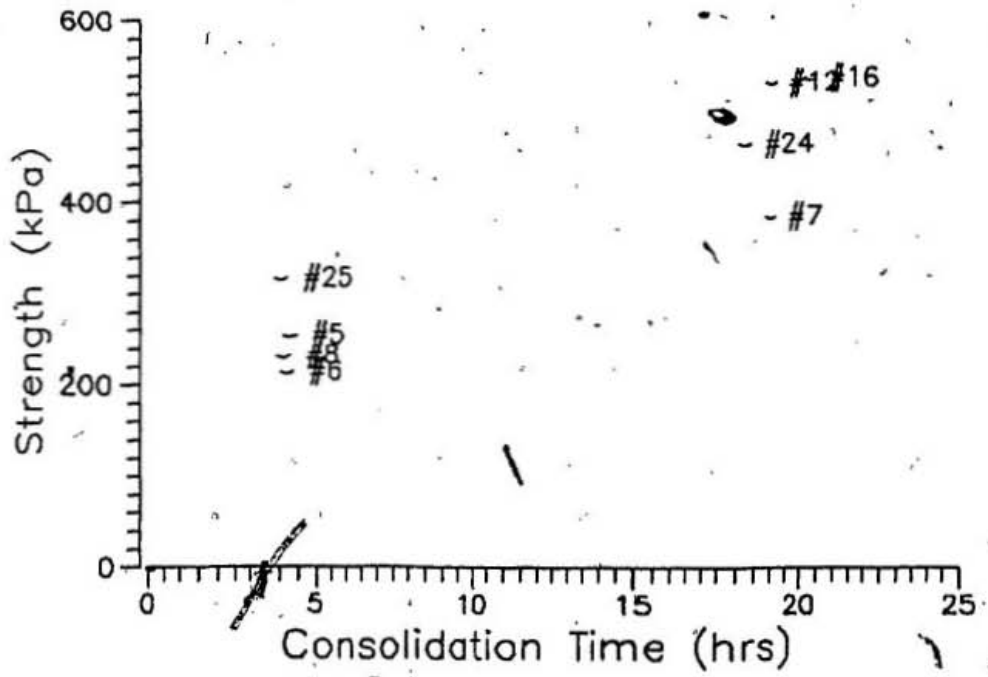

Figure 4.4.15
Strength versus Consolidation Time (86 kPa)

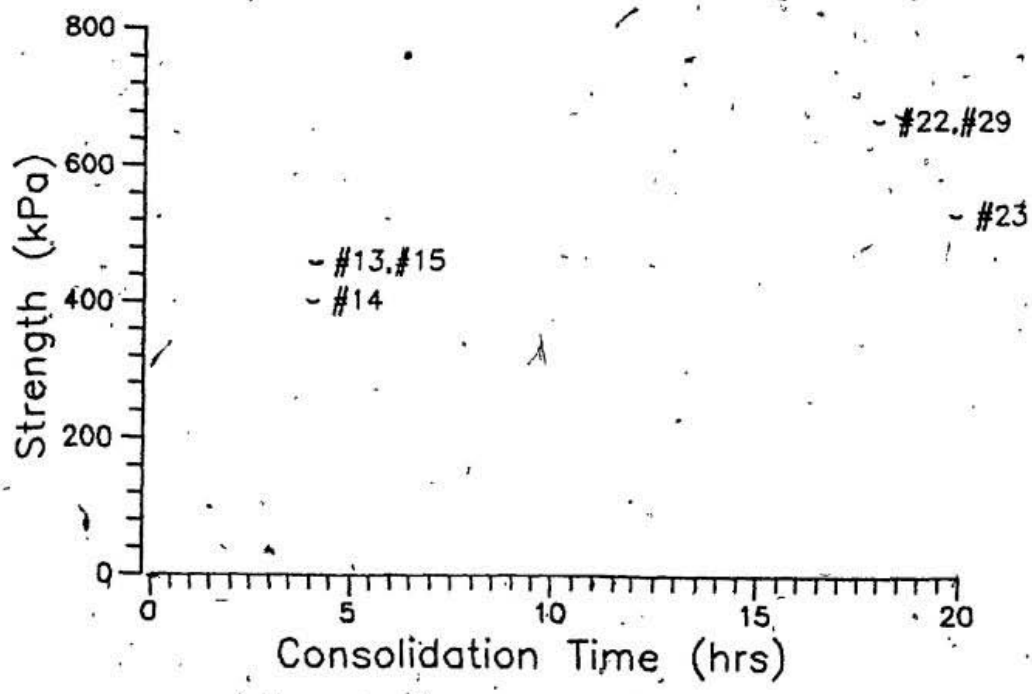

Figure 4.4.16
Strength versus Consolidation Time (172 kPa)

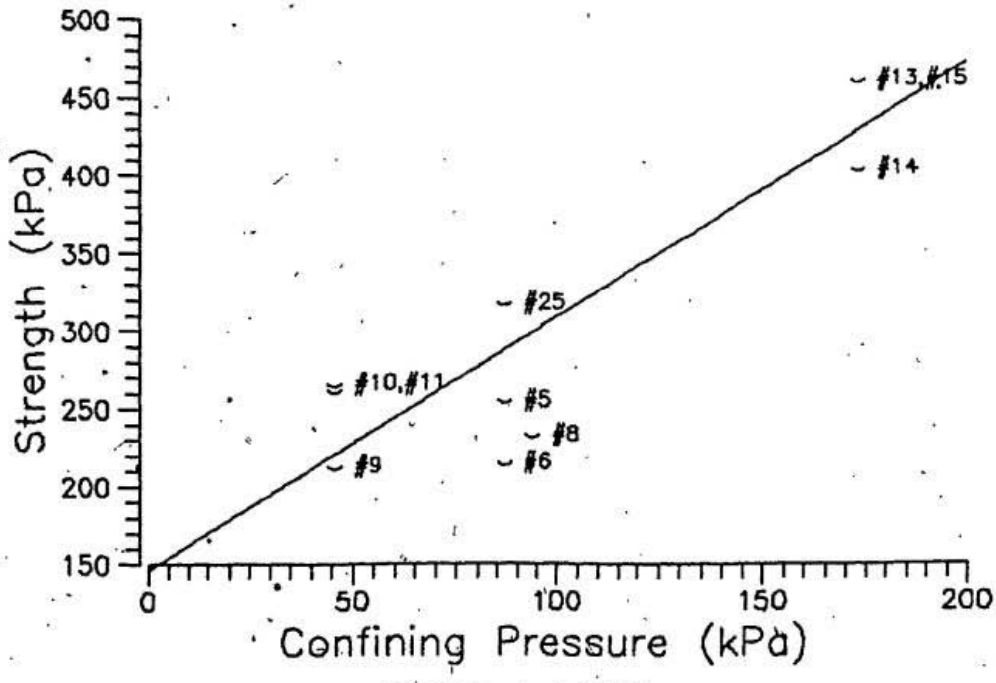

Figure 4.4.17
Strength versus Cell Pressure (4 Hour Consolidation)

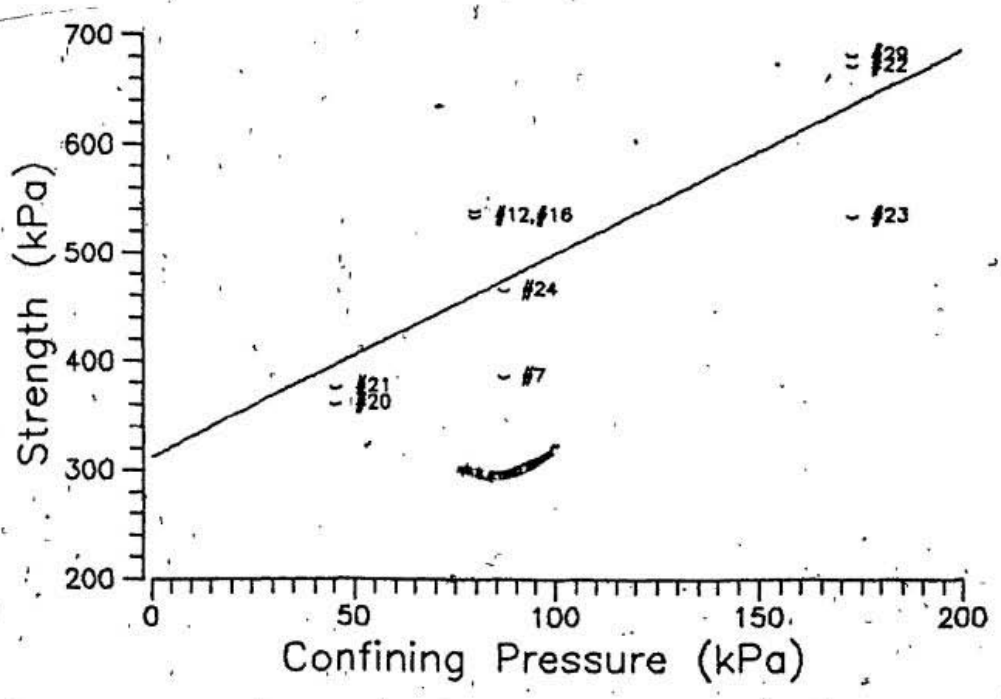

Figure 4.4.18
Strength versus Cell Pressure (19 Hour Consolidation)

strain harden. A temperature increase from -10 to -5 degrees C results solely in a slight decrease in ice strength.

In order to visualize the failure criterion for the material, two representations are used the Mohr's circle plot and the stress path representation. Information on these methods can be derived from most soil mechanics text (Craig, 1974). Figures 4.4.19 and 4.4.20 illustrate the stress paths for all the four and nineteen hour consolidated specimens separately. From the range of cell pressures used in these tests, the failure surface can be approximated by a straight line with a slope, alpha', and y-intercept, a',

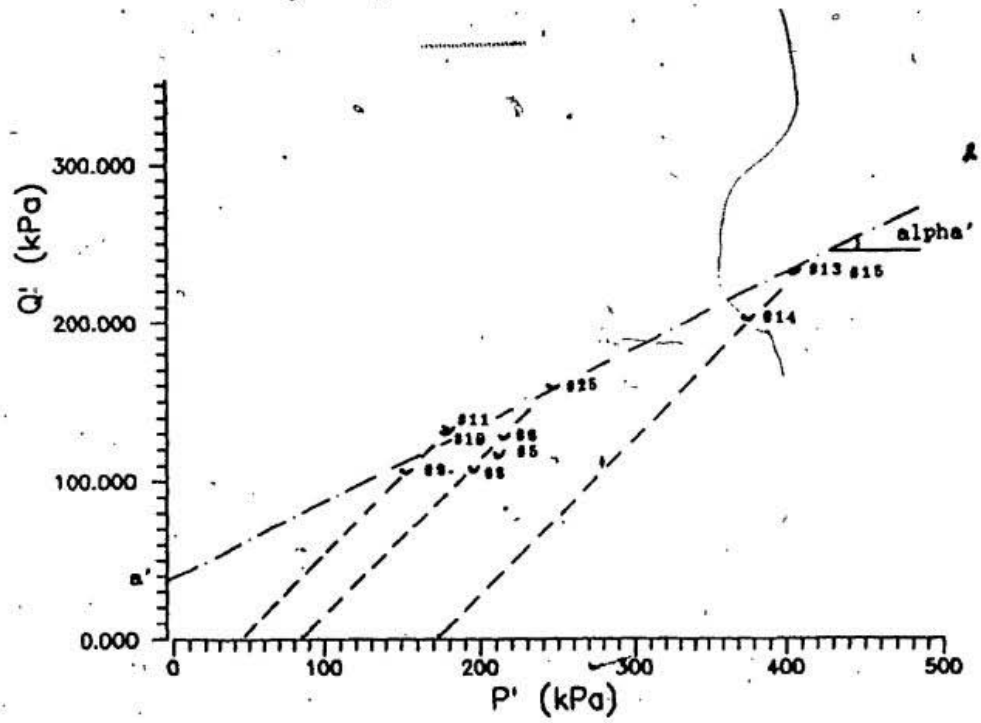

Figure 4.4.19
Stress Path Representation, Test Strength Values
(4 Hour Consolidation)

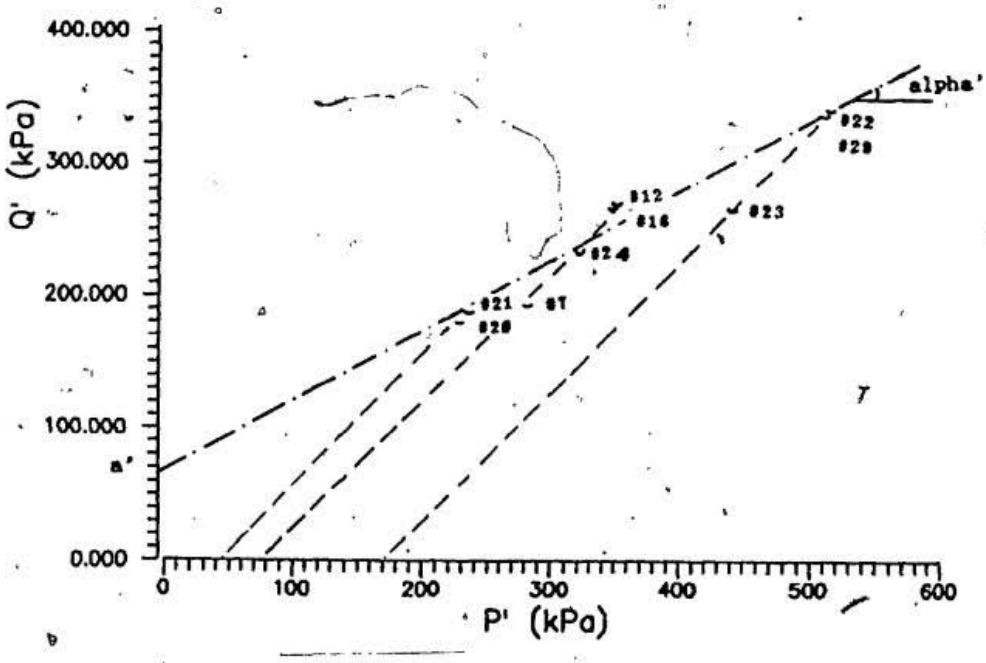

Figure 4.4.20
Stress Path Representation, Test Strength Values
(19 Hour Consolidation)

TABLE OF STRESS PATH AND MOHR'S FAILURE CRITERION RESULTS

Method	Consolidation Time (Hours)	C' kPa	PHI' degrees	a' kPa	alpha' degrees
Mohr's Failure Criterion	4	55	26.6	-	-
	19	75	32.6	-	-
Stress Path Method	4	-	-	35	25.0
	19	-	-	65	28.4
Stress Path Parameter Converted	4	39.6 (36.4% error)	27.8 (6% error)	-	-
	19	77.3/3.1% (3.1% error)	32.7/0.3% (0.3% error)	-	-
		average = 69 kPa	= 28 degrees		

Notes: Formulas for conversions.
PHI' = sin-1 (tan alpha')
C' = a'/ (cos PHI')

Table 4.4.3
Summary of Failure Criterion Results

these modified parameters are indicated in Table 4.4.3. Figures 4.4.21 and 4.4.22 portray the stress paths for the above tests up to the final strains and the associated failure envelope.

The Mohr's circle form of the above groups of tests are depicted in Figures 4.4.23 and 4.4.24. The failure envelope here is described by c', cohesion, and phi', the angle of internal friction. The results are expressed in the Table 4.4.3 along with the percent error calculated when converting the modified parameters to c' and phi'. The average values for the spray-ice were c'= 69 KPa and phi'=

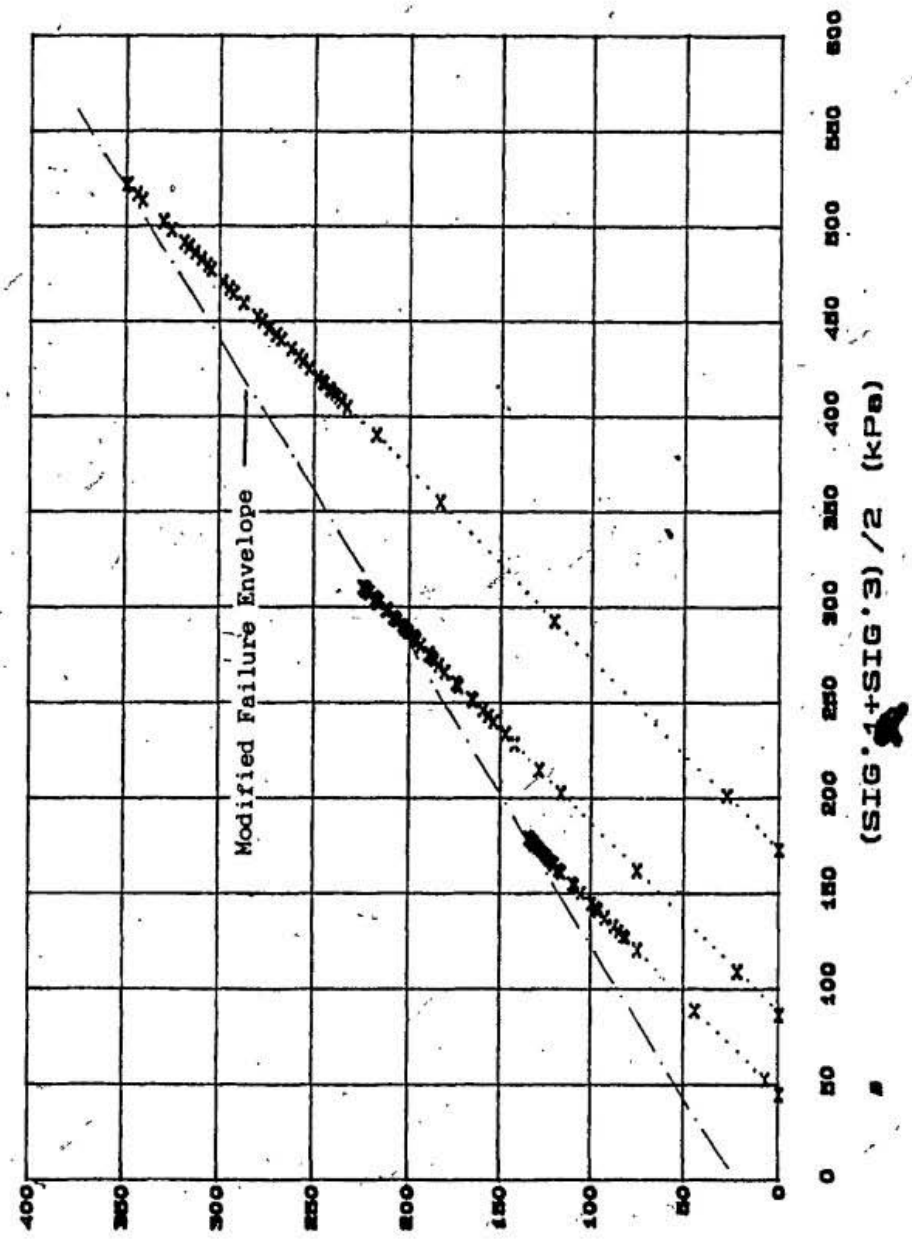

Figure 4.4.21
Stress-Path Representation of Complete Test History
(4 Hour Consolidation)

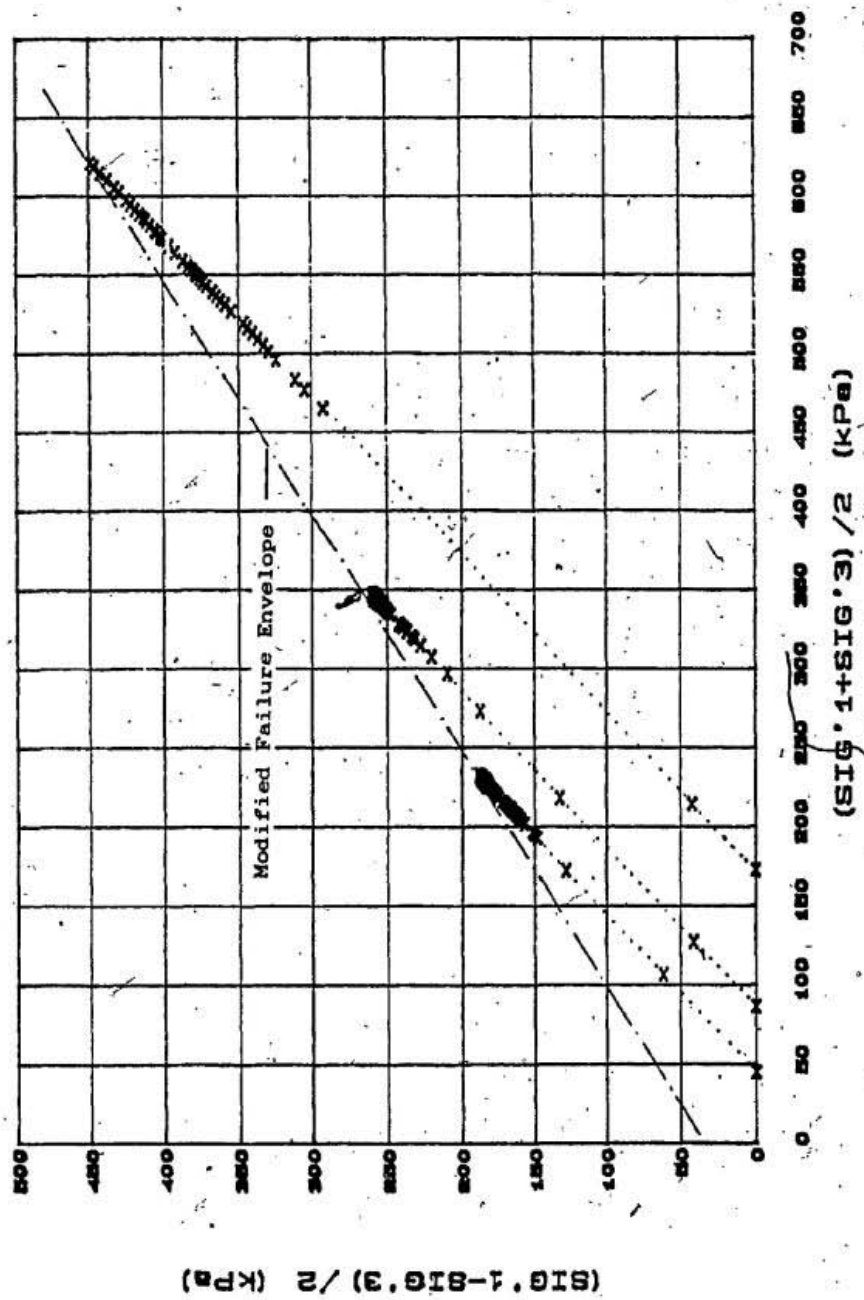

Figure 4.4.22
Stress-Path Representation, Complete Test History
(19 Hour Consolidation)

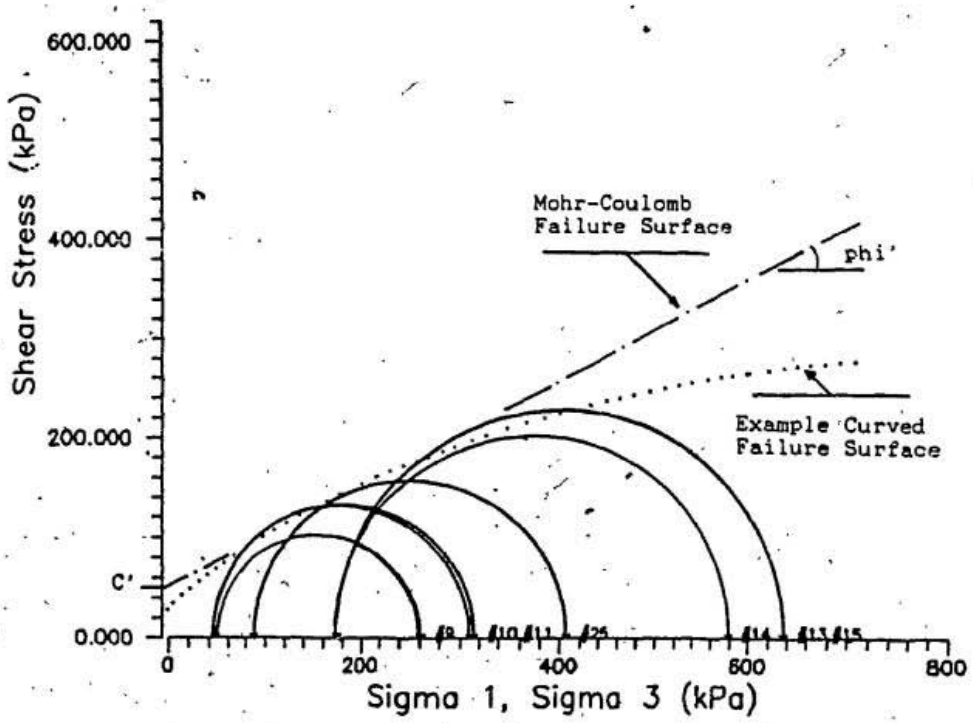

Figure 4.4.23
Mohr Circle Representation, Test Strength Values
(4 Hour Consolidation)

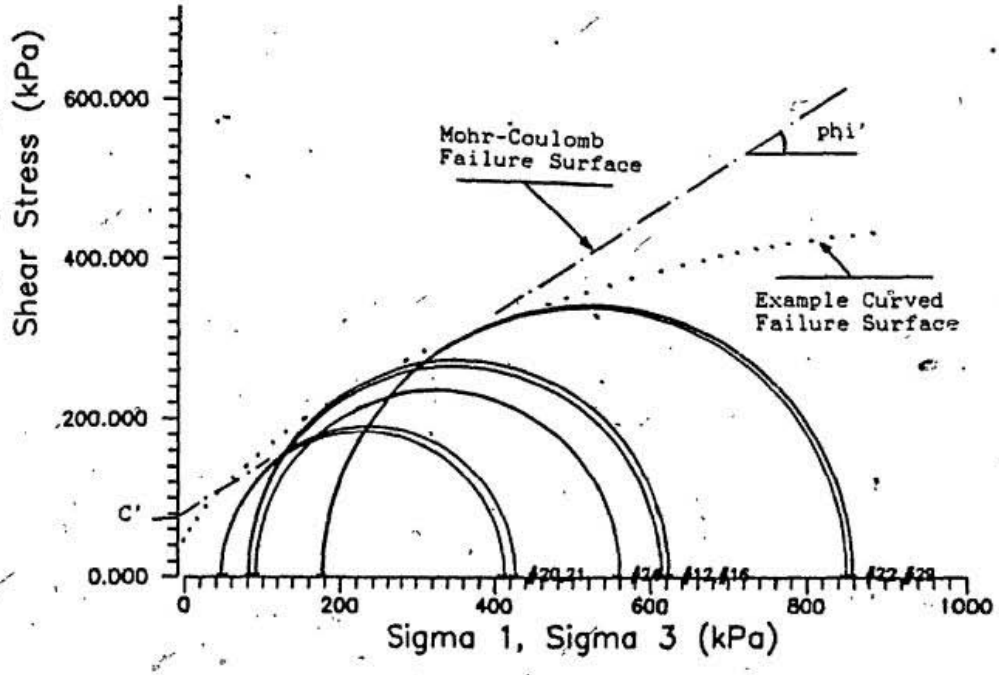

Figure 4.4.24
Mohr Circle Representation, Test Strength Values
(19 Hour Consolidation)

28 degrees, this average did not include the low value for cohesion found in the stress path method. A curved failure surface is also shown on the plots of Mohr's circle, as this may be a more appropriate shape. The shape of the failure envelope will be further discussed in the discussion of results.

The following Table 4.4.4 illustrates some of the ice properties derived from the stress-strain curve. These

TABLE OF SPRAY-ICE PROPERTIES

Test No.	Failure Strain (percent)	Tangent Modulus Ei, (MPa)	Porosity (percent)
5	1.49	28.50	37.6
6	0.24	87.60	35.1
8	3.32	12.10	35.6
25	1.71	69.30	30.5
9	5.15	3965.00	40.2
10	5.12	33.70	30.8
11	2.67	50.70	31.8
13	0.91	70.40	26.3
14	1.58	89.90	30.7
15	0.82	227.10	28.9
7	0.62	174.00	35.5
12	0.96	108.90	29.1
16	0.53	405.90	28.7
24	1.19	121.90	28.7
17	1.01	82.30	20.5
18	0.44	125.80	25.3
19	0.39	106.10	24.2
26	0.71	57.90	33.7
20	8.36	98.30	31.8
21	4.03	165.10	28.4
22	1.57	217.00	25.6
23	1.34	109.60	30.7
29	1.19	178.20	30.1
27	1.68	79.70	30.7
28	1.25	61.70	31.2

Table 4.4.4
Spray-Ice Properties

properties include the percent strain at ice failure, the initial tangent modulus and the porosity. The strain at failure varied from over eight percent to less than half a percent. Generally the higher values are found in the tests with the lowest confining pressure. They did not appear to be a function of sample initial density or consolidation time. The tangent moduli as derived from the initial slope of the stress-strain curve averaged 150 KPa. The initial porosity of the samples were also calculated giving results of 30 percent plus or minus 10 percent.

IV.5 Crystallography of Ice Cores and Samples

IV.5.1 Introduction

In the following paragraphs the crystallography of representative cores taken from the three pressuremeter testing projects and from triaxial test specimens will be described. Before examining the results, the basic ice structure, the ice classification system and the information attained from thin sections will be reported on. Much of this background information was derived from Michel's (1978) text on Ice Mechanics.

The solid ice crystal exhibits a hexagonal structure, which consists of a tetrahedral arrangement of oxygen atoms that are surrounded by pairs of hydrogen atoms. The positions of the hydrogen atoms are not fixed, they move and are often shared by the oxygen atoms. The molecules in the solid ice crystal are concentrated on what is called basal planes. Normal to this basal plane is the axis of principal symmetry called the c-axis. As ice has a very open structure it also has a low density.

The classification system for solid ice includes river, lake and sea ice, not glacier ice. Ice found in nature may consist of several layers; primary, secondary and superimposed. The primary layer is the first formed and grows horizontally, while the secondary layer grows parallel to the heat flow and has a texture which is

controlled by the primary layer. Ice in the secondary layer may be columnar grained in the horizontal or vertical direction and the c-axis can be orientated in a preferred direction. The superimposed ice is formed on top of the primary layer by snow or flooding.

Thin sections are made by cutting very thin slices of ice from a sample, mounting them on a slide and viewing the ice through cross-polaroid lenses. From the thin sections the ice structure, grain size and shape and orientation of preferred c-axis may be evaluated.

The thin sections for this project were made in the cold room of the Institute of Marine Dynamics, St. John's (National Research Council). A slice, approximately 10 mm thick, was first cut from a sample and its orientation labelled. Next, a glass slide was briefly heated and the sample placed on the slide. When the ice was secured to the slide without any visible air pockets the thickness of the ice was further reduced with a band saw. The slide was then placed in a microtome which shaved the ice down to a adequate thickness depending on its structure. The section was the correct thickness when the crystals could be clearly seen between the polaroid lenses. Photographs of thin sections are shown in Appendix C .

IV.5.2 Thin Section Results

Four examples of the ice tested on the LIMEX experiment

are shown in Appendix 'C'. All these thin sections were taken vertically through the ice, perpendicular to the ice surface. What is noticed initially is the variation in the ice type. In section #1 the ice is fine to medium grained, approximately 1 to 3 mm in diameter with mostly sub-rounded grain shape. The grains are not orientated in any particular direction. Sections #2, #3 and #4 show a medium to large grain size and columnar grained as well as equiaxed ice structure. The equiaxed ice has a grain size of approximately 1 to 4 mm and is irregularly shaped. The columnar ice varies from 2 to 10 mm and 5 to 20 mm across its short and long axis respectively. In section #4 two separate layers of columnar ice are evident both vertically orientated. Section #2 shows the ice orientated at approximately 45 degrees to the vertical with fairly large grains. Finally section #4 has columnar ice intermixed with the equiaxed ice structure.

The variation in the ice type is due to the floe formation. The ice floes that were tested were composed of first-year ice that had broken off from shore-fast ice. Over time, the floes may change as snow and water accumulate on their surface and they rotate and join together. Some of the floes are partially composed frozen slush-ice.

A few representative thin sections from the Resolute experiment are also pictured in the appendix. In some cases the damaged area of crushed ice from the indentation tests

can be seen in the photographs; this is not part of the normal ice structure. In total two vertical thin sections and two horizontal thin sections are shown. Photographs 3 and 4 are taken from the same test site. From the vertical sections, the ice appears to be all columnar grained. The grain shape seen in the horizontal sections is very irregular and the grain size is large. The size of the grain is rather difficult to determine due to its structure; but it is in the range of 10 to 25 mm in diameter in the horizontal plane. The length of the columns extend, for the most part, past the length of the sections (approximately 10 cm).

In the appendix four thin sections are shown of the spray-ice cored from close to pressuremeter test #1 during the Calgary tests on spray-ice. The horizontal sections are taken at depths from approximately 0.17 through to 0.5 meters. All of the sections show a similar structure; equiaxed grains that are rounded to subrounded in shape. The grain size of the crystals varies with depth. As the spray-ice was deposited in many layers anywhere from 5 to 20 cm in thickness, the grain size is a function of the conditions while spraying rather than depth. The grain size appears to vary between less than 1 mm to 2 mm. In sections #2 and #4 large crystals are also evident these are from the process of adhering the ice to the slide. The sections had to be cut very thin as the crystal size is so small, thus

holes in the ice can be seen in sections #1, #3 and #4.

Finally, a few sections were performed on the triaxial test specimens. They were taken horizontally from close to the center of the sample. Again some of these sections are in poor conditions due to the thinness that was required. The ice is equiaxed, with subrounded grain shape and grain size mostly between 1 and 2 mm in diameter. It is beneficial to see that the sections of the spray-ice from Calgary are similar in structure and grain size to those of spray-ice formed in the laboratory.

V DISCUSSION OF RESULTS

V.1 Introduction

In the literature review it was shown that spray-ice was a viable construction material but there was a lack of published information on its mechanical properties, partly due to the large expense of field work to collect samples. It was also evident that more experimentation is needed to improve the efficiency of producing spray-ice and its quality. The literature review gave examples of various tests conducted on several types of ice with emphasis on the pressuremeter test.

In the present work, it was decided to establish a means of making spray-ice in the laboratory and to evaluate the material through triaxial tests. As part of the testing program on-site pressuremeter tests were performed on spray-ice and two types of solid ice. Finally a field project, whose objective was to improve the quality and efficiency of making spray-ice, was outlined.

In the following paragraphs the results of the above work will be discussed. First, the production of the spray-ice will be evaluated. Second, the results of the spray-ice pressuremeter tests will be compared with the findings from tests performed with the same equipment and with other pressuremeter tests on ice and soil. Finally, the results from triaxial tests will be evaluated by comparison with previous triaxial tests on spray-ice,

solid, granular ice, snow and soil. In order to view spray-ice as a material it was deemed important to compare it to soil as well as ice. Completing this section are a few remarks on observations made during these experiments and some suggestions for future work.

V.2 Laboratory and Field Production of Spray-Ice

The results of the full-scale project for the production of spray-ice designed and carried out by ERCL and EPR are given in section 2 while the results of the laboratory formation of spray-ice at MUN are detailed in section 3 of the experimental results.

The intention of the Esso project was to improve spray-ice construction techniques. Although some of the detailed objectives of this project could not be met for various reasons, the project was valuable in demonstrating that spray-ice could be made on a large scale outside of the arctic and could be tested for quality and volume during changes in test and field conditions. It further illustrated the benefit of adding compressed air to the spray and the usefulness of employing different nozzle types over the temperature range of -25 to -10 degrees C.

The purpose of manufacturing spray-ice in the laboratory was to provide an adequate amount of test material that was of consistent quality and comparable to that produced in the arctic. From the literature review

conducted it appears that spray-ice had not been produced on a small scale in a cold room previously. Either samples were shipped from sites in the arctic or more recently artificial snow from ski slopes was used for test material. Samples from the arctic were not only expensive to retrieve but also could deteriorate during sampling and shipping and were often inconsistent in nature. Artificial snow may not be exactly the same as spray-ice and is not always available. It is encouraging therefore to be able to produce spray-ice relatively easily in the cold room.

Through experimentation it was possible to attain a spray-ice of the required salinity range and of the correct grain size. The thin sections performed show that the field and laboratory produced spray-ice compare well in grain shape and size. These results also agree with those found in the literature.

V.3 Pressuremeter Test Results

V.3.1 Introduction

A summary of the results from pressuremeter tests completed on spray-ice are outlined in Table 5.3.1 with more detailed information given in section 1 of the experimental results and in Appendix A. The pressuremeter has become widely used as an insitu method of measuring properties of ice as well as soil. However from the literature review conducted few papers have been published

COMPARISON OF PRESSUREMETER RESULTS

Author/ equipment	Material Type	Temperature (deg. C)	Test Type	Time/stage	Rate	Ep (avg) KPa	Pl (avg) KPa	Ep/Pl	Fracture Strength KPa	Compressive Strength KPa
Ladanyi,1978b Menard (G)	sea ice	-4	stress	2 min	100-400 kPa/min	96-212	4.2-6.7	20.20	N/S	N/S
Fougeras,1983 Menard (GC/LLY)	soft clay	N/S	stress	1 min	N/S	1.5/1 %	0.15/0.17	9.60	N/S	N/S
	medium clay	N/S	stress	1 min	N/S	10.9/10.5	0.80/0.73	14.10	N/S	N/S
	stiff clay	N/S	stress	2 min	N/S	26.2/22.5	-/1.60	15.20	N/S	N/S
	loose sand	N/S	stress	2 min	N/S	4.4/3.3	-/0.21	18.30	N/S	N/S
	medium sand	N/S	stress	1 min	N/S	19.3/16.6	2.60/2.20	7.48	N/S	N/S
Michel,1985 high speed, portable	freshwater S1	0.0	strain	immediate	1*10E-3/s	N/S	8.0	-	6.8-7.2	14.1 +/-1.0
	superimposed T2	-5	strain	immediate	1*10E-3/s	N/S	7.9-8.0	-	5.9-7.2	12.8 +/-1.6
	superimposed T3	0.0	strain	immediate	1*10E-3/s	N/S	7.4	-	4.7	12.8
	superimposed T1	0.0	strain	immediate	1*10E-3/s	N/S	5.3	-	2.6-3.0	5.6 +/-0.8
Current Study Resolute,1987 Texam	sea ice	-10 to -15	stress/ strain	2 min	400 kPa/min 2*10E-3/s	63-152 61-104	7.0-9.2 3.1-5.2	13.05 19.30	N/S	N/S
LIMEX,1987 Texam	sea ice	-2	strain	2 min	2*10E-3/s	8.2-31.3	0.47-0.79	26.00	N/S	N/S
Spray-Ice,1988 Texam	freshwater	0.0 to -1	stress/ strain	2 min	37-75kPa/min 2*10E-3/s	4.5-6.8 1.9-3.1	0.734-0.866 0.22-0.35	10.55 9.04	0.289	0.578
Masterson,1987 borehole jack	spray-ice Cape Alison C-47	N/S	N/S	N/S	1*10E-3/s	3814 +/-3553	-	-	N/S	9.07 +/-4.85
	flooded ice East Drake	N/S	N/S	N/S	1*10E-3/s	3583 +/-3288	-	-	N/S	9.24 +/-5.19
Masterson,1988b borehole jack	spray-ice Buckingham 0-68	N/S	N/S	N/S	1*10E-3/s	2396 +/-2371	-	-	N/S	15.3 +/-4.5

Notes:Test #3 not included in spray-ice average.
Masterson's value for Ep is the elastic modulus.
Michel's and the current study values for compressive strength are pressuremeter parameters.
N/S- value not stated in report.

Table 5.3.1
Comparison of Pressuremeter Results

on the pressuremeter in spray-ice although proprietary reports do exist. Thus the use of the pressuremeter in this work is of interest from a results as well as an operational point of view. The results will be compared to those of others found in the literature and those conducted during this work. The success of the operation of this particular pressuremeter in spray-ice and solid ice will also be assessed.

V.3.2 Comparison with Resolute and LIMEX Results

The majority of the pressuremeter tests that have been performed on ice are long-term creep or relaxation tests whose results are not comparable to the short-term strength tests performed in this experiment. The tests conducted in Resolute and on LIMEX are pertinent to this report as the tests were of the same type, conducted under similar conditions with the same equipment.

The pressuremeter used in this experiment was the Roctest, Texam pressuremeter. It had advantages that it was simple to operate and robust. This is important for the field work in a harsh environment as found in the arctic. It was also portable and easy to maintain. A few aspects of its design caused problems during operation, as outlined below. The pressuremeter must be checked before each test to ensure full saturation, especially during large variations in temperature. The metal strips reinforcing the

rubber membrane became distorted during low temperature testing. While testing spray-ice, ice granules became caught between the rubber membrane and the strips. When the metal strips became severely deformed, the membrane was changed and the spray-ice was removed from the probe by disconnecting it and slightly warming the membrane. It would be relatively simple to adapt the probe so that the metal strips were not required. At cold temperatures, a lower viscosity fluid should be used, as the probe did not quickly deflate. Finally to perform creep or other longer term tests it would be useful to connect the control box to a personal computer.

The results of this study will be examined in terms of the pressuremeter modulus (Ep), the pressure limit (Pl) and in some cases the ratio of Ep/Pl, the indentation fracture strength (Ti) and the pressuremeter crushing strength (σop). The pressuremeter modulus is a measure of the materials ability to distort in a deviatoric stress field. Ep should not be compared with the modulus derived from oedometer tests as they are both measured under different conditions. The pressure limit is the limiting state of failure of a material subjected to increasing uniform pressure on the wall of a cylindrical cavity. The pressuremeter crushing strength is not the same as the uniaxial crushing strength due to the tridimensional effect of the probe in the borehole. According to Michel (1985), σop should be compared

with uniaxial tests on samples obtained from the pressuremeter test site to derive a coefficient that relates the parameters. As no uniaxial tests were performed on the samples due to time constraints, the parameters Ti and op are of limited value. Michel (1985) found a coefficient value of 3 for T1, T3 and S1 ice. As the snow ice (T1) is the closest to spray-ice in structure this value may be used to generally compare results.

The values of Ep and Pl are compared with those derived from the LIMEX and Resolute experiments which were all performed at a strain rate of 2x10E-3 s^{-1}, with readings taken after a two minute period and with the same equipment. It was found that Ep for Resolute varied from 61 to 104 MPa, LIMEX from 8.2 to 31.2 MPa and the spray-ice from 1.9 to 6.8 MPa. Spray-ice is thus more deformable than either of the first-year or sea ice tested. It is worth noting that although the LIMEX ice was at close to the same temperature and had in some cases a similar ice structure as the spray-ice it was five times stiffer. The deformability of spray-ice may be partly due to it being formed over the ten days prior to testing and not having adequate time to sinter or freeze completely. Both the sintering and complete freezing of the spray-ice would add to the stiffness and strength of the material.

The values of the limit pressure for Resolute were from 3.1 to 9.2 MPa, for LIMEX from 0.47 to 0.79 MPa and

for spray-ice from 0.224 to 0.866 MPa. The difference in strength between Resolute and LIMEX is approximately one order of magnitude. This is partly due to the temperature difference but also to the looser ice structure found in LIMEX ice. On average the spray-ice had about half the strength of the LIMEX ice for the same type of test. This fact is also reflected by the absence of a limit pressure in several of the stress-controlled tests.

Of the five stress and five strain-controlled tests performed the Ep values for the strain-controlled tests were on average half those for the stress-controlled tests. This agrees with the trend from the Resolute data in which the strain-controlled pressure limit and modulus values were 65 and 10 percent lower respectively than the stress-controlled values. As expected the Pl values for the stress-controlled tests on spray-ice were considerably higher than the strain tests.

The Pl values for the strain-controlled tests on spray-ice varied from the average by only plus or minus 21 percent; while the Ep values varied by plus or minus 22 percent. This shows that the material was of relatively consistent quality over the area tested. One of the stress-controlled tests had a notably higher Ep value. This may have been due to the probe penetrating the ice thickness. Its value was not included in the average.

While testing and coring the spray-ice a few

observations were made. The ice had very definite layers some of which were loose or only partially frozen. The ice ideally should have been thicker for testing. In some cases the probe bulged at the top during tests perhaps due to inadequate confinement by overburden pressure.

V.3.3 Comparison with Soils

The results from other pressuremeter experiments performed on soil, sea ice, and a few types of freshwater ice are outlined in Table 5.3.1. The table also presents the author, type of pressuremeter and test information where available.

A brief look at the table shows that the modulus and pressure limit values are in the same range as those for loose sand. Sand also has a similar sort of granular structure as spray-ice. The soil tests were stress-controlled and should be compared with the similar spray-ice tests.

Soils are sometimes classified according to the ratio of Ep/Pl. The Ep/Pl ratio for spray-ice is on average 9.04 and 10.55 for the strain and stress-controlled tests respectively. These values are lower than that for the LIMEX ice (26.0) but in the range of the Resolute values (13.0 and 19.3). For comparison, soil within this range varies from a clay to between a medium and a loose sand. Ladanyi's (1978) work on sea ice had values averaging 30.3,

considerably higher than spray-ice.

V.3.4 Comparison with Ice and Spray-Ice

During investigation by Michel (1985) a similar type of pressuremeter was employed at close to the same temperatures. The strain rate was half of the one used for this study with immediate rather than two minute readings. From reviewing the spray-ice data, the immediate readings were on average 28 percent higher than those taken after two minutes. It is especially interesting to compare the snow ice (T1) with spray-ice, since their structure is similar. The snow ice is formed when snow falls on top of an ice sheet is flooded and freezes. Generally the snow grain size will be significantly smaller than spray-ice and there will be a higher percentage of solid ice. However in our case the spray-ice was partially submerged and had a high percentage of water in its makeup.

From the Table 5.3.1, the average fracture strength for snow ice was 2.8 MPa while for spray-ice it was 289 kPa, the pressure limit for snow ice was 5.3 MPa and for spray-ice 291 kPa. Due to the difference in the immediate and two minute readings the Pl value for spray-ice could increase to about 373 kPa. However, it remains that both values for spray-ice are in the order of one-tenth of snow ice.

Along with the average fracture strength the pressuremeter crushing strength for the spray-ice was

calculated to be 578 kPa on average. A coefficient of 3 was derived by Michel (1985) for snow ice. This value may or may not be close to the value for spray-ice but is deemed a reasonable estimate. This would mean that the average uniaxial strength for the spray-ice tested is in the order of 193 kPa. The triaxial tests with the lowest confining pressure (40 kPa), that is those most resembling uniaxial tests, had an average deviatoric strength of 248 kPa at -10 degrees C. At -5 degrees C, and a cell pressure of 86 kPa the average strength was 160 kPa. The spray-ice pressuremeter tests were performed at a still higher temperature of close to 0 degrees C. The triaxial strength results on laboratory-made spray-ice appear to be in the range as the values derived from the pressuremeter tests.

The borehole jack results from Masterson (1986a) are expressed in terms of the compressive strength and the elastic modulus. The values are not readily available as previously mentioned. However the pressuremeter modulus is in the order of one one-hundreth of the modulus given by Masterson. Also the compressive strength for these pressuremeter tests, employing the coefficient derived by Michel, is approximately one fourtieth of Masterson's value. It is difficult to fully explain the large difference in these results. Masterson's tests were performed on different ice probably at much lower temperatures, at different strain rates. It should be noted that his values for modulus

varied by close to 100 percent, and the strength values by 50 percent. In addition the borehole jack test is different from the pressuremeter test.

Various parameters have been derived in the literature from the basic pressuremeter data. Unfortunately there seems to be little agreement on what is important to determine besides values for Ep and Pl. It would be of interest to compare the properties established for spray-ice with those of dense snow, but the pressuremeter has not, to the knowledge of the author, been used for testing snow.

V.4 Triaxial Test Results

V.4.1 Introduction

The results of the triaxial tests were described in detail in an earlier section. In the following paragraphs these results will be compared with those found for soils, solid and granular ice, snow and finally other spray-ice experiments. The amount of data published on the triaxial tests on spray-ice is very limited, although some uniaxial tests had been performed on field samples. It is important to understand the behaviour of both saturated and dry spray-ice, but for these experiments dry spray-ice was solely considered. It is the simpler material that is easier to test; the tests do not require saturating the sample or testing near the material's melting point.

V.4.2 Comparison with Soils

The results of the spray-ice triaxial tests can be compared with that of soil. The stress-strain curve for spray-ice was [redacted] the majority of cases a bi-linear relationship with increasing stress and no peak stress. This shape of curve is found in loose sands. A dense sand exhibits a peak in the stress-strain curve. The variation in the shape of the curve for sand is due to the interlocking of the particles. Before failure can take place the interlocking must be overcome as well as the frictional resistance. In the case of spray-ice other

factors are also important. In loose sand there is no initial interlocking to overcome so that the shear stress gradually increases to an ultimate value. A decrease in sample volume with testing is evident in loose sand while an increase is seen with dense sand.

In all the triaxial tests conducted but one, a decrease in sample volume, or increase in density, took place similar to the results from the testing of loose sand. Also, higher final densities were noted in tests conducted at the greater cell pressures. It can be concluded from the shape of the stress-strain curve for spray-ice, that its response under load is similar to a dense sand at low cell pressures, while at higher pressures the response is closer to a loose sand.

From the triaxial tests the phi values vary from 27 to 35 degrees for a loose to dense uniform sand with rounded particles. This value increases as the material became well-graded or has angular particles. Sand exhibits no cohesion while spray-ice does. If the Mohr's failure envelope for spray-ice is approximated with a straight line. The cohesion averages 69 kPa and the angle of internal friction 28 degrees. The cohesion of spray-ice could be due to the sintering and regelation of the granules during consolidation. The cohesion would be dramatically reduced if the failure envelope were curved as shown in Figures 4.4.23 and 4.4.24. This would occur if the particles fracture,

crush or melt rather than move during testing. It is likely that there is some cohesion in spray-ice and that the particles crush and pressure melt, especially at higher cell pressures, strain rates and cold temperatures.

V.4.3 Comparison with Solid, Granular Ice and Snow

A large amount of data has been published on triaxial and uniaxial tests on solid ice with little information on granular ice and no triaxial data readily available on snow. Some of this work was described earlier in the literature review. In this section triaxial tests results of the different materials found in the literature will be addressed generally in terms of factors affecting strength. Then these results will be compared in more detail to spray-ice. The representative results used for comparison are from the following work: a study on sea ice by Richter-Menge et al (1986), on broken ice by Gale et al (1986,87) and uniaxial tests on snow by Jellinek (1957), Landauer (1955) and SIPRE Report #18 (1956).

Solid Ice:

From the papers reviewed the general shape of the stress-strain curve will be described for different types of solid ice. Jones (1982) tests on polycrystalline ice found a rapid increase in stress with strain, a peak stress then strain softening or plastic yielding to a residual stress value. In uniaxial tests brittle fracture may occur. For uniaxial tests on polycrystalline ice at a constant

strain rate (Mellor, 1979) the stress-strain curve had a peak value perhaps with some initial cracking and then ductile behaviour. Richter-Menge et al (1986) considered first-year columnar sea ice and found the following forms of the stress-strain curve from triaxial testing: (1) for unconfined tests, a brittle type of failure, (2) for all tests at low strain rates (10E-5 s^{-1}), a maximum stress with strain softening and plastic flow, (3) at a confining stress/axial stress ratio = 0.5 and strain rate =10E-5 s^{-1}, the curve had no peak value, it flattened with high plasticity, (4) at a confining stress/axial stress ratio = 0.75 , some initial yielding occurred before a peak stress was attained. In general the ductility of the ice increases with increasing confinement.

The failure envelope as derived from the stress-strain curve has often been expressed in terms of the Mohr-Coulomb failure criteria. For the case of solid ice this does not appear to apply exactly. Mellor (1979) and Richter-Menge et al (1986) also suggested that it does not strictly behave as a Tresca or Von Mises material even when failing in a ductile manner. Results from Nadreau et al (1988) and Fokeyev (1976) indicated that the angle of internal friction decreases as the cell pressure increases, and the envelope gradually becomes flatter. Instead, a tear drop model was proposed by Jones (1982) in which the differential stress increases quickly with cell pressure

then gradually decreases as the confining pressure is increased.

The effect of confining pressure on deviatoric stress has already been addressed (Jones, 1982). From Richter-Menge et al (1986) there is evidence that strength increases with strain rate and Nadreau et al (1988) also showed it increased with decreasing temperature. Finally Richter-Menge et al (1986) points out that the failure strain decreases with increasing strain rate, and the initial tangent modulus increased with strain rate and confinement ratio.

Granular Ice:

The general shape of the stress-strain curve for snow ice has been shown by El-Tahan et al (1984) and for cohesionless broken ice by Gale et al (1987). The snow ice was formed from material that was about 1mm in diameter and the tests were uniaxial. Snow ice at high strain rates (10E-2 s^{-1}) exhibited a brittle failure while at lower strain rates a more ductile type of failure. In these tests a peak stress was evident then plastic yielding occurred up to a residual stress. At lower strain rates the peak stress was less pronounced.

The results on the broken ice indicated a distinctive bi-linear stress-strain curve with the breakover stress occurring at low percent strains. This cohesionless ice was described by the Mohr-Coulomb failure criteria after results

from direct shear tests (Gale et al, 1986). The angle of internal friction was between 36 and 45 degrees with no cohesion for material less than 9mm in diameter.

The effect of the various parameters on the ice strength were addressed in each of the papers. The snow ice strength gradually increased with strain rate with a deviation where brittle failure occurred. The elastic modulus also increased with strain rate. For the broken ice the breakover stress was found to increase with cell pressure and consolidation time. The increased consolidation time affected the stiffness and void ratio of the material. At lower consolidation pressures the stress strain curve was flatter. All of the samples displayed contraction during shear. In the paper the ice behaviour was compared to that of a loose Sacramento sand.

Snow:

The following descriptions of snow are based on uniaxial and shear box tests as triaxial information was not available. A stress strain curve for snow is shown in a paper by Landauer (1955). It indicates an increasing stress at a continually decreasing rate. As time progressed stress relaxation occurred and an equilibrium value of stress was approached. The curve does not have a definite break in it like the bi-linear curve described earlier.

It was found that the equilibrium stress was a function of strain rate. The stress increased with strain rate and

was a function of test temperature and sample density. Also the stress values could vary with the snow type.

The SIPRE report #18 showed that the crushing strength of snow cylinders increased with snow density in a linear fashion. The samples deformed by 'mushrooming' at the top or bottom of the sample before rupture. Double shear tests on snow cylinders outlined in this report provided information for a Mohr-Coulomb failure envelope. The strength and lateral pressure points formed a curve which flattened to a residual value rather than a straight line. It was suggested that this could have been due to the nature of the tests; that is the shear rather than triaxial tests. From tension and compression tests a straight failure envelope was formed. It had an angle of internal friction of 19 to 23 degrees and a cohesion of 204 to 1069 kPa.

Jellinek (1957) performed uniaxial tests on snow cylinders to study the strength as a function of age and particle size. The grain size for these tests was less than 1.19 mm. It was found that a small amount of aging increased the compressive strength of the snow dramatically but with increased aging the strength reached a constant value. During this aging of the samples no confining pressures were applied. The age of the snow prior to forming the sample also appeared to affect the strength. Finally an appreciable decrease in strength occurred with a decrease in the particle size. It was suggested that aging process

affected the recrystallization, diffusion and sublimation in the contact areas of the snow particles. As the snow particles become more rounded with time, the system became more stable with age.

In the following paragraphs the spray-ice results will be compared with those described earlier in this section. This comparison will be based on the following; the stress-strain curve, the failure envelope, general trends with the various test conditions and finally actual strength and material property values. Examples of the results of the tests described earlier are outlined in Table 5.4.1, along with sample results from the spray-ice tests. The tests selected from the literature were those whose conditions agreed most closely with those of the spray-ice tests.

The shape of the stress-strain curve for spray-ice most closely follows the findings of Gale on cohesionless broken ice. Both exhibited bi-linear relationships with the breakover stress occurring at low percent strains. Gale found that at lower cell pressures the curve flattened, as with spray-ice. However some of the tests conducted on spray-ice gave peak stresses followed by ductile behaviour. The stress-strain curve for spray-ice changes with test conditions as was found in the report by Richter-Menge. For solid ice the bi-linear relationship was not evident. The uniaxial stress-strain curve for snow had a similar shape

TABLE OF TRIAXIAL AND UNIAXIAL TEST RESULTS ON SOLID AND GRANULAR ICE AND SNOW

Author	Ice Type	Temperature (deg.C)	Test Type	Strain or Loading Rate	Strength (kPa)	Modulus	Failure Strain %	Confining Pressure	Density g/cm^3	Consolidation Time (hrs)
Richter-Menge 1986	columnar first-year	-10	triaxial	10E-3/s	6,560	7.92 GPa	0.125	0	0.904	0
				10E-5/s	1,500	4.88 GPa	0.141	0		
	C-axis at 90 deg.	-10	triaxial	10E-3/s	9,890	6.58 GPa	0.382	R/A=0.25	0.919	0
				10E-5/s	1,370	-	0.292	R/A=0.25		
Gale 1986,87	cohesionless broken ice	-2	triaxial	5.6*10E-5/s	350	N/S	L.T. 0.5	200 KPa	0.596	4.2
		-2	triaxial	5.6*10E-5/s	120	N/S	L.T. 0.5	70 KPa	0.519	4
		-2	triaxial	5.6*10E-5/s	625	N/S	L.T. 1.0	200 KPa	0.639	24.2
SPIRE #18 1956	snow	-10	double shear	34.5 kPa/s	1611	N/S	N/S	207 KPa	0.646-0.65	0
		-10	double shear	34.5 kPa/s	992	N/S	N/S	0	0.65-0.677	0
		-10	uniaxial	51 kPa/s	2200	N/S	N/S	0	0.642	0
Landauer 1955	snow	-10	uniaxial	4*10E-4/s	230-400	N/S	N/S	0	0.42	0
Jellinek 1957	snow	-10	uniaxial	51 kPa/s	330-510	N/S	N/S	0	0.549-0.55	5.9
					360-640	N/S	N/S	0	0.549-0.55	21.7
Current Study	spray-ice	-10	triaxial	1.4*10E-4/s	248	129 MPa	1.10	45 kPa	0.632	4
	spray-ice	-10	triaxial	1.4*10E-4/s	319	62 MPa	1.69	86 kPa	0.639	4
	spray-ice	-10	triaxial	1.4*10E-4/s	443	42 MPa	4.31	172 kPa	0.657	4

Notes: N/S-value not stated in report.
L.T.-less than.
The spray-ice modulus is actually a tangent modulus.
SPIRE #18, tensile and crushing strength tests showed C'=204-1069 kPa and PHI'=19-23 deg.
Gale, direct shear tests gave C'=0 kPa and PHI'=36-45 degrees.
Richter-Menge, confining pressure is given in terms of radial/axial stress (R/A).
Snow consolidation time is sample aging time.

Table 5.4.1
Triaxial and Uniaxial Test Results

as that for spray-ice at the lowest cell pressure and consolidation time. It would be of interest to study the effect of confining pressure on snow through triaxial tests.

The failure envelope has been described for solid ice, granular ice and snow. The available values for cohesion and the angle of internal friction are shown in Table 5.4.1. For solid ice there seems to be an agreement that it does not exactly follow the Mohr-Coulomb failure criteria, as the failure envelope is curved. The direct shear tests that were performed on granular ice gave values of the friction angle with a cohesion of zero. Results from the experiments on snow indicated a curved failure surface similar to that of solid ice. The spray-ice triaxial tests gave a failure surface with a slight curve. More tests are required to confirm these results. It is anticipated that spray-ice would have some cohesion but lower than that for snow.

The results shown in Figures 4.4.12 through 4.4.18 indicate that the spray-ice strength increases with increasing cell pressure, consolidation time and strain rate and in all likelihood decreases with temperature. Also the higher density ice appeared to give greater strength values. These findings agree with those for solid ice, granular ice and snow. The effect of consolidation time was considered for granular ice only while the effect of aging was of interest in snow. The work reviewed on snow did not cover the effect of strain rate and confining pressure. The

effect of temperature was looked at in detail for solid ice and to lesser degree for snow. Mathematical relationships are not proposed for the trends seen in the spray-ice strength, as the amount of data available does not make it appropriate.

The actual strength values for spray-ice are in the range of those for broken ice (Gale et al, 1986, 1987) and low density snow (Landauer, 1955 and Jellinek, 1957). For the majority of the tests on snow the loading rates were higher than those in this work. This would result in an increase in the strength values. The double shear tests with lateral pressure had results that were not readily comparable to the triaxial results for spray-ice.

Modulus values for snow ice and solid ice ranged from 3.25 to 4.88 GPa, while for spray-ice they were between 29 to 227 MPa, about an order of magnitude difference. The failure strain for spray-ice was for most cases between 0.24 to 1.71 percent, while for solid ice it was 0.125 to 0.382 percent and for granular ice from about 0.3 to 1.3 percent. Again, spray-ice more closely resembles granular ice than solid ice. The solid ice being more brittle, it failed at a lower test strain. Finally the porosity values for spray-ice were higher than solid ice as expected. It should be noted that those tests reviewed on ice and snow were performed under different conditions and with different equipment than employed in this experiment which

would affect the results.

From the above discussion it is evident that although spray-ice follows a similar type of failure envelope as snow and solid ice, the shape of the stress-strain curve is notably different. In this way it acts more like the broken ice described by Gale. It's strength is approximately one-tenth that of solid ice, similar to broken ice and snow. The properties derived for solid ice may not be applicable in describing spray-ice. Spray-ice behaviour cannot be adequately described by any of the above categories at least until further work is performed.

V.4.4 Comparison with Spray-Ice

A variety of tests have been performed on spray-ice, both in the field and laboratory. The results of these tests will be discussed in comparison with the results from this investigation. As triaxial tests on dry spray-ice were conducted in this work, these results are mainly of interest; however, due to limited data available other tests will be considered. The information will be compared in terms of: the stress-strain curve, the failure envelope, how factors affect the spray-ice strength and finally actual strength values as outlined in Table 5.4.2.

The shape of the stress-strain curve has been described by Weaver et al (1986) and Prodanovic (1986). Prodanovic

TABLE COMPARING TESTS ON SPRAY-ICE

Author	Location	Test Type	Spray-Ice	Temp. deg. C	Density g/cm^3	Salinity ppt	Strain Rate 1/s	Strength KPa (Std Dev)	Modulus KPa (Std Dev)	Confining Pressure
Kemp 1984	Alark ice pack	confined insitu	1m	-5 to -19.5	540 - 870	15-20	10E-3	7.3	N/S	N/S
		uniaxial on site	1m	-2 to -22	540 - 870	15-20	N/S	0.2 - 3.4	N/S	0
Masterson 1987	Cape Allison C-47	uniaxial	-	N/S	882	7.3-14.2	10E-3	1.96 +/- 1.3	2328 +/- 1102	0
		flatjack confined	-	-24	882	18.3	10E-6	3.94 +/- 0.7	3361 +/- 839	N/S
		borehole jack confined	-	-24	882	18.3	10E-3	9.07 +/- 4.2	3814 +/- 3553	N/S
Masterson 1986b	Buckingham 0-68	uniaxial	-	N/S	847	11.5	10E-3	2.3 (1.02)	1285 (382)	0
		flatjack confined	-	N/S	710	16.3	10E-6	1.87 (0.22)	1060 (285)	N/S
		borehole confined	-	N/S	710	16.3	10E-3	15.2 (4.5)	2396 (2371)	N/S
		triaxial	-	N/S	847	11.5	10E-3	23.3 (1.23)	1672 (911)	10.3 KPa
Masterson 1986a	N/S	unconfined	dry	-5	600-900	N/S	N/S	1.5	2000	0
		compression	dry	-12	600-900	N/S	N/S	3.5	2000	0
		compression	saturated	-2	700-900	N/S	N/S	0.90-1.60	0-1000	0
Weaver 1986	laboratory	triaxial	0.4-0.63	-18	551	0	6.8x10E-5	0.127	N/S	40 KPa
				-5	564	0	7.0x10E-5	0.100	N/S	40 KPa
				-2	548	0	6.8x10E-5	0.87	N/S	60 KPa
				-2	557	0	6.8x10E-5	0.117	N/S	20 KPa
Prodanovic 1984	laboratory	uniaxial	N/S	-10	553-749	2.4-7.2	10E-5	0.236-736	N/S	0
		uniaxial	N/S	-10	657-694	2.8-3.2	10E-3	0.236-995	N/S	0
Current Study 1988	laboratory	triaxial	L.T. 1mm	-10	657 avg.	7.5-17	1.4x10E-4	0.443 avg.	129	172 KPa
				-10	639 avg.	7.5-17	1.4x10E-4	0.319 avg.	62	86 KPa
				-10	632 avg.	7.5-17	1.4x10E-4	0.248 avg.	42	45 KPa
				-5	636 avg.	7.5-17	1.4x10E-4	0.160 avg.	71	86 KPa
				-10	665 avg.	7.5-17	1.4x10E-5	0.219 avg.	91	86 KPa

Notes: Kemp reported C'=50-100 KPa, PHI'=0-10 degrees.
Present study reported C'=69 KPa, PHI'=28 degrees.
N/S-value not stated in report.
Weaver, 1986-strength is yield shear strength.
Current Study-strength is hyd/over deviatoric stress.
-modulus is tangent modulus.

Table 5.4.2
A Comparison of Tests on Spray-Ice

reported on the ice island experiment conducted in Prudhoe Bay in 1978-79. In this case the island was formed by flooding, sprinkling and spraying. The method used for spraying with a gun-type spray nozzle, most closely represents what is commonly used in forming spray-ice, therefore these results will be addressed. Unfortunately, as many of these tests were performed in the field or on field samples, the consistency of the results was poor and it was difficult to verify how factors affected the spray-ice strength. The field samples had imperfections and variations in density, quality and salinity. Also the spray-ice formed in the laboratory is a consistent material while the field samples are expected to have strong and weak lenses as well as a higher ice content.

Results from uniaxial tests showed that the shape of the stress-strain curve varied with strain rate. At low strain rates ($10E\text{-}5s^{-1}$) strain hardening was evident. The strength increased rapidly with stress, then after an inflection point the strength either slightly increased or remained constant to the end of the test. The inflection point was at approximately 0.2 percent strain and the test was completed after 2 percent strain. For the strain rate of $10E\text{-}3\ s^{-1}$ a peak stress was reached at 0.3 percent strain followed by strain softening. At the higher strain rates the spray-ice failed in a brittle fashion by fracturing, surprisingly at a lower strength than found

with the slower strain rate tests.

Weaver et al (1986) reported on tests performed on artificial snow compacted into triaxial samples. Both saturated and dry triaxial tests were performed. The dry samples showed a strong bi-linear stress-strain curve in which the stress increased rapidly to the inflection point, followed by strain hardening. The inflection point occurred at less than 0.5 percent strain and the tests were completed by 20 percent strain. The shape of the stress-strain curve did not vary. All of the dry tests were performed at the same strain rate and for the same consolidation time. As the cell pressure was increased the degree of hardening also increased as displayed by the steeper curves.

The [redacted] mentioned results compare well with the findings of this investigation. The shape of the stress-strain curve in this work was bi-linear in the majority of cases. At low confining pressures a peak stress occurred and a sample underwent strain softening similar to the behaviour reported by Prodanovic on unconfined samples. At higher cell pressures and temperatures the bi-linear relationship occurred. The degree of strain hardening increased with cell pressure in a similar manner as reported by Weaver. The increase in strain hardening was due to the densification caused by pressure melting and the regelation process.

Some of the general trends for strength from the

literature are outlined below. In the work by Weaver, the yield stress (occurring at the inflection point) was not particularly sensitive to temperature, consolidation pressure or the samples' final density. Prodanovic concurred that the strength of spray-ice did not appear to be test rate or sample salinity dependent. Prodanovic stated that while the strength was significantly dependent on sample density, there was no marked difference in strength between the horizontal and vertical samples.

Masterson et al (1986(b)) indicated that spray-ice strength increased with decreasing temperature. Kemp (1984) found that for insitu tests spray-ice strength increased with depth to the waterline. The strength also decreased with higher salinities and lower densities. Finally, he also stated that the strength of spray-ice was isotropic.

In the current investigation the increase in strength with increasing sample density and decreasing test temperature was evident as mentioned above, although the dependence of strength on test temperature was not obvious. It was also found that the strength increased with confining pressure and consolidation time, as well as increasing strain rate. The trend towards an increase in strength with confining pressure is similar to the findings by Kemp. Strength variations with salinity were not addressed in this work.

In Table 5.4.2, some values for spray-ice strength and other properties are provided. It should be noted that the tests were performed, in most cases, at different strain rates, temperatures and sample densities. Generally it can be said that for the spray-ice tested, the strength was in the range of the values provided by Prodanovic and Weaver. All modulus and strength values derived by Masterson were considerably higher than those found in this experiment. This could be partially due to testing field specimens.

There are a few problems with comparing the current tests with those of others. The triaxial tests reported by Masterson et al (1986(b)) were condutted at a confining pressure of 10.3 MPa which was several times larger than those used by Weaver and in the current study. Masterson also reported on uniaxial test results which exhibited standard deviations of approximately half the reported compressive strength. In some cases, the standard deviation was as great for the elastic modulus. The confining pressure for the triaxial results by Kemp were not reported, but the average strength was approximately ten times higher than that found by Weaver, Prodanovic or ourselves. The uniaxial tests by Kemp are closer in range to the current tests, however, the strain rate was not indicated.

Weaver proposed that the strength behaviour for spray-ice "may range from the classical frictional

behaviour of granular materials to the non-linear, visco-elastic behaviour of ice." From the work conducted, it is expected that spray-ice is a material similar to solid poly-crystalline ice and snow in which the Mohr-Coulomb failure envelope is curved, rather than a straight line. From this work it was determined that as with snow and soil, the strength of spray-ice is affected by consolidation time. It is also dependent on strain rate, confining pressure and density.

V.5 Observations and Future Work

During the course of this paper several observations were made concerning equipment and procedures which could have been adapted or changed to improve the experimental technique or the results in some manner. These issues will be reiterated in this section. Also, as work progressed it became apparent that in several areas it would be beneficial if further experimentation or analysis were performed. Some of the ideas for future work will be addressed.

The pressuremeter as a means of finding insitu material properties is a very useful piece of equipment. However, it is worthwhile to mention a few concerns with this model. It was found that the pressuremeter could have operated more efficiently at low temperatures if its fluid were less viscous. Problems with the probe membrane leaking suggest that they could be better designed. Finally, the probe also caused problems when the exterior metal strips deformed severely or when spray-ice built up under the metal strips. The borehole for the pressuremeter tests were made with an ice auger for the LIMEX and Resolute experiments. It formed a fairly rough walled hole, which could cause discrepancies in the results. The three inch core barrel used in Calgary was far more suitable for the job.

The production of spray-ice and the triaxial tests were

performed with few difficulties. The major problem was the inconsistent operation of the cold room used both for forming the spray-ice and the triaxial testing. It especially caused concern when storing the spray-ice. The density of the triaxial samples varied by plus or minus ten percent. The error could have been reduced if an accurate higher capacity scale was available. This would have prevented the testing of samples that were not within the required density range. It should also be possible to transfer the incoming data directly to a personal computer, which would make it possible to collect more data points during tests with longer consolidation times and to perform tests more easily at faster and slower strain rates.

Examples of future work that could be completed with the given equipment are: 1) Pressuremeter tests could be performed on spray-ice in the laboratory through the use of a large drum-like container. This would enable various vertical loads to be applied while performing controlled tests on laboratory spray-ice. 2) Creep tests and constant strain tests at various rates could be conducted with the pressuremeter. 3) The ice cores from the field experiments could be used for uniaxial, triaxial or other testing. 4) The triaxial tests performed were very successful but further work could be done at higher and lower strain rates and other temperatures.

It would be of interest to compare the results in this

experiment with tests performed on ice that is formed by salt water spray. This ice is often a problem in the shipping industry. Another comparison could be completed with the crushed ice formed from an ice sheet impinging on a structure. The additional work would further explain the behaviour of spray-ice in relation to other materials.

VI CONCLUSIONS

1) In general the results, including the stress-strain curves and the strength values, of the triaxial tests performed compare well with those previously conducted on spray-ice. It was found that these results are close to those attained for granular ice.

2) The behaviour of spray-ice is similar to that of granular ice and the failure envelope has a shape in agreement with solid ice or snow. It can be said that spray-ice does not act purely as a granular material. It's cohesive properties cause it to behave as a visco-elastic material similar to snow or solid ice.

3) From the triaxial tests conducted the following strength dependencies are realized.

The strength appears to increase slightly with decreasing temperature as it does with solid ice and snow.

The higher confining pressures cause greater strength values and an increase in the strain hardening of the material, as with granular ice.

The longer consolidation times result in an increase in the strength of the ice.

Finally, the lower strain rate and lower sample density

gave slightly lower strength values.

4) Although the results of the pressuremeter tests are considerably lower than those previously reported, they do compare roughly with the triaxial tests performed herein and the variation in the results is small. The pressuremeter tests on spray-ice in the literature provided only values of compressive strength and elastic modulus, and it would require further testing to accurately derive these parameters for this work. Generally the pressuremeter operated well in the harsh conditions. Its continued use to determine spray-ice properties is recommended with the improvements already mentioned.

5) The ERCL experiment completed in Calgary demonstrated that it is possible to perform large-scale tests on spray-ice outside of the arctic and to improve productivity through experimentation.

6) The laboratory production of spray-ice was very successful. Large quantities of good quality material were made in a relatively short period of time.

Through the work performed on spray-ice a clearer understanding of its behaviour has been formulated. There

still exists many options for future work to confirm these findings and to further explain this important and interesting material.

REFERENCES

Baguelin, F., Jezequel, J.F., Lemee, E., Le Mehaute, A., "Expansion of Cylindrical Probes in Cohesive Soils", Jour. Soil Mechanics and Foundations Div., Proc. ASME, Vol. 98, No. SM11, Paper 9377, Nov., 1972.

Baguelin, F., Jezequel, J.F., Shields, D.H., The Pressuremeter and Foundation Engineering, Trans Tech Pub., Clausthal, Germany, 1978.

Baguelin, F., Jezequel, J.F., Shields, D.H., "The prediction of Horizontal Soil Forces using the Pressuremeter", Civil Engineering in the Oceans, Proc. 4th, ASCE, San Francisco, CA, Vol2, pp. 732-744, 1979.

Bishop, R.F., Hill, R., Mott, N.F., " Theory of Indentation and Hardness Tests", Proc. Phys. Soc., Vol. 57, 1945.

Butkovich, T.R., "Studies of the Age Hardening of Processed Snow", CRREL Report #99, June, 1962.

Cox, G., Richter-Menge, J.A., "Triaxial Compression Testing of Ice", Proc. Conference Arctic '85/ ASCE, San Francisco, CA, 1985.

Cox, G.F.N., Utt, M.E., "Ice Properties in a Grounded Man-Made Ice Island" Proc. OMAE, Vol. 4, Tokyo, 1986.

Craig, R.F., Soil Mechanics, Van Nostrand Reinhold Co., Berkshire, England, 1974.

Duthweiller, F.C., Utt, M.E., "Ice as a Construction Material in the Offshore Arctic", Civil Engineering in the Arctic Offshore, Proceedings, 1985.

El-Tahan, H., Swamidas, A.S.J., Arockiasamy, M., Reddy, D.V.,"Strength of Iceberg and Artificial Snow Ice under High Strain Rates and Impact Loads", Proc. 3rd OMAE, Vol. 3, 1984.

Faugeras, J.C., Gourves, R., Meunier,P., Nagura, M.,Matsubara, L., Sugauara, N., "On the Various Factors Affecting Pressuremeter Test Results", Symposium International, Essais in Place In-Situ Testing, Vol. 2, Paris, 1983.

Fokeyev, N.V., "Determination of the Compressive Strength of Artificial Ice Specimens of Different Salinities under Conditions of Combined Stress", Proc. of the Arctic and Antarctic Research Inst., Vol 331, 1976.

Frederking, R.M.W., "Plane-Strain Compressive Strength of Columnar-Grained and Granular-Snow Ice", Jour. of Glaciology, Vol.18, No. 80, 1977.

Frederking, R., Hausler, F., "The Flexural Behavior of Ice from In-situ Cantilever Beam Tests", Proc. IAHR Ice Symp., Lulea, Sweden, 1978.

Funegard, E.G., Nagel, R.H., Olson, G.G., "Design and Construction of the Mars Spray Ice Island", OMAE, Houston, Texas, 1987.

Gale, A.D., Sego, D.C., Morgenstern, N.R., "Behavior of Cohesionless Broken Ice", Canadian Conf. on Marine Geotechnical Engineering, St. John's, Nfld, 1986.

Gale, A.D., Wong, T.T., Sego, D.C. and Morgenstern, N.R. "Stress-Strain Behaviour of Cohesionless Broken Ice", 9th Intn'l POAC, Fairbanks, Alaska, 1987.

Gibson, R.E., Anderson, W.F., "Insitu Measurement of Soil Properties with the Pressuremeter", Civil Eng. and Public Works Review, Vol. #56, No. 658, May, 1961.

Goff, R.D., Thomas, G., Maddock, W., "Applications of Spray Ice and Rubble for Arctic Offshore Exploration", OMAE, Houston, Texas, 1987.

Goff, R.D., Masterson, D.M., "Construction of a Sprayed Ice Island for Exploration", Proc. OMAE, Tokyo, Japan, 1986.

Gold, L.W., "The Initial Creep of Columnar Grained Ice", Canad. Jour. of Physics, Vol. 43, 1965.

Haas, W.H., Bott, M.W., "The CBR Test Applied to Processed and Compacted Snow", Cold Regions Engineering, 1985.

Hausler, F., "Multiaxial Compressive Strength Tests on Saline Ice with Brush-Type Loading Platens", Proc. IAHR, Quebec City, 1981.

Jahns, H.O., Petric, D.H., Lockett, A.V., "CIDS Spray Ice Barrier", OTC, Houston, Texas, 1986.

Jellinek, H., "Compressive Strength Properties of Snow", SIPRE Report #34, Aug., 1957.

Jones, S.J., "The Confined Compressive Strength of Polycrystalline Ice", Jour. of Glaciology, Vol. 28, No. 98, 1982.

Juvkam-Wold, H.C., "Spray Ice Islands evaluated for Arctic Drilling Structures", Oil and Gas Journal, April, Vol. 86, No. 86, 1986.

Keinonem, Nyman, "An Experimental Model Scale Study on the Compressible, Frictional and Cohesive Behavior of Broken Ice Mass", Proc. IAHR Ice Symposium, Part 2, 1978.

Kemp, "Grounded Ice Pads as Drilling Bases in the Beaufort Sea", Proc. IAHR Ice Symposium, Hamburg, 1984.

Ladanyi, B., "Etude Theorique et Experimentale de L'expansion dans un Sol Pulverulent d'une Cavite Presentant une Symetrie Spherique ou Cylindrique", Ann. Trav. Public. Belg., 1961.

Ladanyi, B., "Expansion of a Cavity in a Saturated Clay Medium", Proc. ASCE, 89, SM4, pp.127-161, 1963.

Ladanyi, B., "In-Situ Determination of Undrained Stress-Strain Behavoir of Sensitive Clays with the Pressuremeter", Ecole Polytechnigue, Montreal, April, 1972.

Ladanyi, B., "Quasi-Static Expansion of a Cylindrical Cavity in Rock", Proc. 3rd Symp. CSCE, Vol. #2, 1976.

Ladanyi, B., Barthelemy, E., Saint-Pierre, R.," In-Situ Determination of Creep Properties of Ice Covers by means of Borehole Creep and Relaxation Tests", Proceedings of Workshop on the Bearing Capacity of Ice Covers, Winnipeg, 1978(a).

Ladanyi, B., Saint-Pierre, R.," Evaluation of Creep Properties of Sea Ice by means of a Borehole Dilatometer ", IAHR Symposium on Ice Problems, Lulea, Sweden, 1978(b).

Ladanyi, B., "Borehole Creep and Relaxation Tests in Ice-Rich Permafrost ", Proc. 4th Canadian Permafrost Conference, Calgary, 1981.

Ladanyi, B., "Borehole Creep and Relaxation Tests in Ice-Rich Permafrost", Proc. 4th Canad. Permafrost Conf., the R.J.E. Brown Mem. Vol., Nat. Res. Council, Ottawa, pp.406-415, 1982.

Ladanyi, B., "Borehole Dilatometer Test", Proc. IAHR Ice Symposium, Hamburg, Germany, 1984(a).

Ladanyi, B., Murat, J.R., Huneault, P., "A Parametric Study of Long-term Borehole Dilatometer Tests in Ice", IAHR Ice Symposium, Hamburg , Germany, 1984(b).

Ladanyi, B., Huneault, P., "Use of the Borehole Dilatometer Stress-Relaxation Test for Determining the Creep Properties of Ice", Proc. OMAE, Houston, Texas, 1987.

Lane, J.F., "On the Strengths of Sea Ice and a Correlation between the Various Strength Tests ", Div. of Mechanical Engineering, NRC, Report LTR-LT-104, Sept., 1979.

Landauer, J.K., "Stress-Strain Relations in Snow under Uniaxial Compression", SIPRE Report #12, Feb., 1955.

Man, C.S., "Creep Settlement of Artificial Ice Islands", Proc. OMAE, Houston, Texas, 1988.

Masterson, D.M., Gamble, R.P., "Current Ice Road and Structure Design and Construction Procedures", International Polar Transportation Conf., Vancouver, BC, May 1986(a).

Masterson, D.M., Pare, A., Gamble, R.P., "Construction and Performance of a Floating Ice Platform Built from Sprayed Ice", Arctic Offshore Technology Conf. & Exp., Calgary, Alta., 1986(b).

Masterson, D.M., Baudais, D.T., Pare, A., Bourns, M., "Drilling of a Well from a Sprayed Floating Ice Platform: Cape Allison C-47", OMAE, Houston, Texas, 1987.

Mellor, M., "Snow Mechanics", Applied Mechanics Reviews, Vol.19, No. 5, 1966.

Mellor, M., "Mechanical Properties of Polycrystalline Ice", Proc. IUTAM Symposium, Copehagen, Denmark, 1979.

Menard, L., "Mesure In-situ des Proprietes Phsiques des sols", Annales des Ponts et Chaussees, Paris, No.14, pp.357-377, 1957.

Michel, B., Ice Mechanics, Les Presses de L'Universite Laval, Quebec, 1978.

Michel, B., "A High Speed Borehole Pressuremeter to Measure the Crushing Strength of Ice", M.I.T., Cambridge, Mass., 1986.

Nadreau, J.P., Nawwar, A.H. and Wang, Y.S., "Triaxial Testing of Freshwater Ice at Low Confining Pressures", Proc. OMAE, Houston, Texas, 1988.

Neth, V.M., Smith, T.R., Wright, B.D., "Design, Construction and Monitoring of the Tarsuit Relief Ice Pad", Proc. POAC, Helsinki, 1983.

Pare, A., Carlson, L.E., Bourns, M., and Karim, N., "The Use of an Additive in Sprayed Sea Water to Accelerate Ice Structure Construction", International Symposium on Cold Regions Heat Transfer, 1987.

Peyton, "Sea Ice Strength", Geophysical Inst. U. of Alaska, UAG R-182, Dec., 1966.

Potter, R.E., "Development of New Structures Combined with the Use of Rubble Fields", Proc. AOTC, Calgary, 1984.

Pounder, E., Little, E., "Some Physical Properties of Sea Ice", Can. Journal of Physics, Vol. 37, 1959.

Prodanovic, A., "Ice Island Experiment, Ice Strength and Crystallography", AOGA Project #49, Vol. 3, 1981(a).

Prodanovic, A., "Ice Island Experiment, Summer Monitoring Report", AOGA Project #49, Vol. 4, 1981(b).

Prodanovic, A., "Man-Made Ice Island Performance", Proc. OMAE, Tokyo, Japan, 1986.

Ramseier, R., Keeler, C., "The Sintering Process of Snow", CRREL Report #226, 1967.

Richter-Menge, J.A., Cox, G.F.N., Perron, N., Durell, G., Bosworth, H.W., "Triaxial Testing of First Year Sea Ice", CRREL, Report 86-16, Dec., 1986.

Richter-Menge, J.A., "Confined Compressive Strength of Horizontal First-Year Sea Ice", Proc. OMAE, Houston, Texas, 1987.

Roctest Ltd., "Interpretation and Application of Pressuremeter Test Results", Sols Soils, No. 26, 1975.

Sackinger, Sackinger, "On the Freezing of Sprayed Sea Water to Produce Artificial Sea Ice", M.I.T., Dept. of Chem., 1978.

Shields, D.H., Ladanyi,B, Murat, J.R., Clark, J.I., "Stresses in Icebergs - Will the Pressuremeter Work ?", Proc. Canad. Conf. Geot. Eng., Montreal, 1986.

SIPRE Report #18, "Strength Studies of High-Density Snow", Oct., 1956.

Spence, J., Hult, J.A.H., "Simple Approximations for Creep Relaxation", Int. Jour. of Mechanical Sciences, Pergamon Press, Vol. 15, pp. 741-755, 1973.

Stordal, A., Janbu, N., "Shear Strength Parameters obtained from Pressuremeter Tests", Proc. 11th Inter. Conf. on Soil Mechanics and Foundation Engineering, San Francisco, 1985.

Urabe, N., Iwasaki, T., Yoshitake, A., "Fracture Toughness of Sea Ice", CRST, Vol. 3, No. 1, pp. 29-37, 1980.

Vyalov, S.S., Emakov, V.F., "Simplified Method of Testing Ice for Creep and Relaxation", Proc. Conf. Physics of Snow and Ice, Part 1, 1966.

Weaver, J.S., McKeown, S., "Observations of the Strength Properties of Spray Ice", Proc. OMAE, Tokyo, Japan, 1986.

Weaver, J.S. and Gregor, L.C., "The Design, Construction and Verification of the Angasak Spray Ice Exploration Island", Proc. OMAE, Houston, Texas, 1988.

Williams, R., "Spray Ice Island Technology Advancing in the Arctic", Oil and Gas Journal, Sept., 1985.

Wong, T.T, Gale, A.D., Sego, D.C. and Morgenstern, N.R., "Shear Box Tests on Broken Ice", 9th Intn'l POAC, Fairbanks, Alaska, 1987.

Zarling, J., "Heat and Mass Transfer from Freely Falling Drops at Low Temperatures", CRREL Report #18, 1980.

APPENDIX A

Uncorrected and corrected pressuremeter test results for Calgary experiments.

Table of ice core information for pressuremeter experiments.

Calibration curves for pressuremeter experiments.

Corrected pressuremeter curves for Calgary spray-ice experiments.

CALGARY PRESSUREMETER TEST #1

Volume (cc)	Pressure (KPa)	Corrected Volume (cc)	Corrected Pressure (KPa)
0	0	0.00	0.00
60	25	59.04	0.00
120	40	118.46	1.94
180	60	177.69	13.41
240	85	236.72	29.91
300	115	295.57	51.44
360	145	354.41	72.96
420	175	413.26	94.49
480	220	471.52	131.10
540	260	529.98	162.68
600	300	588.44	194.26
660	335	647.09	220.82
720	370	705.74	247.37
780	395	764.78	263.87
840	425	823.62	285.40
900	435	883.24	286.81
960	455	942.46	298.29
1020	485	1001.31	319.81
1080	495	1060.92	321.23
1140	500	1120.73	317.61
1200	510	1180.34	319.03

CALGARY PRESSUREMETER TEST #2

Volume (cc)	Pressure (KPa)	Corrected Volume (cc)	Corrected Pressure (KPa)
0	0	0.00	0.00
60	0	60.00	0.00
120	20	119.23	0.00
180	45	178.27	0.00
240	65	237.49	9.80
300	90	296.53	26.30
360	120	355.38	47.83
420	165	413.64	84.44
480	198	472.37	108.98
540	230	531.14	132.52
600	255	590.17	149.02
660	280	649.21	165.51
720	305	708.25	182.01
780	335	767.09	203.54
840	355	826.32	215.01
900	375	885.55	226.48
960	395	944.78	237.95
1020	420	1003.81	254.45
1080	435	1063.24	260.89
1140	450	1122.66	267.34
1200	470	1181.89	278.81

CALGARY PRESSUREMETER TEST #3

Volume (cc)	Pressure (KPa)	Corrected Volume (cc)	Corrected Pressure (KPa)
0	0	0.00	0.00
60	0	60.00	0.00
120	20	119.23	0.00
180	50	178.07	3.36
240	95	236.33	39.97
300	150	294.21	86.63
360	200	352.28	128.27
420	245	410.55	164.88
480	285	469.00	196.46
540	325	527.46	228.05
600	355	586.30	249.57
660	390	644.95	276.13
720	420	703.80	297.65
780	445	762.83	314.15
840	470	821.87	330.65
900	480	881.48	332.07
960	500	940.71	343.54
1020	505	1000.52	339.93
1080	520	1059.94	346.37
1140	530	1119.55	347.78
1200	535	1179.36	344.17

CALGARY PRESSUREMETER TEST #4

Volume (cc)	Pressure (KPa)	Corrected Volume (cc)	Corrected Pressure (KPa)
0	0	0.00	0.00
60	0	60.00	0.00
120	0	120.00	0.00
180	15	179.42	0.00
240	35	238.65	0.00
300	65	297.50	1.16
360	105	355.96	32.74
420	150	414.23	69.35
480	180	473.07	90.88
540	220	531.53	122.46
600	245	590.57	138.96
660	275	649.41	160.48
720	300	708.45	176.98
780	325	767.49	193.48
840	350	826.53	209.98
900	375	885.56	226.48
960	400	944.60	242.98
1020	435	1003.25	269.53
1080	450	1062.68	275.97
1140	470	1121.91	287.45
1200	485	1181.33	293.89

CALGARY PRESSUREMETER TEST #5

Volume (cc)	Pressure (KPa)	Corrected Volume (cc)	Corrected Pressure (KPa)
0	0	0.00	0.00
60	0	60.00	0.00
120	4	11[illegible].85	0.00
180	25	17[illegible].04	0.00
240	50	238.08	0.00
300	70	297.31	6.19
360	100	356.15	27.71
420	140	414.61	59.30
480	175	473.26	85.85
540	200	532.30	102.35
600	230	591.15	123.88
660	265	649.80	150.43
720	285	709.03	161.90
780	300	768.45	168.34
840	325	827.49	184.84
900	345	886.72	196.31
960	355	946.33	197.73
1020	365	1005.95	199.14
1080	385	1065.18	210.61
1140	400	1124.60	217.06
1200	415	1184.02	223.50

CALGARY PRESSUREMETER TEST #6

Volume (cc)	Pressure (KPa)	Corrected Volume (cc)	Corrected Pressure (KPa)
0	0	0.00	0.00
79.9	75	77.01	42.91
142.5	150	136.73	109.31
208	225	199.34	175.30
285	300	273.45	239.62
371	375	356.56	302.66
459	450	441.68	365.40
592	525	571.79	421.66
729	600	705.90	477.35
865	675	839.01	533.18
1018	750	989.13	586.57

CALGARY PRESSUREMETER TEST #7

Volume (cc)	Pressure (KPa)	Corrected Volume (cc)	Corrected Pressure (KPa)
0	0	0.00	0.00
125.5	75	122.61	36.34
205.5	150	199.73	100.24
284.5	225	275.84	164.28
371	300	359.45	227.24
463.5	375	449.06	289.34
576	450	558.68	348.55
699	525	678.79	406.25
836	600	812.90	461.94
972	675	946.01	517.77
1124.8	750	1095.93	571.19

CALGARY PRESSUREMETER TEST #8

Volume (cc)	Pressure (KPa)	Corrected Volume (cc)	Corrected Pressure (KPa)
0	0	0.00	0.00
147.5	75	144.61	33.18
230.4	150	224.63	96.65
304.9	225	296.24	161.34
389	300	377.45	224.65
480	375	465.56	286.96
585	450	567.68	347.25
706	525	685.79	405.25
838	600	814.90	461.65
965	675	939.01	518.78
1111	750	1082.13	573.17

CALGARY PRESSUREMETER TEST #9

Volume (cc)	Pressure (KPa)	Corrected Volume (cc)	Corrected Pressure (KPa)
0.0	0	0.00	0.00
238.1	100	234.25	45.27
323.2	200	315.50	133.57
380.6	300	369.05	225.86
428.4	400	413.00	319.53
477.7	500	458.45	412.98
527.5	600	504.40	506.37
584.0	700	557.05	598.78
653.0	800	622.20	689.40
732.0	900	697.35	778.58
826.4	1000	787.90	865.54

CALGARY PRESSUREMETER TEST #10

Volume (cc)	Pressure (KPa)	Corrected Volume (cc)	Corrected Pressure (KPa)
0	0	0.00	0.00
328	150	322.22	82.60
463	300	451.44	213.99
574	450	556.66	348.84
696	600	672.88	482.11
848	750	819.10	611.05
1042	900	1007.31	733.95

INDEX OF ICE CORE SAMPLES

LIMEX		Resolute		Calgary	
Test No.	Sample Size (cm)	Label No.	Sample Size (cm)	Test No.	Sample Size (cm)
1(stbd)	38.1	12	12.7x21.6x14	1,6	100
1	15.2,35.6,28,17.8	15	12.7x21.6x14	2,7	90
2	43.2,40.6	16	10.2x20.3x17.8	3,8	100
2(floe)	27.9,26.7,33	22	14x16.5x15.2	4,9	75
5	20.3,25.4	25	16.5x15.2x17.8	5,10	85
6	22.9,27.9	26	20.3x14x10.2		
7,8	36.8,38.1,29.2,33	27	14x20.3x20.3		
11	33,38.1,35.6	?	12.7x17.8x17.8		
		?	10.2x21.6x17.8		
		?	16.5x10.2x16.5		
		?	16.5x16.5x17.8		
		?	16.5x17.8x16.5		
		Test 9	25.4 4/17.8 cm each		

Note: Resolute samples were in block form except for test #9.
All the rest of the samples were taken from cores.

Pressuremeter Calibration #1, Resolute

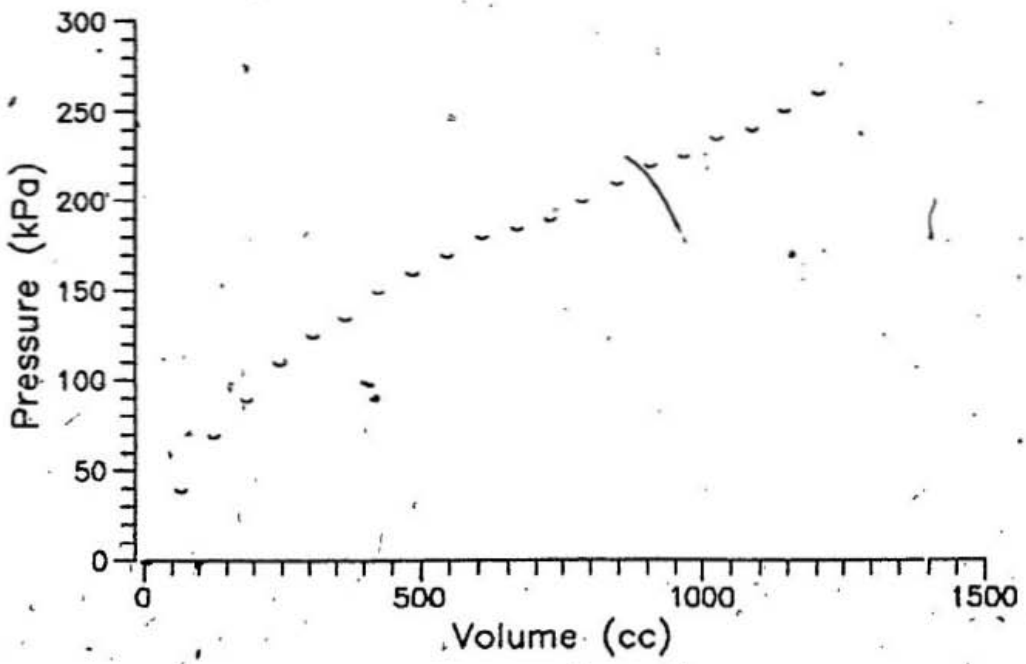

Volume Calibration #1, Resolute

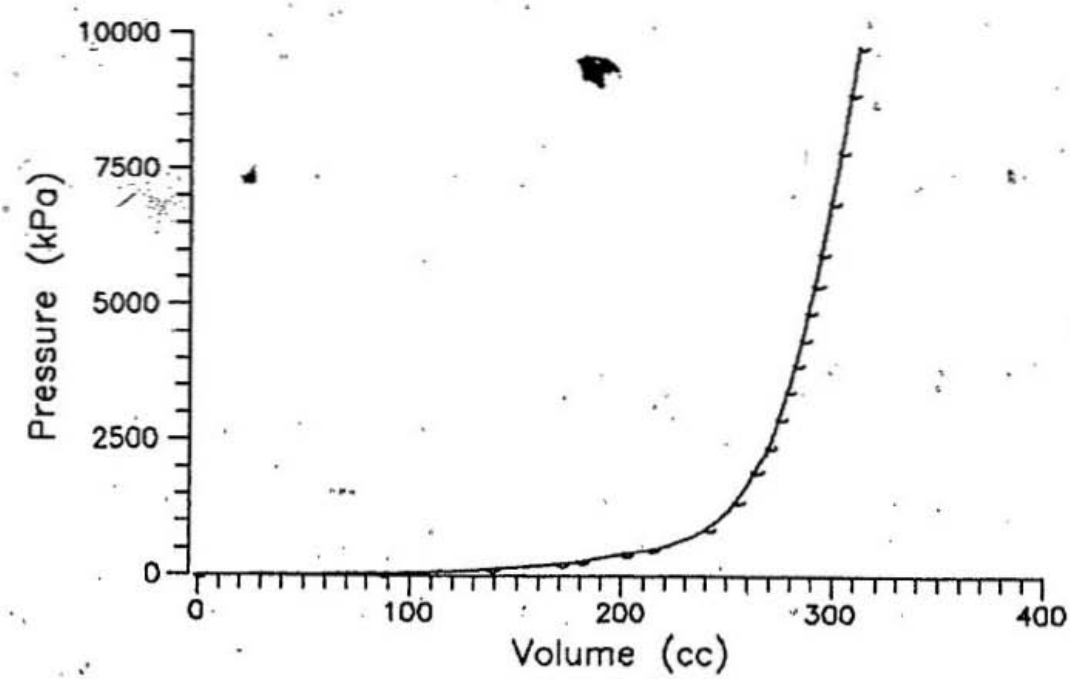

Pressure Calibration #2, Resolute

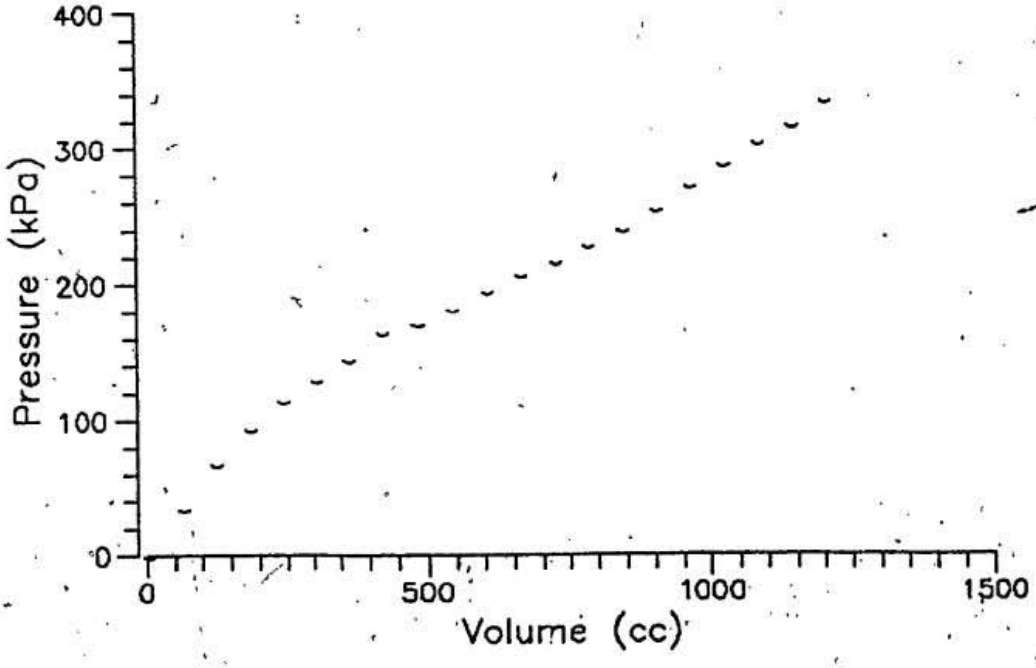

Volume Calibration #2, Resolute

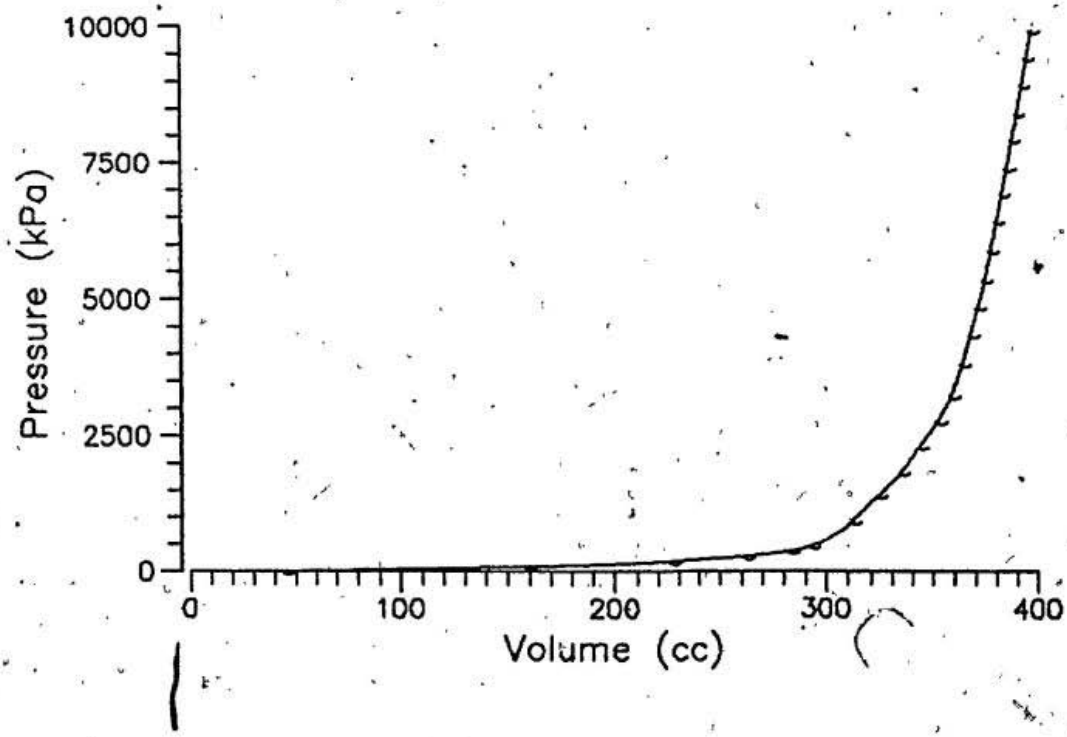

Pressure Cailbration, LIMEX

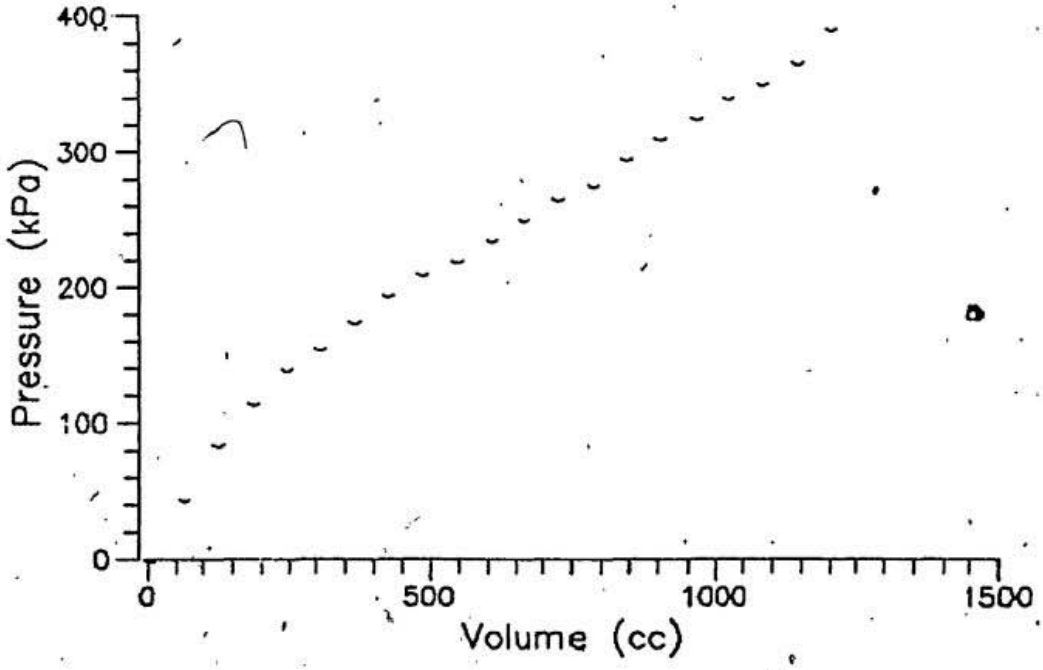

Volume Calibration, LIMEX

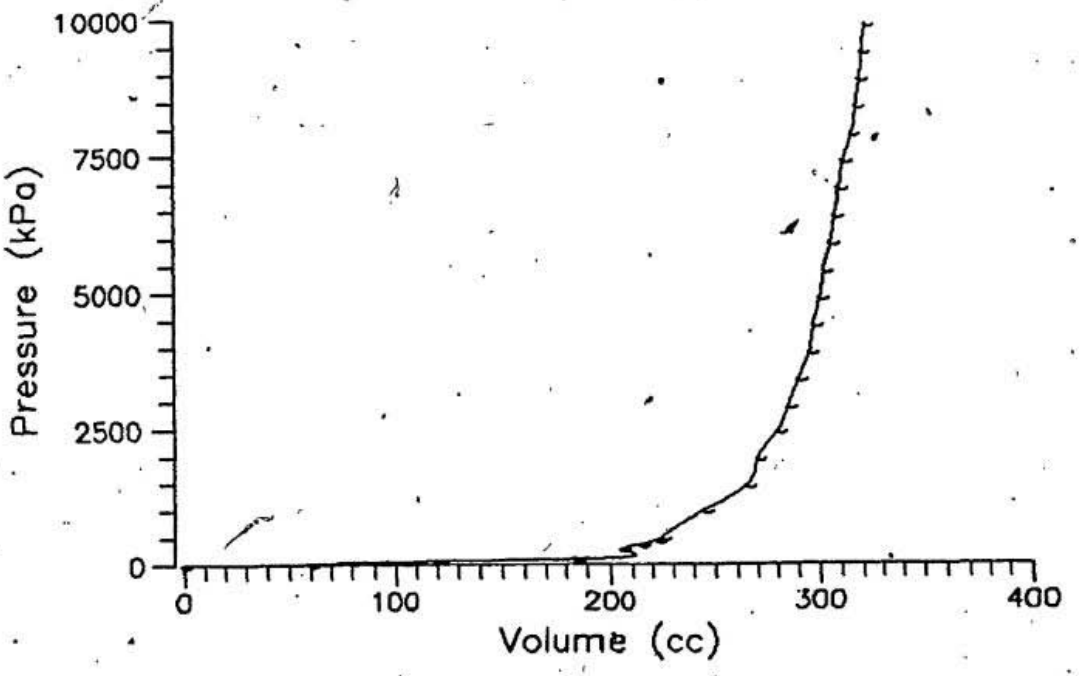

Pressure Calibration, Calgary

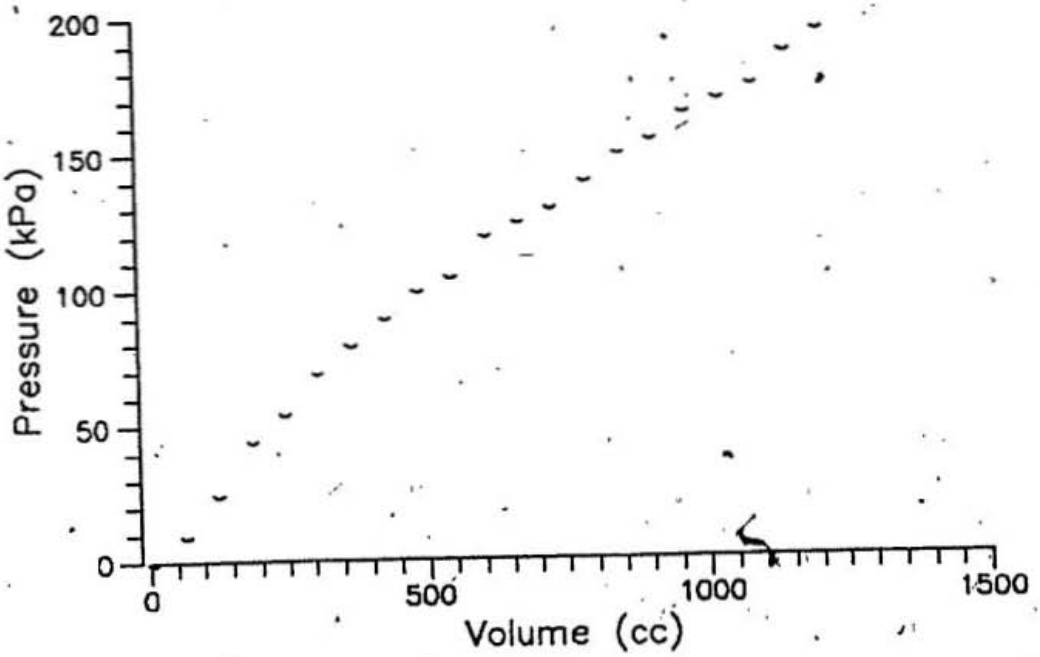

Volume Calibration, Calgary

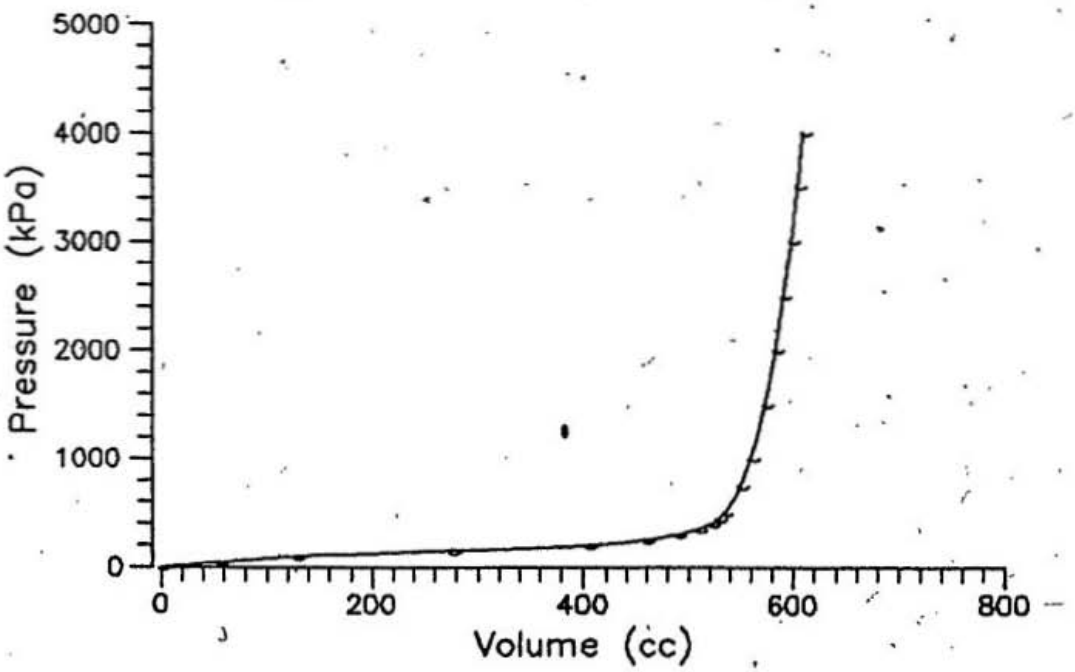

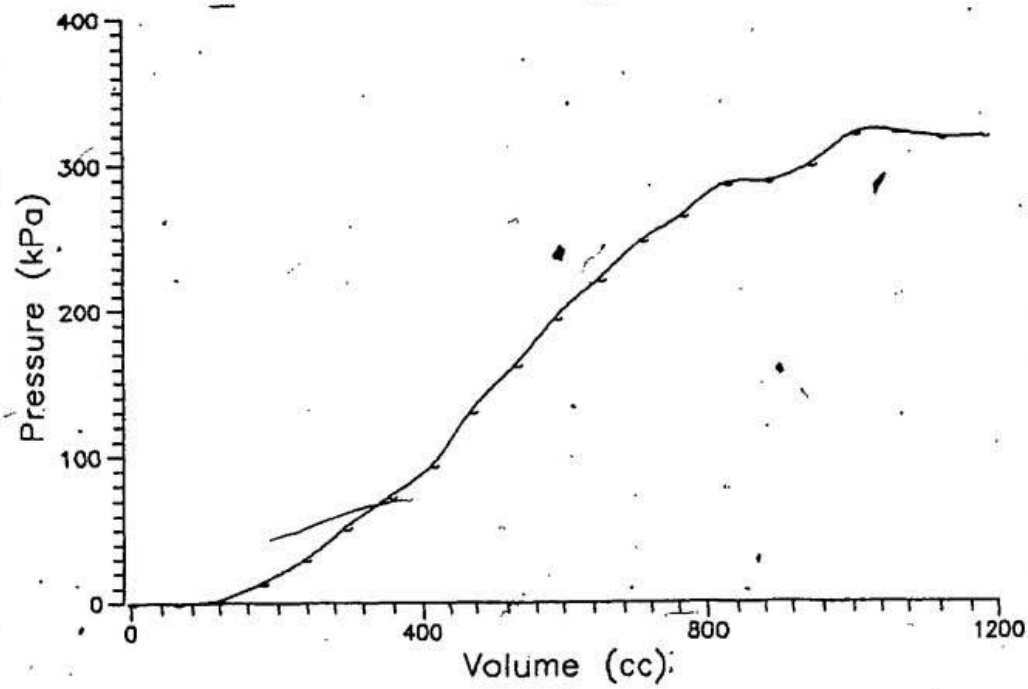

PRESSUREMETER TEST #1

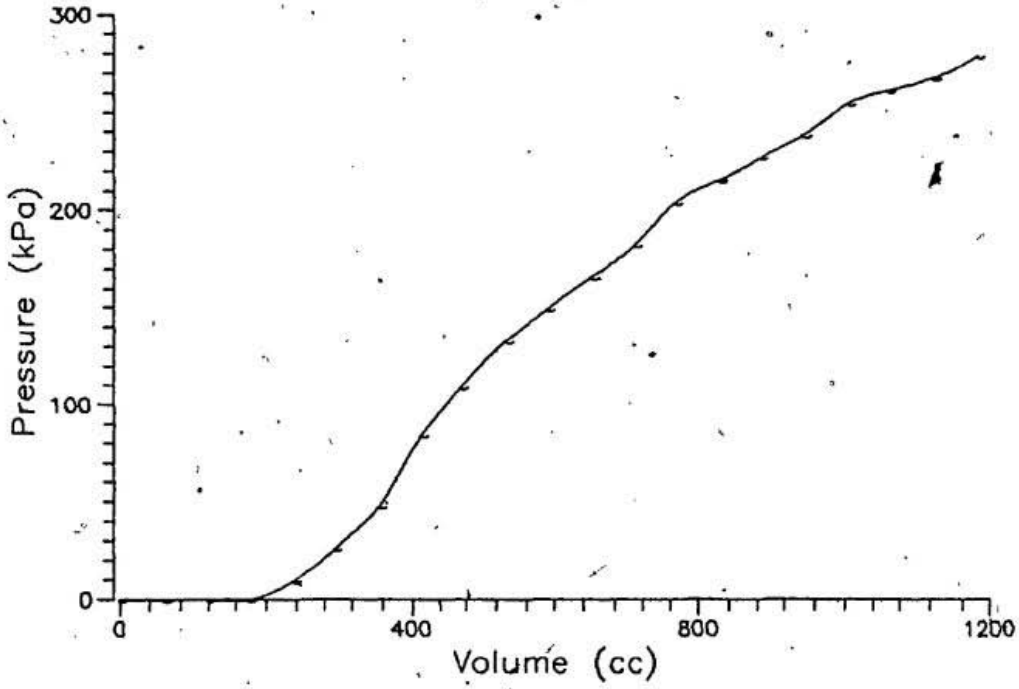

PRESSUREMETER TEST #2

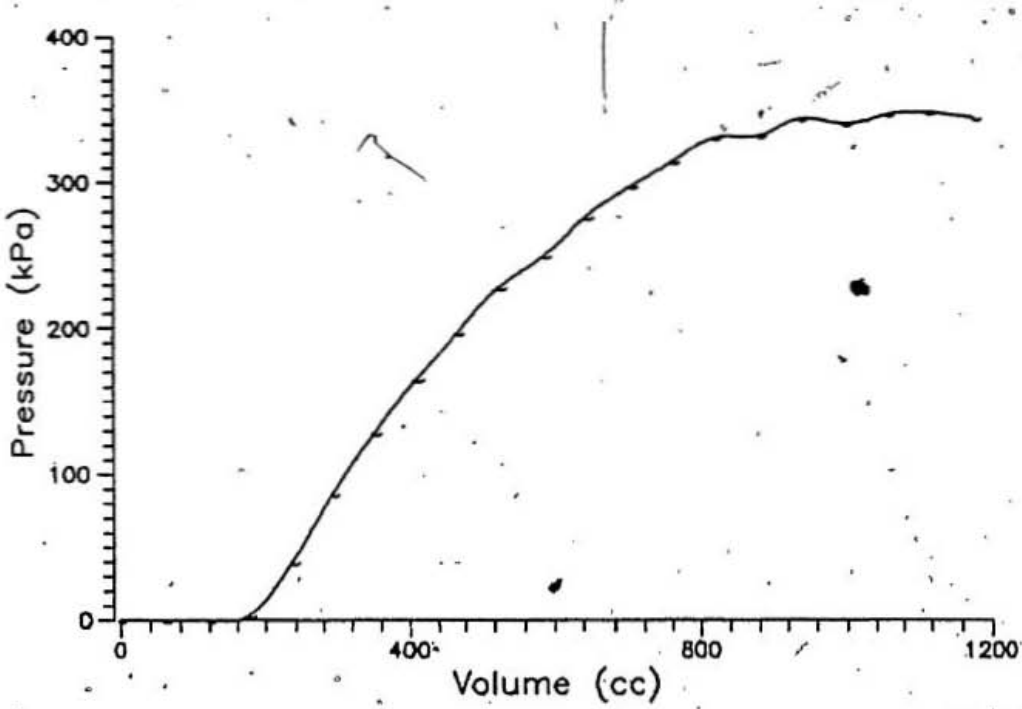

PRESSUREMETER TEST #3

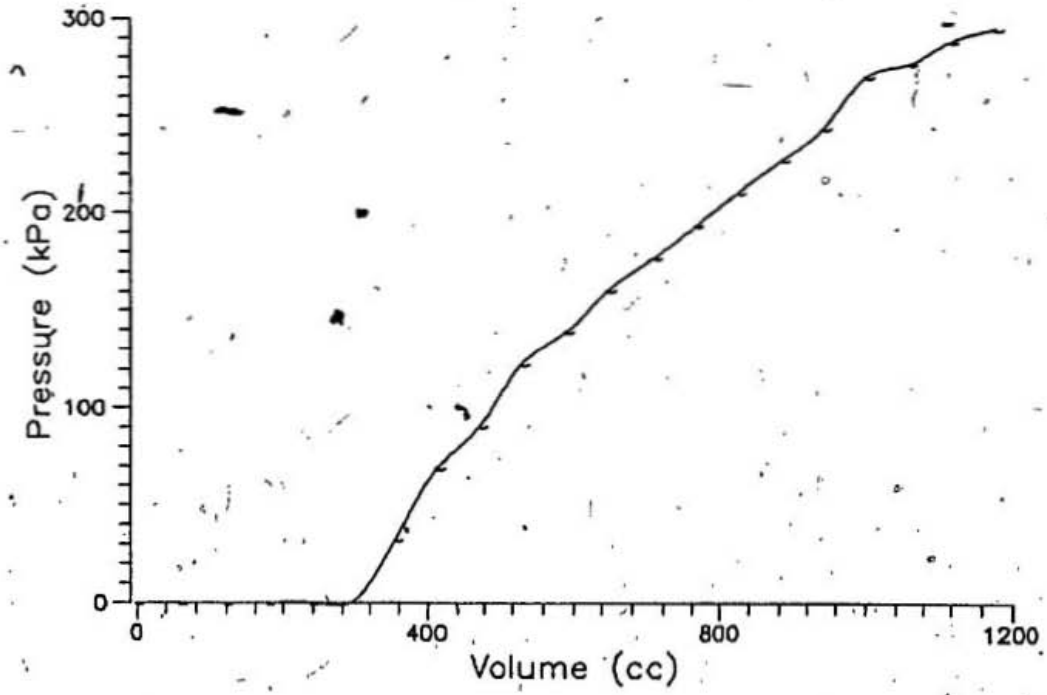

PRESSUREMETER TEST #4

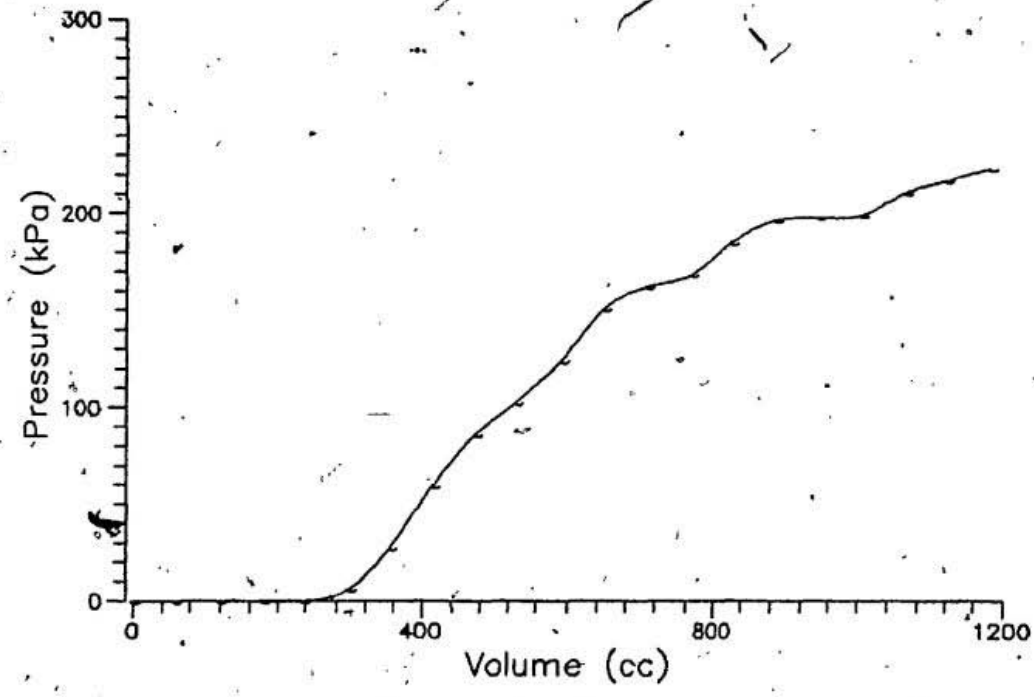

PRESSUREMETER TEST #5

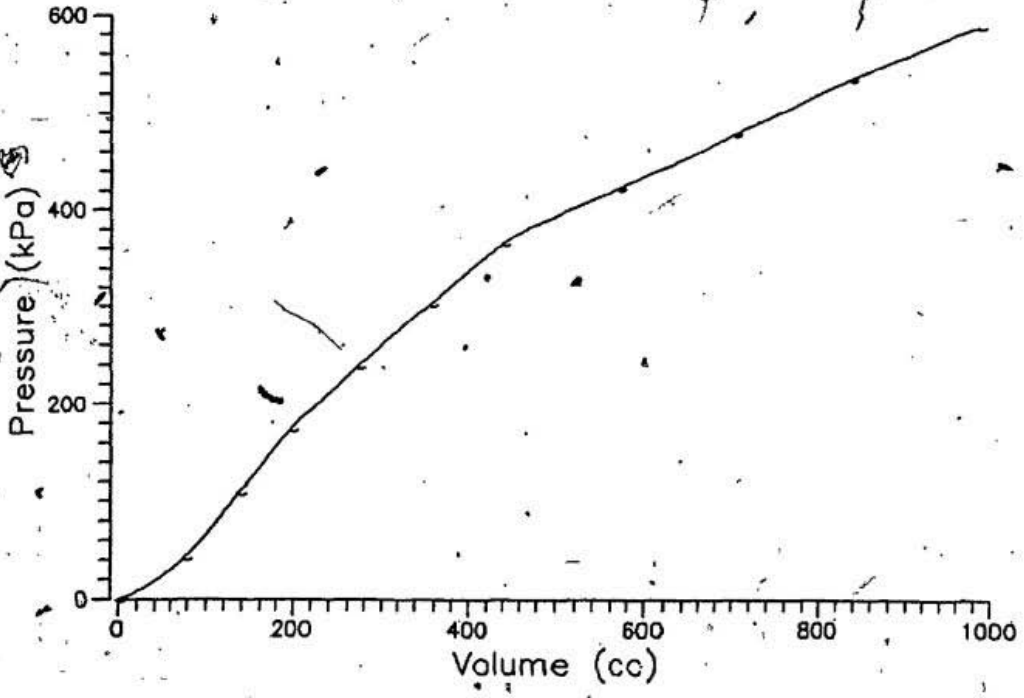

PRESSUREMETER TEST #6

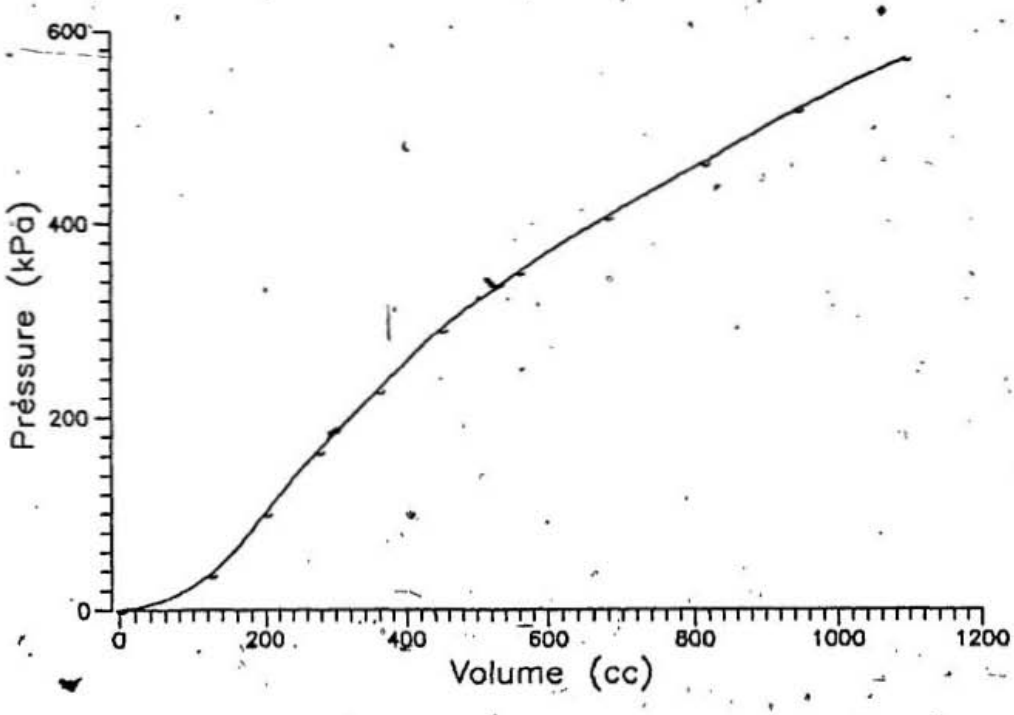

PRESSUREMETER TEST #7

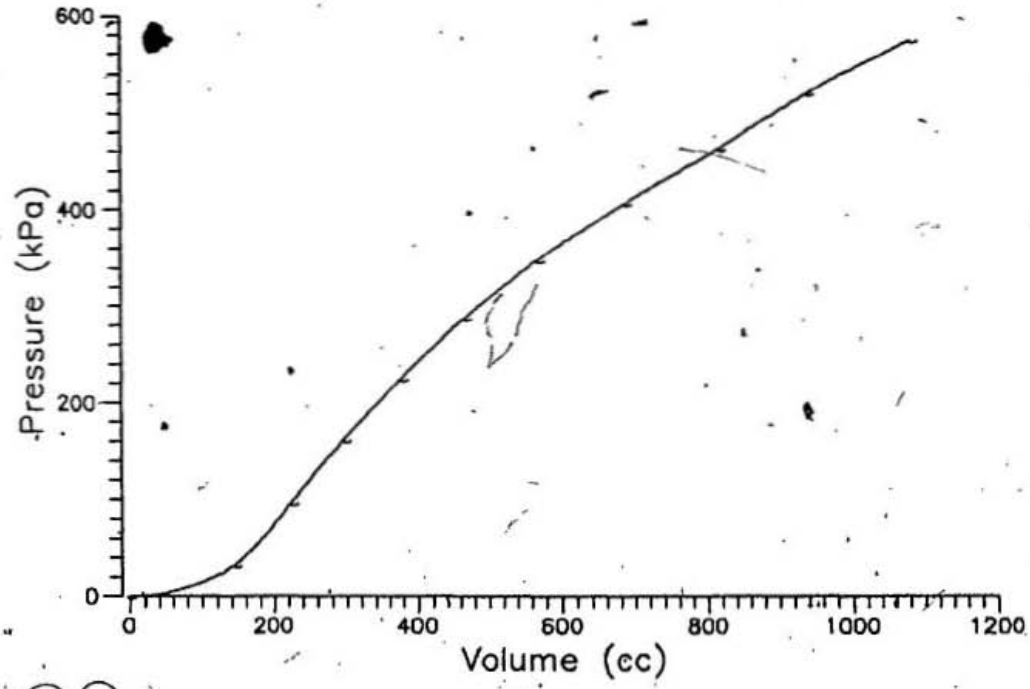

PRESSUREMETER TEST #8

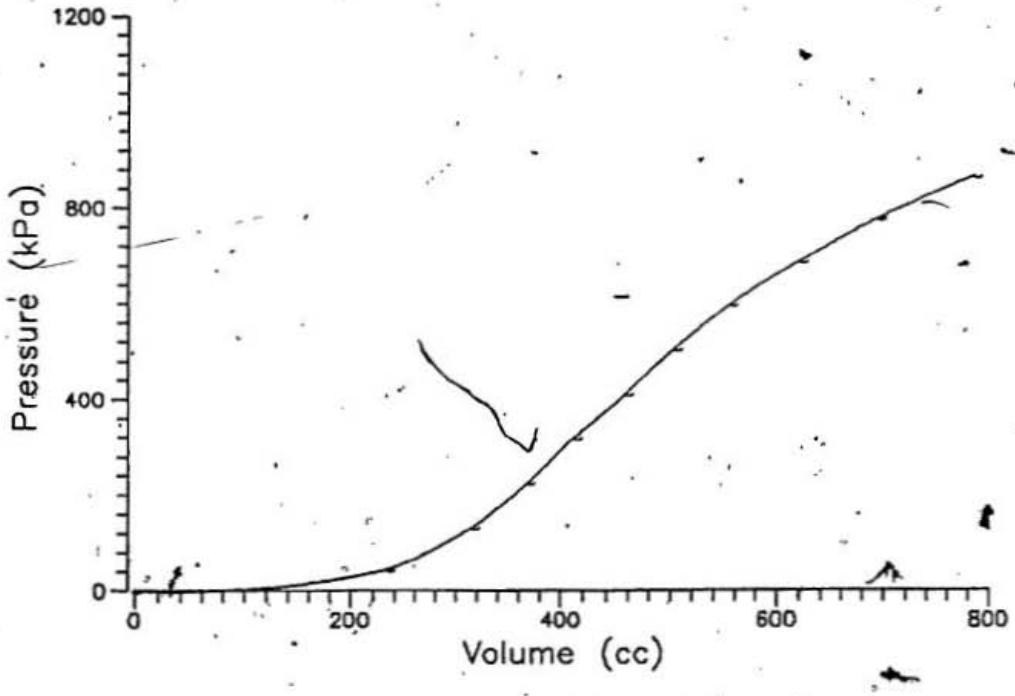

PRESSUREMETER TEST #9

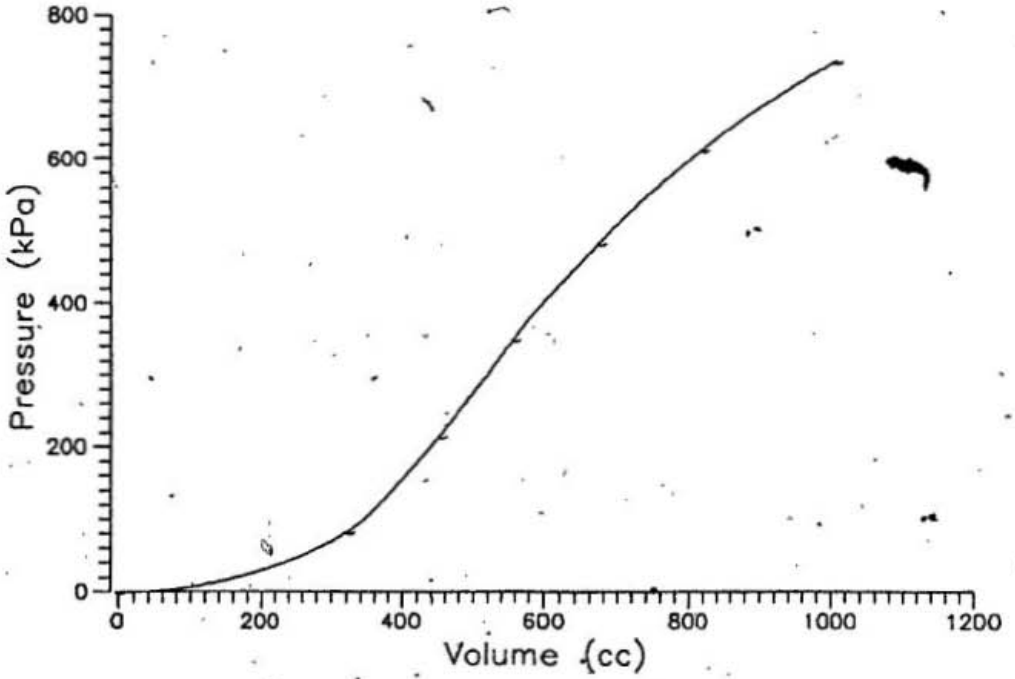

PRESSUREMETER TEST #10

APPENDIX B

Table of salinity results and load cell, LVDT and thermistor calibrations.

Triaxial test information, calibrations and initial results for each test.

Stress-strain curves for each group of tests.

Photographs of triaxial samples.

RECORD OF SALINITY RESULTS

Date Tested	Test No.	Capacitance (mvolt, avg.)	Salinity 0/00 (at 20 deg. C)
Oct.30/87	9	12.5	8.0
Nov.17/87	10	15.9	10.3
Nov.17/87	13	14.4	9.3
Nov.20/87	none	25.6	17.0
Nov.20/87	none	24.6	16.5
Nov.20/87	none	25.1	16.7
Nov.23/87	17	13.5	8.5
Nov.25/87	18	14.3	9.2
Nov.26/87	19	15.4	10.0
Dec.2/87	20	15.1	9.7
Dec.2/87	21	17.7	11.5
Dec.4/87	22	20.9	14.0
Dec.4/87	23	22.8	15.7
Dec.7/87	24	17.6	11.7
Dec.8/87	25	13.5	8.5
Dec.8/87	26	10.4	6.8
Dec.9/87	27	14.5	9.5
Dec.11/87	28	13.3	8.2
Dec.11/87	29	12.0	7.5

Note: Sample taken either day before or day tested.
Sample stored in sealed container while melting.
Sample brought close to 20 deg. C before testing.
Three tests performed for each sample.

LVDT #1 Calibration, Oct 19/87

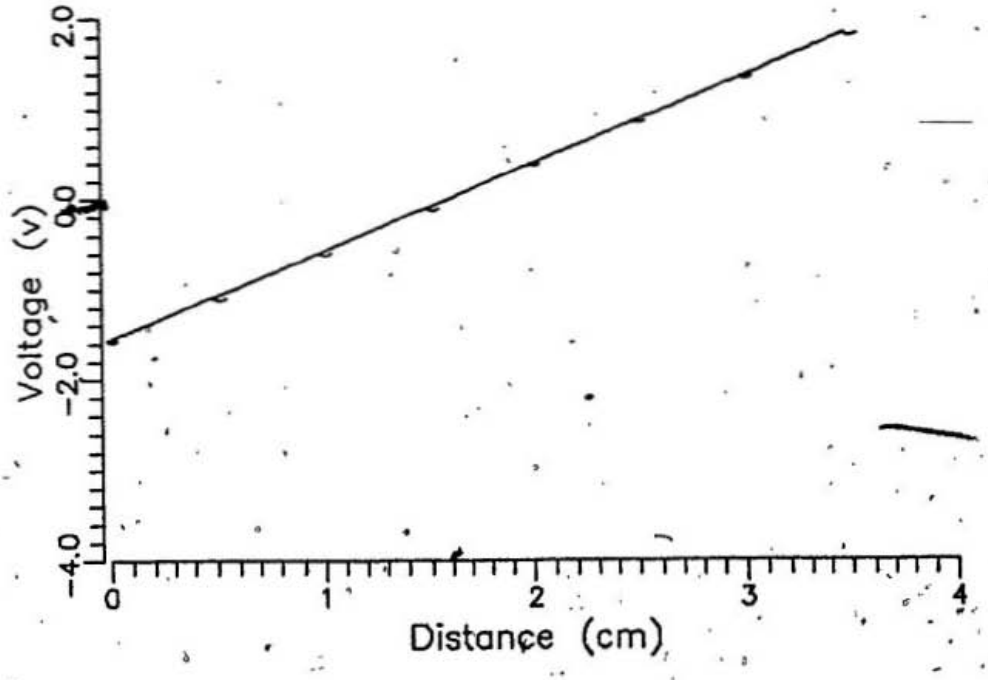

LVDT #2 Calibration, Oct 28/87

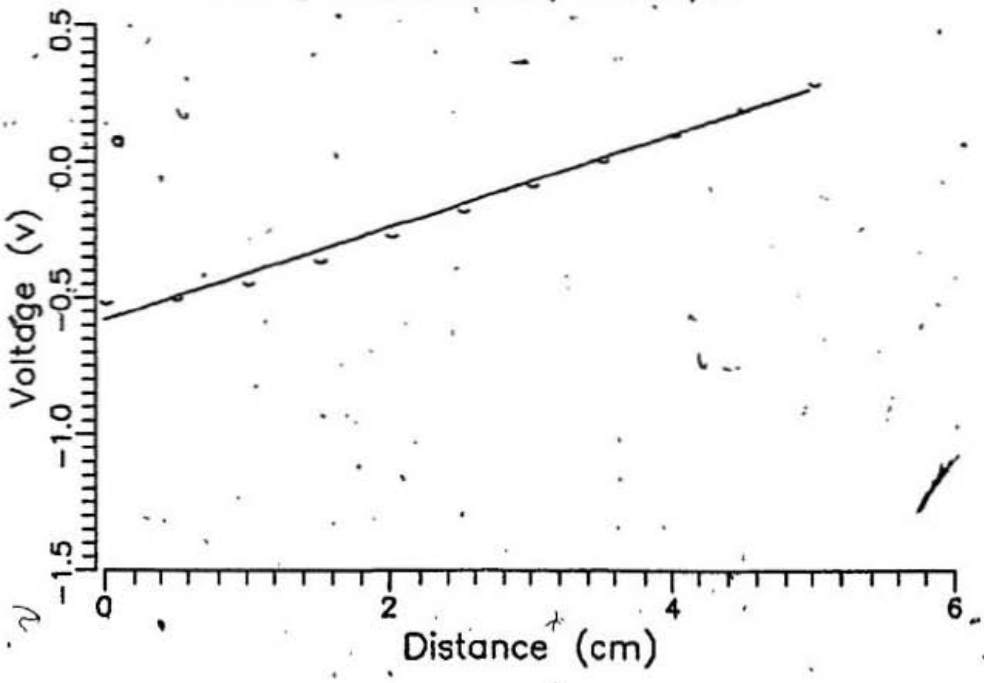

LVDT #3 Calibration, Oct 29/87

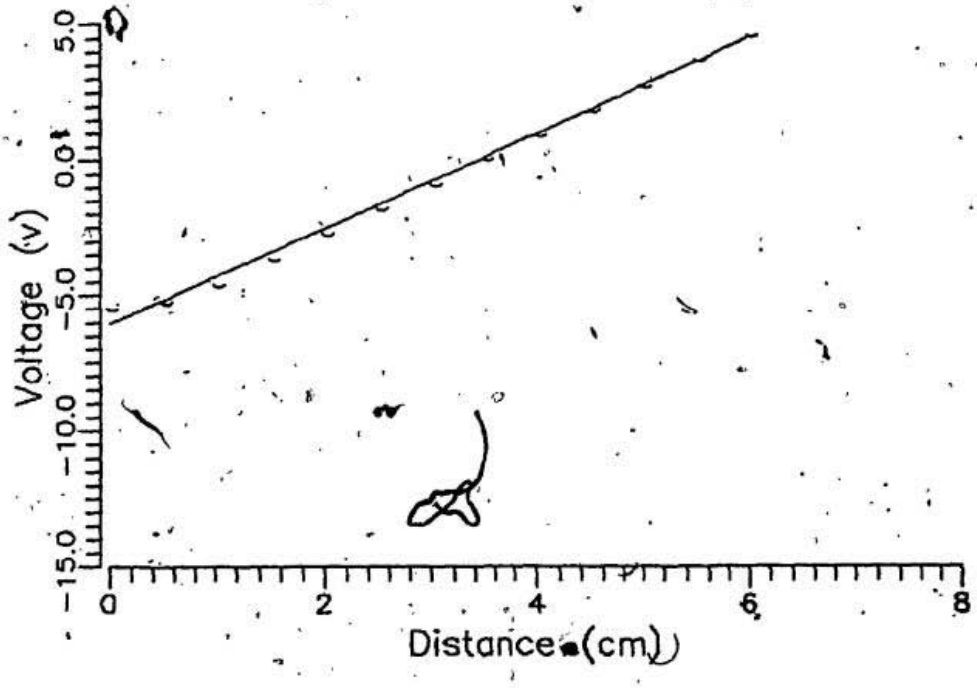

LVDT #4 Calibration, Nov. 23/87.

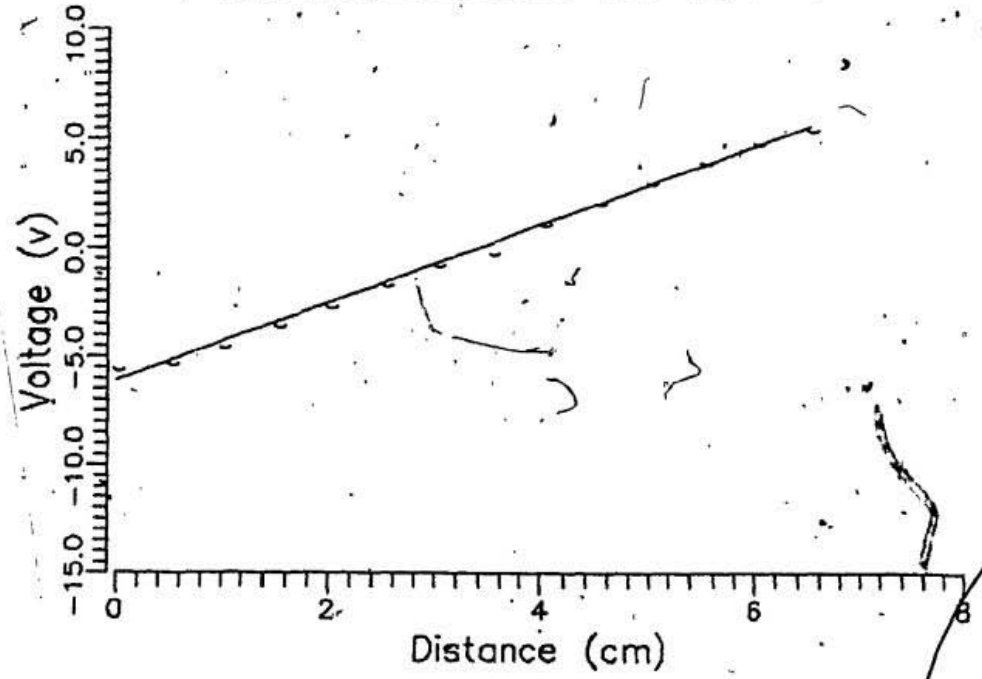

Load Cell Calibration by Weight

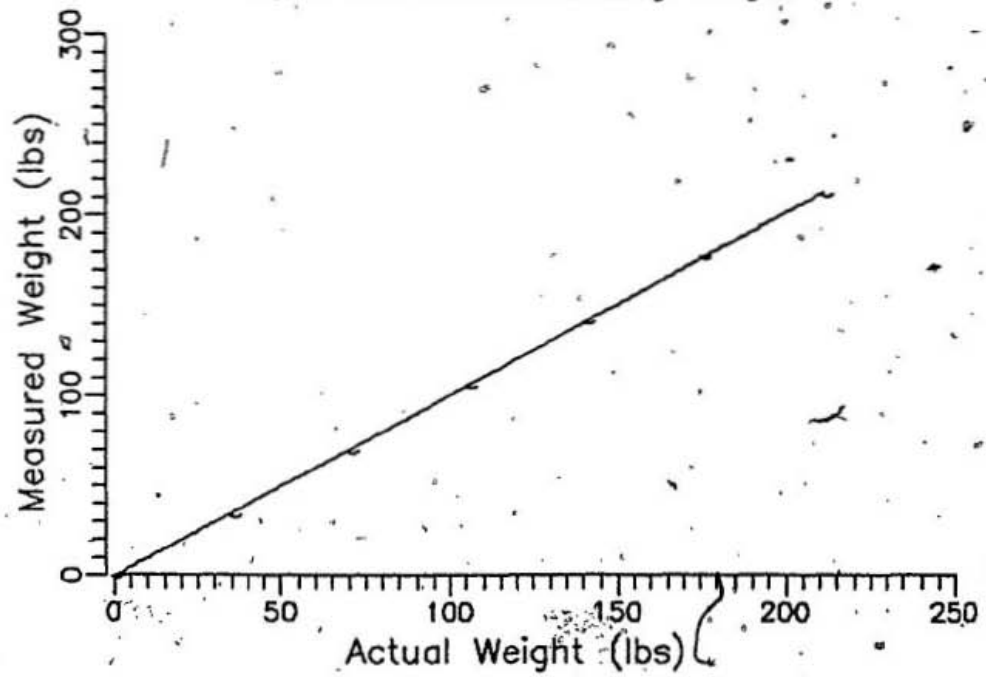

Load Cell Calibration with Voltmeter

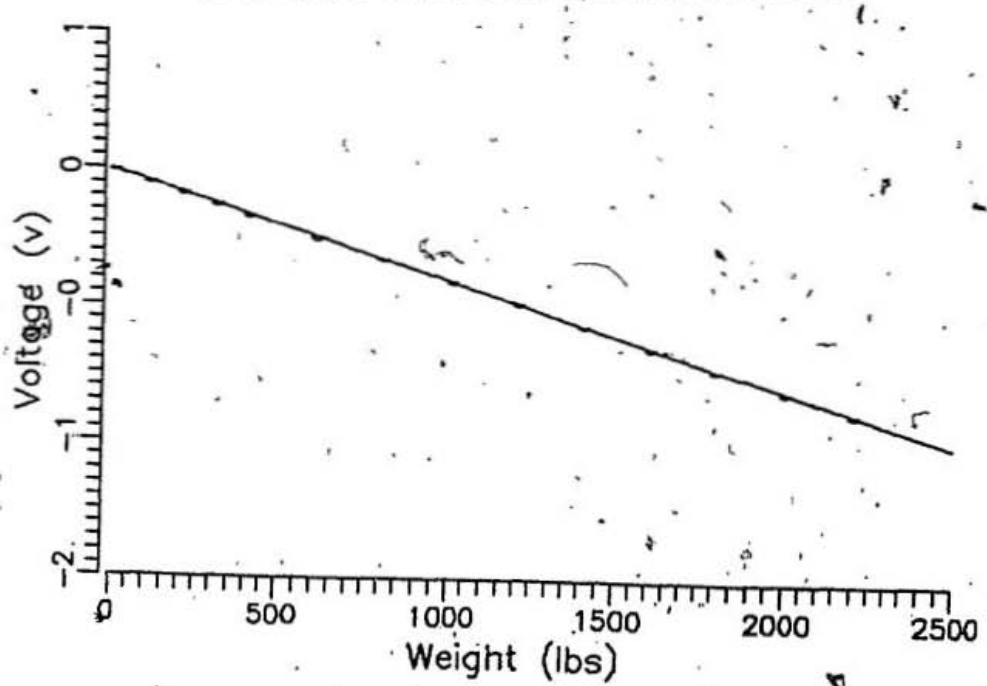

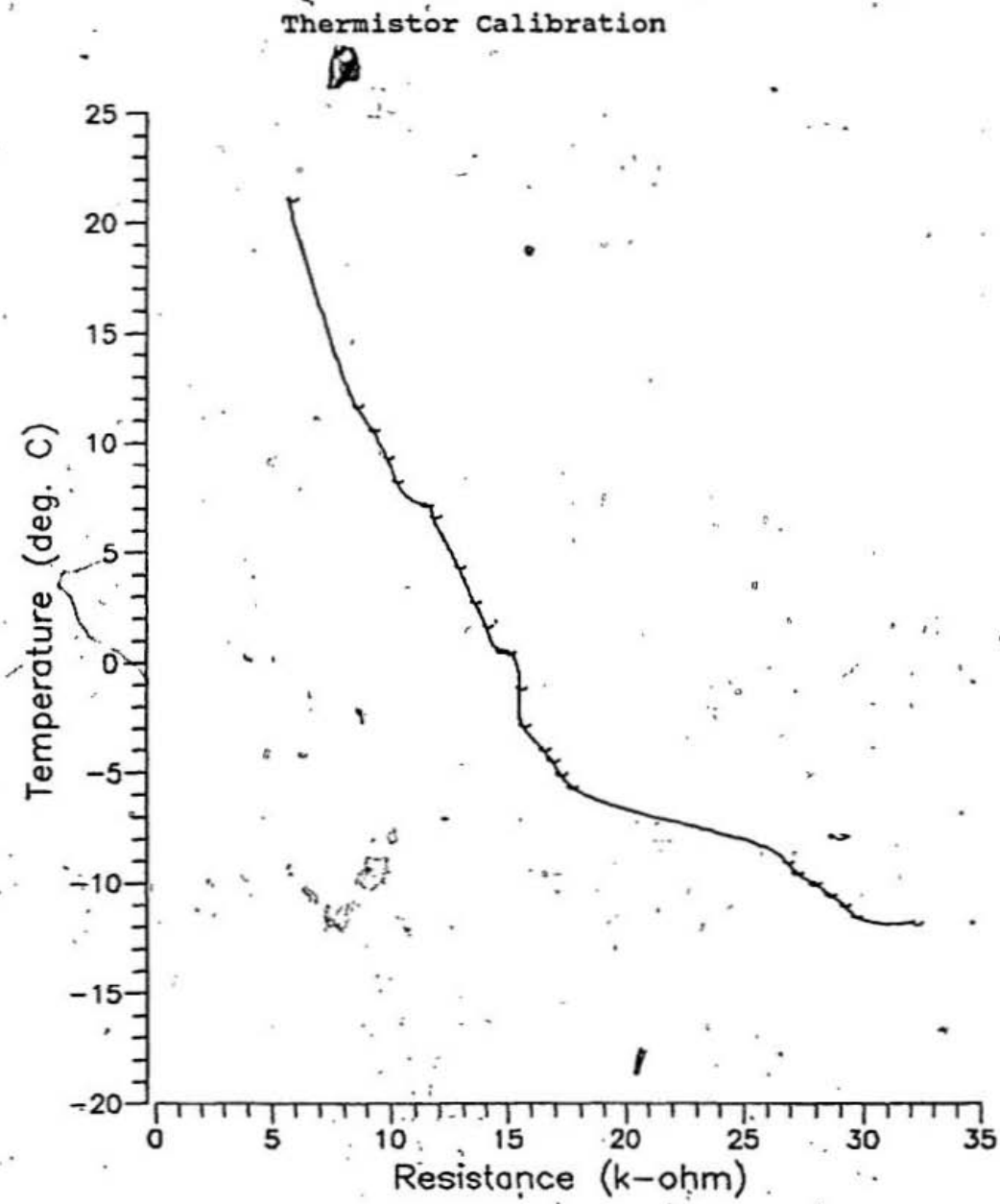
Thermistor Calibration
Temperature (deg. C)
25
20
15
10
5
0
-5
-10
-15
-20
0
5
10
15
20
25
30
35
Resistance (k-ohm)

Triaxial Test Information

triaxial test #5

INITIAL DIAMETER OF SPECIMEN (MM) = 71.70
FINAL HEIGHT OF SPECIMEN (MM) = 112.30
FINAL DIAMETER OF SPECIMEN (MM) = 75.50
LATERAL CELL PRESSURE (kPa) = 86.19

INITIAL LOAD CELL READING (UNIT OF READINGS)= 4.000000
CALIBRATION COEFF. FOR LOAD CELL (KN/UNIT) = 0.004448
INITIAL LVDT READING (UNIT OF READINGS) = -1.080000
CALIBRATION COEFF. FOR LVDT (MM/UNIT) = 10.283800

triaxial test #6

INITIAL DIAMETER OF SPECIMEN (MM) = 71.70
FINAL HEIGHT OF SPECIMEN (MM) = 106.55
FINAL DIAMETER OF SPECIMEN (MM) = 75.88
LATERAL CELL PRESSURE (kPa) = 86.19

INITIAL LOAD CELL READING (UNIT OF READINGS)= 4.000000
CALIBRATION COEFF. FOR LOAD CELL (kN/UNIT) = 0.004448
INITIAL LVDT READING (UNIT OF READINGS) = -0.272000
CALIBRATION COEFF. FOR LVDT (MM/UNIT) = 53.868000

triaxial test #7

INITIAL DIAMETER OF SPECIMEN (MM) = 71.70
FINAL HEIGHT OF SPECIMEN (MM) = 107.00
FINAL DIAMETER OF SPECIMEN (MM) = 80.52
LATERAL CELL PRESSURE (kPa) = 86.19

INITIAL LOAD CELL READING (UNIT OF READINGS)= 4.000000
CALIBRATION COEFF. FOR LOAD CELL (kN/UNIT) = 0.004448
INITIAL LVDT READING (UNIT OF READINGS) = -0.240000
CALIBRATION COEFF. FOR LVDT (MM/UNIT) = 53.860001

Triaxial Test Information

triaxial test #8

INITIAL DIAMETER OF SPECIMEN (MM)	=	71.70
FINAL HEIGHT OF SPECIMEN (MM)	=	108.05
FINAL DIAMETER OF SPECIMEN (MM)	=	79.19
LATERAL CELL PRESSURE (kPa)	=	93.08
INITIAL LOAD CELL READING (UNIT OF READINGS)	=	4.000000
CALIBRATION COEFF. FOR LOAD CELL (kN/UNIT)	=	0.004448
INITIAL LVDT READING (UNIT OF READINGS)	=	-0.274000
CALIBRATION COEFF. FOR LVDT (MM/UNIT)	=	53.862598

triaxial test #9

INITIAL DIAMETER OF SPECIMEN (MM)	=	71.70
FINAL HEIGHT OF SPECIMEN (MM)	=	110.17
FINAL DIAMETER OF SPECIMEN (MM)	=	84.28
LATERAL CELL PRESSURE (kPa)	=	44.82
INITIAL LOAD CELL READING (UNIT OF READINGS)	=	2.000000
CALIBRATION COEFF. FOR LOAD CELL (kN/UNIT)	=	0.004448
INITIAL LVDT READING (UNIT OF READINGS)	=	-0.222100
CALIBRATION COEFF. FOR LVDT (MM/UNIT)	=	53.860001

triaxial test #10

INITIAL DIAMETER OF SPECIMEN (MM)	=	71.70
FINAL HEIGHT OF SPECIMEN (MM)	=	109.55
FINAL DIAMETER OF SPECIMEN (MM)	=	79.82
LATERAL CELL PRESSURE (kPa)	=	44.82
INITIAL LOAD CELL READING (UNIT OF READINGS)	=	2.000000
CALIBRATION COEFF. FOR LOAD CELL (kN/UNIT)	=	0.004448
INITIAL LVDT READING (UNIT OF READINGS)	=	-3.010000
CALIBRATION COEFF. FOR LVDT (MM/UNIT)	=	5.494500

Triaxial Test Information

triaxial test #11

INITIAL DIAMETER OF SPECIMEN (MM)	=	71.70
FINAL HEIGHT OF SPECIMEN (MM)	=	108.60
FINAL DIAMETER OF SPECIMEN (MM)	=	82.20
LATERAL CELL PRESSURE (kPa)	=	44.80
INITIAL LOAD CELL READING (UNIT OF READINGS)	=	2.000000
CALIBRATION COEFF. FOR LOAD CELL (kN/UNIT)	=	0.004448
INITIAL LVDT READING (UNIT OF READINGS)	=	-3.560000
CALIBRATION COEFF. FOR LVDT (MM/UNIT)	=	-5.351700

triaxial test #12

INITIAL DIAMETER OF SPECIMEN (MM)	=	71.70
FINAL HEIGHT OF SPECIMEN (MM)	=	106.25
FINAL DIAMETER OF SPECIMEN (MM)	=	78.23
LATERAL CELL PRESSURE (kPa)	=	79.28
INITIAL LOAD CELL READING (UNIT OF READINGS)	=	4.000000
CALIBRATION COEFF. FOR LOAD CELL (kN/UNIT)	=	0.004448
INITIAL LVDT READING (UNIT OF READINGS)	=	-3.540000
CALIBRATION COEFF. FOR LVDT (MM/UNIT)	=	5.454000

triaxial test #13

INITIAL DIAMETER OF SPECIMEN (MM)	=	71.70
FINAL HEIGHT OF SPECIMEN (MM)	=	117.05
FINAL DIAMETER OF SPECIMEN (MM)	=	75.96
LATERAL CELL PRESSURE (kPa)	=	172.37
INITIAL LOAD CELL READING (UNIT OF READINGS)	=	6.000000
CALIBRATION COEFF. FOR LOAD CELL (kN/UNIT)	=	0.004448
INITIAL LVDT READING (UNIT OF READINGS)	=	-2.930000
CALIBRATION COEFF. FOR LVDT (MM/UNIT)	=	5.351700

Triaxial Test Information

triaxial test #14

INITIAL DIAMETER OF SPECIMEN (MM)	= 71.70
FINAL HEIGHT OF SPECIMEN (MM)	= 116.80
FINAL DIAMETER OF SPECIMEN (MM)	= 74.78
LATERAL CELL PRESSURE (kPa)	= 172.37
INITIAL LOAD CELL READING (UNIT OF READINGS)	= 6.000000
CALIBRATION COEFF. FOR LOAD CELL (kN/UNIT)	= 0.004448
INITIAL LVDT READING (UNIT OF READINGS)	= -2.074000
CALIBRATION COEFF. FOR LVDT (MM/UNIT)	= 5.351700

triaxial test #15

INITIAL DIAMETER OF SPECIMEN (MM)	= 71.70
FINAL HEIGHT OF SPECIMEN (MM)	= 110.30
FINAL DIAMETER OF SPECIMEN (MM)	= 75.54
LATERAL CELL PRESSURE (kPa)	= 172.37
INITIAL LOAD CELL READING (UNIT OF READINGS)	= 6.000000
CALIBRATION COEFF. FOR LOAD CELL (kN/UNIT)	= 0.004448
INITIAL LVDT READING (UNIT OF READINGS)	= -2.786000
CALIBRATION COEFF. FOR LVDT (MM/UNIT)	= 5.351700

triaxial test #16

INITIAL DIAMETER OF SPECIMEN (MM)	= 71.70
FINAL HEIGHT OF SPECIMEN (MM)	= 117.30
FINAL DIAMETER OF SPECIMEN (MM)	= 79.87
LATERAL CELL PRESSURE (kPa)	= 79.30
INITIAL LOAD CELL READING (UNIT OF READINGS)	= 4.000000
CALIBRATION COEFF. FOR LOAD CELL (kN/UNIT)	= 0.004448
INITIAL LVDT READING (UNIT OF READINGS)	= -2.330000
CALIBRATION COEFF. FOR LVDT (MM/UNIT)	= 5.351700

Triaxial Test Information

triaxial test #17

INITIAL DIAMETER OF SPECIMEN (MM)	=	71.70
FINAL HEIGHT OF SPECIMEN (MM)	=	116.08
FINAL DIAMETER OF SPECIMEN (MM)	=	78.12
LATERAL CELL PRESSURE (kPa)	=	86.19
INITIAL LOAD CELL READING (UNIT OF READINGS)	=	8.000000
CALIBRATION COEFF. FOR LOAD CELL (kN/UNIT)	=	0.004448
INITIAL LVDT READING (UNIT OF READINGS)	=	-3.480000
CALIBRATION COEFF. FOR LVDT (MM/UNIT)	=	5.351700

triaxial test #18

INITIAL DIAMETER OF SPECIMEN (MM)	=	71.70
FINAL HEIGHT OF SPECIMEN (MM)	=	118.95
FINAL DIAMETER OF SPECIMEN (MM)	=	75.42
LATERAL CELL PRESSURE (kPa)	=	86.19
INITIAL LOAD CELL READING (UNIT OF READINGS)	=	4.000000
CALIBRATION COEFF. FOR LOAD CELL (kN/UNIT)	=	0.004448
INITIAL LVDT READING (UNIT OF READINGS)	=	-3.280000
CALIBRATION COEFF. FOR LVDT (MM/UNIT)	=	5.351700

triaxial test #19

INITIAL DIAMETER OF SPECIMEN (MM)	=	71.70
FINAL HEIGHT OF SPECIMEN (MM)	=	116.55
FINAL DIAMETER OF SPECIMEN (MM)	=	76.22
LATERAL CELL PRESSURE (kPa)	=	86.19
INITIAL LOAD CELL READING (UNIT OF READINGS)	=	2.000000
CALIBRATION COEFF. FOR LOAD CELL (kN/UNIT)	=	0.004448
INITIAL LVDT READING (UNIT OF READINGS)	=	-2.375000
CALIBRATION COEFF. FOR LVDT (MM/UNIT)	=	5.351700

Triaxial Test Information

triaxial test #20

INITIAL DIAMETER OF SPECIMEN (MM)	= 71.70
FINAL HEIGHT OF SPECIMEN (MM)	= 111.30
FINAL DIAMETER OF SPECIMEN (MM)	= 78.64
LATERAL CELL PRESSURE (kPa)	= 44.82
INITIAL LOAD CELL READING (UNIT OF READINGS)	= 2.000000
CALIBRATION COEFF. FOR LOAD CELL (kN/UNIT)	= 0.004448
INITIAL LVDT READING (UNIT OF READINGS)	= -2.260000
CALIBRATION COEFF. FOR LVDT (MM/UNIT)	= 5.351700

triaxial test #21

INITIAL DIAMETER OF SPECIMEN (MM)	= 71.70
FINAL HEIGHT OF SPECIMEN (MM)	= 113.80
FINAL DIAMETER OF SPECIMEN (MM)	= 80.78
LATERAL CELL PRESSURE (kPa)	= 44.82
INITIAL LOAD CELL READING (UNIT OF READINGS)	= 4.000000
CALIBRATION COEFF. FOR LOAD CELL (kN/UNIT)	= 0.004448
INITIAL LVDT READING (UNIT OF READINGS)	= -3.050000
CALIBRATION COEFF. FOR LVDT (MM/UNIT)	= 5.351700

triaxial test #22

INITIAL DIAMETER OF SPECIMEN (MM)	= 71.70
FINAL HEIGHT OF SPECIMEN (MM)	= 110.05
FINAL DIAMETER OF SPECIMEN (MM)	= 75.96
LATERAL CELL PRESSURE (kPa)	= 172.37
INITIAL LOAD CELL READING (UNIT OF READINGS)	= 6.000000
CALIBRATION COEFF. FOR LOAD CELL (kN/UNIT)	= 0.004448
INITIAL LVDT READING (UNIT OF READINGS)	= -3.130000
CALIBRATION COEFF. FOR LVDT (MM/UNIT)	= 5.351700

Triaxial Test Information

triaxial test #23

INITIAL DIAMETER OF SPECIMEN (MM) =	71.70
FINAL HEIGHT OF SPECIMEN (MM) =	108.05
FINAL DIAMETER OF SPECIMEN (MM) =	76.20
LATERAL CELL PRESSURE (kPa) =	172.37
INITIAL LOAD CELL READING (UNIT OF READINGS) =	4.000000
CALIBRATION COEFF. FOR LOAD CELL (kN/UNIT) =	0.004448
INITIAL LVDT READING (UNIT OF READINGS) =	-2.447000
CALIBRATION COEFF. FOR LVDT (MM/UNIT) =	5.351700

triaxial test #24

INITIAL DIAMETER OF SPECIMEN (MM) =	71.70
FINAL HEIGHT OF SPECIMEN (MM) =	112.80
FINAL DIAMETER OF SPECIMEN (MM) =	78.46
LATERAL CELL PRESSURE (kPa) =	86.19
INITIAL LOAD CELL READING (UNIT OF READINGS) =	4.000000
CALIBRATION COEFF. FOR LOAD CELL (kN/UNIT) =	0.004448
INITIAL LVDT READING (UNIT OF READINGS) =	-2.630000
CALIBRATION COEFF. FOR LVDT (MM/UNIT) =	5.351700

triaxial test #25

INITIAL DIAMETER OF SPECIMEN (MM) =	71.70
FINAL HEIGHT OF SPECIMEN (MM) =	113.05
FINAL DIAMETER OF SPECIMEN (MM) =	77.54
LATERAL CELL PRESSURE (kPa) =	86.19
INITIAL LOAD CELL READING (UNIT OF READINGS) =	4.000000
CALIBRATION COEFF. FOR LOAD CELL (kN/UNIT) =	0.004448
INITIAL LVDT READING (UNIT OF READINGS) =	-2.300000
CALIBRATION COEFF. FOR LVDT (MM/UNIT) =	5.351700

Triaxial Test Information

triaxial test #26

INITIAL DIAMETER OF SPECIMEN (MM)	= 71.70
FINAL HEIGHT OF SPECIMEN (MM)	= 115.17
FINAL DIAMETER OF SPECIMEN (MM)	= 74.92
LATERAL CELL PRESSURE (kPa)	= 82.74

INITIAL LOAD CELL READING (UNIT OF READINGS)	= 2.000000
CALIBRATION COEFF. FOR LOAD CELL (kN/UNIT)	= 0.004448
INITIAL LVDT READING (UNIT OF READINGS)	= -2.610000
CALIBRATION COEFF. FOR LVDT (MM/UNIT)	= 5.351700

triaxial test #27

INITIAL DIAMETER OF SPECIMEN (MM)	= 71.70
FINAL HEIGHT OF SPECIMEN (MM)	= 110.55
FINAL DIAMETER OF SPECIMEN. (MM)	= 75.98
LATERAL CELL PRESSURE (kPa)	= 82.74

INITIAL LOAD CELL READING (UNIT OF READINGS)	= 2.000000
CALIBRATION COEFF. FOR LOAD CELL (kN/UNIT)	= 0.004448
INITIAL LVDT READING (UNIT OF READINGS)	= -2.790000
CALIBRATION COEFF. FOR LVDT (MM/UNIT)	= 5.351700

Triaxial Test Information

triaxial test #28

INITIAL DIAMETER OF SPECIMEN (MM)	= 71.70
FINAL HEIGHT OF SPECIMEN (MM)	= 111.05
FINAL DIAMETER OF SPECIMEN (MM)	= 77.00
LATERAL CELL PRESSURE (kPa)	= 82.74
INITIAL LOAD CELL READING (UNIT OF READINGS)	= 4.000000
CALIBRATION COEFF. FOR LOAD CELL (kN/UNIT)	= 0.004448
INITIAL LVDT READING (UNIT OF READINGS)	= -3.300000
CALIBRATION COEFF. FOR LVDT (MM/UNIT)	= 5.351700

triaxial test #29

INITIAL DIAMETER OF SPECIMEN (MM)	= 71.70
FINAL HEIGHT OF SPECIMEN (MM)	= 113.55
FINAL DIAMETER OF SPECIMEN (MM)	= 75.04
LATERAL CELL PRESSURE (kPa)	= 172.37
INITIAL LOAD CELL READING (UNIT OF READINGS)	= 12.000000
CALIBRATION COEFF. FOR LOAD CELL (kN/UNIT)	= 0.004448
INITIAL LVDT READING (UNIT OF READINGS)	= -3.260000
CALIBRATION COEFF. FOR LVDT (MM/UNIT)	= 5.351700

Stress-Strain Curve
(86 kPa, 1.45x10E-4/s, 4 hrs, -10 deg.C)

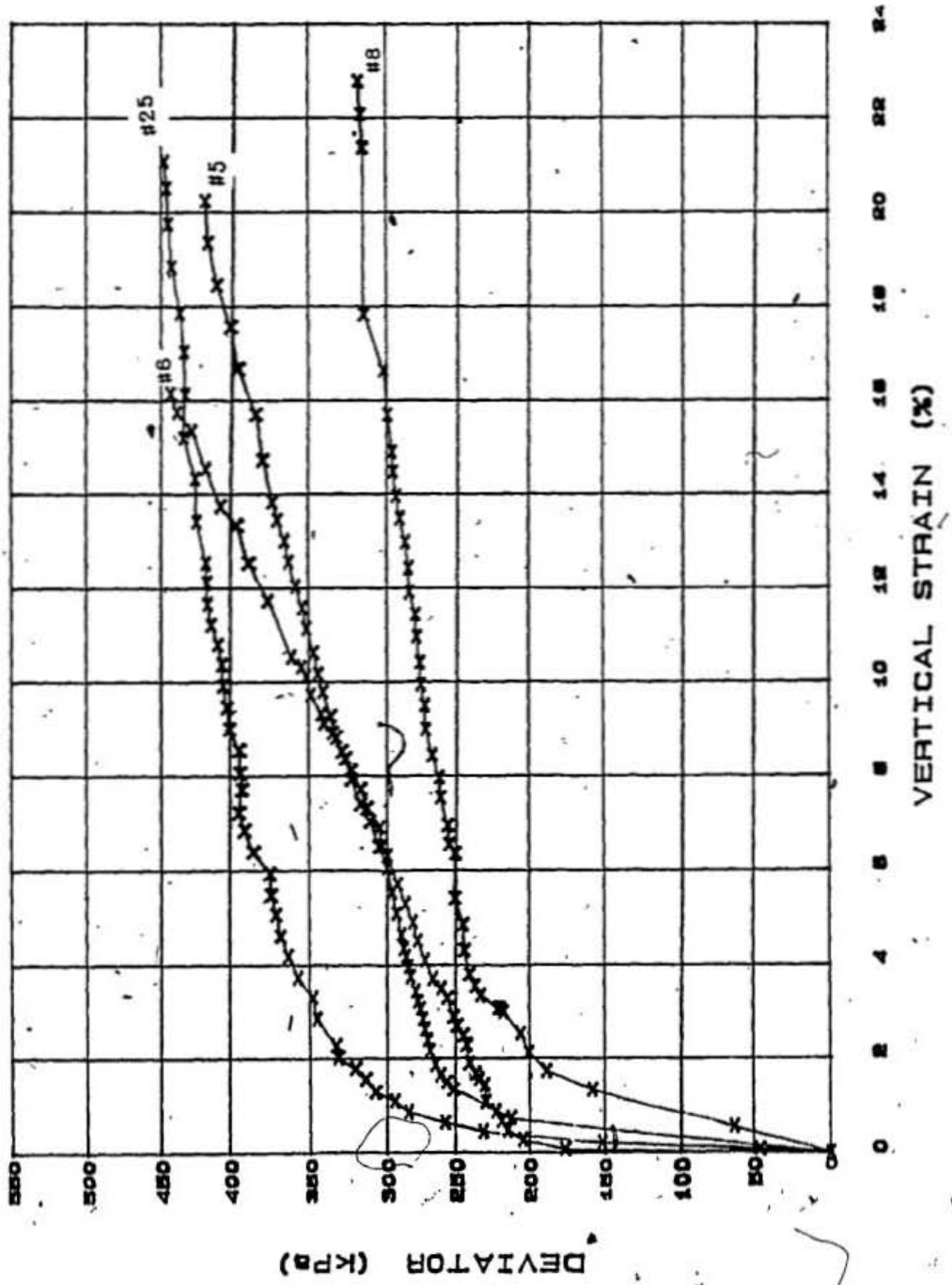

Stress-Strain Curve
(45 kPa, 1.45x10E-4/s, 4 hrs, -10 deg.C)

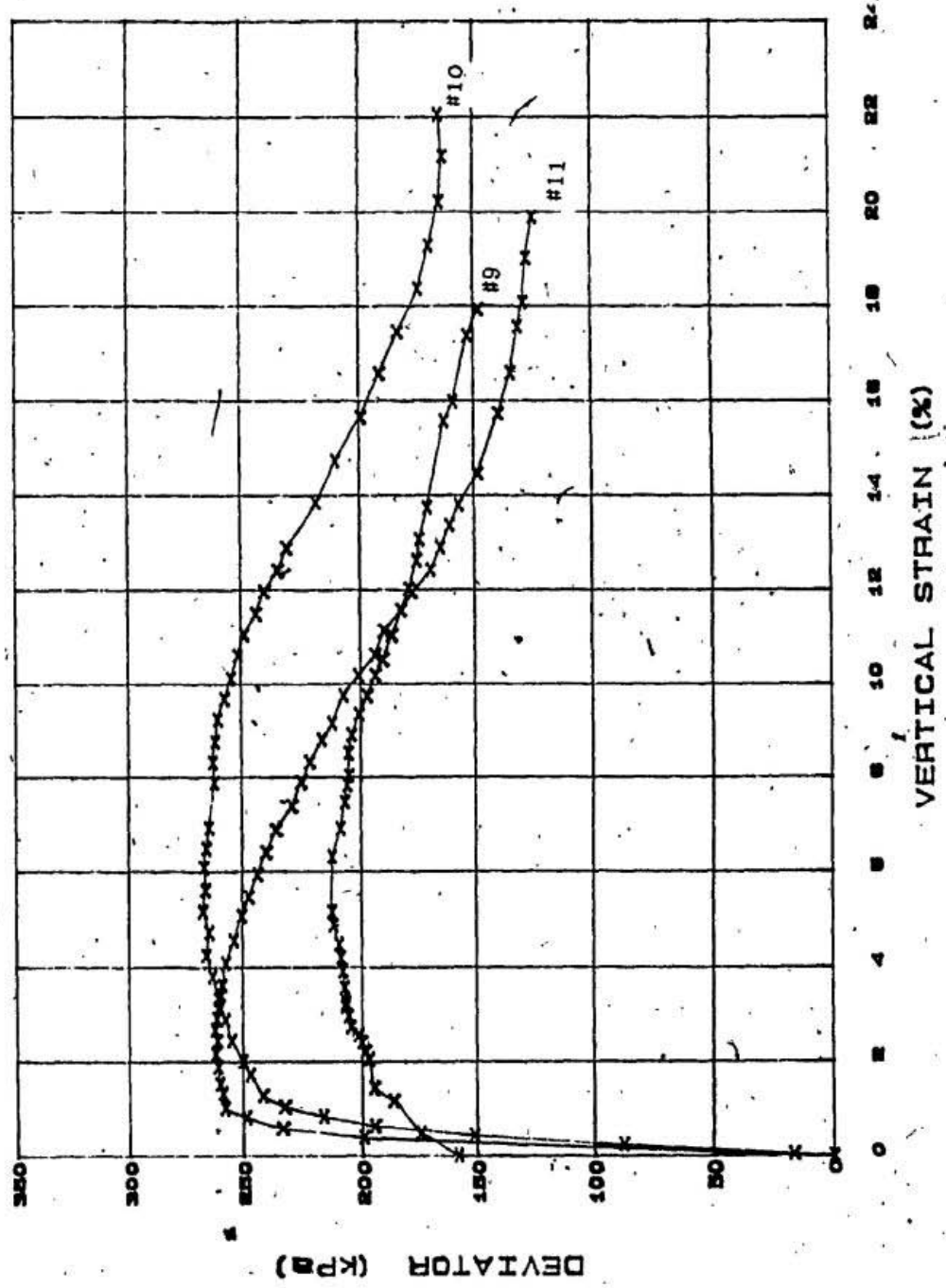

Stress-Strain Curve
(172 kPa, 1.45x10E-4/s, 4 hrs, -10 deg.C)

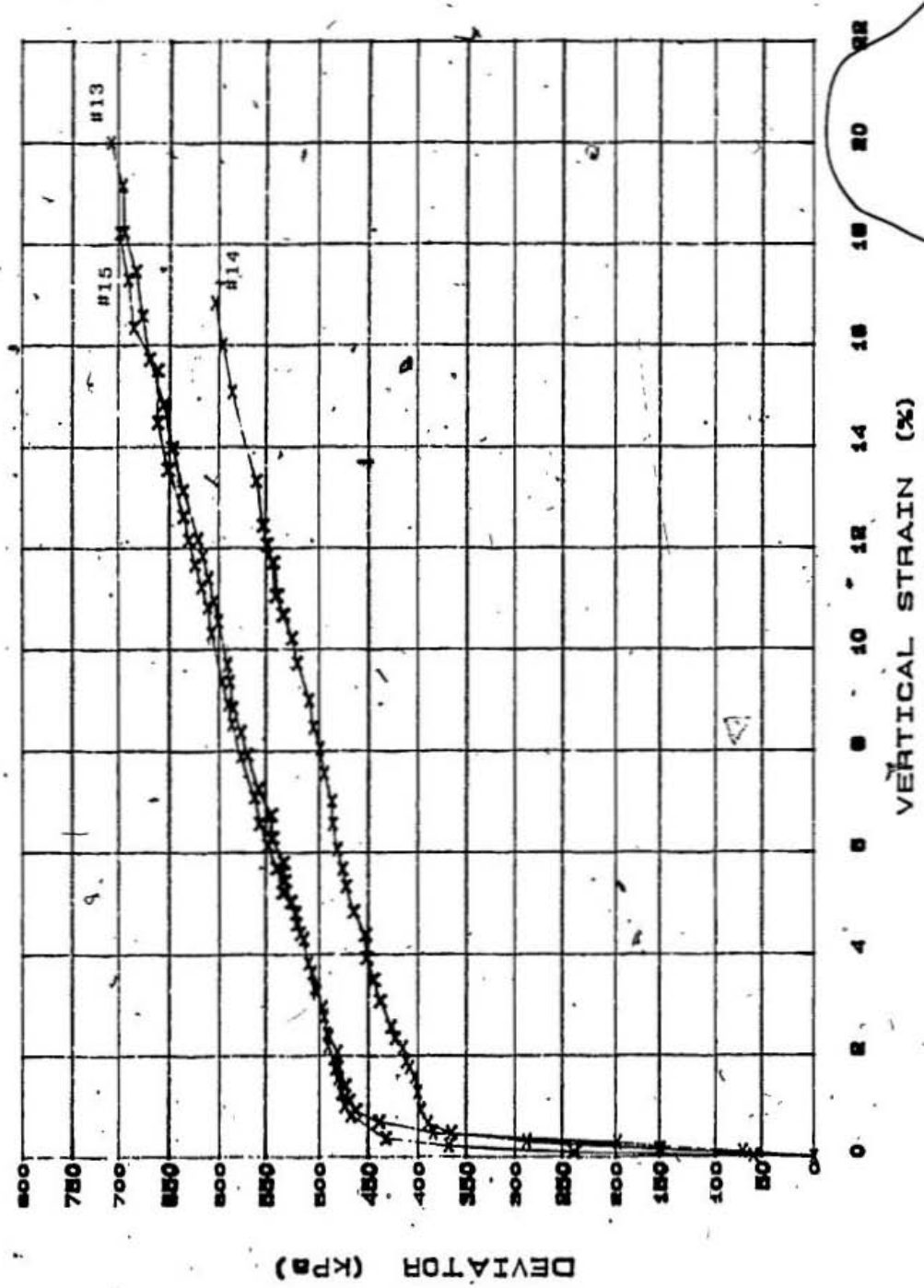

Stress-Strain Curve
(86 kPa, 1.45x10E-4/s, 19 hrs, -10 deg.C)

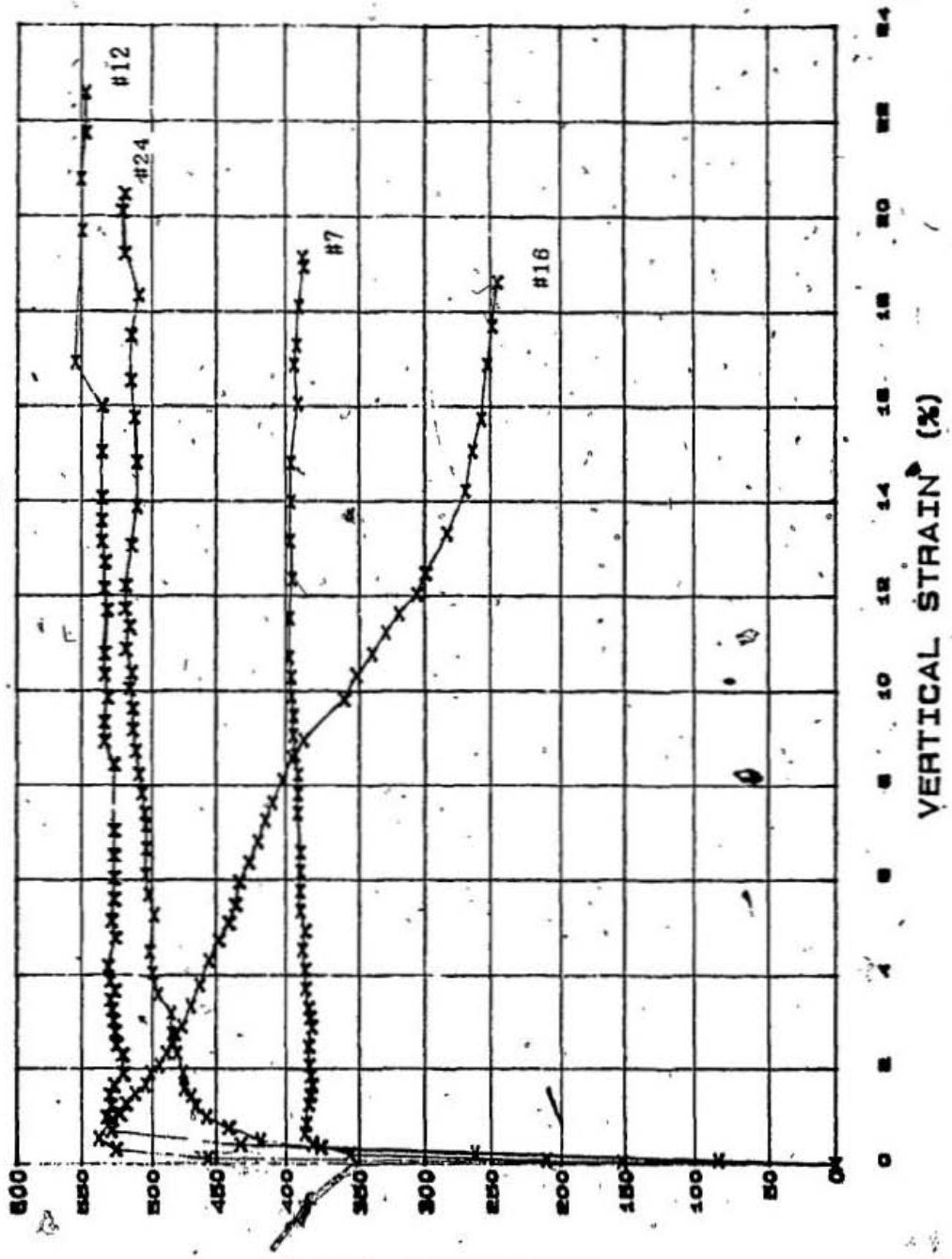

Stress-Strain Curve
(86 kPa, 1.78x10E-5/s, 4 hrs, -10 deg.C)

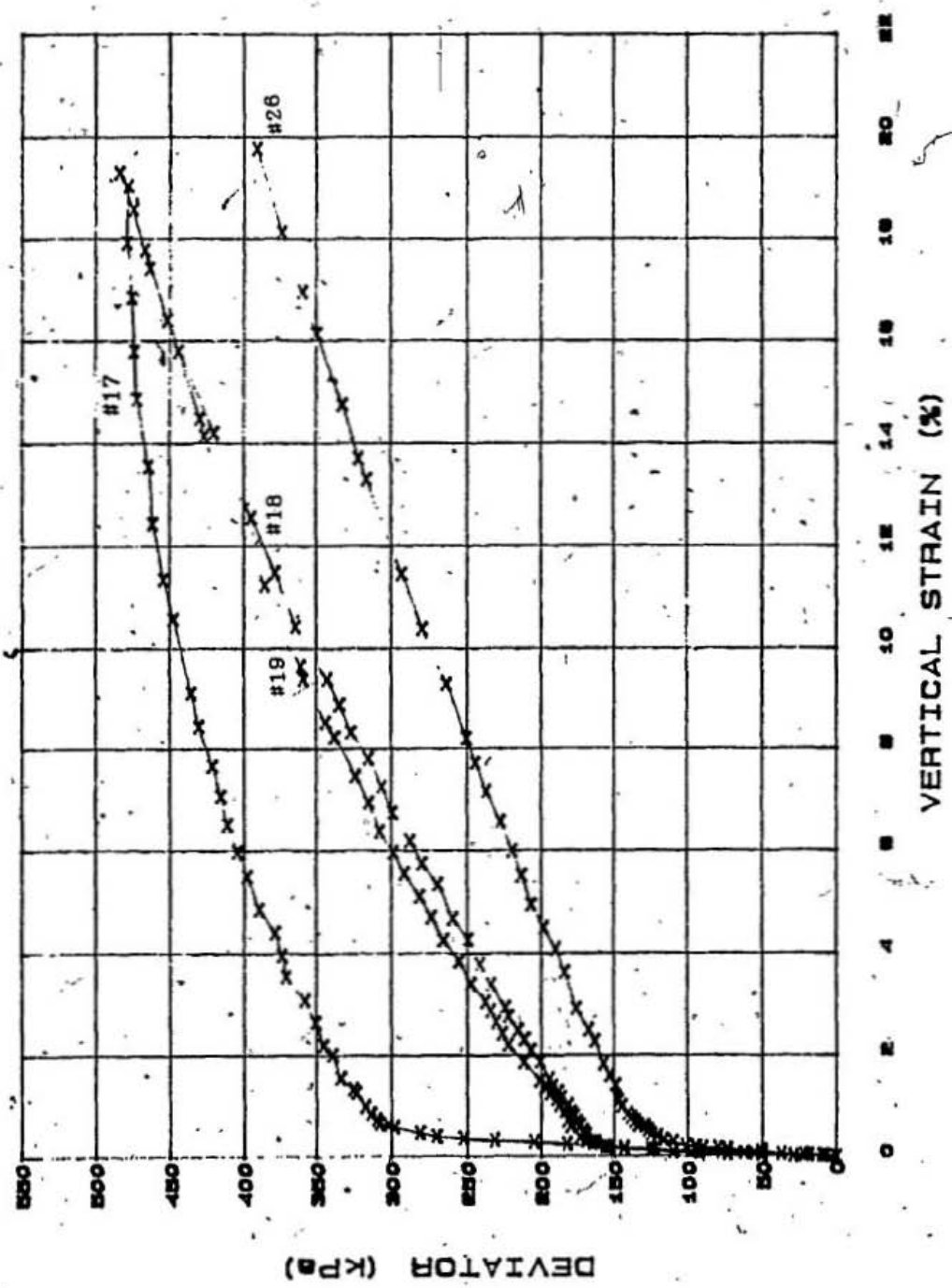

Stress-Strain Curve
(45 kPa, 1.45x10E-4/s, 19 hrs, -10 deg.C)

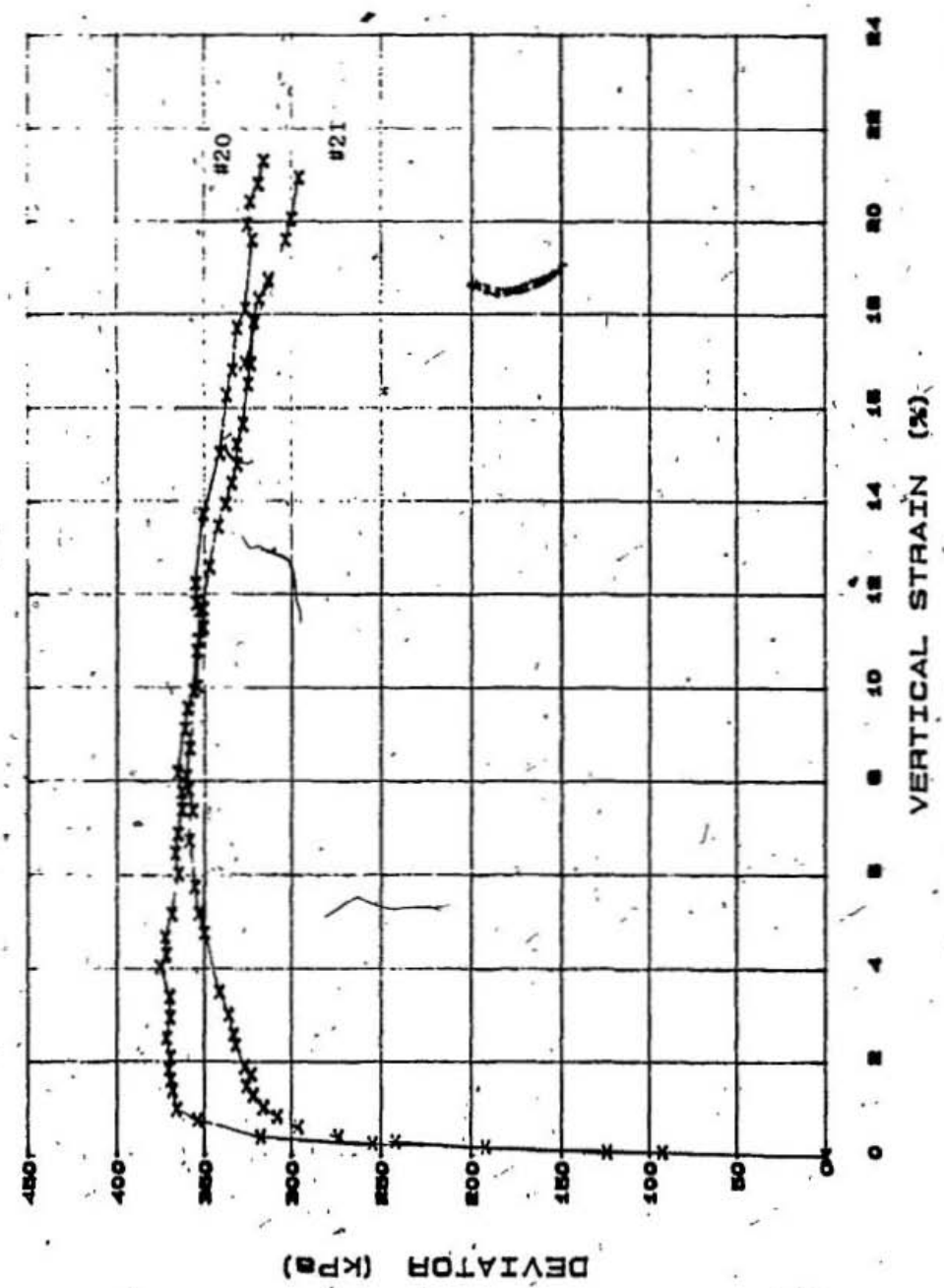

Stress-Strain Curve
(172 kPa, 1.45x10E-4/s, 19 hrs, -10 deg.C)

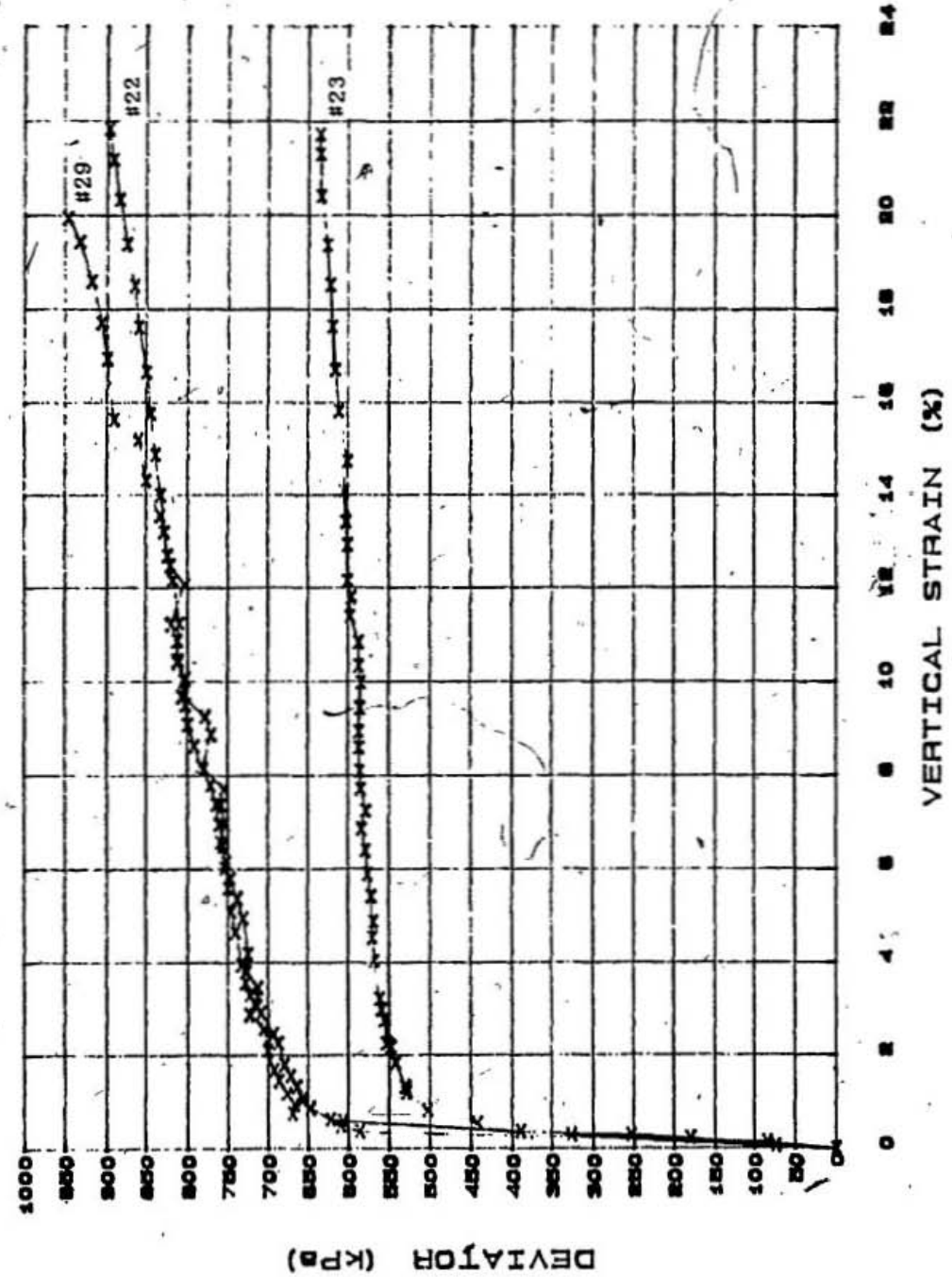

Stress-Strain Curve
(86 kPa, 1.45x10E-4/s, 4 hrs, -5 deg.C)

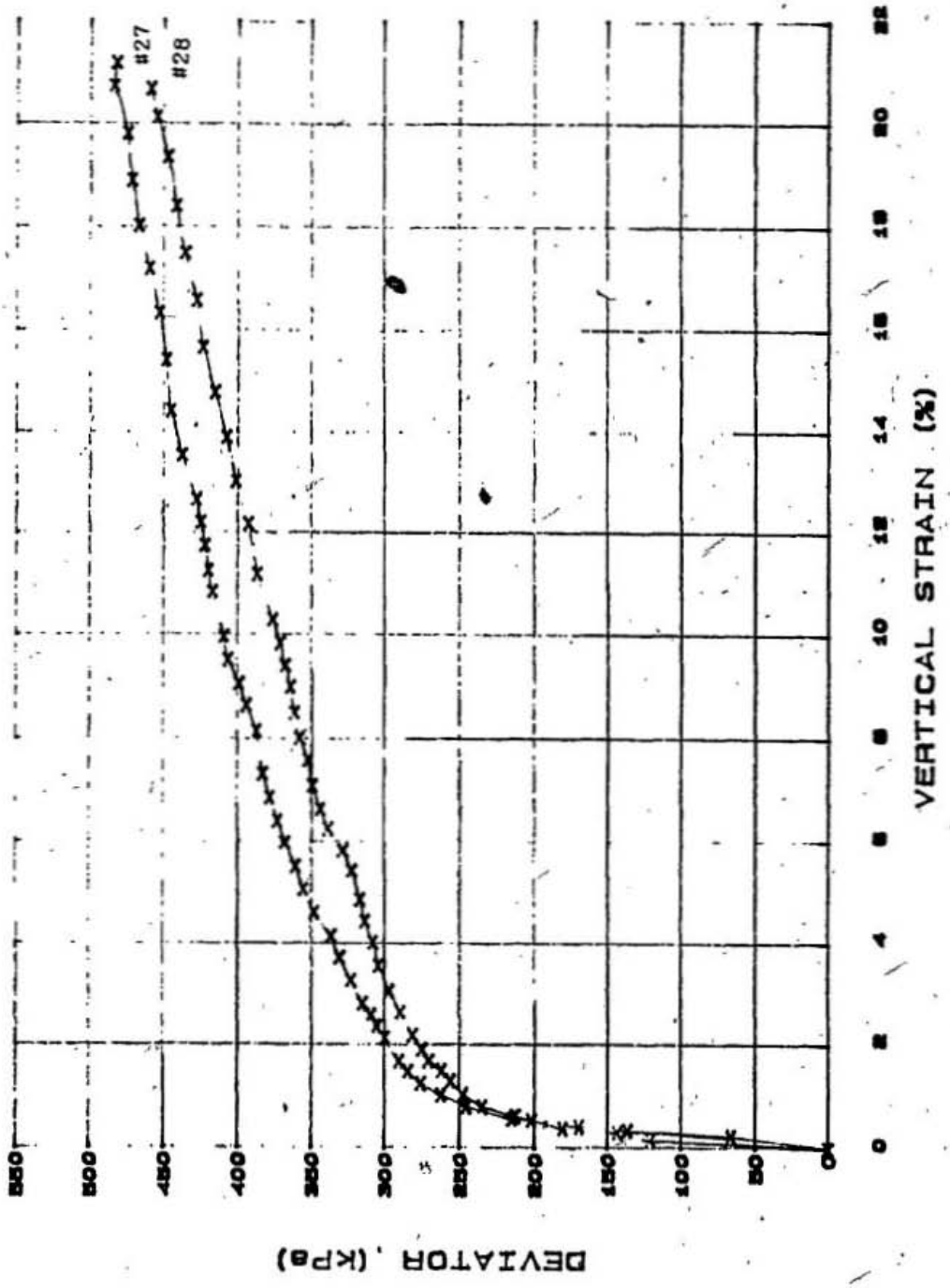

Photographs of Triaxial Samples

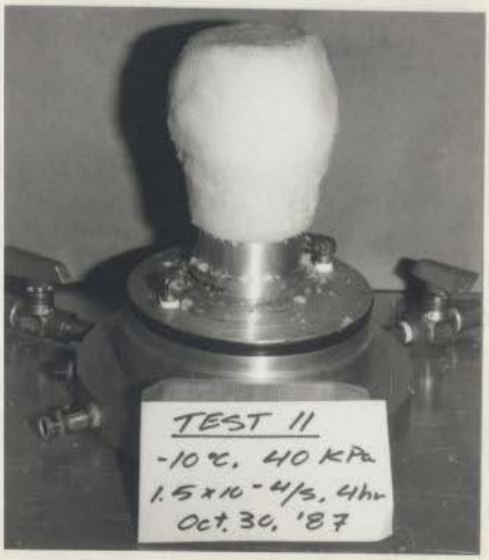

Photographs of Triaxial Samples

Photographs of Triaxial Samples

Photographs of Triaxial Samples

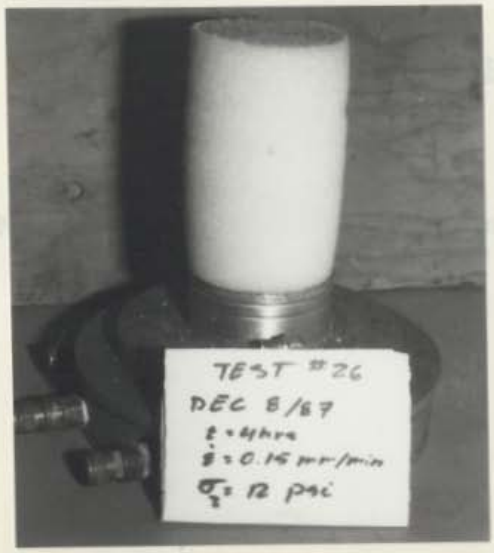

APPENDIX C

Photographs of thin sections on samples from Resolute, LIMEX and Calgary experiments and the triaxial tests.

Resolute Thin Sections

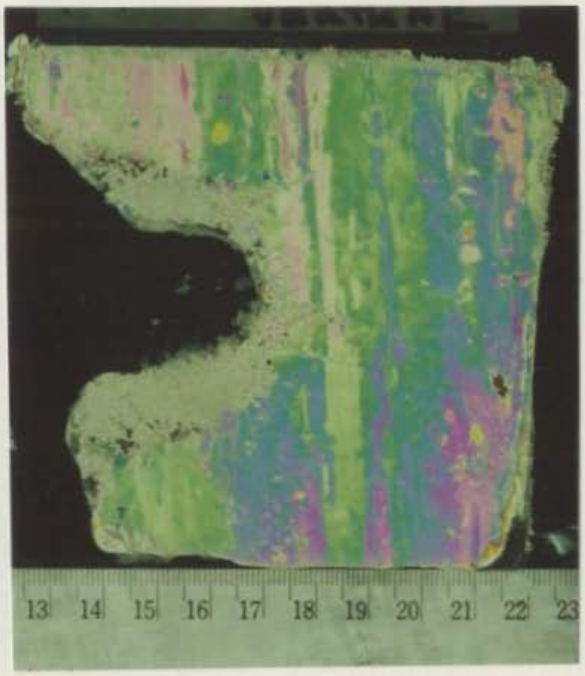

#1

#2

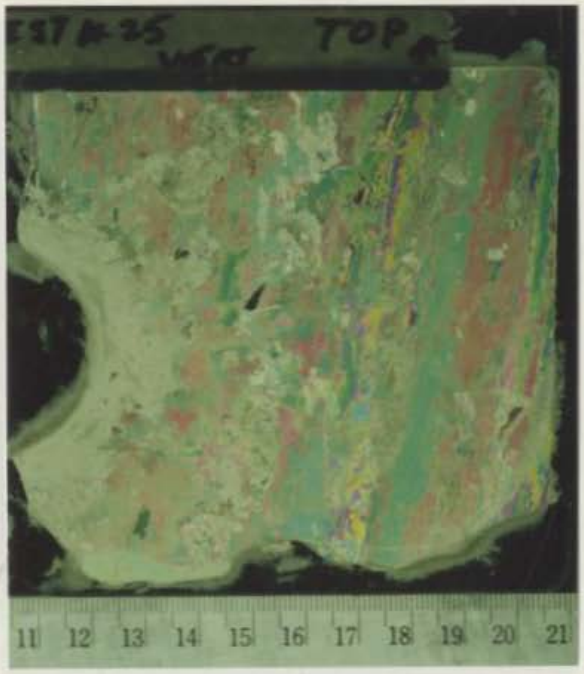

#3

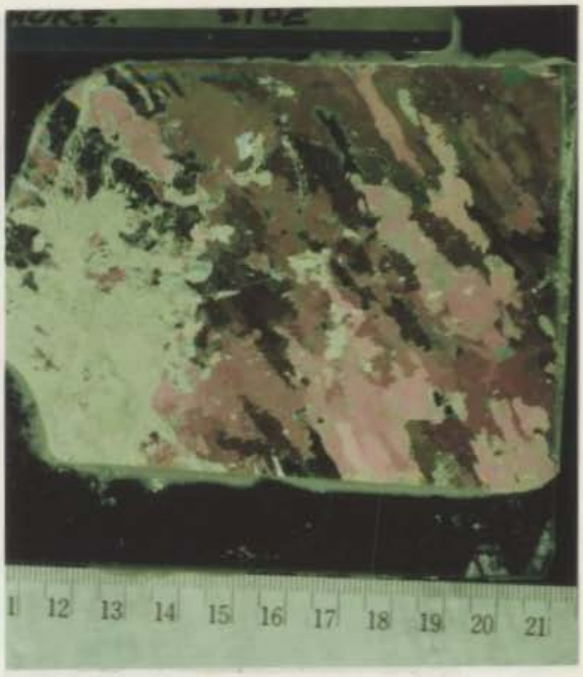

#4

LIMEX Thin Sections

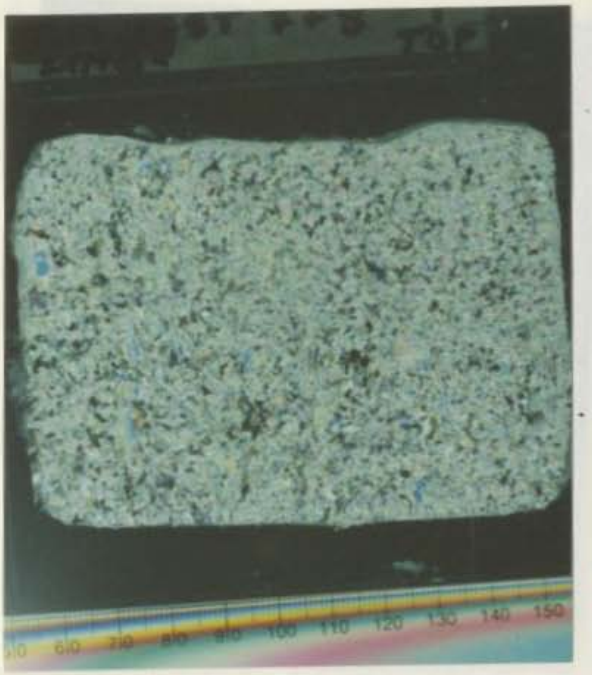

#1

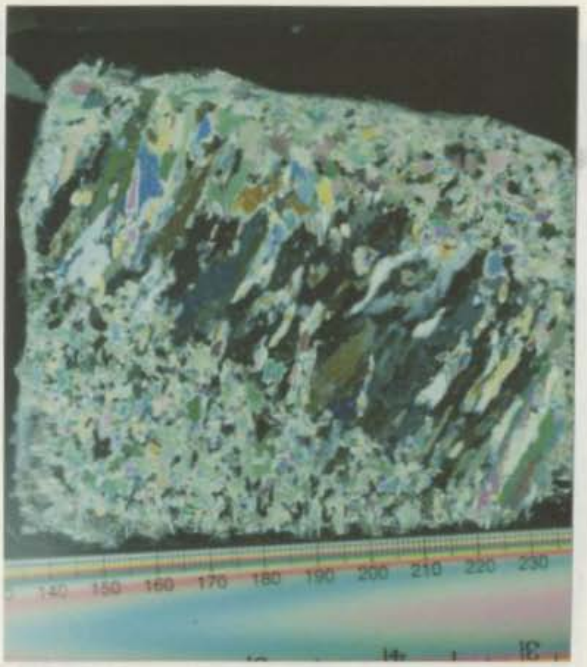

#2

#3

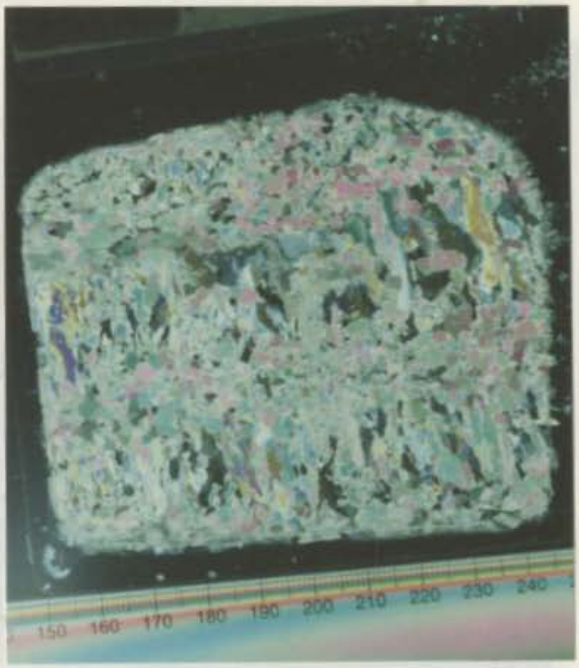

#4

Calgary Thin Sections

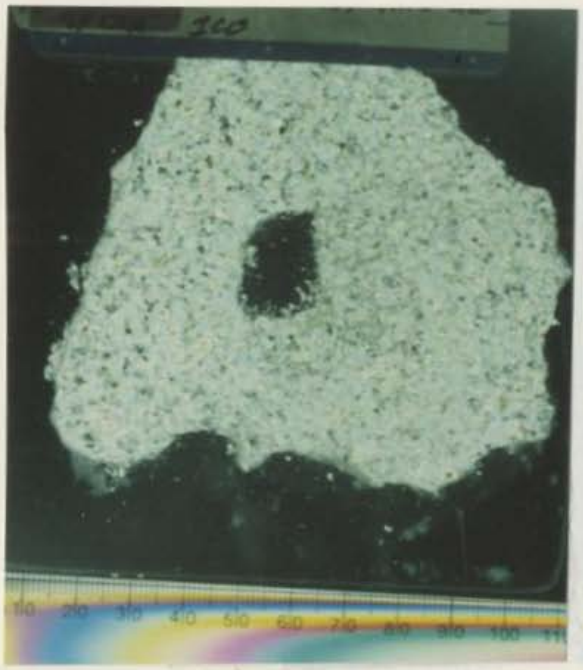

#1(0.50m)

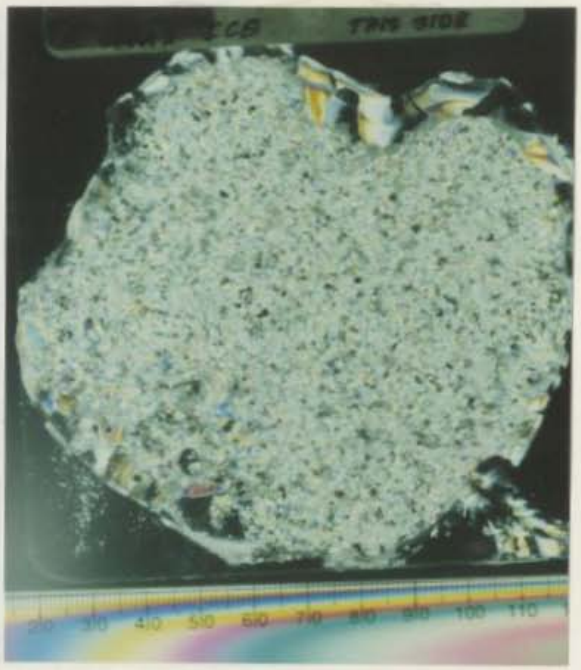

#2(0.17m)

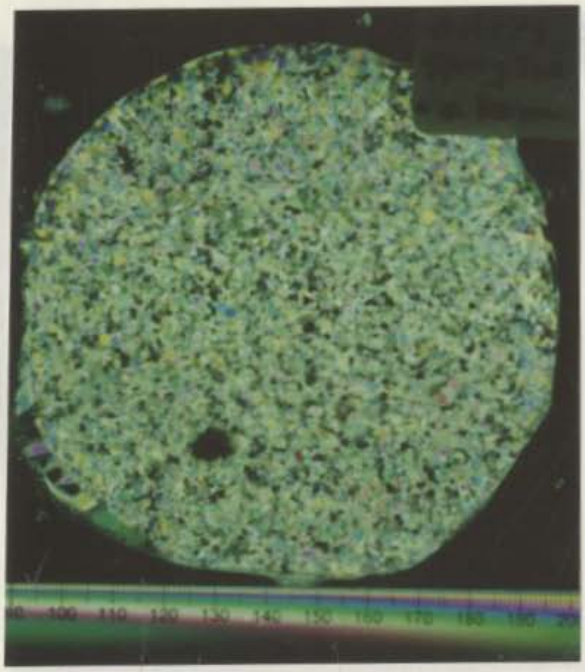

#3(0.30m)

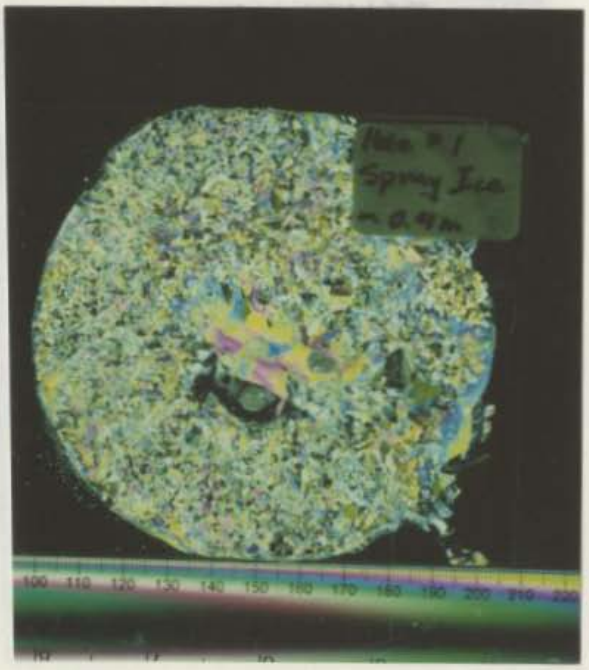

#4(0.40m)

Triaxial Thin Sections